A human iPSC-based model to investigate the effects of psychiatric risk gene CACNA1C on neuronal development and network activity

A thesis presented for the award of

Doctor of Philosophy

Gemma Wilkinson

October 2021

Acknowledgements

First, I would like to thank my supervisors Professor Adrian Harwood and Professor Jeremy Hall for their guidance and insight throughout this project. I have enjoyed working with them in such a supportive and collaborative environment.

Next, I would like to thank everyone in the institute that has given me help and support. Thank you to the other members of the Harwood lab past and present who are always available to discuss results and help troubleshoot. I would like to particularly thank Mouhammed for helping me with many techniques during my PhD, particularly the MEA experiments. Thanks to Ian for generating the iCas9 cell line and setting up our CRISPR screening pipeline. Thank you to Olena for generating the patient iPSCs. Thank you to Kerrie for all the support you gave me following the unexpected interruptions to lab work. Additional thanks to Emma and all the technicians for ensuring smooth running of the lab and institute, particularly during a global pandemic.

I would like to thank my family and friends for their support over the last few years. A special thanks to my partner Tom, you have supported me in so many ways during my PhD and made working from home during a pandemic much more enjoyable.

A final thanks to the GW4 BioMed doctoral training programme and the Medical Research Council who funded my PhD.

Impact of Covid

The COVID-19 pandemic had a significant impact on my PhD research. In March 2020, when the UK went into lockdown, the university closed and access to the lab was halted. This disrupted experiments I was carrying out at the time, primarily neuronal differentiation experiments. I was 40 days into a 100-day time-course which had to be stopped when the university closed. This experiment had to be repeated from the beginning once access to the lab was resumed as cells at this time-point cannot be frozen down. I was unable to access the lab for over 4 months until mid-August, which led to a significant reduction in the amount of time available to carry out experiments. On return to the lab, access was limited to half-days and the requirement for social distancing meant access to equipment, particularly cell culture hoods, was also limited. This limited the number of experiments that I could carry out at once. The restrictions to lab access meant that there was not time to carry out the original number of repeats planned for the experiments. Therefore, the data in my thesis shows results from 1-2 independent differentiations for each experiment, when 3 independent differentiations would have been ideally carried out.

Abstract

CACNA1C encodes the pore-forming subunit of the L-type voltage gated calcium channel Cav1.2. Genome wide association studies have consistently shown that variation in CACNA1C increases risk for psychiatric diseases, including bipolar disorder, schizophrenia, and autism spectrum disorder (ASD). In addition, *de novo* mutations in the gene cause Timothy Syndrome (TS), a multi-system disorder with symptoms that include ASD, developmental delay and epilepsy. This thesis investigates the role of CACNA1C on cortical neuronal development and neuronal network activity. CRISPR/Cas9 gene editing was used in human induced pluripotent stem cells (iPSCs) to derive homozygous CACNA1C knockout lines. In addition to this an iPSC line was derived from an atypical TS patient carrying a novel mutation in CACNA1C that was predicted to have a gain-of-function effect. Differentiation of these lines into cortical neurons demonstrated changes to the expression of neuronal markers and rosette numbers following alterations to CACNA1C expression/function. Alterations to CACNA1C also led to changes in the activation of downstream signalling pathways and the expression of enzymes responsible for GABA production. Functional analysis of neuronal network activity showed alterations to the pattern of neuron bursting behaviour in both the knockout and patient lines. These changes could be rescued using pharmacology targeting either L-type calcium channels or GABA-A receptors. Overall, this data demonstrates that CACNA1C plays a role in cortical neuronal development and neuronal network activity. The results suggest that changes to GABAergic signalling may be responsible for the changes seen to neuronal network activity.

Contents

Acknowledgements i

Impact of Covid ii

Abstract iii

List of tables ix

List of figures x

List of abbreviations xii

1 Introduction 1

1.1 Relevance of CACNA1C in psychiatric disorders 1

1.1.1 Introduction 1

1.1.2 Schizophrenia 1

1.1.3 Bipolar Disorder 3

1.1.4 Autism Spectrum Disorder 4

1.1.5 Genetics of psychiatric disorders 5

1.1.6 Timothy Syndrome 11

1.2 Cav1.2 calcium channel biology 19

1.2.1 Voltage-gated calcium channels 19

1.2.2 L-type calcium channels 21

1.2.3 Cav1.2 calcium channel (CACNA1C) 22

1.2.4 Role of Cav1.2 in neurodevelopment 26

1.2.5 Role of Cav1.2 in neuronal activity 28

1.3 The use of human iPSCs to model psychiatric disorders 31

1.3.1 Human induced pluripotent stem cells (iPSCs) 31

1.3.2 Generation of cortical neurons from iPSCs 32

1.3.3 iPSC-based research using patients with psychiatric disorders.....35
1.3.4 Genome editing using CRISPR-Cas9.....37
1.4 Project Aims.....40
2 General Methods.....42
2.1 Stem Cell Culture.....42
2.1.1 Cell lines and maintenance.....42
2.1.2 iPSC passaging.....43
2.1.3 iPSC freezing.....43
2.1.4 iPSC sub-cloning.....44
2.1.5 Differentiation of glutamatergic neurons from iPSCs.....44
2.1.6 Cell Transfection.....47
2.2 CRISPR Guide Design.....47
2.3 PCR.....47
2.3.1 DNA sample collection.....47
2.3.2 PCR amplification.....48
2.4 Mutation detection assay.....49
2.5 minION sequencing.....49
2.5.1 Barcoding Samples.....49
2.5.2 Library preparation.....50
2.5.3 Sequencing Analysis.....51
2.6 Western Blot.....52
2.6.1 Protein sample collection.....52
2.6.2 Protein concentration measurement.....52
2.6.3 Gel electrophoresis and protein transfer.....53
2.6.4 Immunoblotting.....53
2.7 qPCR.....54

2.7.1 RNA sample collection 54
2.7.2 Conversion to cDNA 55
2.7.3 qPCR 55
2.8 Immunocytochemistry 56
2.8.1 Cell preparation and staining 56
2.8.2 Imaging and analysis 57
2.9 Multi electrode array culture and recording 58
2.9.1 Plating neurons onto multi electrode array plates 58
2.9.2 Astrocyte-conditioned media 58
2.9.3 MEA recordings and analysis 58
2.10 Study Design and Statistical Analysis 59
3 Generation and validation of CACNA1C mutant iPSC lines and an Atypical Timothy Syndrome patient iPSC line 61
3.1 Introduction 61
3.1.1 Chapter Aims 62
3.2 Results 63
3.2.1 Generation of CACNA1C knockout lines 63
3.2.2 Off target screening in knockout lines 66
3.2.3 Validation of loss of CACNA1C expression 69
3.2.4 Characterisation of Atypical Timothy Syndrome line 73
3.3 Discussion 75
3.3.1 Conclusion 79
4 Phenotypic analysis of CACNA1C knockout and atypical Timothy Syndrome iPSC lines during cortical differentiation 80
4.1 Introduction 80
4.1.1 Chapter Aims 81

4.2 Results 82
4.2.1 Phenotypic analysis of NPC markers 82
4.2.2 Impact of CACNA1C on the generation of neurons 84
4.2.3 Analysis of neuronal subtypes 88
4.2.4 Analysis of downstream ERK1/2 and CREB signalling 94
4.3 Discussion 98
4.3.1 Conclusion 108
5 The effect of loss of CACNA1C and an ATS point mutation on neuronal network activity 109
5.1 Introduction 109
5.1.1 Chapter Aims 110
5.2 Results 112
5.2.1 Overview of MEA experiment design 112
5.2.2 Formation of synchronised network activity in CACNA1C knockout line 114
5.2.3 Effect of GABA-A receptor activation on network activity in CACNA1C knockout line 117
5.2.4 Formation of synchronised network activity in ATS line 120
5.2.5 Effect of LTCC antagonism on network activity in ATS line 123
5.2.6 Effect of GABA-A receptor antagonism on network activity in ATS line 126
5.2.7 Effect of MEK inhibitor on network activity in ATS line 130
5.3 Discussion 135
5.3.1 Conclusion 140
6 General Discussion 142
6.1 Summary of findings 142

6.1.1 Chapter 3: Generation and validation of CACNA1C mutant iPSC lines and an Atypical Timothy Syndrome patient iPSC line 142

6.1.2 Chapter 4: Phenotypic analysis of CACNA1C knockout and atypical Timothy Syndrome iPSC lines during cortical differentiation..... 142

6.1.3 Chapter 5: The effect of loss of CACNA1C and an ATS point mutation on neuronal network activity..... 143

6.2 Context and points of discussion 144

6.2.1 Neuronal development..... 144

6.2.2 GABAergic signalling 146

6.3 Study Limitations..... 148

6.3.1 Residual Cav1.2 protein expression..... 148

6.3.2 Unknown effect of ATS mutation on Cav1.2 function..... 149

6.3.3 Variability in differentiation of iPSCs..... 149

6.3.4 Variability in MEA recordings..... 150

6.4 Future Directions..... 151

6.4.1 Comparison of different TS mutations 151

6.4.2 GABAergic signalling 152

6.4.3 Neuronal rosette formation and maintenance 152

6.5 Conclusions..... 153

References 154

List of tables

Table 1.1 Summary of single nucleotide polymorphisms (SNPs) in CACNA1C that have been associated with psychiatric disorders. 9
Table 1.2 Summary of published Timothy Syndrome mutations, symptoms, and effect on channel function. 16
Table 1.3 Summary of the different classes of voltage gated calcium channels. 20
Table 2.1 Neural differentiation media formulations. 45
Table 2.2 Guide sequences used for CRISPR gene knockout. 47
Table 2.3 Primers used for PCR amplification. 48
Table 2.4 Barcoded primers for multiplexing of samples for sequencing. 50
Table 2.5 Primary and Secondary Antibodies used for Western Blot 54
Table 2.6 Primers used for qPCR experiments 56
Table 2.7 Primary and secondary antibodies used for immunofluorescence. 57
Table 3.1 Possible off-target sites that were screened in the CACNA1C knockout lines. 67
Table 4.1 Summary of statistics for gene expression of Nestin, Pax6 and FoxG1. 84
Table 4.2 Summary of statistics for gene expression of Map2 and β-III-tubulin. 86
Table 4.3 Summary of statistics for gene expression analysis of glutamatergic and GABAergic markers at day 50. 90
Table 4.4 Summary of statistics for gene expression analysis of cortical layer markers at day 50. 94
Table 4.5 Summary of statistics for western blot analysis of iCas9 and Hom lines 95
Table 4.6 Summary of statistics for western blot analysis of Control and ATS lines. 97
Table 5.1 Summary of statisitcs for effect of diazepam on excitability and network characteristics in Control and Hom neurons. 120
Table 5.2 Summary of statisitcs for effect of diltiazem on excitability and network characteristics in Control and ATS neurons. 126
Table 5.3 Summary of statisitcs for effect of bicuculline on excitability and network characteristics in Control and ATS neurons. 130
Table 5.4 Summary of statisitcs for effect of selumitnib after 1 hour and 21 hours on excitability and network characteristics in Control and ATS neurons. 134

List of figures

Figure 1.1 (A) UCSC genome browser screenshot of CACNA1C isoforms annotated in GENCODE V38. 7
Figure 1.2 Location of point mutations discovered in CACNA1C. 18
Figure 1.3 Subunit structure of high voltage-activated calcium channels. 20
Figure 1.4 Cav1.2 channels contribute to the regulation of gene expression via CREB. 24
Figure 1.5 Schematic of a neuronal action potential. 30
Figure 1.6 Methods of gene knockdown that can be utilised in induced pluripotent stem cells (iPSCs). 40
Figure 2.1 Overview of protocol for differentiation of iPSCs into cortical neurons. . 45
Figure 3.1 Screening of CACNA1C-mutant iPSCs. 65
Figure 3.2 Sequencing of possible off-targets. 68
Figure 3.3 Western blot for CACNA1C. 70
Figure 3.4 CACNA1C transcripts in knockout lines.. 72
Figure 3.5 ATS line mutation and expression. 74
Figure 4.1 Gene expression of NPC markers during the first 20 days of neuronal differentiation.. 83
Figure 4.2 Relative gene expression of Map2 and β-III-tubulin from day 30 to 50 of neuronal differentiation. 85
Figure 4.3 Immunostaining of MAP2 (green) and DAPI (blue) at day 50 in iCas9, Hom, control and ATS neurons. 87
Figure 4.4 Relative gene expression of Glutamatergic and GABAergic markers at Day 50 of neuronal differentiation. 89
Figure 4.5 GAD65 and GAD67 immunostaining in day 50 neurons. 91
Figure 4.6 Relative gene expression of cortical layer markers at day 50 of neuronal differentiation.. 93
Figure 4.7 Phosphorylation of ERK1/2 and CREB in iCas9 and CACNA1C Hom lines. 95
Figure 4.8 Phosphorylation of ERK1/2 and CREB in Control and ATS lines. 97
Figure 4.9 Proposed pathway of GAD65 and GAD67 transcription. 107
Figure 5.1 Raster and ASDR plots showing MEA analysis measures. 113

Figure 5.2 Neuronal network activity of Control and Hom neurons on MEAs 60 days after plating. 116
Figure 5.3 Effect of GABA-A receptor activation on neuronal network activity of Control and Hom iPSC-derived neurons. 118
Figure 5.4 Neuronal excitability and network characteristics following application of 50nM diazepam in control and Hom iPSC-derived neurons. 119
Figure 5.5 Neuronal network activity of Control and ATS neurons on MEAs 50 days after plating. 122
Figure 5.6 Effect of blockade of LTCCs on neuronal network activity of Control and ATS iPSC-derived neurons. 124
Figure 5.7 Neuronal excitability and network characteristics following application of 5µM diltiazem in control and ATS iPSC-derived neurons. 125
Figure 5.8 Effect of blockade of GABA-A receptors on neuronal network activity of Control and ATS iPSC-derived neurons. 128
Figure 5.9 Neuronal excitability and network characteristics following application of 10µM bicuculline in control and ATS iPSC-derived neurons. 129
Figure 5.10 Effect of blockade of MEK signalling on neuronal network activity of Control and ATS iPSC-derived neurons. 132
Figure 5.11 Neuronal excitability and network characteristics 1 hour and 21 hours after application of 1µM selumitinib in control and ATS iPSC-derived neurons 133

List of abbreviations

ACSF	artificial cerebrospinal fluid
ADHD	attention deficit-hyperactivity disorder
AHP	afterhyperpolarisation
ASD	autism spectrum disorder
ASDR	array-wide spike detection rate
ATS	atypical Timothy syndrome
BDNF	brain-derived neurotrophic factor
BMP	bone-morphogenetic protein
BPD	bipolar disorder
CaM	calmodulin
CaMK	calmodulin kinase
CaMKK	CaMK kinase
CCAT	calcium channel associated transcriptional regulator
CDI	calcium dependent inactivation
CNV	copy number variant
CRE	cAMP response element
CREB	cAMP response element binding protein
CRISPR	clustered-regularly interspaced short palindromic repeat
DHP	dihydropyridine
DPP	days post-plating
ECG	electrocardiogram
ERK1/2	extracellular signal regulated kinases 1/2
ESCs	embryonic stem cells
GABA	y-aminobutyric acid
GAD	glutamic acid decarboxylase
gRNA	guide RNA
GWAS	genome wide association study
HDR	homology directed repair
HVA	high-voltage activated
iCas9	inducible Cas9

iPSCs	induced pluripotent stem cells
LQTS	long QT syndrome
LTCC	L-type calcium channel
LTP	long term potentiation
LVA	low-voltage activated
MAPK	mitogen-activated protein kinases
MDD	major depressive disorder
MEA	multi-electrode array
MEK	mitogen-activated protein kinase kinase
mQTL	methylation quantitative trait loci
MRI	magnetic resonance imaging
mRNA	messenger RNA
NFAT	nuclear factor of activated T-cells
NHEJ	non-homologous end joining
NMDA	N-methyl-D-aspartate
NPCs	neural progenitor cells
PAM	protospacer adjacent motif
PET	positron emission tomography
PV	parvalbumin
qRT-PCR	quantitative reverse transcription PCR
RyR2	type 2 ryanodine receptors
SB	synchronised burst
SNP	single nucleotide polymorphism
TALENs	transcription activator-like effector nucleases
TGFβ	transforming growth factor beta
TS	Timothy syndrome
VDI	voltage dependent inactivation
VGCC	voltage gated calcium channel
VZ	ventricular zone

1 Introduction

1.1 Relevance of CACNA1C in psychiatric disorders

1.1.1 Introduction

Psychiatric conditions, including schizophrenia, bipolar disorder (BPD) and autism spectrum disorder (ASD) are highly complex disorders that are prevalent worldwide (Demyttenaere et al. 2004; Charlson et al. 2019). Schizophrenia and BPD are both in the top 20 causes of global burden of disease (Vigo et al. 2016). These disorders also cause an enormous personal burden which lead to reduced quality of life and life expectancy (Ngui et al. 2010). They have a high heritability, however until recently it was unclear which genes were implicated in these diseases (Gejman et al. 2010). This is paired with a lack of understanding of the underlying pathophysiology of psychiatric diseases. The treatments for different psychiatric disorders are ineffective in many people and the unknown etiology makes the development of new drugs difficult. This is particularly apparent in schizophrenia where the majority of anti-psychotics act by targeting the dopaminergic system, a mechanism which was discovered over 50 years ago (Jašović-Gašić et al. 2012). New genomic techniques, including genome wide association studies (GWAS) have been used to elucidate the genes involved in psychiatric disorders with the hope to highlight possible genetic targets for research and future treatments. Research is now needed to investigate the functional effects of these risk genes and how they may lead to disease. In this thesis I address this by investigating the effects of CACNA1C, one of the most highly associated risk genes, on neuronal development and network activity.

1.1.2 Schizophrenia

Schizophrenia is a neurodevelopmental disorder that affects approximately 1% of the population (Szegedi and Egan 2012; Owen et al. 2016). Heritability of the disorder is estimated around 80% (Cardno and Gottesman 2000; Sullivan et al. 2003; Hilker et al. 2018). It is characterised by symptoms that are classified into three groups. Positive symptoms which include hallucinations and delusions, negative symptoms such as anhedonia and affective flattening and cognitive symptoms which affect

working memory, executive function, learning and social cognition (Szegedi and Egan 2012). The neurodevelopmental hypothesis of schizophrenia suggests that genetic and environmental factors during the prenatal and postnatal period influence brain development, which can then lead to schizophrenia later in life (Weinberger 1987; Rund 2018). Most patients develop schizophrenia in late adolescence or early adulthood, with a slightly later age of onset in females (Gogtay et al. 2011). Patients can recover or improve over time, however roughly one third of patients do not show any response to medication, providing a large unmet clinical need for new, effective treatments (Lally et al. 2016).

Current treatments for schizophrenia act largely by targeting the dopaminergic system, specifically dopamine D_2 receptors (Miyamoto et al. 2012). However, many anti-psychotics also act at other receptors, and there is evidence to suggest multiple neurotransmitter systems are involved in schizophrenia pathology. *N*-methyl-D-aspartate (NMDA) receptor antagonists, such as ketamine, induce positive, negative and cognitive schizophrenia-like symptoms in humans and animal models, implicating the glutamatergic system (Krystal et al. 1994; Coyle 2012). Changes in levels of γ-aminobutyric acid (GABA) interneuron subtypes have also been found in post-mortem studies (Akbarian et al. 1995; Beasley and Reynolds 1997). In addition, GWAS have shown that over 100 genes have been linked to schizophrenia (Ripke et al. 2014; Li et al. 2017). One of these genes is DRD2, supporting the hypothesis that the D_2 dopamine receptor is involved in schizophrenia pathogenesis. However, single nucleotide polymorphisms (SNPs) at this locus increase risk of schizophrenia by under 10% (Ripke et al. 2014). Other genes that have been implicated in schizophrenia have roles in neurodevelopment, synaptic signalling, neuroimmunology and histone methylation and one of the most consistently implicated groups of genes is voltage-gated calcium channels (VGCCs) (O'dushlaine et al. 2015; Xiao et al. 2017). GWAS have shown that the genetic contribution towards schizophrenia is highly heterogenous, which may account for the large number of patients that don't respond to current treatments.

1.1.3 Bipolar Disorder

Bipolar disorder (BPD) is a chronic mood disorder characterised by episodes of depression and episodes of abnormally elevated mood which can include psychosis in some patients (Charney et al. 2017). These episodes of elevated mood are known as mania or hypomania dependent on severity and duration of the symptoms. Age of onset usually occurs in adulthood between 20 and 40 years old (Prabhakar and Balon 2010). BPD affects roughly 2% of the population and twin and family studies have shown heritability to be between 60 and 85% (P et al. 2003; Merikangas et al. 2007; Edvardsen et al. 2008; Song et al. 2015; Johansson et al. 2019). BPD has many overlapping symptoms with schizophrenia and MDD; cognitive dysfunction and psychotic symptoms can be present in both BPD and schizophrenia and mood symptoms are common in all three disorders.

The current gold-standard treatment for BPD is lithium but only 40-50% of patients show an adequate response and some become non-responsive after continued use (Kujawa and Nemeroff 2006). The mechanism for lithium treatment is unclear as it affects multiple cellular pathways. Research has shown that lithium can repair oxidative stress caused by excitotoxicity, prevent apoptosis, alter calcium signalling and modulate multiple neurotransmitter systems (Malhi and Outhred 2016). Other treatments for BPD include antipsychotics, such as olanzapine and risperidone, and anticonvulsants, such as valproic acid and lamotrigine (Kato 2019). Like schizophrenia, the mechanisms underlying BPD are largely unknown. Positron emission tomography (PET) studies have shown reductions in the dopamine D1 receptor and serotonin 2 receptor during mania (Suhara et al. 1992; Yatham et al. 2010). Mitochondrial function has also been linked to BPD. Post-mortem studies have shown changes to the mRNA levels of mitochondrial genes, however this is affected by drug treatment (Konradi et al. 2004; Iwamoto et al. 2005; Sun et al. 2006). A study using iPSCs from patients with bipolar disorder has also shown mitochondrial dysfunction, which was rescued by lithium treatment in cells derived from lithium-responsive patients (Mertens et al. 2015). This suggests one of the pathways that leads to bipolar disorder involves mitochondrial function, which may have

downstream effects, such as alterations in calcium signalling (Kato 2008). However, it is likely that other pathways are also involved in BPD as lithium has multiple targets and its mechanism of action is unclear. Additionally, not all BPD patients respond to lithium, highlighting the heterogeneity underlying psychiatric diseases.

1.1.4 Autism Spectrum Disorder

Autism spectrum disorder (ASD) is a group of neurodevelopmental disorders that affects roughly 1.7% of children and is usually diagnosed by 2 years old (Mazurek et al. 2014; Baio et al. 2018). The estimated heritability of ASD ranges from 56 to 95% (Colvert et al. 2015; B et al. 2016; Xie et al. 2020). The core symptoms of ASD are reduced language skills, deficits in social interaction and repetitive or stereotypic behaviours (Grzadzinski et al. 2013). ASD is highly heterogenous and symptoms can vary significantly between patients and at different ages; with some individuals displaying intellectual disability while others are highly intelligent (Grzadzinski et al. 2013). There are currently no treatments for ASD, but risperidone and aripiprazole, which are dopamine and 5-HT receptor antagonists can be used to help manage some symptoms of ASD. Both these treatments have similar efficacy in reducing irritability, hyperactivity and stereotypic behaviours in patients (Ghanizadeh et al. 2014). However these treatments are not effective at treating sociability defects (McCracken et al. 2002; McDougle et al. 2005).

Magnetic resonance imaging (MRI) studies have shown that ASD patients show altered activation in the cerebellum and the presence of anatomical abnormalities (Allen and Courchesne 2003; Allen et al. 2004; Hazlett et al. 2005). It has been hypothesised that alterations in brain connectivity may be responsible for these anatomical abnormalities. In general patients have over-connectivity in local areas but under-connectivity between brain regions (Herbert et al. 2004; Just et al. 2007). There is also evidence that the balance of excitatory and inhibitory signalling is altered. Both glutamate and GABA systems are altered in ASD patients, which may contribute to alterations in connectivity (Fatemi et al. 2002; Aldred et al. 2003; Yip et al. 2009; Shimmura et al. 2011).

ASD has a strong genetic component, concordance rates can vary from 60-90% in monozygotic twins to 20% in siblings (Le Couteur et al. 1995; Hallmayer et al. 2011; Ozonoff et al. 2011; Ramaswami and Geschwind 2018). The genetic component of ASD varies widely between patients. ASD in many patients is attributed to common genetic variation that is present in over 1% of the population, these common variants have an additive effect that lead to the development of ASD (Klei et al. 2012; Gaugler et al. 2014). Rare gene variants occur in approximately 10-15% of patients, these patients have single-gene disorders or copy number variants (CNVs) that often have additional phenotypes such as facial dysmorphism, epilepsy and intellectual disability (Hagberg 1995; Folstein and Rosen-Sheidley 2001; Splawski et al. 2004; Veltman et al. 2005; Yoo 2015; Wong et al. 2019). These disorders include Timothy Syndrome (CACNA1C), fragile x (FMR1), tuberous sclerosis complex (TSC1 and TSC2), Rett syndrome (MeCP2), 16p11.2 deletions, FoxG1 syndrome and neurofibromatosis (NF1). Although these genes have varying functions, they can be used to determine shared biological pathways that may contribute to ASD.

1.1.5 Genetics of psychiatric disorders

Schizophrenia, BPD and ASD are all highly heritable disorders. However, for the majority of patients the genetic contribution of these disorders results from multiple common variants that increase the risk of developing one of these conditions. Genome wide association studies (GWAS) have been used to determine which SNPs contribute to this increased risk (Ripke et al. 2014; Li et al. 2017; Grove et al. 2019). In order to do this GWAS require large sample sizes in order to compare the frequencies of hundreds of SNPs between patients and matched controls. The effect size of SNPs associated with psychiatric disorders is small (odds ratio of <1.2), however they have an additive effect so together can account for a large degree of the heritability of psychiatric disorders (Bray and Hill 2016). These SNPs often occur in non-coding areas of the genome so further research is required to determine whether they cause a direct biological effect on a specific gene or if they are in linkage disequilibrium with other variants (Edwards et al. 2013; Roussos et al. 2014).

Pathway analysis of significant SNPs suggests that VGCCs may play an important role in development of psychiatric disorder and one of the genes that has been consistently associated with psychiatric disorders is CACNA1C (Smoller et al. 2013; O'dushlaine et al. 2015). This gene encodes the pore-forming subunit of Cav1.2, an L-type voltage gated calcium channel. All the SNPs that have been associated with psychiatric diseases occur in intron 3 of CACNA1C (Figure 1.1). The SNP rs1006737 was the first to be associated with BPD and this has been supported by subsequent GWAS with larger sample sizes (Ferreira et al. 2008; Sklar et al. 2008; Green et al. 2013; Ruderfer et al. 2014). This SNP and others within CACNA1C have also been associated with schizophrenia and to a lesser extent major depressive disorder (MDD), ASD and attention deficit-hyperactivity disorder (ADHD), as summarised in Table 1.1. A cross-disorder GWAS for schizophrenia, BPD, MDD, ASD and ADHD found four genome-wide significant SNPs, two of which occurred in genes for L-type calcium channel subunits (Smoller et al. 2013). The SNPs occurred in CACNA1C (rs1024582) and CACNB2 (rs2799573), an auxiliary subunit that is involved in trafficking of L-type calcium channels. The study also found significant enrichment for a set of calcium channel genes, suggesting that variation in calcium channel activity may be associated with symptoms that converge across all these disorders.

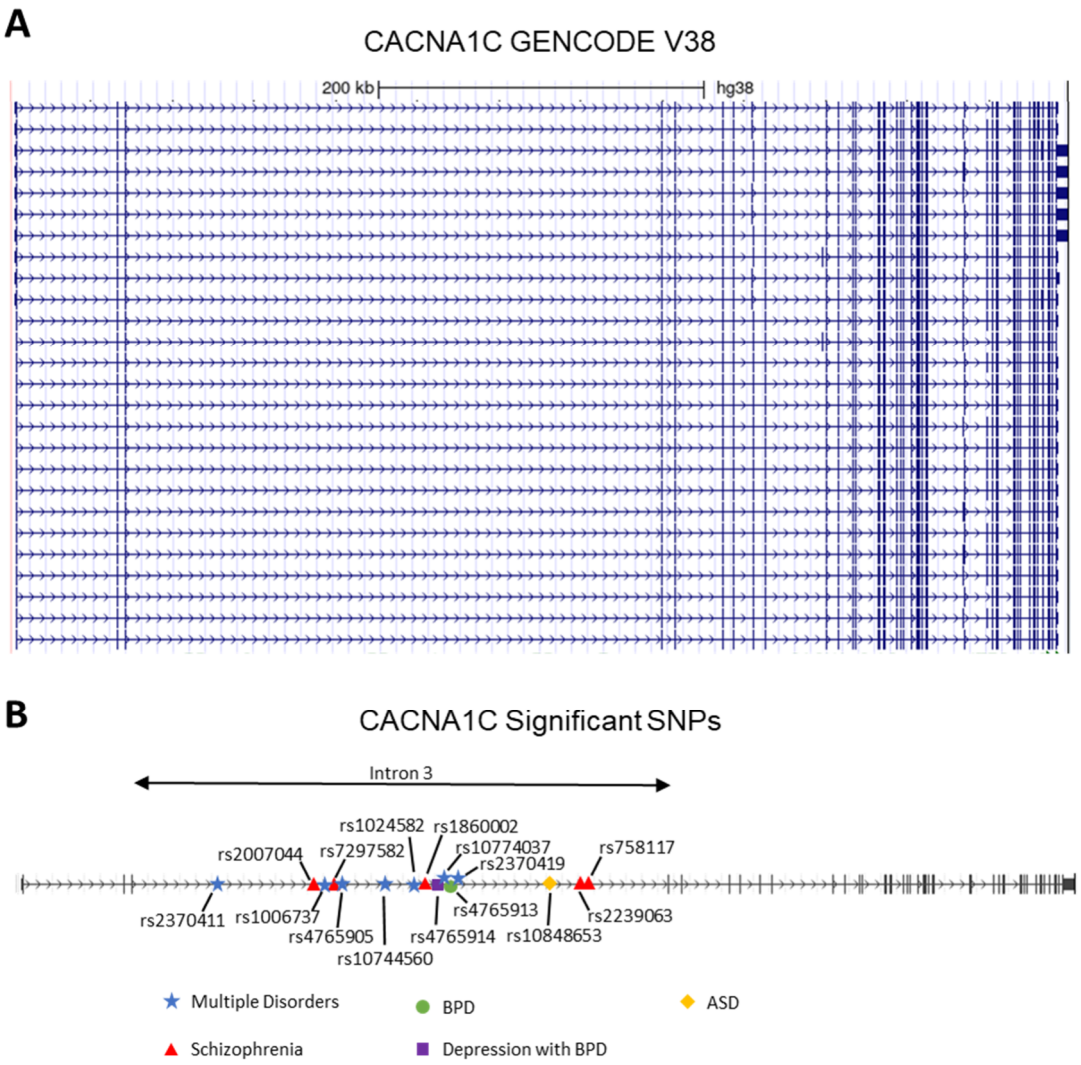

Figure 1.1 (A) UCSC genome browser screenshot of CACNA1C isoforms annotated in GENCODE V38. Transcripts starting with Exon 1 but not 1a are shown as 1a isoforms are only expressed in cardiac tissue. Exons are indicated by vertical bars. (B) Location of SNPs associated with psychiatric disorders in CACNA1C. Blue stars indicate SNPs that have been associated with more than one psychiatric disorder. Red triangles indicate SNPs associated with schizophrenia. Green circles indicate SNPs associated with bipolar disorder (BPD). Purple squares indicate SNPs associated with broad depression with BPD. Yellow diamonds indicate SNPs associated with ASD.

SNP	Disorder	P value	Study Type	References
rs1006737	BPD	3.15E-06	GWAS	(Sklar et al. 2008)
		7.00E-08	GWAS	(Ferreira et al. 2008)
		7.43E-08	GWAS	(Ruderfer et al. 2014)
		4.09E-04	Previous BPD associated SNPs analysed	(Green et al. 2013)
	SCZ	3.40E-02	SNP specifically tested for association	(Green et al. 2010)
		5.20E-12	GWAS	(Ripke et al. 2013)
		1.08E-02	Only CACNA1C SNPs analysed	(Zheng et al. 2014)
		1.37E-02	CACNA1C & miR137 SNPs analysed	(Guan et al. 2014)
		1.40E-03	Only CACNA1C SNPs analysed	(He et al. 2014)
		1.50E-02	SNP specifically tested for association	(Nyegaard et al. 2010)
	MDD	3.90E-04	SNP specifically tested for association	(Green et al. 2010)
		7.00E-04	Only CACNA1C SNPs analysed	(He et al. 2014)
	BPD, SCZ	5.50E-13	GWAS	(Ruderfer et al. 2014)
	BPD, MDD	3.10E-08	Meta-analysis of BPD & MDD GWAS	(Liu et al. 2011)
	ASD	3.50E-02	Family based association study	(Li et al. 2015)
rs2007044	SCZ	3.22E-18	GWAS	(Ripke et al. 2014)
		5.63E-20	GWAS	(Pardiñas et al. 2018)
		9.10E-18	GWAS	(Periyasamy et al. 2019)
		5.30E-03	Only CACNA1C SNPs analysed	(Zheng et al. 2014)
rs7297582	BPD, MDD	3.40E-08	Meta-analysis of BPD & MDD GWAS	(Liu et al. 2011)
rs4765905	SCZ	1.20E-08	GWAS	(Hamshere et al. 2013)
		3.22E-18	GWAS	(Takahashi et al. 2015)
		4.00E-02	CACNA1C & miR137 SNPs analysed	(Guan et al. 2014)
	ASD	3.50E-02	Family based association study	(Li et al. 2015)

rs10848653	ASD	1.30E-06	Family based association study	(Lu et al. 2012)
rs4765913	BPD	1.52E-08	GWAS	(Sklar et al. 2011)
		9.78E-10	Previous BPD associated SNPs analysed	(Green et al. 2013)
		3.12E-09	GWAS	(Charney et al. 2017)
rs10744560	BPD	3.60E-06	GWAS	(Stahl et al. 2019)
rs4765914	Broad depression with BPD	5.25E-09	GWAS with bivariate analysis	(Amare et al. 2019)
rs10774037	BPD	7.00E-08	GWAS	(Ferreira et al. 2008)
	Broad depression with SCZ	7.94E-12	GWAS with bivariate analysis	(Amare et al. 2019)
rs2370419	BPD, MDD (females only)	1.40E-04	Only CACNA1C SNPs analysed	(Dao et al. 2010)
rs2370411	BPD, MDD (females only)	1.90E-04	Only CACNA1C SNPs analysed	(Dao et al. 2010)
rs758117	SCZ	1.68E-08	GWAS	(Li et al. 2017)
rs2239063	SCZ	4.76E-09	GWAS	(Ikeda et al. 2018)
rs1860002	SCZ	1.27E-17	GWAS	(Ikeda et al. 2018)
rs1024582	SCZ	1.27E-17	GWAS	(Ikeda et al. 2018)
		6.28E-04	Previous BPD associated SNPs analysed	(Green et al. 2013)
		6.20E-03	Only CACNA1C SNPs analysed	(Zheng et al. 2014)
	BPD, SCZ, MDD, ASD, ADHD	1.87E-08	Cross-disorder GWAS	(Smoller et al. 2013)

Table 1.1 Summary of single nucleotide polymorphisms (SNPs) in CACNA1C that have been associated with psychiatric disorders. (BPD = bipolar disorder, SCZ = schizophrenia, MDD = major depressive disorder, ASD = autism spectrum disorder, ADHD = attention deficit hyperactivity disorder, GWAS = genome wide association study)

Although rs1006737 is the most commonly associated SNP with psychiatric disorders, and therefore the most highly investigated, it is also in linkage disequilibrium (R^2 > 0.8) with many other SNPs within CACNA1C (including rs1024582, rs2159100, rs7965923, rs769087, rs12315711, rs11062170, rs4765905, rs758170, rs10774035, rs10774036, rs10744560, rs12311439, rs4298967) (Roussos et al. 2014; Eckart et al. 2016). This means that the alleles expressed at these loci are correlated with each other. Studies have shown that these SNPs are associated with CACNA1C expression. The risk allele (A) for rs1006737 is associated with increased mRNA expression of CACNA1C in the dorsolateral prefrontal cortex of post-mortem brains and induced human neurons (Bigos et al. 2010; Yoshimizu et al. 2015; Eckart et al. 2016). However, this is not consistent across all brain regions. The risk allele for rs1006737 is also associated with decreased expression of CACNA1C transcripts in the superior temporal gyrus and cerebellum but no changes were found in the parietal cortex (Gershon et al. 2014; Eckart et al. 2016). CACNA1C undergoes extensive splicing and has over 50 potential coding transcripts that are differentially expressed across the brain (Clark et al. 2020). These SNPs may alter the expression of specific transcripts, thus explaining the differences seen between brain regions.

Most of the SNPs associated with psychiatric disease occur within a 68kb region in intron 3 that has been shown to interact with the CACNA1C promoter (Roussos et al. 2014; Eckart et al. 2016). Luciferase reporter assays have shown that the risk variants for rs4765905 and rs2159100 are associated with reduced transcriptional activity (Roussos et al. 2014; Eckart et al. 2016). Therefore, they may be responsible for the correlation of CACNA1C expression with SNPs, including rs1006737, in the 68kb region within intron 3. One of the main regulators of gene expression is DNA methylation. It has been shown five CpG sites in intron 3 of CACNA1C are hypermethylated in BPD patients (Starnawska et al. 2016). Multiple SNPs (rs2239030, rs2238056, rs10848634, rs1006737) were methylation quantitative trait loci (mQTL) for these CpG sites. All the associated SNPs were located in the risk locus in intron 3. The most significant mQTL was rs2238056, however all these SNPs are in high linkage disequilibrium.

In addition to SNPs in non-coding regions of the genome, exome sequencing has identified *de novo* mutations within the coding region of CACNA1C in patients with schizophrenia. The study found that patients with schizophrenia had an increased number of disruptive mutations compared to controls (Purcell et al. 2014). Voltage-calcium channel genes were particularly enriched, including two in CACNA1C. One of the mutations occurred at a splice donor site in exon 21. Exon 21 is mutually exclusive with exon 22 and is the dominant exon expressed in the brain (Andrade et al. 2019). This mutation is likely to alter splicing of these exons and therefore the ratio of exon 21:22 containing transcripts in the brain. The second mutation found in CACNA1C is a missense mutation and introduces a premature stop codon in exon 29 of CACNA1C causing a truncated protein (Purcell et al. 2014).

Mutations in calcium channels have also been found in exome sequencing studies of patients with ASD, including CACNA2D3, CACNA1D and CACNAB2 (Breitenkamp et al. 2014; De Rubeis et al. 2014). One of these mutations was G407R in exon 8a of CACNA1D. This is in a very similar position as the mutation in CACNA1C that causes Timothy Syndrome. Both of these mutations cause impaired voltage-dependent inactivation of the channel (Pinggera et al. 2015). This suggests that prolonged calcium influx may be an important mechanism that contributes to ASD. *De novo* mutations in CACNA1C have been associated with developmental disorders (Kaplanis et al. 2020). A rare missense mutation in CACNA1C has also identified in a patient with autism spectrum disorder (Jiang et al. 2013). However, the mutation was also present in unaffected family members, therefore it is unclear if the mutation was causative.

1.1.6 Timothy Syndrome

Timothy Syndrome (TS) is a rare autosomal dominant disorder characterised by syndactyly, congenital heart disease and long QT syndrome (LQTS), however many patients show severe developmental delay, ASD and seizures (Splawski et al. 2004). It is a multi-system disorder, which often leads to death by 2.5 years (Splawski et al. 2005). The genetic cause was first discovered in 2004, when a mutation (G1216A) in

exon 8a of CACNA1C was discovered after analysis of the DNA samples of 13 individuals with TS. This mutation caused a substitution of glycine to arginine (G406R) at the C-terminal end of the sixth transmembrane segment of domain I (Splawski et al. 2004).

Shortly after, two new mutations in the alternatively spliced exon 8 were found in individuals with severe forms of TS (Splawski et al. 2005). One of the mutations (G406R) is analogous to the mutation in classic Timothy Syndrome (TS1), the other is a substitution of glycine to serine at position 402 (G402S). Patients with mutations in exon 8 tend to have more severe phenotypes but do not have syndactyly and were classified as having type 2 Timothy Syndrome (TS2). Since then, the spectrum of TS-causing mutations has expanded and the G402S mutation has been reclassified as atypical TS (Bauer et al. 2021). One patient that was diagnosed with TS2 (G406R) survived into adulthood and developed bipolar disorder (Gershon et al. 2014). The mutations in CACNA1C that lead to TS1 and TS2 cause impaired voltage-dependent channel inactivation of Cav1.2 channels, which produces maintained inward calcium currents and prolonged action potentials (Splawski et al. 2004; Splawski et al. 2005). Cav1.2 is widely expressed in tissues such as the heart, brain, smooth muscle and immune system, explaining its severe, multi-system phenotype. Exons 8 and 8a are mutually exclusive and it has been shown that around 80% of Cav1.2 mRNA in the heart and brain contain exon 8, with the remaining expressing exon 8a (Splawski et al. 2005). This expression pattern explains why TS2 patients often have more severe symptoms.

In addition to the mutations found in Exon 8 and 8a, more mutations have been discovered in CACNA1C that lead to TS-like disorders and are classified as atypical Timothy Syndrome. These patients have a range of symptoms, which are summarised in Table 1.2**Error! Reference source not found.**. One of these patients carries a mutation in exon 9 (E407A), directly adjacent to the mutation found in TS1 and TS2 patients (Figure 1.2) (Colson et al. 2019). Therefore, it may have a similar effect on channel function as G406R mutations. However, studies have not been carried out to confirm this. Studies that have investigated the effect of atypical TS point

mutations on Cav1.2 channel function have demonstrated alterations to current density, activation, ion selectivity and voltage dependent inactivation. The point mutations at exon 14 (S6435) and exon 28 (I1166T) both cause impaired voltage dependent inactivation as seen for G406R and G402S mutations (Boczek et al. 2015; Wemhöner et al. 2015; Ozawa et al. 2018). However, these mutations also altered Cav1.2 current density and I1166T caused a gain of function shift in activation of the channel. These mutations in general cause a gain-of function phenotype leading to prolongation of action potentials and calcium influx. However the point mutation E115K in exon 27 causes a loss of ion selectivity, leading to reduced inward calcium current and allows flux of potassium and sodium ions through the channel (Ye et al. 2019). This specific mutation was also identified in a patient with Brugada syndrome, which is characterised by cardiac arrythmia and a high risk of ventricular fibrillation, however it is unclear if this patient had any additional extra-cardiac symptoms (Burashnikov et al. 2010).

Recently, a paper was published describing 25 individuals containing novel heterozygous mutations in CACNA1C (Rodan et al. 2021). Fourteen of these individuals had missense mutations and have been summarised in Table 1.2. The other 11 contained truncating mutations that are likely to lead to nonsense-mediated decay, for clarity these have not been included in the table. The individuals carrying missense mutations displayed a range of phenotypes, but all of them showed developmental delay or intellectual disability. Although only one individual was diagnosed with autism, many of the other patients also displayed symptoms of ASD such as stereotypies and abnormal socialisation. Most of the patients also had a history of seizures. Interestingly, of the 11 individuals that had had an electrocardiogram (ECG), 9 of them were normal, one had LQTS and the other had ventricular conduction delay. This suggests these mutations had less cardiac effects and a greater effect on brain development and function. As all the missense mutations were *de novo,* they may not be present in cardiac cells, explaining the lack of LQTS phenotype in these patients. Of these mutations, 4 were assessed using patch clamp analysis; measuring the effect of the mutations on current density and voltage-dependent activation (Table 1.2; L614R, L614P, L657F, L1408V). The

mutations generally led to a gain-of-function effect, except L1408V which caused a reduction in current density. The truncating mutations described in this paper are also likely to lead to loss of function of Cav1.2. Individuals with these mutations had more normal motor development than patients carrying missense mutations. However, five of eleven had been diagnosed with ASD, suggesting a common phenotype between gain- and loss-of-function of Cav1.2. Only one had a history of seizures, suggesting this symptom is more specific to gain-of function. Of the 5 individuals that had ECGs, all were normal. Overall, this paper highlights that both loss and gain-of-function mutations in Cav1.2 can lead to a complex multi-system disorder, and neurological abnormalities are a common phenotype in these patients.

Mutation	Location	Symptoms	Effect on Cav1.2 function	References
F166L	Exon 4	Motor delay, hypotonia, ASD symptoms, intellectual disability, seizures, facial dysmorphism		(Rodan et al. 2021)
K177R	Exon 4	Motor delay, speech delay, learning disability, seizures, hip dysplasia		(Rodan et al. 2021)
R324W	Exon 7	Motor delay, hypotonia, anxiety, learning disability, dyslexia, seizures		(Rodan et al. 2021)
G402S	Exon 8	LQTS, developmental delay, facial dysmorphism, syndactyly	Impaired VDI	(Splawski et al. 2005; Dufendach et al. 2018)
V403M	Exon 8/8a	Motor delay, hypotonia, language delay, ASD symptoms, developmental delay		(Rodan et al. 2021)
S405R	Exon 8/8a	Syndactyly, developmental delay		(Dufendach et al. 2018)
G406R	Exon 8a	LQTS, congenital heart defects, cardiac arrhythmia, syndactyly, developmental delay, ASD, facial dysmorphism	Impaired VDI, reduced CDI	(Splawski et al. 2004; Splawski et al. 2005; Walsh et al. 2018)
G406R	Exon 8	LQTS, congenital heart defects, cardiac arrhythmia, developmental delay, ASD, facial dysmorphism, muscoskeletal problems	Impaired VDI, reduced CDI	(Splawski et al. 2005; Walsh et al. 2018)
E407G	Exon 9	LQTS, syndactyly, ASD, facial dysmorphism, seizures, dyspraxia		(Po' et al. 2019)
E407A	Exon 9	LQTS, ventricular tachycardia, syndactyly, learning difficulties, seizures		(Colson et al. 2019)
G419R	Exon 9	LQTS, syndactyly, mild neurodevelopmental delay, left ventricular noncompaction cardiomyopathy	decreased $V_{1/2}$ of activation, increased window current	(Bisabu et al. 2020)
L601R	Exon 13	Motor delay, hypotonia, language delay, ASD symptoms, intellectual disability, facial dysmorphism		(Rodan et al. 2021)
M611T	Exon 13	Motor delay, hypotonia, tremor, ASD symptoms, developmental delay, seizures		(Rodan et al. 2021)
L614R	Exon 13	Motor delay, hypotonia, language delay, ASD symptoms, developmental delay, seizures, clubfoot	Non-significant increased current	(Rodan et al. 2021)
L614P	Exon 13	Motor delay, hypotonia, language delay, ASD, intellectual disability, seizures, facial dysmorphism	Increased current, decreased $V_{1/2}$ of activation	(Rodan et al. 2021)

S643F	Exon 14	LQTS, ASD, intellectual disability	Increased late Cav1.2 currents, reduced peak current, decreased $V_{1/2}$ of activation, impaired VDI	(Ozawa et al. 2018)
L657F	Exon 14	Motor delay, language delay, ASD symptoms, intellectual disability, seizures, facial dysmorphism	Increased current, decreased $V_{1/2}$ of activation, increased expression	(Rodan et al. 2021)
I743del	Exon 16	Motor delay, hypotonia, language delay, ASD symptoms, sleep difficulties, developmental delay, clubfoot, facial dysmorphism		(Rodan et al. 2021)
C1021R	Exon 19	LQTS, syndactyly, developmental delay, facial dysmorphism, congenital heart defects, hypoglycaemia, seizures, segmental intestinal dilatation		(Dufendach et al. 2018; Nugud et al. 2021)
R1024G	Exon 24	Syndactyly, joint contractures, developmental delay, pulmonary hypertension		(Kosaki et al. 2018)
E1115K	Exon 27	LQTS, bradycardia, ASD, hyperglycaemia	Loss of selectivity filter; no inward calcium current, outward potassium and inward sodium currents	(Ye et al. 2019)
I1166T	Exon 28	LQTS, seizures, cerebral & cerebellar atrophy, facial deformities, respiratory failure	Altered current density*, decreased $V_{1/2}$ of activation, decreased SSI	(Boczek et al. 2015; Wemhöner et al. 2015)
V1187A	Exon 28	Motor delay, hypotonia, language delay, sensitivity to sensory stimuli, seizures, syndactyly		(Rodan et al. 2021)
L1408V	exon 35	Motor delay, hypotonia, laguage delay, intellectual disability, seizures, ventricular delay, hearing loss	reduced current density	(Rodan et al. 2021)
V1411L	exon 35	LQTD, motor delay, hypotonia, language delay, abnormal social development, intellectual disability, developmental delay, seizures, facial dysmorphism		(Rodan et al. 2021)
A1473G	Exon 38	LQTS, syndactyly, developmental delay, cortical blindness, seizures, joint contractures, limited movement		(Gillis et al. 2012)
G1911R	Exon 47	LQTS, syndactyly, developmental delay, facial dysmorphism, hypoglycaemia, seizures	Impaired VDI, increased window current, decreased $V_{1/2}$ of activation	(Hennessey et al. 2014)

*Table 1.2 Summary of published Timothy Syndrome mutations, symptoms, and effect on channel function. (LQTS = Long QT Syndrome, ASD = Autism Spectrum Disorder, VDI = Voltage dependent inactivation, CDI = Calcium dependent inactivation). *Alteration in current density differs between studies.*

Many other mutations in CACNA1C have been found that cause long QT syndrome in patients, specifically long QT syndrome 8 (LQTS8). However, these mutations do not cause any extra-cardiac phenotypes (Antzelevitch et al. 2007; Boczek et al. 2013; Fukuyama et al. 2014; Wemhöner et al. 2015; Landstrom et al. 2016; Gardner et al. 2019). It was initially hypothesised that mutations at the end of one of the 6th transmembrane segments is what led to extra-cardiac phenotypes via alterations in downstream signalling (Boczek et al. 2015). However, some of the mutations that cause LQTS8 are also present in these locations and mutations have been discovered that cause atypical TS that are not at the end of a 6th transmembrane segment (Figure 1.2). For example, two point mutations have been discovered at amino acid position 1166 in exon 28; one causes a TS-like phenotype and the other a LQTS only phenotype (Wemhöner et al. 2015). The only difference between these mutations is the isoleucine at this position became either a threonine or valine, respectively. It is likely that the specific amino acids differently alter channel function. Both Isoleucine and valine have non-polar side chains, whereas threonine has a polar side chain. Therefore, a mutation to threonine is more likely to have a larger effect on Cav1.2 structure and function than a valine mutation. This explains the more severe TS-like phenotype found in both patients with the I1166T mutation, but this hypothesis does not fit for all the mutations found in CACNA1C. An additional explanation is that as these mutations are often de novo, they may not occur in all tissues thus leading to a range of phenotypes. This genetic mosaicism has been shown to occur in both TS patients and parents of children with TS (Dufendach et al. 2013; Baurand et al. 2017; Walsh et al. 2018). Additionally, CACNA1C is a complicated gene with over 50 potentially functional splice variants that may differ between tissues, if the mutation is not present in all splice variants it may not affect all tissues (Clark et al. 2018).

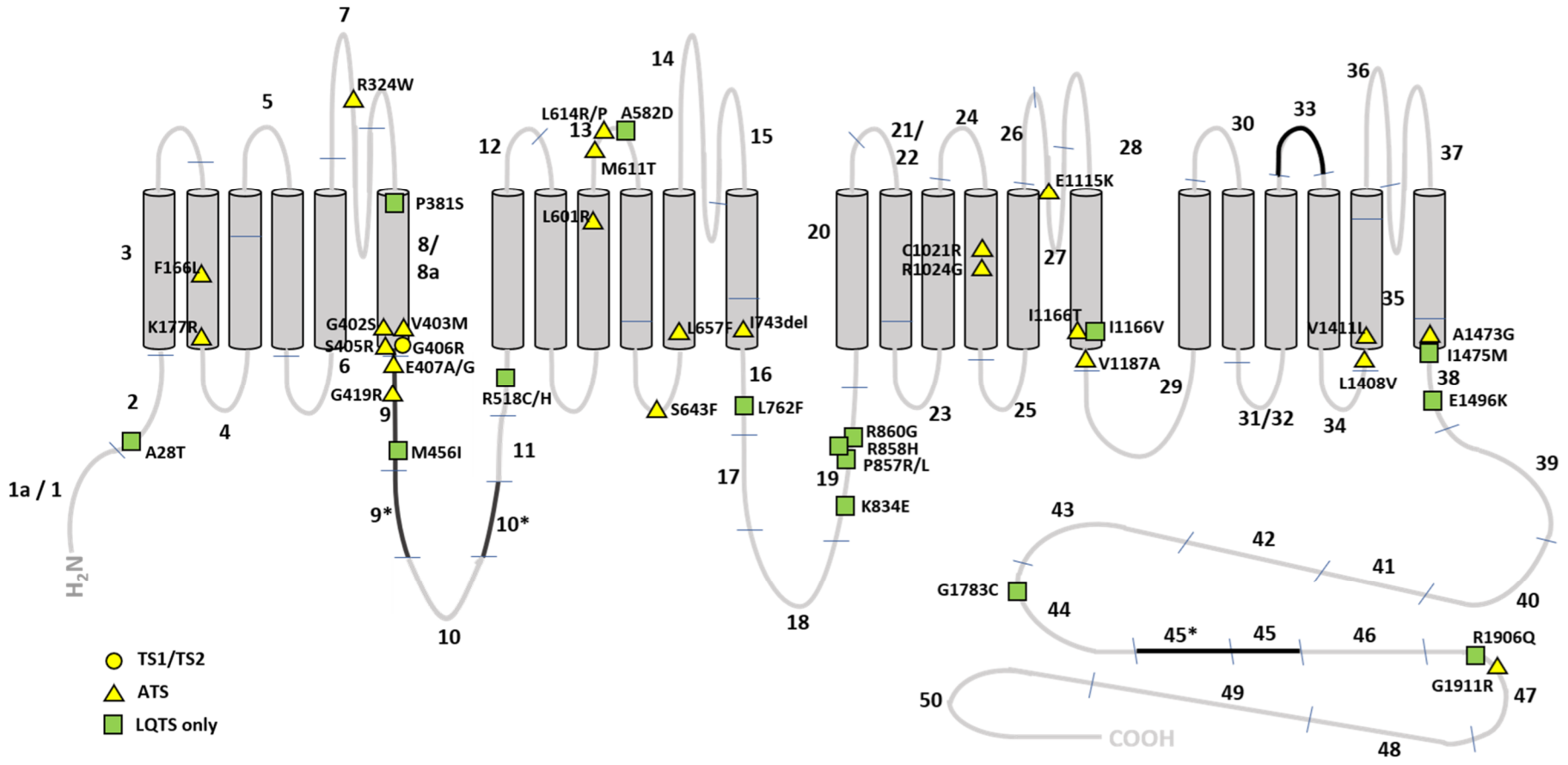

Figure 1.2 Location of point mutations discovered in CACNA1C. Black exons denote alternate exons. Yellow symbols show mutations that cause extra-cardiac phenotypes, including Timothy Syndrome (TS, yellow circles) and TS-like diseases (yellow triangles). Green squares show mutations that cause long QT syndrome only and do not have an extra-cardiac phenotype. Position of mutation is based on previously published diagrams and UniProt database and therefore are not necessarily aligned to the same reference transcript

1.2 Cav1.2 calcium channel biology

1.2.1 Voltage-gated calcium channels

There are two major types of voltage-gated calcium channels (VGCCs); high voltage-activated (HVA) and low voltage-activated (LVA) channels. HVA channels are hetero-multimeric proteins containing a pore-forming Cavα1 subunit and ancillary subunits, Cavβ, Cavα2δ and Cavγ, whereas LVA channels lack these ancillary subunits (Figure 1.3) (Simms and Zamponi 2014). VGCCs are further categorised by the Cavα1 subunit and form three major families, summarised in Table 1.3**Error! Reference source not found.**. Cav1 encodes L-type calcium channels (LTCCs), Cav2 channels are highly diverse and can form P/Q-, N- or R-type calcium channels, Cav3 channels all form T-type calcium channels (Catterall et al. 2005).

All Cavα1 subunits have a similar structure, they contain four transmembrane domains that each have six transmembrane segments (Figure 1.2). Segment 4 is positively charged and important for controlling voltage dependent activation of the channel (Catterall 2010). The re-entrant loop between segments 5 and 6 contains a highly conserved glutamic acid which form a pore highly selective for cations, such as calcium (Yang et al. 1993). The intracellular linker regions are important for interactions with downstream proteins and other 2nd messengers, therefore these regions have the most sequence variation between different Cavα1 subunits (Simms and Zamponi 2014).

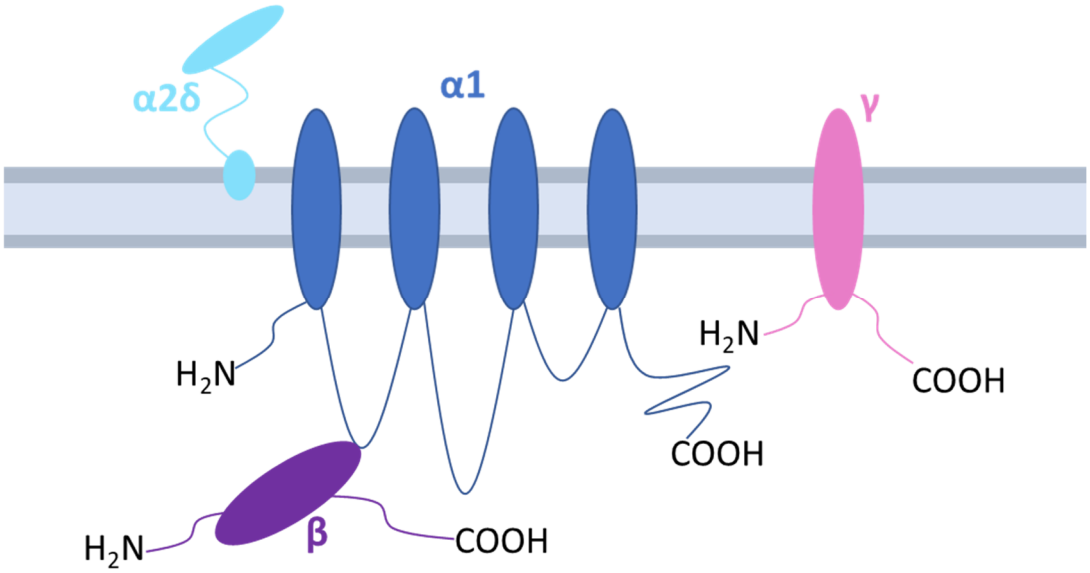

Figure 1.3 Subunit structure of high voltage-activated calcium channels. The α1 subunit (dark blue) is the pore-forming subunit made up of 4 membrane-spanning domains. The auxiliary subunits; α2δ (light blue), β (purple) and γ (pink) are important for expression, trafficking and gating properties of the channel.

Class	Family	Channel	Cavα1 Subunit	Ancillary Subunits	Channel Type
HVA	Cav1	Cav1.1	CACNA1S	Cavβ, Cavα2δ, Cavγ	L-type
		Cav1.2	CACNA1C		
		Cav1.3	CACNA1D		
		Cav1.4	CACNA1F		
	Cav2	Cav2.1	CACNA1A	Cavβ, Cavα2δ, Cavγ	P/Q-type
		Cav2.2	CACNA1B		N-type
		Cav2.3	CACNA1E		R-type
LVA	Cav3	Cav3.1	CACNA1G	None	T-type
		Cav3.2	CACNA1H		
		Cav3.3	CACNA1I		

Table 1.3 Summary of the different classes of voltage gated calcium channels. (HVA = high voltage activated, LVA = low voltage activated)

Cavβ subunits are intracellular and associate with Cavα1 subunits at the linker between domain 1 and 2. There are 4 different Cavβ subunits and they are important for determining the gating properties of the channel and trafficking to the cell surface (Opatowsky et al. 2004). Association of this subunit inhibits ubiquitination and degradation of the channel (Altier et al. 2011). There are also 4 types of Cavα2δ subunits, which are attached extracellularly to the plasma membrane via a

glycophosphatidylinositol anchor. They have a small effect on channel function and have been shown to be important in the membrane expression level and location of VGCCs (Hoppa et al. 2012). LTCCs also have a Cavγ subunit and eight different isoforms have been identified so far. These subunits have not been well studied, but some types have been shown to affect calcium current density and they also interact with other proteins such as AMPA receptors (Chen et al. 2007).

1.2.2 L-type calcium channels

LTCCs are widely expressed throughout the body and have diverse functions. They are differentiated from other VGCCs due to their slow voltage-dependent activation and sensitivity to dihydropyridines (DHPs) (Randall and Tsien 1995). Under normal resting condition the intracellular concentration of calcium is in the 100nM range. When LTCCs are activated, allowing calcium influx, levels rise to a high micromolar range (Wadel et al. 2007). In neurons, influx of calcium is important for a range of processes including gene transcription, neurotransmitter release and action potential firing (Simms and Zamponi 2014). However prolonged elevation of calcium is toxic to cells, therefore LTCCs are tightly regulated (Stanika et al. 2012).

LTCCs can be inactivated by two different mechanisms. Voltage dependent inactivation (VDI) occurs when prolonged membrane depolarisation causes a conformational change so that the linker between domains 1 and 2 block the pore (Stotz et al. 2004). The other mechanism is calcium dependent inactivation (CDI) where calcium binds to calmodulin (CaM), a calcium sensor that is associated with the C-terminus of Cav1 subunits. The binding of calcium to CaM allows additional interactions with the N-terminus of Cav1, thus causing a conformational change and inactivation of the channel (Peterson et al. 2000; Johny et al. 2013).

The expression pattern of LTCCs varies between different channels. Cav1.1 is mostly expressed in skeletal muscle and Cav1.4 is mainly restricted to the retina and immune cells (Tanabe et al. 1988; McRory et al. 2004). Cav1.2 and Cav1.3 are more widely expressed in tissues including the heart, pancreas and brain. These two channels are

often co-expressed in the brain, however Cav1.2 accounts for roughly 90% of LTCCs in the brain and Cav1.3 the remaining 10% (Sinnegger-Brauns et al. 2009). Both channels are expressed postsynaptically on the soma and in the spines and shafts of dendrites (Obermair et al. 2004; Di Biase et al. 2008). They have different channel properties and downstream effects. Cav1.3 has faster activation kinetics than Cav1.2 and activates at more negative voltages, around -55mV versus -30mV for Cav1.2. Cav1.3 channels also display slower and less complete VDI than Cav1.2 channels and are less sensitive to DHPs (Koschak et al. 2001; Xu and Lipscombe 2001).

1.2.3 Cav1.2 calcium channel (CACNA1C)

The pore-forming alpha 1c subunit of Cav1.2 is encoded by the gene CACNA1C, which is located on chromosome 12 in humans. CACNA1C is a complex gene with over 50 exons that can be spliced to form at least 90 different transcripts in the human brain. These splice variants have significantly different channel properties, and their expression varies across both brain regions and development (Tang et al. 2004; Bartels et al. 2018; Clark et al. 2020). Mutually exclusive exons 8 and 8a, which is where mutations for TS1 and TS2 occur, show a switch in abundance during corticogenesis in mice and also during the differentiation of human induced pluripotent stem cells (iPSCs) from neural progenitor cells (NPCs) to neurons (Panagiotakos et al. 2019). The Cav1.2 gene also encodes calcium channel associated transcriptional regulator (CCAT), which is transcribed by activation of a promoter in exon 46 of CACNA1C (Gomez-Ospina et al. 2013). The expression of CCAT is developmentally regulated, independent of Cav1.2 expression. However, it has been shown that it can repress transcription of Cav1.2, in addition to regulating the expression of other genes, such as connexin 31.1 and NR3 (Gomez-Ospina et al. 2006; Schroder et al. 2009)

Cav1.2 is an important mediator of excitation-transcription coupling that leads to transcription of genes involved in synaptic plasticity, neurodevelopment and adult neurogenesis (Murphy et al. 1991; Thompson et al. 1995; Dolmetsch et al. 2001; Li et al. 2016). Activation of Cav1.2 channels by membrane depolarisation triggers

intracellular signalling pathways that cause phosphorylation of cAMP response element binding protein (CREB). It has been shown that there are two main pathways that cause Cav1.2 dependent CREB phosphorylation (Figure 1.4). When Cav1.2 channels are activated they open to allow Ca influx and undergo a voltage dependent conformational change, both of which are required for phosphorylation of CREB (Li et al. 2016). Calcium binds and activates the Cav1.2-associated protein calmodulin (CaM), which is then able to interact with various kinases (Deisseroth et al. 1998; Dolmetsch et al. 2001). Rapid phosphorylation of CREB occurs via CaM kinases (CaMK) (Wu et al. 2001). Upon depolarisation, the association of α-CaMKII with Cav1.2 increases, α/β-CaMKII are required for phosphorylation of γ-CaMKII, which then shuttles calcium-bound CaM (Ca-CaM) to the nucleus (Deisseroth et al. 1998; Ma et al. 2014; Li et al. 2016; Cohen et al. 2018). Ca-CaM activates CaMK kinase (CaMKK), which phosphorylates and activates CaMKIV, thus leading to phosphorylation of CREB (Tokumitsu and Soderling 1996; Ma et al. 2014).

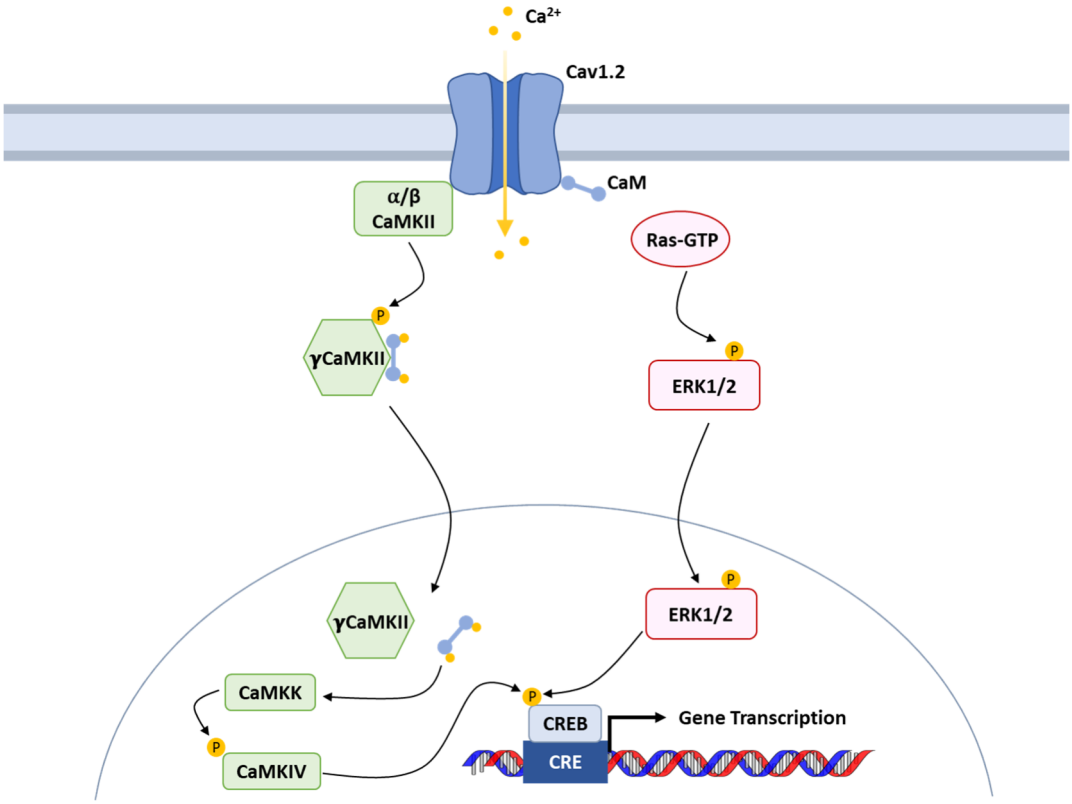

Figure 1.4 Cav1.2 channels contribute to the regulation of gene expression via CREB. When Cav1.2 opens following membrane depolarisation an influx of calcium occurs. Calcium then binds to and activates calmodulin (CaM). Phosphorylation of γ-Ca2+/calmodulin- dependent protein kinase II (γ-CaMKII) by α/β-CaMKII allows Ca-CaM to bind. This complex is then shuttled to the nucleus where Ca-CaM activates CaMK kinase (CaMKK). CaMKK phosphorylates CaMKIV, which then phosphorylates CREB, leading to CREB-dependent gene transcription. CREB can also be phosphorylated by the Ras-ERK pathway. Conformational change of Cav1.2 following depolarisation leads to activation of Ras and thus phosphorylation of extracellular signal-regulated kinases 1/2 (ERK1/2). ERK1/2 is translocated to the nucleus where it phosphorylates CREB. Phosphorylated CREB binds to the cAMP response element (CRE) to promote the expression of immediate early genes such as c-fos.

Slow, late-phase phosphorylation of CREB occurs via mitogen-activated protein kinases (MAPKs) (Wu et al. 2001). Following depolarisation extracellular signal-regulated kinases 1/2 (ERK1/2) are phosphorylated via activated Ras-GTP and pERK1/2 is translocated to the nucleus where it mediates CREB phosphorylation (Figure 1.4). In a Cav1.2 knockout mouse model expression of pERK1/2 was reduced in both the dendrites and nucleus of cortical neurons following depolarisation and also showed a reduction in sustained phosphorylation of CREB (Moosmang et al. 2005). This finding of reduced pERK1/2 and pCREB has also been shown to occur in a Cav1.2 heterozygous rat model (Tigaret et al. 2021). The pathway for Cav1.2-dependent phosphorylation of CREB via ERK1/2 is not as well studied as the CaMK pathway, however it has been shown to be independent of calcium influx and subsequent activation of CaM (de Hoog et al. 2000; Servili et al. 2019). Therefore, it is likely that activation of the Ras-MAPK pathway is dependent on a voltage dependent conformational change of the Cav1.2 channel.

Following phosphorylation CREB binds to cAMP response element (CRE) to promote gene expression. Blockade of either the CaMK or MAPK pathway has been shown to inhibit CRE-dependent gene expression, suggesting both pathways are important for coupling Cav1.2 to gene transcription (Bading et al. 1993; Moosmang et al. 2005). CREB leads to the transcription of immediate early genes, which encode transcription factors such as c-fos, jun-B, fos-B, zif268. These transcription factors activate late response genes that encode proteins involved in neuronal plasticity and development (Murphy et al. 1991; Thompson et al. 1995). Blockade of LTCCs during differentiation of rat neural stem cells inhibited CREB phosphorylation and led to reduced neuronal differentiation and synapse formation, highlighting the importance of LTCC-dependent gene transcription in the brain (Lepski et al. 2013).

In addition to CREB, LTCCs have also been shown to activate the transcription factor nuclear factor of activated T-cells (NFAT) in hippocampal neurons. Following activation of Cav1.2 channels, the calcium-dependent phosphatase calcineurin is recruited to the C-terminus of Cav1.2 by AKAP79/150 (Oliveria et al. 2007; Li et al. 2012). Calcineurin is then able to dephosphorylate NFAT, allowing it to translocate

to the nucleus to regulate gene expression (Graef et al. 1999). Like CREB, NFAT signalling has been shown to play a role in neuronal development and synaptic plasticity (Kipanyula et al. 2016).

1.2.4 Role of Cav1.2 in neurodevelopment

Calcium signalling has been shown to play an important role in neuronal development. It is involved in the specification of neurotransmitter specification, axonal pathfinding, dendritic growth, differentiation into different neuronal subtypes and radial migration (reviewed in Rosenberg and Spitzer, 2011). Radial glial cells in the ventricular zone (VZ) of the developing cortex show spontaneous calcium waves, which increase during corticogenesis and are generated due to the activation of VGCCs (Weissman et al. 2004; D'Ascenzo et al. 2006). In primary culture, when mouse NPCs are differentiated in the presence of the LTCC antagonist nifedipine, they form less β-III-tubulin and MAP2 positive neurons. However in the presence of the LTCC activator Bay K 8644, they generate more β-III-tubulin and MAP2 positive neurons (D'Ascenzo et al. 2006). NPCs differentiated in the presence of nifedipine also formed neurons that were more poorly differentiated with reduced synapse formation (Lepski et al. 2013).

It is possible that LTCCs influence the number of neurons by modulating neuronal survival. NeuroD is a marker of neuronal differentiation and is essential for neuronal survival. It has been shown in adult hippocampal NPCs that nifedipine decreases NeuroD expression but increases the expression of glial fate genes Hes1 and Id2, whereas Bay K 8644 and the LTCC agonist FPL64176 have the opposite effect (Deisseroth et al. 2004; Teh et al. 2014). Additionally, the fraction of apoptotic neurons was increased by nimodipine and decreased by Bay K 8644. It is likely that this mechanism in adult NPCs would be similar during corticogenesis, suggesting that LTCC activity may be important for the survival of new-born neurons. Modulation of NeuroD expression may occur via type 2 ryanodine receptors (RyR2). When RyR2 knockout embryonic stem cells (ESCs) are differentiated into neurons they show a reduction in the percentage of β-III-tubulin -positive neurons and reduced levels of

NeuroD. When wild-type ESCs were differentiated in the presence of Bay K 8644 it promoted neuronal differentiation, however Bay K 8644 had no effect on RyR2 knockout cells or in the presence of RyR inhibitors (Yu et al. 2008). This suggests that the co-operation of LTCCs and RyR2 is required for neurogenesis.

These studies show that LTCCs are a key component of neuronal development. However, the compounds they use are not specific to Cav1.2 or Cav1.3 so it is hard to determine the contribution of each channel. To do this, genetic approaches are required. The majority of these studies have looked at the effects of CACNA1C deletion in adult neurogenesis, where it is possible the role of Cav1.2 may differ from neuronal development. Multiple studies have shown that deletion of Cav1.2 leads to a decrease in the number of immature neurons and was also associated with a decrease in cell proliferation (Lee et al. 2016; Temme et al. 2016). In a forebrain-knockout mouse model they found that there was no difference in BrdU, which marks dividing cells, an hour after injection but there was a decrease after 30 days. These mice also showed a decrease in the protein expression of brain-derived neurotrophic factor (BDNF) and they hypothesised that these differences were due to a decrease in the survival of new-born neurons (Lee et al. 2016). Deletion of CACNA1C in rat NPCs also showed a decrease in proliferation and neuron production. However, they suggested that Cav1.2 has a role in neuronal fate choice as CACNA1C deficient NPCs gave rise to fewer neurons, but more astroglia (Völkening et al. 2017). A heterozygous rat model of CACNA1C also showed a decrease in proliferation in the adult hippocampus but did not find any changes to the number of immature neurons (Moon et al. 2018). This may be due to a gene dosage effect, as all the other models were conditional homozygous knockouts of CACNA1C.

TS models are another way to elucidate the contribution of Cav1.2 toward neurodevelopment. These models have shown alterations in the expression of markers for different cortical layers. Patient iPSC-derived neurons show a decrease in the number of lower-layer neurons expressing SATB2 and increased CTIP2 expression. The decreased expression of SATB2 was replicated in a mouse model, however there was no change in CTIP2 (Paşca et al. 2011). Although SATB2 is mainly

expressed in layers II-IV of the cortex it is also expressed in layer V cells that project through the corpus callosum to the contralateral hemisphere. Whereas CTIP2 is expressed in layer V neurons that project to subcortical structures and the spinal cord (Chen et al. 2005; Alcamo et al. 2008; Chen et al. 2008). When Cav1.2 channels containing the G406R mutation found in TS (Cav1.2-TS) were electroporated into mice at E13.5, when layer V is formed, they also caused a decrease in SATB2 and increase in CTIP2 expressing cells by E17.5, when the majority of layer V has formed (Panagiotakos et al. 2019). They also investigated the effect of CACNA1C knockout and found it had the opposite effect. Loss of one copy of CACNA1C led to a reduction in CTIP2 positive cells but an increase in SATB2 cells. There was also a reduction in the transcription factor TBR1, which is required for the formation of layer VI cortico-thalamic projection neurons (Hevner et al. 2001). This suggests that Cav1.2 plays an important role in the generation of different cortical neuron subtypes during neuronal development.

1.2.5 Role of Cav1.2 in neuronal activity

The electrical coupling of neurons is important in memory and learning processes. When one neuron repeatedly activates another the synaptic connection between the neurons is strengthened, causing long term potentiation(LTP), an important process for memory storage (Sweatt 2010). There are two forms of LTP, NMDA-dependent and NMDA-independent LTP. Blockade of LTCCs both *in vitro* and *in vivo* has been shown to reduce formation of NMDA-independent LTP (Morgan and Teyler 1999; Weisskopf et al. 1999; Bauer et al. 2002; Freir and Herron 2003). Various knockout models of Cav1.2 have shown that this channel reduces LTP in the amygdala and hippocampus (Moosmang et al. 2005; Langwieser et al. 2010; Tigaret et al. 2021). However knockout of Cav1.3 had no effect on NMDA-independent LTP in the hippocampus, which suggests Cav1.2 alone is required for NMDA-independent LTP (Clark et al. 2003).

These synaptic connections allow neurons to form patterns of synchronous activity in the brain but patients with psychiatric disorders have deficits in neuronal

connectivity (Herbert et al. 2004; Just et al. 2007; Williams and Boksa 2010; Kato 2019). It has been demonstrated that LTCCs have a role in oscillatory activity. Both neuronal oscillations and synchronous calcium transients, which result from synchronised bursting of neurons, have been shown to be dependent on LTCCs in rodent neurons (Przewlocki et al. 1999; Jun He et al. 2005; Bukalo et al. 2013; Hansen et al. 2014). It has also been shown in human iPSC-derived neurons that blockade of LTCCs alters the pattern of synchronised bursting activity. Blockade of LTCCs had no effect on the basal firing rate of neurons but caused an increase in the number of synchronised bursts and reduction in the interval between the bursts. Whereas, blockade of P/Q- or T-type calcium channels had no effect on neuronal activity (Plumbly et al. 2019). Functional magnetic resonance imaging (fMRI) has also shown that the risk SNP rs1006737 in CACNA1C is associated with increased connectivity in the hippocampus during working memory or emotional processing tasks in healthy humans. However these studies found conflicting results in the prefrontal cortex (Bigos et al. 2010; Paulus et al. 2014).

Models of epileptic activity have also implicated LTCCs in neuronal firing. During epileptiform activity large synchronous depolarisations of neurons occur, which are associated with an influx of calcium (Empson and Jefferys 2001). Blockade of LTCCs has been shown to both reduce and potentiate epileptiform activity. In hippocampal and neocortical slices from guinea pigs, nifedipine reduced epileptiform activity in a Mg^{2+} free model of epilepsy (Straub et al. 1999). Additionally, other LTCC blockers have been shown to have anti-epileptic effects (Bingmann and Speckmann 1989; Aicardi and Schwartzkroin 1990). However, in a model induced by GABAergic antagonism they showed that calcium influx through LTCCs was required to terminate epileptiform activity and blockade with nifedipine increased neuronal excitability (Empson and Jefferys 2001). These conflicting findings may be due to the different methods used to induce epileptic activity, but they also suggest that LTCCs play multiple roles in shaping neuronal activity.

Influx of calcium through LTCCs is associated with neuronal depolarisation and Cav1.2 plays an important role in shaping action potentials (Figure 1.5) (Bean 2007). VGCCs are activated following depolarisation and affect the width of action potentials. iPSC-derived neurons from patients with TS have wider action potentials than controls due to the prolonged opening of Cav1.2, leading to prolonged depolarisation (Paşca et al. 2011). However LTCCs, specifically Cav1.2, have also been shown to associate with calcium and voltage activated potassium (BK_{Ca}) channels (Shah and Haylett 2000; Berkefeld et al. 2006; Lima and Marrion 2007; Berkefeld and Fakler 2008). These channels are important in the afterhyperpolarisation phase (AHP) of action potentials. Empson and Jefferys (2001) showed that nifedipine reduced the amplitude of the post-burst AHP during epileptiform activity. BK_{Ca} channels have been shown to associate specifically with Cav1.2, Cav2.1 and Cav2.2 channels. This ensures robust activation of BK_{Ca} channels following depolarisation and calcium influx (Berkefeld et al. 2006).

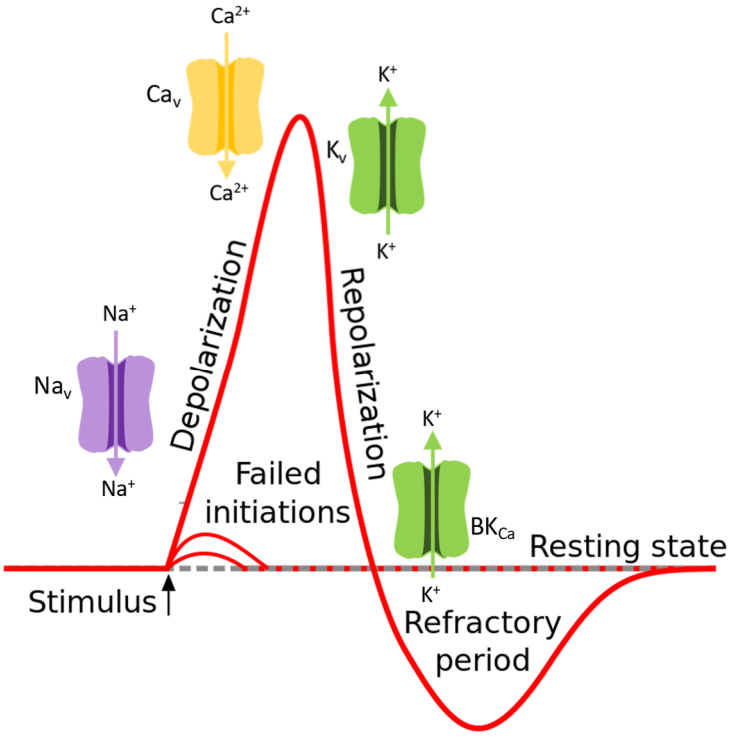

Figure 1.5 Schematic of a neuronal action potential. Following a stimulus of sufficient strength voltage gated sodium channels (Nav) are opened leading to depolarisation. Calcium channels (Cav) have slower activation kinetics and are typically activated near the peak of the action potential so do not contribute towards the rising phase. Following depolarisation potassium channels (Kv) are activated leading to a net inward current and repolarisation. Calcium channels also associate with calcium-activated potassium (BK) channels. These channels are involved in the later stages of repolarisation, specifically the afterhyperolarisation refractory period.

VGCCs have distinct expression patterns and activation properties and these channels have been shown to differentially modulate the properties of BK_{Ca} channels (Berkefeld and Fakler 2008). BK_{Ca} channels associated with Cav1.2 required longer action potentials in order to be activated and do not remain open as long as channels associated with Cav2.1. As Cav2.1 and Cav2.2 channels are expressed presynaptically, whereas Cav1.2 channels are expressed postsynaptically, it is likely that these kinetics are important for the different roles of BK_{Ca} channels within neurons, such as neurotransmitter release in presynaptic compartments (Raffaelli et al. 2004). AHPs can be split into three components. Medium and fast AHPs occur after single action potentials and are important in regulating the frequency of action potentials within a burst of firing but slow AHPs occur after trains of action potentials. BK_{Ca}-Cav1.2 complexes play a role in slow AHPs as they are partially blocked by LTCC antagonists (Shah and Haylett 2000; Lima and Marrion 2007). Slow AHPs play an important part in neuronal activity and are involved in the regulation of synaptic plasticity (Sah and Bekkers 1996; Lancaster et al. 2001).

1.3 The use of human iPSCs to model psychiatric disorders

1.3.1 Human induced pluripotent stem cells (iPSCs)

The study of psychiatric disorders in the past has mainly relied on post-mortem studies and animal models. However, these techniques come with a variety of caveats. Post-mortem studies only represent the end stage of diseases and are often confounded by variables such as preservation method, patient's drug treatment and cause of death. Additionally, functional assays cannot be carried out on post-mortem tissue. Animal models overcome these caveats but have shown poor translation into human therapies (Dragunow 2008). This is likely due to the complexity of psychiatric diseases, as CNVs and/or a large amount of common genetic variation can contribute towards these diseases (Girirajan et al. 2012; Ripke et al. 2013; Li et al. 2017; Grove et al. 2019). These genetic changes are hard to model in rodents. Additionally, humans and rodents have been shown to display differences in neuronal

development, an important factor in psychiatric disease (Molnár and Clowry 2012; Gabdoulline et al. 2015).

The discovery of how to generate human iPSCs in 2007 has provided us with a method that overcomes many of these caveats (Takahashi et al. 2007; Yu et al. 2007). iPSCs are reprogrammed from adult somatic cells, such as skin fibroblasts, keratinocytes or blood cells, by the expression of a set of pluripotency-related transcription factors; Oct3/4, Sox2, Klf4, c-Myc, Nanog and Lin28. In order to be classed as pluripotent stem cells, like embryonic stem cells (ESCs), they must be able to self-renew and differentiate into the three germ layers; mesoderm, endoderm and ectoderm (Takahashi et al. 2007). When cells are reprogrammed into iPSCs it is possible they may retain some of their epigenetic signature (Kim et al. 2011). This may be useful for the study of some diseases where the environment and epigenetic modifications contribute towards the disease. However, these epigenetic markers may also affect the differentiation potential of iPSCs and efficiency of reprogramming (Roost et al. 2017). Additionally, cells may accumulate mutations during reprogramming, which can lead to chromosomal instability and partially explain why iPSCs show more variability than ESCs, both between and within cell lines (Hu et al. 2010; Gore et al. 2011). However, iPSCs offer two distinct advantages over the use of ESCs. The first is that human ESCs need to be obtained from human embryos and therefore there is a limited supply of ESC lines due to ethical issues. The second, and more significant advantage is that iPSCs can be obtained from patients, allowing us to study complex diseases such as ASD and schizophrenia in human neurons.

1.3.2 Generation of cortical neurons from iPSCs

Although iPSCs can be used to model many different tissues, they are particularly useful in neuroscience research due to the lack of accessibility to human brain tissue. There are many different types of neurons within the brain that have been linked to psychiatric disease and various methods have been developed to generate these cells. These include cortical, GABAergic, dopaminergic, serotonergic, hippocampal, hypothalamic and medium spiny neurons (Chambers et al. 2009; Boissart et al. 2013;

Liu et al. 2013; Maroof et al. 2013; Kwon et al. 2014; Yu et al. 2014; Arber et al. 2015; Wang et al. 2015; Lu et al. 2016). The most established of these methods is for the generation of forebrain cortical neurons. These protocols generate mostly glutamatergic excitatory neurons with a forebrain identity.

There are two main methods for the generation of forebrain neurons, one based on the formation of embryoid bodies and the other using monolayer cultures. The first method involves culturing cells in suspension to form 3D aggregates that produce neurons (Muratore et al. 2014). This method produces a high yield and purity of neurons but has been mostly replaced by the simpler dual-SMAD inhibition monolayer protocol. This involves culturing iPSCs at a high density in the presence of inhibitors for bone-morphogenetic protein (BMP) and transforming growth factor beta (TGFβ) pathways, which leads to the induction of neuroepithelial cells with a forebrain identity (expression of FoxG1 and Pax6) (Chambers et al. 2009). These neural progenitor cells then generate cortical forebrain projection neurons.

Generation of forebrain cortical neurons using dual-SMAD inhibition mimics human cortical development. Neurons are produced sequentially with deep layer neurons formed first followed by upper layers (Shi et al. 2012). The gene expression profile of iPSC-derived cortical neurons has also been shown to spatially correlate with the expression profile of cortical neurons relative to the Allen Brain Atlas. However, they most closely resembled fetal neurons between the first and second trimester (Brennand et al. 2015). In addition, iPSC-derived neurons have been shown to be immature when looking at electrophysiological measures, such as resting membrane potential, ability to fire action potentials and synaptic currents (Dolmetsch and Geschwind 2011; Shi et al. 2012; Bardy et al. 2015). This has led to the development of protocols aiming to generate more physiologically mature neurons.

The use of astrocytes to promote neuronal maturation is one avenue that has been investigated. Astrocytes are important for neuronal survival and synapse formation (Pfrieger and Barres 1997; Hama et al. 2004; Ullian et al. 2004). Neurons and astrocytes can be co-cultured, either by plating iPSC-derived neurons onto primary

astrocytes or by differentiation of NPCs into both neurons and astrocytes. These studies have shown that co-culture improves dendritic complexity, ion-channel and receptor expression, resting membrane potential, and both spontaneous and induced electrical activity of neurons (Tang et al. 2013; Gunhanlar et al. 2017). However, it is difficult to control the growth of astrocytes in these cultures and prevent them from overgrowing the post-mitotic neurons. Another approach is the use of astrocyte-conditioned media, where astrocytes are cultured in neuronal media for several days before it is added to neuronal cultures, exposing them to any factors secreted by the astrocytes. Although astrocytes are unable to physically interact with neurons using this approach, it can improve the functional maturation of neurons demonstrated by their ability to generate complex and spontaneous neuronal activity (Rushton et al. 2013).

Studies have also shown that changing the components of neuronal media can promote maturation and neuronal activity. Rushton and colleagues showed that supplementing with Ca^{2+} or GABA could recapitulate the effects of astrocyte-conditioned media (Rushton et al. 2013). Telezhkin and colleagues used small-molecule inhibitors in addition to Ca^{2+} and GABA. These inhibit the notch pathway and cylcin-dependent kinase 4/6 (CDK4/6) to promote cell cycle exit and therefore differentiation. Neurons differentiated in this media had increased spontaneous and induced electrical activity and increased synaptic currents, indicating increased maturation (Telezhkin et al. 2016). The standard media used for neuronal differentiations was optimised to promote neuronal differentiation and survival. However, it causes neurons to have a consistently depolarised membrane potential, therefore silencing neuronal activity and impairing synaptic function. Bardy and colleagues developed a new media (BrainPhys) which has a concentration of ions closer to physiological levels with the exclusion of neuroactive amino acids. Neurons cultured in this media showed similar Na^{+} and K^{+} currents and Ca^{2+} activity compared to neurons cultured in artificial cerebrospinal fluid (ACSF), the standard for *ex vivo* electrophysiological recordings. Neurons were also able maintain spontaneous electrical activity for several weeks to months in this media and both expression of synaptic proteins and synaptic activity improved over time (Bardy et al. 2015).

1.3.3 iPSC-based research using patients with psychiatric disorders

Psychiatric disorders have a degree of heritability. However, as mentioned earlier, the genetic contribution towards these diseases is varied and complex and is therefore hard to model in rodents. Increasingly, patient-derived iPSCs are being used to identify common cellular mechanisms that may contribute to psychiatric disease and potential pathways that could be targeted for future treatments. The first study to use iPSC-derived neurons from patients with schizophrenia showed that these neurons displayed altered connectivity and dendritic morphology (Brennand et al. 2011). They also showed altered gene expression in WNT signalling-related genes, a pathway that is also altered in NPCs from schizophrenia patients (Topol et al. 2015). Another study differentiated cells into dopaminergic and glutamatergic neurons. They found deficits in the differentiation of both these types of neurons, but dopaminergic neurons displayed a much more severe phenotype in terms of morphology and impaired mitochondrial function (Robicsek et al. 2013).

Studies using iPSC-derived neurons from patients with idiopathic forms of ASD have found alterations in GABAergic markers, synaptic proteins and cell cycle length (Mariani et al. 2015; Liu et al. 2017; Marchetto et al. 2017). However, these changes are not consistent across studies. Mariani and colleagues differentiated patient iPSCs into telencephalic organoids and found an increase in neuron (MAP2) and synapse density. Patient organoids had an increased expression of multiple GABAergic markers, but no differences in glutamatergic markers. They also found that ASD iPSCs had a decrease in cell cycle length (Mariani et al. 2015). Marchetto and colleagues similarly found decreased cell cycle length in NPCs derived from ASD patient iPSCs. They also found an increase of GABAergic markers in NPCs alongside a decrease in glutamatergic markers, however there was a decrease in the number of GABA-positive neurons. This study also investigated the electrical activity of ASD neurons using multi-electrode arrays. They found decreased activity in ASD neurons compared to controls and a decrease in the synchronisation of neuronal bursts (Marchetto et al. 2017). Liu and colleagues also found a reduction in spontaneous

activity in ASD patient iPSC derived neurons. However they found no differences in the expression of synaptic proteins, unlike Mariani and colleagues (Liu et al. 2017). Although the results across these studies is not consistent they support the hypothesis that the excitatory/inhibitory balance is disrupted in ASD leading to altered brain connectivity (Fakhoury 2015).

In the context of BPD, alterations in mitochondrial function, expression of ion channel subunits and neuronal activity have been found in patient iPSC-derived neurons. Madison and colleagues showed decreased expression of WNT pathway related genes and differential expression of ion channels. Patient-derived NPCs showed a proliferation deficit that could be rescued by activation of the WNT pathway (Madison et al. 2015). Chen and colleagues found an increase in gene expression of ion channels and membrane bound receptors. Neurons displayed a more ventral identity compared to controls and showed increased calcium transients, both of which could be rescued by lithium treatment (Chen et al. 2014). Mertens and colleagues also showed that BPD neurons were more excitable and found an increase in mitochondrial function. However they found that the excess excitability was only rescued in lithium-responsive patient neurons and had no effect in lithium non-responsive patient neurons, which suggest iPSC-derived neurons may have good predictive validity for drug-screening in the future (Mertens et al. 2015). Kathuria and colleagues' findings conflict with these studies. They found that BPD neurons had decreased endoplasmic reticulum-mitochondrial membrane interactions, suggesting decreased mitochondrial function. They also found that BPD cerebral organoids displayed the same spontaneous activity as controls, however when they were electrically stimulated or depolarised they displayed a diminished response compared to controls (Kathuria et al. 2020).

These studies have provided insights into some of the pathways implicated in psychiatric disorders and have confirmed findings from animal and post-mortem studies, such as altered mitochondrial function in BPD (Konradi et al. 2004; Iwamoto et al. 2005; Sun et al. 2006). However, results between studies using patient iPSCs are often conflicting. This may be due to differences in methods and the types of

neurons that are generated, but it is also likely to be due to the polygenic nature of psychiatric disorders. Instead, investigation of psychiatric disorders caused by specific gene mutations or CNVs can be carried out to help reduce variability and identify mechanisms that may be hidden by the genetic heterogeneity of patients with idiopathic forms of psychiatric disorders.

Study of psychiatric conditions with a defined genetic cause has been most commonly carried out in ASD, where syndromes including Timothy, Rett, FoxG1, Angelman and Prader-Willi syndrome account for roughly 10-15% of ASD cases (Folstein and Rosen-Sheidley 2001). Studies investigating TS using iPSC-derived neurons have found upregulation of tyrosine hydroxylase expressing neurons and altered expression of different subtypes of cortical neurons (Paşca et al. 2011; Panagiotakos et al. 2019). TS neurons also show increased activity-dependent dendritic retraction and deficits in migration of interneurons (Krey et al. 2013; Birey et al. 2017). Gene expression analysis has shown that genes associated with ASD and synaptic proteins are upregulated in TS neurons (Tian et al. 2014). Studies using iPSC-derived neurons from patients with Rett and FoxG1 syndrome have both shown increased expression of GluD1, a glutamate receptor subunit that has been shown to induce the formation of GABAergic synapses (Livide et al. 2015; Patriarchi et al. 2016). FoxG1 neurons showed an increase in GABAergic markers and Rett neurons have been shown to have a decrease in excitatory synapses and spontaneous calcium transients (Marchetto et al. 2010; Patriarchi et al. 2016). This further implies that an imbalance in excitatory and inhibitory signalling may be a common feature of ASD. It is evident from these studies that the use of both idiopathic and genetically defined patient iPSCs would be advantageous for helping to further elucidate common cellular mechanisms that cause psychiatric diseases.

1.3.4 Genome editing using CRISPR-Cas9

Human iPSCs provide the opportunity to use patient-specific cells that can be differentiated into disease-relevant neuronal cell types. This is particularly useful for studying diseases where the underlying genetic contribution is unknown or variable

between patients. However, due to the variability in genetic background between patients the results from studies are often inconsistent. To overcome this, studies need to use a large number of different patient lines but reprogramming and differentiation of iPSCs is costly and time-consuming. Instead, we can study genes that have been implicated in psychiatric disorders using gene editing. Working with a genetically modified cell line and isogenic control will reduce variability and therefore the workload required to identify phenotypes.

The discovery and rapid development of clustered-regularly interspaced short palindromic repeat (CRISPR) technology in recent years has allowed a more high-throughput approach to gene editing compared to programmable nucleases such as zinc-finger nucleases and transcription activator-like effector nucleases (TALENs) (Gupta and Musunuru 2014). CRISPR-Cas9 is a part of the adaptive immune response in bacteria. They contain a CRISPR array in their genome, which is regions of repetitive DNA separated by protospacers (foreign DNA sequences). These arrays are often close to the Cas9 gene. Guide RNA (gRNA) is transcribed from these arrays, composing of two parts, the crRNA and tracrRNA (Barrangou et al. 2007). The crRNA sequence is complementary to the foreign DNA and the tracrRNA is a repetitive region of DNA which binds to the Cas9 protein. This allows the Cas9 protein to be guided to specific DNA sequences where it binds to and cuts the DNA leading to a double strand break (Figure 1.6a). This system also requires the presence of a protospacer adjacent motif (PAM) upstream of the complementary DNA sequence.

This simple system has since been utilized in mammalian cells to introduce mutations in target genes and create knockout lines. The generation of a double strand break by Cas9 induces DNA repair mechanisms in the cell; non-homologous end joining (NHEJ) and homology directed repair (HDR). NHEJ is the dominant method of DNA repair as it is faster because it does not require a template for repair. However, this means it is also more prone to errors, which can lead to INDELs at the target site (Ran et al. 2013). Delivery of Cas9 and a gRNA targeted to your gene of interest is all that is required for this system and can be done via expression vectors or ribonucleoproteins using a variety of transfection methods (Kabadi et al. 2014;

Hashimoto and Takemoto 2015; Zuris et al. 2015). Additionally stem cell lines have been generated that allow inducible expression of the Cas9 protein, so that only transfection of gRNA is required when creating a new knockout line (González et al. 2014).

CRISPR-Cas9 technology is rapidly evolving and alternative gene editing techniques using Cas9 have been generated. Specific base editing can be carried out by utilising HDR and transfection of a DNA repair template (Ran et al. 2013). This technique may be useful for generating disease-associated SNPs in isogenic lines that have been identified from GWAS or correcting genetic mutations in patient lines. Nuclease dead Cas9 (dCas9) fused to transcriptional repressors or activators can be used to modulate gene expression in a reversible way without permanent modification to the genome (Figure 1.6b) (Gilbert et al. 2014; Mandegar et al. 2016). More recently Cas13 has been discovered, which target mRNA rather than DNA to allow for reversible gene knockdown that is more specific than RNA interference (Figure 1.6c-d) (Abudayyeh et al. 2017; Cox et al. 2017; Konermann et al. 2018). This adaptability to different techniques highlights how CRISPR may be used to help elucidate the role that specific risk genes may have in disease pathology.

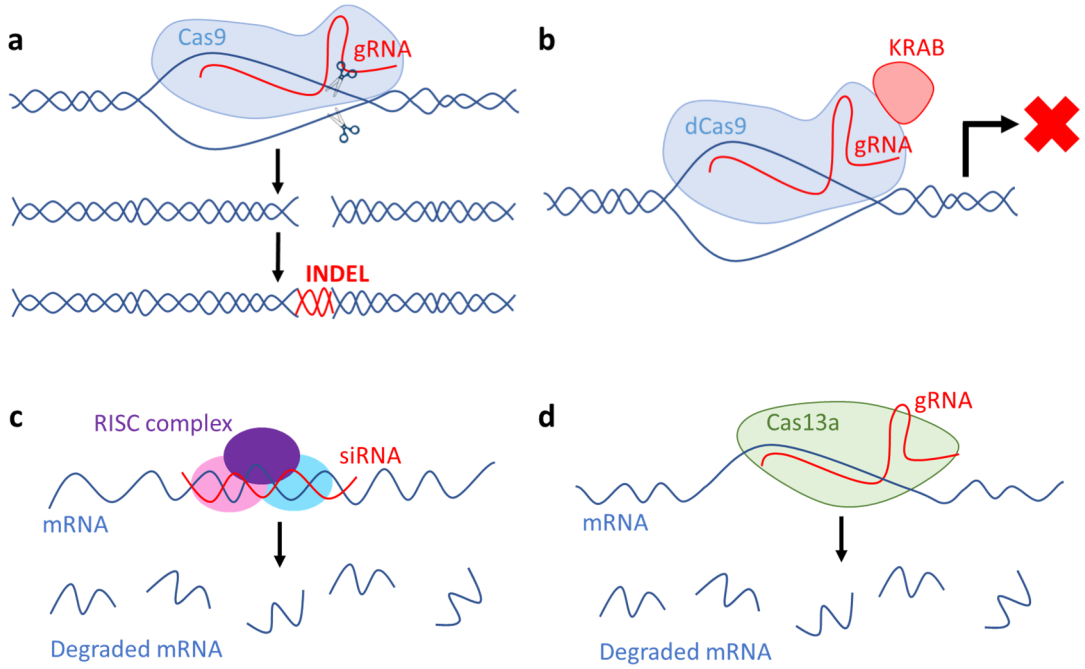

Figure 1.6 Methods of gene knockdown that can be utilised in induced pluripotent stem cells (iPSCs). (a) Heterozygous or homozygous knockout of a gene can be obtained using the Cas9 protein. A guide RNA (gRNA) complementary to a region in the gene of interest guides the Cas9 protein to the DNA site, where it cleaves both strands of DNA. The Cas9 protein can repeatedly cut the DNA until a mistake is made during DNA repair, leading to an insertion or deletion (INDEL) that disrupts the gene sequence. (b) Nuclease-dead Cas9 (dCas9) fused to a transcriptional repressor (e.g. KRAB) is targeted to a region around the transcription start site by the gRNA. Binding of dCas9-KRAB inhibits gene expression. (c) small interfering RNA (siRNA) associate with endogenous proteins; dicer, argonaute 2 and TRBP, to form an RNA-induced silencing complex (RISC). This complex binds complementary messenger RNA (mRNA) and inhibits gene expression by either degradation or translational repression. (d) Cas13 forms a complex with gRNA, which then guides it to complementary mRNA sequences. Cas13 cleaves and degrades this mRNA, thus inhibiting gene expression.

1.4 Project Aims

CACNA1C has been shown to be highly associated with psychiatric disorders including BPD and schizophrenia. Mutations in the gene also lead to Timothy Syndrome, a rare developmental disorder that includes ASD as a common symptom. Based on this clear association with psychiatric disease the overall objective of this project is to identify how Cav1.2 alters neuronal development and activity. To achieve this the project has the following aims:

- The first results chapter aims to generate and validate a CACNA1C knockout line using an inducible Cas9 iPSC line.

- The second results chapter investigates the effect of loss and gain of function of Cav1.2 on neuron generation. This will be done using the CRISPR-generated knockout lines and an ATS patient line. Expression of different neuronal markers will be measured using qRT-PCR and immunocytochemistry. Associated downstream signalling pathways will also be investigated to provide a potential mechanism for changes to neuronal differentiation.
- The third results chapter will investigate the effect of loss and gain of function of Cav1.2 on neuronal network activity using multi-electrode arrays. Pharmacology will be used to further investigate any changes to network activity.

2 General Methods

2.1 Stem Cell Culture

2.1.1 Cell lines and maintenance

The cell lines used in this thesis were the IBJ4, iCas9, CACNA1C knockout and atypical Timothy syndrome (ATS) human induced pluripotent stem cell lines (iPSCs). The IBJ4 iPSC line was a gift from Josh Chenoweth from the Lieber Institute for Brain Development, MD, USA. The iCas9 lines were derived from the IBJ4 line and contain the Cas9 gene, in the AAVS1 locus under a tetracycline inducible promoter. It was generated via electroporation of AAVS1-TALEN-L (Addgene # 59025) and AAVS1-TALEN-R (Addgene # 59026) plasmids which were a gift from Danwei Huangfu, and the pAAVS1-PDi-CRISPRn plasmid (Addgene # 73500) which was a gift from Bruce Conklin. This line was generated by Ian Tully based on methods from the Conklin lab (Mandegar et al. 2016; Tully 2020). CACNA1C knockout lines were generated from the iCas9 line, as described in Chapter 3. The ATS line was derived by Olena Petter from a patient carrying a missense mutation (p(Ala1521Pro)) in CACNA1C. Written informed consent was gained from primary carers and the participant. The protocol was approved by the NHS London Queen Square research ethics committee." The IMAGINE-ID website and paper has further information; https://imagine-id.org/healthcare-professionals/study-documents-downloads-page/ https://pubmed.ncbi.nlm.nih.gov/31056457/. qPCR and immunocytochemistry were carried out by Olena Petter to confirm generation of pluripotent stem cells that are vector-free.

All iPSCs were maintained in feeder-free cultures in E8 medium (Thermo Fisher, #A1517001) on a matrix layer of Matrigel (Corning, #354234). To prepare cell culture plates, thawed aliquots of frozen Matrigel were diluted 1:100 in DMEM/F12 (Thermo Fisher, #11320033) and plated at 1 ml / 9.6 cm^2. Coated plates were incubated for at least 1 hour at 37°C, they were then washed with DPBS (Thermo Fisher, #14190250) and placed at 37°C until needed. Used Matrigel was reused once on another plate before being discarded.

Frozen 1 mL vials of iPSCs were thawed at 37 °C, diluted in E8 media and centrifuged at 200 g for 5 minutes. The media was aspirated, and cells resuspended in 2 mL of E8 media

with 10 μM Rock inhibitor Y27632 (Stem Cell Technologies, #72302). The resuspended cells were plated into 1 well of a coated 6-well plate and left to settle overnight. The media was then aspirated, cells washed with DPBS to remove cell debris and 2 mL of fresh E8 without Y27 was added. Cells were maintained in E8 with media changes every other day until 70-80% confluency. At this point cells were passaged using either Gentle Cell Dissociation Reagent (Stem Cell Technologies, #07174) or ReLeSR (Stem Cell Technologies, #05872).

2.1.2 iPSC passaging

For standard passaging of iPSCs, E8 media was aspirated from cells and 1 mL of Gentle cell dissociation reagent added per well that was passaged. Cells were incubated at 37°C for 3 minutes. The Gentle cell reagent was then aspirated and 1 mL of E8 added. Cells were dissociated from the bottom of the well by gently scratching with a stereological pipette. Cells were then diluted in E8 to the desired concentration and transferred into plates already coated with matrigel.

When regions of cells within a well appeared to be undergoing spontaneous differentiation ReLeSR was used to isolate the pluripotent cells. E8 media was aspirated, and cells washed with DPBS. 1 mL ReLeSR was added to each well for 30 seconds and then aspirated off. Cells were incubated at 37°C without any medium for 2 minutes and then 1 ml of E8 media was added to the well. The plate was firmly tapped against the palm of the hand for 30-60 seconds. The detached cells were collected and diluted in E8 to the desired concentration before being transferred into coated plates.

2.1.3 iPSC freezing

Cells were grown to confluency in a 6-well plate prior to freezing. Cells were then pre-treated with 10 μM Y27 for at least 1 hour. Following Y27 pre-treatment cells were dissociated from the well using Gentle cell dissociation reagent as described for standard cell passaging. After the Gentle cell reagent was aspirated, 1 mL of E8 containing 10% dimethyl sulfoxide (DMSO, Sigma Aldrich, #D2650) was added to the well and the cells were detached by scratching with a stereological pipette. The cell

suspension was then transferred to a cryovial, placed in a CoolCell freezing box and transferred to a -80°C freezer. Cells were transferred to liquid nitrogen for long term storage within 48 hours.

2.1.4 iPSC sub-cloning

For sub-cloning, cells were passaged into single cells and plated at low density so that colonies grown from single cells could be picked into new plates. Cells were grown to confluency in a 6-well plate. Cells were treated with Revitacell (1:100, Thermo Fisher, #A2644501) 2 hours prior to passage. Following pre-treatment E8 media was aspirated from cells and they were incubated with 1 mL of Accutase (Thermo Fisher, #A1110501) at 37 °C for 10 minutes or until cells were lifting off the plate. Cells were transferred into a 1.5 mL tube and singularised by carefully pipetting up and down 3-4 times using a 1000 µL pipette. They were the centrifuged at 150 g for 3 minutes and the Accutase aspirated. Cells were resuspended in 1 mL E8 and plated at a 1:50-1:100 dilution onto 100 mm coated dishes containing E8 media with Revitacell (1:100).

Cells were grown in E8 media for 5-7 days until the majority of the colonies were big enough to pick but were not merging together. Prior to picking, cells were pre-treated with Revitacell (1:100) for 2 hours. Cells were picked under an Evos XL core microscope using a 200 µL pipette to scratch the colonies off the plate and transfer into a precoated 48- or 96-well plate containing E8 with Revitacell (1:100).

2.1.5 Differentiation of glutamatergic neurons from iPSCs

Written below is the basic protocol for production of cortical glutamatergic neurons. This protocol is based on the dual-SMAD inhibition methods described by Chambers *et al.* (2009) and Shi *et al.* (2012). Media components are summarised in Table 2.1. The basic outline of the protocol is shown in Figure 2.1.

Components	Media		
	N2B27-RA	N2B27+RA	BrainPhys
DMEM/F12 (Thermo Fisher, #12634028)	100 mL	100 mL	
Neurobasal (Thermo Fisher, #21103049)	50 mL	50 mL	
Brain Phys Basal (Stem Cell, #05790)			150 mL
B27-RA (50X) (Thermo Fisher, #12587010)	1 mL		
B27+RA (50X) (Thermo Fisher, #17504044)		1 mL	3 mL
N2 (100X) (Thermo Fisher, #17502001)	1 mL	1 mL	
PSG (100X) (Thermo Fisher, #10378016)	1.5 mL	1.5 mL	1.5 mL
β-mercaptoethanol (Sigma, #M3148)	150 µL	150 µL	
Ascorbic Acid (200 mM) (Sigma, #A4403)			75 µL
BDNF (20 µg/mL) (Tocris, #2837)			150 µL

Table 2.1 Neural differentiation media formulations. (RA = Retinyl acetate, PSG = Penicillin-Streptomycin-Glutamine, BDNF = Brain-derived neurotrophic factor)

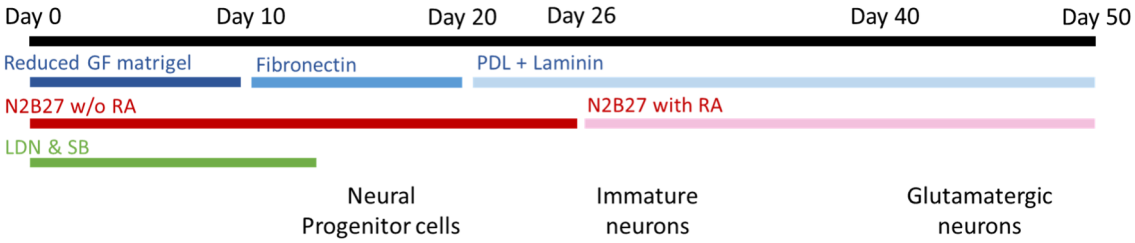

Figure 2.1 Overview of protocol for differentiation of iPSCs into cortical neurons. Dual SMAD inhibition using LDN193189 (LDN) and SB431542 (SB) in N2B27-RA medium was used for neural induction. Cells are passaged onto fibronectin at day 10 and LDN and SB removed at day 13. At day 20 NPCs are passaged onto poly-D-lysine (PDL) and laminin coated plates. Once neurons have started to form at day 26 cells are switched to N2B27 media with vitamin A (retinyl acetate) to improve neuronal maturation. Cells are maintained in this media until the end of the protocol at day 50, unless needed for MEA experiments.

Before the start of neural induction (D0), confluent wells of iPSCs were collected as described for standard iPSC passaging and plated onto 12-well plates (1:2 passage ratio) coated with reduced growth factor Matrigel (Corning, #354230). Cells were maintained in E8 media until 90-100% confluent after which they washed with DPBS and N2B27-RA media containing 100 nM LDN193189 (LDN, Sigma-Aldrich, #SML0559) and 10 nM SB431542 (SB, Sigma-Aldrich, #S4317) was added.

iPSCs were maintained in this media for 10 days, with half-media changes every 2 days. After this point multi-layered colonies of cells could be seen. For the 1st passage cells were pre-treated with 10 µM Y27 for 1 hour. The medium was then removed from cells and kept for later use. Cells were washed with DPBS and 500 µL of Versene (Thermo Fisher, #15040066) was added to each well for 2 minutes at 37 °C. The Versene was aspirated and 1 mL of the previously collected N2B27-RA medium was added to each well. Cells were detached from the plate by scratching with a stereological pipette and collected cells were pooled together into a 50 mL tube. Cells were diluted with fresh N2B27-RA containing LDN, SB and Y27 to a passage ratio of 2:3 and to allow plating of 1.5 mL of cells per well. Cells were then plated onto fresh 12-well plates pre-coated with fibronectin (Millipore, #FC010) for 1 hour. On day 13 of the induction protocol, the medium was switched to N2B27-RA alone. Cells were then maintained with half medium changes every two days until day 20. At day 20 multilayer colonies comprising neural rosettes were visible, at this point cells were deemed to be neural precursor cells (NPCs).

To continue differentiation NPCs were passaged at day 20 onto plates coated with 0.1 mg/mL poly-D-lysine (Sigma-Aldrich, #P7886) and 20 µg/mL laminin (Roche, #11243217001). 2 hours prior to passage cells were pre-treated with 10 µM Y27 for 2 hours. The medium was then removed from cells and kept for later use. Cells were washed with DPBS and 500 µL of Versene was added to each well for 2 minutes at 37 °C. The Versene was aspirated and 1.5 mL of the previously collected N2B27-RA medium was added to each well. Cells were detached from the plate by scratching with a stereological pipette and collected cells were pooled together into a 50 mL tube. Cells were diluted with fresh N2B27-RA to a passage ratio of 1:2 and to allow plating of 1.5 mL of cells per well. On day 26, once cells displayed neuronal morphology, the medium was changed to N2B27+RA. Cells were then maintained with half medium changes every two days until the end of the protocol at day 50. Wells intended for culture on multi-electrode arrays (MEAs) were switched to astrocyte conditioned BrainPhys media roughly 1 week before plating.

2.1.6 Cell Transfection

Cells were grown in a 6-well plate until 70% confluent. crRNA (10 µM) and tracrRNA (10 µM) (Both Sigma, #VC40003 and #TRACRRNA05N-5NMOL) were annealed in a thermocycler (95 °C for 5 mins, ramp down to 25 °C at 0.3 °C/sec). Annealed guide RNA was transfected into the cells using Lipofectamine CRISPRMAX (ThermoFisher, # CMAX00008). 10 µL guide RNA was combined with 5 µL Lipofectamine™ CRISPRMAX™ Reagent in 125 µL Opti-MEM™ I Medium. 7.5 µL Lipofectamine™ CRISPRMAX™ Reagent was added to 125 µL Opti-MEM™ I Medium. Both solutions were incubated for 5 minutes at room temperature before being mixed together. Following incubation for a further 10 minutes the guide RNA-transfection reagent complex was added to cells. Cells were left for 2-3 days before passage and/or DNA extraction.

2.2 CRISPR Guide Design

Guides were designed to target exon 2 of CACNA1C, the first constitutive exon, so that an out of frame mutation would stop protein production. Two of the guides used were previously validated by Sanjana and colleagues and one was designed using CRISPOR (Sanjana et al. 2014; Haeussler et al. 2016). Guide RNA contained an added sequence to anneal to the tracrRNA (Both Sigma, #VC40003 and #TRACRRNA05N-5NMOL). Guide sequences are summarised in Table 2.2

Gene	Guide Sequence	Comments
CACNA1C	CGATGGCCGCCTGCCACGAC	Validated guide
	CCCTCCGGATGGGGTTCTTC	Validated guide
	TGAATGCCAATGCGGCAGCG	CRISPOR-designed guide

Table 2.2 Guide sequences used for CRISPR gene knockout.

2.3 PCR

2.3.1 DNA sample collection

DNA was extracted from cells using QuickExtract DNA Extraction Solution (Lucigen, #QE09050). Cells were dissociated from plates using Gentle cell dissociation reagent as previously described. Cells were then added to 30-100 µL of QuickExtract solution. This

solution was vortexed for 30 seconds and then incubated at 65 °C for 6 minutes. The solution was vortexed again and incubated at 98 °C for 2 minutes. Samples were placed on ice or stored at -20 °C until required for PCR.

2.3.2 PCR amplification

Genomic DNA was amplified by PCR using the GoTaq G2 Mastermix (Promega, #M7832). The reaction was set up to contain the Mastermix at 1 X concentration, 10 µM forward primer, 10 µM reverse primer, <100 ng genomic DNA and nuclease-free water up to 25 µL or 50 µL. Primers are summarised in Table 2.3. The PCR reaction was then amplified in a thermocycler (Eppendorf, Mastercycler X50s). The programme consisted of an initial denaturation step at 98 °C for 30 seconds, followed by 30 amplification cycles and a final extension step at 72 °C for 2 minutes. Each cycle included 10 seconds denaturation at 98 °C, 30 seconds annealing at 55 °C to 60 °C (primer-dependent) and 30 seconds/kilobase extension at 72 °C. PCR reactions were then run on an agarose gel to verify specific amplification of the DNA.

Target	Forward Primer (5'-3')	Reverse Primer (5'-3')
M13 Tags	GTAAAACGACGGCCA	GGAAACAGCTATGACCATG
CACNA1C Exon 2	GGTGAGGCAAGGAGACTAGAGC	GATTCATCCAGTCTAGGGCGGG
CACNA1C Exon 1-4	CATTTCTTCCTCTTCGTGGCTGC	TAGTAGGTTCCAGCCGTTGC
ARHGAP35	AAAAGCCACGTCCCAAGCCACC	GCAGGAAGCAAAACCAAGGCGG
CACNA1D	TGGATGCTGGCTTGGCTGATGC	CTGCAACCCGAAGAGACAGGAAGG
CYFIP2	ATCCGCTACTGATGGTGCCTGG	TTTGTCCTCAAGCAGCAGCCCC
HMGA2	ATGGCCCTTGTTGAACCTGGGG	TGCCAGGGCTGTACAACAATGGG
KCNK10	TGGCCACCCATCCCAGTTTTCC	TCCGTTCTCCAACTCAGCGTGC
MLXIPL	ATTGTTGCTTCCAGGGCCGAGC	AAAGTGATGCAGTTGGCCCCGC
NRIP3	TTGTCATCAGCTGCGAGCAGGG	TTTAGGCACCAAGATGAGGGCC
PAMR1	TGCCTTCCCCATCCTCTTTGCG	TGGCTGCTGACATGCTAAGGGG
PPM1N	AACCCCGCTTTGTAGGTGCAGG	AGACACGTGTCCAACAGCTGCG
SELPLG	TGCTGCAAGGCGTTCTACTGGC	ACCTCGGCTGAAATGTGGCTGG
SH3BP5	AAGAGCCAAAGCAGCACCTCCC	TAACAGTTTGAAAGAGGGTTGC
TP53BP2	TGCCCAGAATCAACAGCAGCACC	TGCCCTCACTCCATCCAGAACC

Table 2.3 Primers used for PCR amplification. M13 tags were added 5' to primers if barcoding was required

2.4 Mutation detection assay

The Surveyor® Mutation Detection Kit (IDT, 706025) was used to screen for mutations following transfection of guides into Cas9 cells. The PCR amplification of the region of interest was placed in a thermocycler at 95 °C for 5 minutes, then ramped down to 25 °C at 0.3 °C/s. The sample was then incubated with 1 µL Surveyor Enhancer S, 2 µL Surveyor Nuclease S and 0.15 M $MgCl_2$ solution ($1/10^{th}$ total volume) at 42 °C for 1 hour. Stop solution ($1/10^{th}$ reaction volume) was added to the reaction which was then run on an agarose gel.

2.5 minION sequencing

2.5.1 Barcoding Samples

DNA was amplified by PCR, as described in section 2.3. Primers were designed using the Primer wizard on Benchling to amplify the region of interest with M13 tags added to the 5' end of each primer. The PCR product was then diluted 1 in 100 before being reamplified by PCR using barcoded primers designed by Ian Tully (Table 2.4). These primers allowed the PCR product of up to 96 samples from subcloned cells to be pooled together for sequencing, as the barcodes where used to identify individual samples (Tully 2020).

Primer	Sequence (5' to 3')
Barcode Fwd 1	AAGAAAGTTGTCGGTGTCTTTGTGGTAAAACGACGGCCA
Barcode Fwd 2	TCGATTCCGTTTGTAGTCGTCTGTGTAAAACGACGGCCA
Barcode Fwd 3	GAGTCTTGTGTCCCAGTTACCAGGGTAAAACGACGGCCA
Barcode Fwd 4	TTCGGATTCTATCGTGTTTCCCTAGTAAAACGACGGCCA
Barcode Fwd 5	CTTGTCCAGGGTTTGTGTAACCTTGTAAAACGACGGCCA
Barcode Fwd 6	TTCTCGCAAAGGCAGAAAGTAGTCGTAAAACGACGGCCA
Barcode Fwd 7	GTGTTACCGTGGGAATGAATCCTTGTAAAACGACGGCCA
Barcode Fwd 8	TTCAGGGAACAAACCAAGTTACGTGTAAAACGACGGCCA
Barcode Fwd 9	AACTAGGCACAGCGAGTCTTGGTTGTAAAACGACGGCCA
Barcode Fwd 10	AAGCGTTGAAACCTTTGTCCTCTCGTAAAACGACGGCCA
Barcode Fwd 11	GTTTCATCTATCGGAGGGAATGGAGTAAAACGACGGCCA
Barcode Fwd 12	CAGGTAGAAAGAAGCAGAATCGGAGTAAAACGACGGCCA
Barcode Rev A	AGAACGACTTCCATACTCGTGTGAGGAAACAGCTATGACCATG
Barcode Rev B	AACGAGTCTCTTGGGACCCATAGAGGAAACAGCTATGACCATG
Barcode Rev C	AGGTCTACCTCGCTAACACCACTGGGAAACAGCTATGACCATG
Barcode Rev D	CGTCAACTGACAGTGGTTCGTACTGGAAACAGCTATGACCATG
Barcode Rev E	ACCCTCCAGGAAAGTACCTCTGATGGAAACAGCTATGACCATG
Barocde Rev F	CCAAACCCAACAACCTAGATAGGCGGAAACAGCTATGACCATG
Barcode Rev G	GTTCCTCGTGCAGTGTCAAGAGATGGAAACAGCTATGACCATG
Barcode Rev H	TTGCGTCCTGTTACGAGAACTCATGGAAACAGCTATGACCATG

Table 2.4 Barcoded primers for multiplexing of samples for sequencing.

2.5.2 Library preparation

Barcoded PCR products were pooled together and purified using Wizard® SV Gel and PCR Clean-Up System (Promega, A9281). Membrane binding solution was added to the PCR products in an SV Minicolumn. After incubation for a minute the mixture was centrifuged at 16,000 RCF for 1 minute. The Minicloumn was washed twice with Membrane Wash Solution and the membrane dried by centrifugation at 16,000 RCF for 1 minute. The DNA bound to the membrane was eluted in 50 µL of nuclease-free water by centrifugation at 16,000 RCF for 1 minute.

1µg of purified DNA was then prepared for sequencing using the $1D^2$ sequencing kit (Oxford Nanopore, SQK-LSK308). The DNA was incubated with Ultra II End-prep reaction buffer and enzyme mix for 5 minutes at 20 °C and 5 minutes at 65 °C. AMPure XP beads (Beckman, #A63880) where then added to the mixture and incubated for 5 minutes at room temperature with constant agitation. The sample was pelleted on a magnet and

washed with 70% ethanol, before being resuspended in nuclease free water. The sample was incubated for 2 minutes and then pelleted on a magnet. The eluate was removed and incubated with 1D2 Adapter and Blunt/TA Ligase Master Mix (NEB, #M0367L) for 10 minutes at room temperature. AMPure XP beads were added to the sample and incubated for 10 minutes with constant agitation. The sample was pelleted on a magnet and washed with 70% ethanol, before being resuspended in nuclease free water. The eluate was removed and incubated with Barcode Adapter Mix and Blunt/TA Ligase Master Mix for 10 minutes at room temperature. AMPure XP beads were added to the sample and incubated for 10 minutes with constant agitation. The sample was pelleted on a magnet and washed with ABB buffer before being resuspended in Elution buffer. The sample was incubated for 10 minutes before the beads were pelleted on a magnet and the eluate was transferred into a clean 1.5 mL tube.

The sample was then loaded onto a SpotON flow cell (ONT, #R9.4.1). The flow cell was inserted into the MinION (ONT, #MIN-101B). A small amount of buffer was drawn back from the priming port of the flow cell to remove any bubbles. 800 µL priming mix (576 µL Running buffer with Fuel Mix 624 µL of nuclease-free water) was loaded into the flow cell via the priming port and incubated for 5 minutes. The remaining 200 µL of priming mix was added to the flow cell. The prepared DNA sample was mixed with Running buffer with Fuel Mix and Library Loading Beads and loaded onto the flow cell via the sample port. The MinION was then connected to a computer with the MinKNOW programme. The sequencing run was then started via this programme after selecting the flow cell type. The sequencing was run until around 400,000 reads were acquired.

2.5.3 Sequencing Analysis

The reads were base-called using Albacore to generate FASTQ files and sorted into folders according to their barcodes. The sequences where then aligned to the reference genome for CACNA1C Exon 2. A custom script, was used to identify if deletions were present for each set of barcoded sequences (Tully 2020). These barcoded reads were then checked on Integrative Genomics Viewer to confirm the presence and frequency of the deletions.

2.6 Western Blot

2.6.1 Protein sample collection

At least one confluent well of cells in a 12-well plate was required for adequate protein extraction from cells. E8 media was aspirated from cells and Gentle cell dissociation reagent or Versene was added to cells for a minute, dependent on if they were iPSCs or differentiated cells respectively. The dissociation reagent was aspirated, cells were carefully washed with DPBS and then fresh DPBS added to the well. Cells were dissociated from the bottom of the well by gently scratching with a stereological pipette and collected in a 1.5 mL Eppendorf tube. The cell suspension was centrifuged at 900 g for 5 minutes at 4 °C and the supernatant aspirated leaving the cell pellet.

The cells were then resuspended in 150 µL RIPA buffer (Sigma, #R0278-50ML) containing MS-SAFE Protease and Phosphatase Inhibitor (Sigma, MS-SAFE-1VL) and incubated on ice for 30 minutes with vortexing every 5 minutes. Cells were then centrifuged at 14000 rpm for 5 minutes at 4 °C. 120 µL of the supernatant was added to LDS sample buffer (4 X) and sample reducing agent (DTT, 10 X) (Both Thermo Fisher, #NP0007 and #NP0004) and incubated at 95 °C for 5 minutes to denature the proteins before transfer to a -80 °C freezer for storage until required. The remaining supernatant was stored at -80 °C until required for protein concentration measurement.

2.6.2 Protein concentration measurement

5 µL of each sample and BSA protein standards (125-2000 µg/mL, Thermo Fisher, #23208) were added in triplicate into a 96-well plate. 25 µL of working solution A (20 µL reagent S plus 1 mL reagent A, (BioRad, #5000113 and #5000115)) was added to each well. 200 µL of reagent B (BioRad, #5000114) was then added to the wells and the plate was gently agitated to mix. The samples were incubated for 15 minutes at room temperature before the absorbance was read at 750 nM using a CLARIOstar microplate reader. The average reading of each sample and protein standard was calculated from the 3 wells and the protein standard readings plotted on a graph against their known concentration. The equation for the line of best fit was then used to calculate the

concentration of each sample that was measured and thereafter the concentration of the protein sample stored with LDS and DTT.

2.6.3 Gel electrophoresis and protein transfer

Protein samples in LDS and DTT were thawed on ice, 20-50 µg of sample (dependent on protein of interest) was diluted in RIPA buffer with LDS and DTT so that all samples were the same volume for loading. Samples were then loaded onto a Bolt Bis-Tris 4-12% gradient gel (Thermo Fisher, #NP0323BOX) with Protein colour standard (5 µL, NEB, #P7719). The gel was run at 120 V for 2-3 hours, dependent on the size of protein of interest, in Bolt MES running buffer (Thermo Fisher, #B000202). The gel was then sandwiched against a nitrocellulose membrane (Sigma, #GE10600114) and run at 120 V for 1 hour 45 minutes at 4°C in Bolt transfer buffer (Thermo Fisher, #BT00061) to transfer the proteins to the nitrocellulose membrane.

2.6.4 Immunoblotting

The nitrocellulose membrane was soaked in tris buffered saline (TBS, Formedium, #TBSL1000) and then blocked for 1 hour at room temperature in TBS containing 5% milk powder. The membrane was then incubated overnight at 4°C with the primary antibody in 5% milk-TBS. The membrane was washed 3 times for 5 minutes with TBS containing 0.1% Tween-20 (Sigma, #P9416) and then incubated for 1 hour at room temperature with the secondary antibody. The membrane was then washed 3 times for 5 minutes with TBS-Tween and washed once with TBS before visualisation using an Odessey CLx imager. Antibodies used are summarized below (Table 2.5). Images were analysed using the Image Studio Lite programme.

Primary Antibodies			
Antibody	**Supplier**	**Species**	**Dilution**
GAPDH	Abcam (ab9485)	Rabbit	1:1000
CACNA1C	Millipore (AB5156)	Rabbit	1:200
ERK1/2	CST (4695)	Rabbit	1:1000
Phospho-ERK1/2	CST (9106)	Mouse	1:1000
CREB	CST (9104)	Mouse	1:1000
Phospho-CREB	CST (9198)	Rabbit	1:1000
Secondary Antibodies			
Antibody	**Supplier**	**Species**	**Dilution**
IRDye® 680RD anti-Mouse IgG	Licor (926-68070)	Goat	1:10,000
IRDye® 800CW anti-Rabbit IgG	Licor (926-32211)	Goat	1:10,000

Table 2.5 Primary and Secondary Antibodies used for Western Blot

2.7 qPCR

2.7.1 RNA sample collection

RNA was extracted from cells using the RNeasy Mini kit (Qiagen, #74104). E8 media was aspirated from cells and they were carefully washed with DPBS. Fresh DPBS was added to each well. Cells were dissociated from the bottom of the well by gently scratching with a stereological pipette and collected in a 1.5 mL Eppendorf tube. The cell suspension was centrifuged at 200 g for 5 minutes and the supernatant aspirated leaving the cell pellet. 600 µL RLT buffer was then added to the sample, vortexed briefly and the solution passed through a x-gauge needle 5 times. 600 µL of 70% ethanol was added to the samples. The sample was spun through a column at 8000 g for 15 seconds and the flow through discarded. Buffer RWT, followed by Buffer RPE were then spun through the column at 8000 g for 15 seconds each. Fresh Buffer RPE was added to the column and centrifuged at 8000 g for 2 minutes. 40 µL nuclease free water was added to the column and collected in a fresh centrifuge tube via centrifugation at 8000 g for 1 minute. The RNA concentration was measured using a spectrometer.

2.7.2 Conversion to cDNA

RNA was converted to cDNA using miScript II RT Kit (Qiagen, #218160). 1 µg of each RNA sample was combined with 5 x miScript HiFlex buffer, 10 x miScript Nucleics mix and miScript Transcriptase mix up to a total volume of 20 µL. The reverse-transcriptase reactions were incubated for 60 minutes at 37 °C and 5 minutes at 95 °C. The cDNA concentration was then measured using a BioSpectrometer (Eppendorf) and samples were diluted to 100 ng/µL.

2.7.3 qPCR

Quantitative PCR was carried out using QuantiTect SYBR Green PCR Kit (Qiagen, #204145). Each sample was run in triplicate using 2.5 µL (250 ng) of DNA per PCR reaction. A master mix containing 12.5 µL of 2 x QuantiTect SYBR Green PCR Master Mix, 0.5 µM of forward and reverse primers (Table 2.6), and RNAse-free water up to 22.5 µL was added to each sample in a 96-well plate. The plate was run on a Real-Time PCR instrument (Applied Biosystems®) with an initial incubation at 95 °C for 15 minutes followed by 40 cycles of 94 °C for 15 seconds, 55 °C for 30 seconds, 70 °C for 30 seconds. A melting curve was also generated to check primer specificity. Data was exported to Microsoft Excel and analysed using the ΔΔCt method for relative quantification (Livak and Schmittgen 2001).

Gene	Forward Sequence (5'-3')	Reverse Sequence (5'-3')	Reference
CACNA1C	TGACTATTTTTGCCAATTGTGTGG	GCGGAGGTAGGCATTGGG	-
CTIP2	CTCCGAGCTCAGGAAAGTGTC	TCATCTTTACCTGCAATGTTCTCC	(Arber et al. 2015)
CUX1	GCTCTCATCGGCCAATCACT	TCTATGGCCTGCTCCACGT	-
FoxG1	AGGAGGGCGAGAAGAAGAAC	TCACGAAGCACTTGTTGAGG	-
GAD65	GGCTTTTGGTCTTTCGGGTC	GCACAGTTTGTTTCCGATGCC	(Paşca et al. 2011)
GAD67	GCCAGACAAGCAGTATGATGT	CCAGTTCCAGGCATTTGTTGAT	(Paşca et al. 2011)
GAPDH	AGGCTGGGGCTCATTTG	CAGTTGGTGGTGCAGGAG	-
LHX6	TGAGAGTCAGGTACAGTGCG	GCCCATCCATATCGGCTTTGA	-
Map2	CTGCTTTACAGGGTAGCACAA	TTGAGTATGGCAAACGGTCTG	(Paşca et al. 2011)
Nestin	AGCAGGAGAAACAGGGCCTAC	CTCTGGGGTCCTAGGGAATTG	-
Pax6	GTGTCCAACGGATGTGTGAG	CTAGCCAGGTTGCGAAGAAC	-
SatB2	CCGCACACAGGGATTATTGTC	TCCACTTCAGGCAGGTTGAG	(Paşca et al. 2011)
Tbr1	GGGCTCACTGGATGCGCCAAG	TCCGTGCCGTCCTCGTTCACT	(Kmet et al. 2013)
β-III-tubulin	ATGAGGGAGATCGTGCACAT	GCCCCTGAGCGGACACTGT	(Kwon et al. 2012)
VGAT	CCGAGTGGTGAACGTAGCG	GTGGCGATAATGGACCAGGAC	(Paşca et al. 2011)
vGLUT1	CGACGACAGCCTTTTGTGGT	GCCGTAGACGTAGAAAACAGAG	(Paşca et al. 2011)
vGLUT2	GGGAGACAATCGAGCTGACG	CAGCGGATACCGAAGGAGATG	(Paşca et al. 2011)

Table 2.6 Primers used for qPCR experiments.

2.8 Immunocytochemistry

2.8.1 Cell preparation and staining

Neurons were fixed on 12- or 24-well plates using 4% paraformaldehyde solution (PFA, Sigma #P6148). Following medium aspiration, cells were washed with DPBS. 0.5-1 mL of PFA was added to each well and incubated at 4 °C for 20 minutes. PFA was then removed, and cells were washed 3 times with DPBS before being stored in DPBS at 4 °C in the dark until use.

For staining, cells were washed with 0.1% Triton X-100 (Sigma X100PC) diluted in PBS (PBS-T) for 5 minutes. Cells were then blocked to prevent non-specific binding with 5%

donkey serum in PBS-T. Primary antibodies, diluted in PBS-T with donkey serum, were incubated overnight at 4 °C (Table 2.7). The next day cells were washed 3 times for 5 minutes each with PBS-T. Then secondary antibodies diluted in PBS-T and donkey serum were incubated for 1 hour at room temperature in the dark (Table 2.7). Cells were then washed with PBS before counterstain with DAPI (1:1000 in PBS) for 5 minutes. Cells were then washed twice with PBS. All PBS was removed from the cells and coverslips were carefully placed over the cells with DAKO fluorescence mounting medium (Agilent #S3023). Cells were stored in the dark at 4 °C at least overnight, until visualisation.

Primary Antibodies			
Antibody	**Supplier**	**Species**	**Dilution**
MAP2	Abcam (ab32454)	Rabit	1:500
GAD65	Millipore (MAB351)	Mouse	1:500
GAD67	Millipore (MAB5406)	Mouse	1:500
Secondary Antibodies			
Antibody	**Supplier**	**Species**	**Dilution**
Alexa Fluor 488 anti-rabbit	Thermo Fisher (A32790)	Donkey	1:1000
Alexa Fluor 594 anti-mouse	Thermo Fisher (A21203)	Donkey	1:1000

Table 2.7 Primary and secondary antibodies used for immunofluorescence.

2.8.2 Imaging and analysis

Cells were imaged using a Leica DMI6000 inverted microscope with Las X software. An average of 10 random fields was acquired for each well at 20x magnification. Analysis was caried out using FIJI Image J software. To calculate the area of staining each channel was thresholded dependent on the protein that was being stained and the area was then determined. MAP2 staining was calculated proportional to the area of DAPI staining. GAD65 and GAD67 staining was calculated proportional to MAP2 area. The number of rosettes were counted manually based on morphology relative to the area of DAPI.

2.9 Multi electrode array culture and recording

2.9.1 Plating neurons onto multi electrode array plates

Neurons were plated between day 48 and day 52 of neuronal differentiation onto CytoView MEA 24-well plates (Axion Biosystems, #M384-tMEA-24W-5, 4X4 electrode grid). 1 week prior to plating neuronal differentiation media was gradually replaced with astrocyte-conditioned BrainPhys media. Plates were coated overnight with 0.1% polyethylenimine (Sigma) and washed with DPBS before use. Neurons were singularised with accutase as previously described and resuspended in 1 mL of medium. Cells were counted using a haemocytometer and diluted to 30,000 cells/µL in BrainPhys media containing 10 µg/mL Laminin. They were then plated as a 10µL droplet into the centre of each well at roughly 300,000 cells per well. Following incubation at 37 °C for 1 hour, 500 µL of BrainPhys media was carefully added to each well, taking care not to displace the neurons. Neurons were maintained in Astrocyte-conditioned BrainPhys medium with twice-weekly half-media changes. Two days after plating, neurons were treated with DAPT (10 µM) for 1 week to remove any remaining NPCs and allow synchronised networks to form.

2.9.2 Astrocyte-conditioned media

Normal human astrocytes in flasks at 60-80% confluency were used to condition media. Astrocytes were cultured in 20 mL BrainPhys media at 37 °C. After 72 hours the conditioned media was removed from flasks and replaced with fresh media. The conditioned media was sterilised using a 0.22 µm syringe PVDF filter and stored at 4 °C for use within 7 days or 20 °C for longer storage. This process was repeated every 3-4 days until the required amount of medium was acquired. Conditioned medium was used 1:1 with fresh medium for neurons plated on MEAs.

2.9.3 MEA recordings and analysis

Electrophysiological activity was recorded every 10 days using hardware (Maestro Pro complete with Maestro 768 channel amplifier) and software (AxIS 1.5.2) from Axion Biosystems. Channels were sampled simultaneously with a gain of 1000× and a sampling rate of 12.5 kHz/channel. During the recording, the temperature was maintained at 37

°C. All active electrodes were included in the analysis. Before every recording, wells were rigorously quality controlled to check that the cells had not clumped or lifted, and that they covered at least 80% of the electrodes. Any well that did not meet these criteria were excluded from analysis.

A Butterworth band-pass filter (with a high-pass cut-off of 200 Hz and low-pass cut-off of 3000 Hz) was applied along with a variable threshold spike detector set at 5.5× standard deviation on each channel. Offline analysis was achieved with custom scripts written in MATLAB. Briefly, spikes were detected from filtered data using an automatic threshold-based method set at −5.5×σ, where σ is an estimate of the noise of each electrode based upon the median absolute deviation 1. Spike timestamps were analysed to provide statistics on the general excitability of cultures. Neuronal bursting was detected based on three parameters: interburst period longer than 200 ms, more than three spikes in each burst and a maximum inter-spike (intra-burst) interval of 300 ms. Network activity was illustrated by creating array–wide spike detection rate (ASDR) plots with a bin width of 200 ms.

2.10 Study Design and Statistical Analysis

When designing iPSC experiments several factors must be considered in order to reduce variability. First cells used should be a low and similar passage number to each other. During routine cell culture, genetic mutations can accumulate over time which can alter the characteristics of the cell line and introduce greater variability (Yoshihara et al. 2017)yo. Therefore, cells within 5 passages of each other were used to start neuronal differentiations. For the ATS patient line and IBJ4 line, which was used as a control for the ATS line, the passage number was between 15 and 20 when starting differentiation for all experiments. The CACNA1C lines were derived from the iCas9 line, which was derived from the IBJ4 line and thus had already surpassed passage 50 by the time they were generated. Differentiations using the iCas9 and CACNA1C Hom lines were started using cells between passage number 54 and 59.

Next, cells can show a high degree of variability between independent differentiations. Therefore, multiple differentiations must be carried out to account for this variability

(McNeill et al. 2020; Volpato and Webber 2020). Ideally, each independent differentiation would count as one biological replicate (or N number), with multiple samples from the same differentiation counting as technical replicates. Due to restricted lab access during the COVID pandemic, only 1-2 differentiations could be carried out for experiments in this thesis. Therefore, to increase power each well was treated as a biological replicate for statistical analysis in this thesis.

All statistics were carried out using GraphPad Prism 8. Data was first analysed using the Anderson-Darling normality test to determine the use of parametric or non-parametric tests. Where groups of data from the same experiment had contrasting distributions, parametric tests were used as they are generally more robust than non-parametric tests. Additionally, data was checked for outliers using the ROUT method (Q=1%), and any outliers were removed from the dataset before statistical analysis. When two groups were being compared at one specific time point a T-test was used to determine statistical significance. Corrections for multiple testing using the Holm-Sidak method was applied when analysing multiple genes/proteins. One-way ANOVA was used when comparing 3 cell lines. Two-way ANOVA was used to compare cell lines across multiple time-points. The statistical tests for each experiment are described in the relevant results sections. All p-values are two-tailed. Summary plots of data show mean and standard error, unless otherwise stated. N numbers vary and are reported for individual experiment.

3 Generation and validation of CACNA1C mutant iPSC lines and an Atypical Timothy Syndrome patient iPSC line

3.1 Introduction

Psychiatric disorders are complex and caused by a combination of environmental and genetic factors. GWAS studies have shown that common variants can increase the genetic risk of these disorders. One of the most consistently associated genes linked to psychiatric disorders is CACNA1C, which encoded the pore-forming subunit of the L-type calcium channel Cav1.2 (Sklar et al. 2008; Ripke et al. 2013; Smoller et al. 2013; Ruderfer et al. 2014). The associated SNPs within intron 3 of CACNA1C have been shown to alter the expression of the gene (Bigos et al. 2010; Gershon et al. 2014; Yoshimizu et al. 2015; Eckart et al. 2016). There is also a rare disorder specifically associated with point mutations within CACNA1C known as Timothy Syndrome (TS). It is characterised by syndactyly, congenital heart disease and long QT syndrome but a large proportion of the patients also show developmental delay, ASD and intellectual disability (Splawski et al. 2004; Splawski et al. 2005).

The use of iPSCs offers an advantageous method to study the role of CACNA1C in psychiatric disease as cells from patients with TS can be generated and differentiated into neurons (Paşca et al. 2011). However, as TS encompasses a range of point mutations with varying symptoms the phenotypes in cell lines is also likely to differ between patients (Splawski et al. 2005; Gillis et al. 2012; Ozawa et al. 2018; Colson et al. 2019). Therefore, it is important not to generalise results between different forms of TS, unless multiple patient lines have been studied. These mutations often cause a gain-of function effect on the Cav1.2 channel due to an impairment in voltage-dependent inactivation of the channel (Splawski et al. 2004; Boczek et al. 2015; Wemhöner et al. 2015; Ozawa et al. 2018). However, psychiatric GWAS-linked SNPs affect expression of CACNA1C, so models that alter CACNA1C expression would also be useful (Bigos et al. 2010; Gershon et al. 2014; Yoshimizu et al. 2015; Eckart et al. 2016). One way of doing this would be to use iPSCs containing the GWAS-linked SNPs, either from participants that carry the SNP or by genetic modification to allow for an isogenic control (Yoshimizu et al. 2015). However, these SNPs have a very small

effect size on increasing risk of psychiatric disease and on their own are not pathogenic, so changes are likely to be very small, if at all measurable.

An alternative method is to generate knockout lines, which can be used in combination with patient iPSCs to study the role of CACNA1C in psychiatric disease. This has been made relatively easy due to the discovery of the CRISPR/Cas9 system and its optimisation for use in iPSCs using the iCRISPR platform (González et al. 2014). This involves using an iPSC line containing the Cas9 gene under a doxycycline inducible promoter. Alternative methods involve transfection of the Cas9 protein or expression vector in addition to the guide RNAs (Kabadi et al. 2014; Hashimoto and Takemoto 2015; Zuris et al. 2015). However, this method only requires transfection with the gRNA once expression of Cas9 has been induced with doxycycline and has been shown to have efficiencies of up to 40% (González et al. 2014). Therefore, this method will be used to generate CACNA1C mutant lines that will be studied alongside an atypical Timothy Syndrome patient line.

3.1.1 Chapter Aims

This chapter presents the generation of cell lines used for experiments in future results chapters. The aims were to develop CACNA1C knockout iPSC lines using the iCRISPR system. The lines were validated by screening for off-targets and by confirmation of loss of CACNA1C protein expression. This chapter will also characterise the atypical TS patient line using *in silico* analysis to classify the mutation and investigation of whether the point mutation affects the expression of CACNA1C.

3.2 Results

3.2.1 Generation of CACNA1C knockout lines

CACNA1C knockout lines were generated from iCas9 cells. The iCas9 line is the IBJ4 iPSC line that has been genetically modified to contain the Cas9 gene under a doxycycline inducible promoter in the AAVS1 safe-harbour locus. The iCas9 cells were incubated with doxycycline to induce expression of the Cas9 nuclease and transfected with guide RNA targeting CACNA1C. Initially one guide RNA was used at a time, however this did not produce any mutations in the cells. In order to increase the chance of insertions or deletions (indels) 3 different guides targeting exon 2 of CACNA1C were transfected at once. Exon 2 was chosen as the target as it is the first constitutive exon in CACNA1C.

Following this, a Surveyor Mutation Detection kit was used on DNA extracted from the transfected cells and control (non-transfected) cells. This was to check if any mutations had occurred in the pooled population of cells before sub-cloning and checking individual colonies. A PCR reaction was carried out to amplify the targeted region. The products were then heated to separate the double-stranded DNA and re-annealed. If mutations in the DNA were present and they reannealed to wildtype DNA, they would be cleaved by a nuclease that cleaves at locations of mismatched DNA due to the presence of insertions or deletions. The sample from the transfected cells had an extra band at 700bp following incubation with the nuclease, suggesting an indel had occurred in some of the cells (Figure 3.1a).

The remaining transfected cells were then dissociated into single cells and plated at a low density for sub-cloning as described in Chapter 2. Individual colonies were manually isolated and expanded. Colonies were screened for mutations using the ONT minION sequencing system. Genomic DNA was extracted from half of the cells for each clone and the target region was amplified by PCR. Barcoding of primers allowed sequencing of up to 96 samples at once. The sequences for each cell colony was identified based on the forward and reverse barcode primer and aligned to the

reference genome to check for mutations. This led to the identification of two clones that contained homozygous deletions in the target region (Figure 3.1b-d). These clones were further subcloned to ensure purity. The deletions in both lines all occur around the expected cut sites of the guides and cause frameshift mutations. In clone 20, allele 1 contains a 224bp deletion occurring between guide 1 and guide 3. The 2nd allele contains two deletions; a smaller 8bp deletion at the guide 3 cut site, and a 183bp deletion starting at the guide 1 cut site and ending between the cut sites for guide 2 and 3. For clone 29, allele 1 contains a 6bp deletion at the guide 1 cut site and a 176bp deletion between guides 2 and 3. Allele 2 contains a 47bp deletion between guides 1 and 2. All of these mutations lead to the introduction of a stop codon in the third amino acid position of exon 3, which is constitutive, and thus should prevent the generation of Cav1.2 protein (Figure 3.1e). Both lines were used for the experiments presented in this thesis and will be referred to as CACNA1C Hom1 (clone 20) and Hom2 (clone 29).

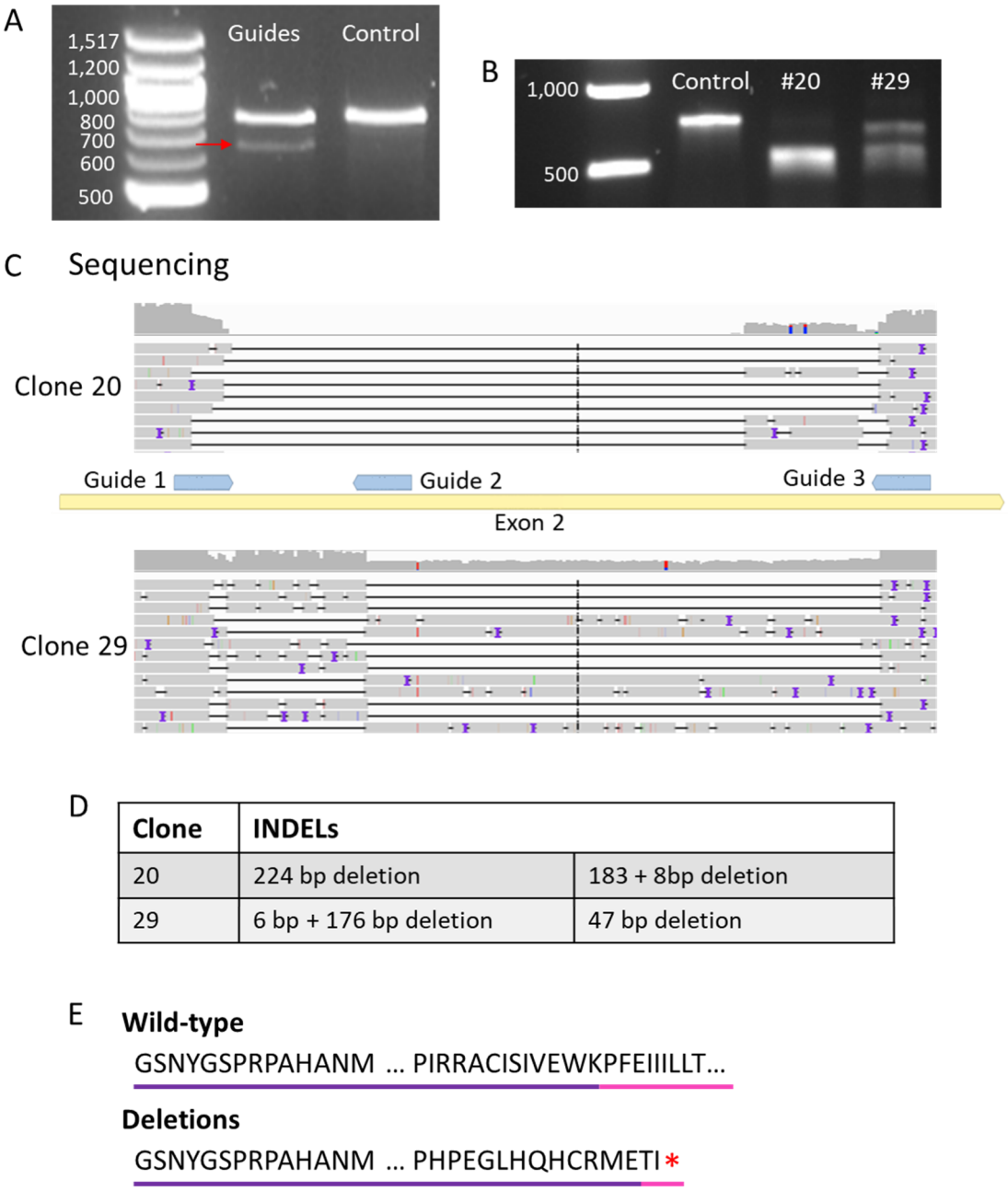

D

Clone	INDELs	
20	224 bp deletion	183 + 8bp deletion
29	6 bp + 176 bp deletion	47 bp deletion

E

Wild-type

GSNYGSPRPAHANM … PIRRACISIVEWKPFEIIILLT…

Deletions

GSNYGSPRPAHANM … PHPEGLHQHCRMETI*

*Figure 3.1 Screening of CACNA1C-mutant iPSCs. (A) Surveyor mutation assay of DNA from cells transfected with guides and untransfected cells (control). Transfected cells show an additional band around 700 bp. (B) PCR product of target region in iCas9 iPSCs (control) and the two clones that contained indels (20 and 29). (C) Sequencing results of the two clones that contained indels. Each row is an individual read from the sequencing and the black lines denote deletions when compared to the reference genome. The position of the guides on exon 2 is shown and is the same scale as the sequencing data. (D) Summary of INDELs present in clones. (E) Amino acid sequence of wild type and deletion alleles starting from exon 2 of CACNA1C. Exon 2 is underlined in purple and exon 3 in pink. The deletions lead to a frameshift altering the downstream amino acid sequence and introducing a stop codon at the start of exon 3, denoted by a *.*

3.2.2 Off target screening in knockout lines

CRISPR is an efficient method for gene editing but it has been shown to cause off targets. Research has shown that off-target cleavage can occur with up to 5 base pair mismatches between the guide and DNA sequence (Fu et al. 2013; Hsu et al. 2013; Pattanayak et al. 2013; Cho et al. 2014). However, the rate of off-targets appears to be rare in human pluripotent stem cells specifically (Smith et al. 2014; Veres et al. 2014). In order to determine whether off-targets have occurred online prediction tools can be used to generate a list of off-target sequences for each guide. These sites can then be screened using targeted amplicon sequencing.

CACNA1C Hom1 and Hom2 were both screened for possible off-targets using targeted amplicon sequencing. Off target sites for each guide were chosen using CRISPOR and RGEN Cas Off-finder databases. CRISPOR provides a list of off-target sites for guides based on base-pair mismatches (Concordet and Haeussler 2018). RGEN Cas Off-finder generates predicted off targets based on mismatches but can also allow for bulges in either the DNA or guide RNA sequence (Bae et al. 2014). The parameters of up to 4 mismatches with 0 bulges and up to 2 mismatches with 1 bulge were used to narrow down the list of potential off targets. The list was further reduced by discarding off target sites located in introns. Genes were then ranked based on brain expression levels according to the UCSC genome browser. Up to 5 off-target sites for each guide were screened for possible off-targets sites and are summarised in Table 3.1.

Guide	Gene	Function	Mismatch	Bulge	Off target position
1	KCNK10	Potassium channel	4	0	625
1	NRIP3	Binding protein	4	0	934
1	SH3BP5	Binding protein	4	0	789
2	ARHGAP35	Repressor of glucocorticoid receptor transcription	2	1	336
2	CACNA1D	L-type calcium channel	4	0	805
2	HMGA2	Transcriptional regulating factor	2	1	521
2	PAMR1	Regeneration associated muscle protease	3	0	513
3	CYFIP2	FMR1-interacting protein	4	0	330
3	MLXIPL	Transcription factor	3	0	368
3	SELPLG	P-selectin receptor	3	0	1109
3	SH3BP5L	Binding protein	4	0	671
3	TP53BP2	Bcl2-binding protein	4	0	589

Table 3.1 Possible off-target sites that were screened in the CACNA1C knockout lines. The off-target position corresponds to its position within the PCR amplification.

A 750-12500bp region encompassing the possible off-target site was amplified by PCR for each gene in the iCas9 line and both CACNA1C knockout lines. The PCR products were then barcoded and sequenced using the Oxford Nanopore Technologies minION. The sequencing results are shown in Figure 3.2. The sequence 100 bp either side of the PAM site for each gene was examined for indels. Neither of the knockout lines contained indels when compared to the control line. For some genes (ARHGAP35, CACNA1D and CYFIP2) there was a nucleotide present that contained a mixture of reads in the iCas9 line that didn't appear present in one or both knockout lines. However, when looking closely at the data the consensus sequence was the same. For example, in CACNA1D the nucleotide at position 782 has roughly 80% G reads and 20% C reads, so would be labelled G. Both knockout lines also had a G nucleotide at this position. This is also the case for ARHGAP35 and CYFIP2. The appearance of a small percentage of reads with a different base is likely to be due to either miscalling during sequencing or errors in PCR amplification. Therefore, none of the lines contained indels or point mutations at the screened sites.

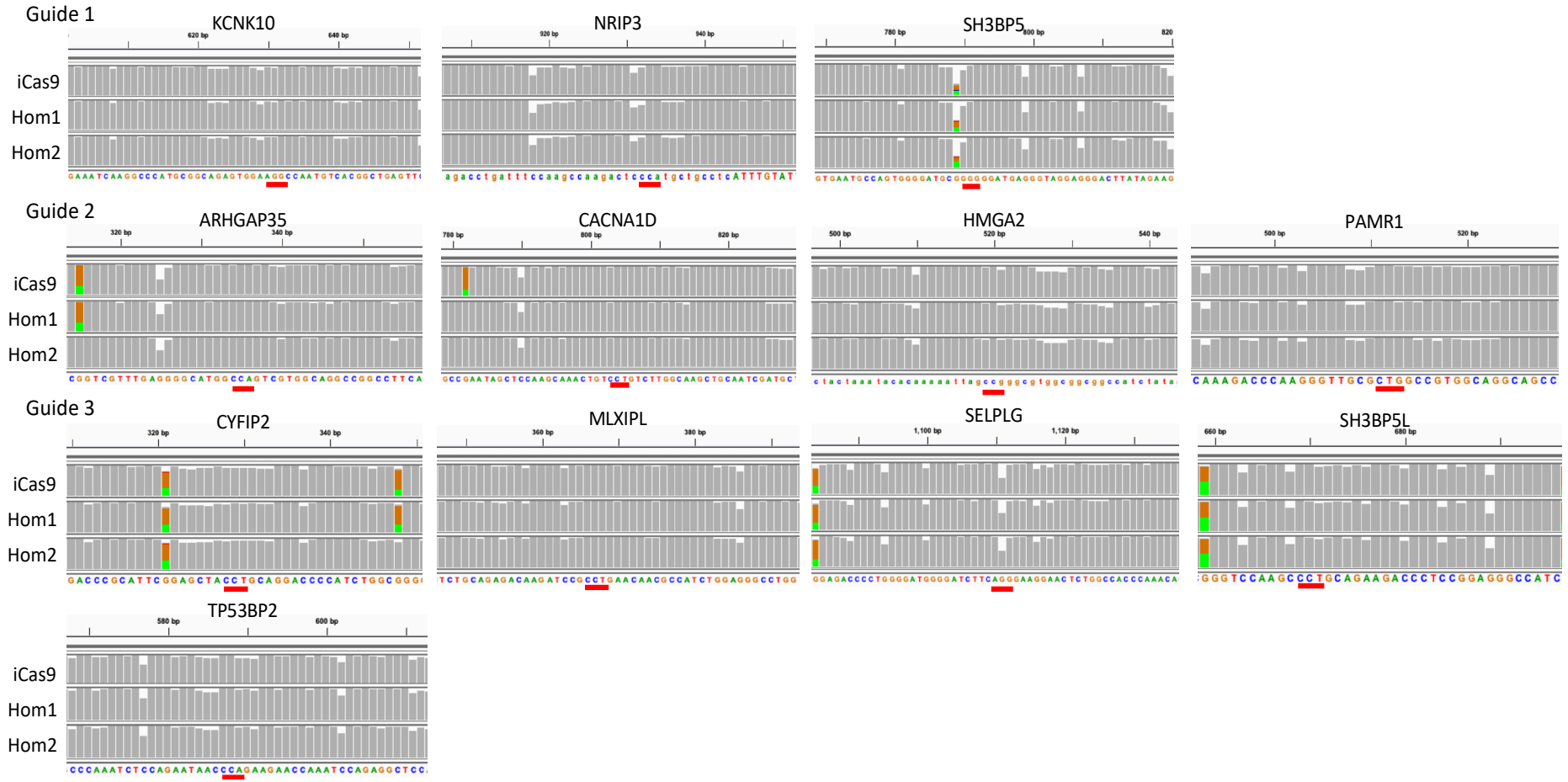

Figure 3.2 Sequencing of possible off-targets. Genomic DNA from iCas9, CACNA1C Hom1 and CACNA1C Hom2 cell lines was screened to identify if any off-target mutations occurred in the mutant lines. The height of the grey bars is proportional to the read coverage for each nucleotide. Coloured bars denote the nucleotide letter if it is mixed or differs from the reference sequence. The number of G (brown) and A (green) nucleotide reads is proportional to the size of each colour. The red lines denote the PAM sites for the guides. CACNA1C Hom1 and Hom2 sequences match the control iCas9 sequences and do not contain any indels.

3.2.3 Validation of loss of CACNA1C expression

Knockout of CACNA1C in the homozygous lines was verified at the protein level by western blot. Previous studies have shown that functional voltage gated calcium channels (VGCCs) are not expressed in human stem cells (Forostyak et al. 2016). Therefore, a time-course was carried out in the control iCas9 line to verify when CACNA1C is expressed during neuronal differentiation. Samples were collected between day 10 and day 50 of the differentiation. The results show that the expression of CACNA1C increases over time. There is no visible expression of CACNA1C at Day 10 of the differentiation (neural stem cells) (0.00113 ± 0.00113). Once neurons have been produced at Day 30 there are low levels of expression (0.00232 ± 0.000423). However, expression of CACNA1C increases over time until day 50 of the neuronal differentiation, when it is highest (0.0217 ± 0.00872) (Figure 3.3a). Therefore, this time-point was used to verify loss of expression in the knockout lines. Hom1 and Hom2 showed a significant reduction, but not complete loss, of CACNA1C expression in both lines as determined by one-way ANOVA with Tukey's post hoc test ($F(2,14) = 8.6$, $p = 0.0037$) (Figure 3.3b). CACNA1C Hom1 (0.000718 ± 0.000228) showed a 76% reduction in CACNA1C expression compared to iCas9 (0.00302 ± 0.000688) ($p = 0.0079$). CACNA1C Hom2 (0.000842 ± 0.000129) showed a 72% reduction compared to iCas9 ($p = 0.0084$). There was no significant difference in CACNA1C expression between Hom1 and Hom2 ($p = 0.9796$).

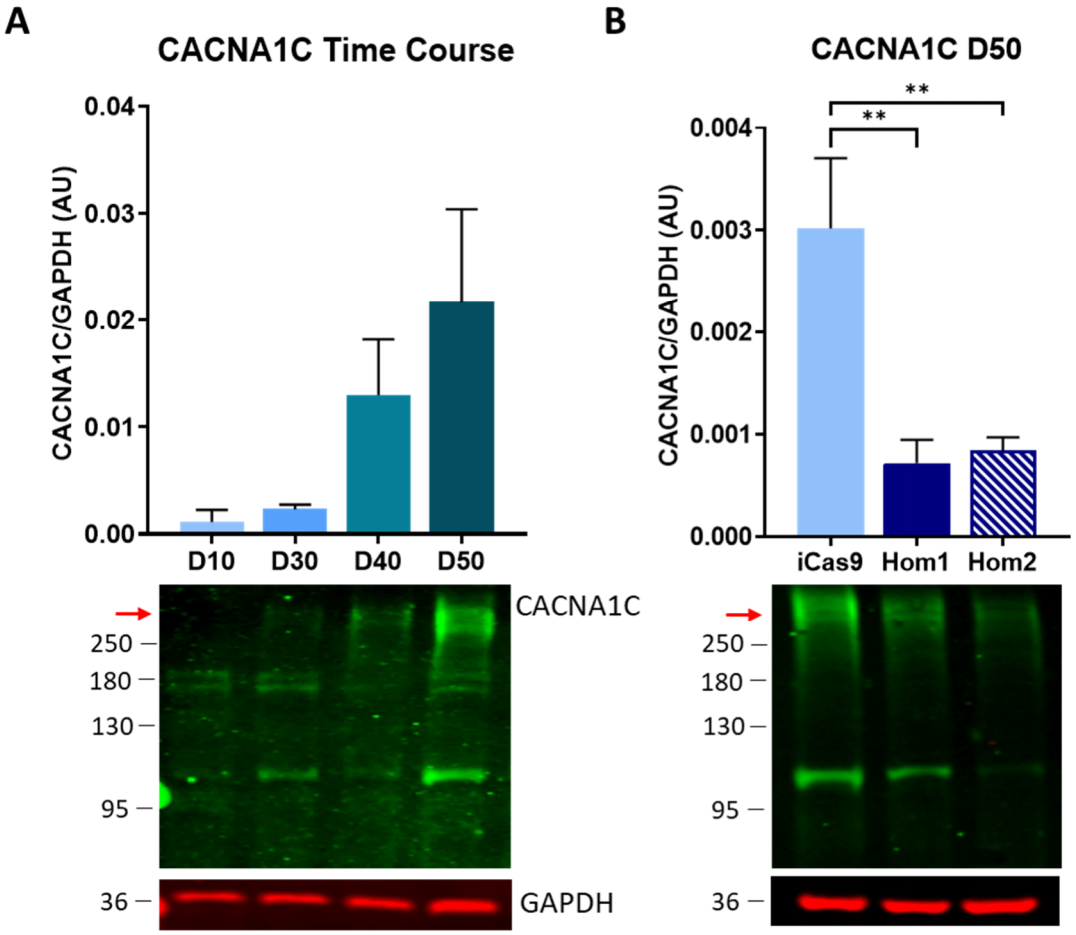

*Figure 3.3 Western blot for CACNA1C. (A) Expression of CACNA1C in iCas9 line at different time points during a neuronal differentiation. (B) Expression of CACNA1C in Day 50 neurons in the iCas9, CACNA1C Hom1 and Hom2 lines (** p<0.01). CACNA1C expression was normalised to GAPDH. Figure A shows summary data from 3 samples across one differentiation. Figure B shows summary data from 6 samples across two differentiations.*

In order to determine why there was some residual protein expression in the knockout lines RNA expression of CACNA1C at day 50 was also analysed (Figure 3.4a). qRT-PCR with primers targeting exon 3 to exon 4 of the gene, downstream of the deletions, was carried out. There was no significant difference in CACNA1C mRNA expression between iCas9, Hom1 and Hom2 lines, as determined by one-way ANOVA ($F(2,15) = 0.9988$, $p = 0.3915$), which suggests a lack of nonsense-mediated decay. It has been shown that residual protein expression can occur in lines containing out-of-frame deletions due to either exon-skipping or translation re-initiation (Smits et al. 2019). CACNA1C shows a highly complex splicing profile so it was possible that exon skipping may be responsible for the residual protein expression (Clark et al. 2020). Therefore, exon 1 to exon 4 of the RNA was amplified to determine if exon skipping

was occurring. The PCR products from the Hom1 and Hom2 lines were of the expected size and did not amplify any wild type transcripts. However, all 3 lines contained an additional band just over 200 bp (Figure 3.4b). This matches the size of DNA that would be amplified if exon 2 and 3 were skipped (216 bp). To verify if this was the case the PCR samples were barcoded according to the cell line and sequenced using the ONT minION (Figure 3.4c). The sequencing data did not show any sequences aligned to the CACNA1C transcript that were missing exon 2 and 3, suggesting the extra band was amplification of an unrelated product and not a product of exon skipping.

The other explanation for residual protein expression is translation re-initiation, due to the presence of methionine downstream of the deletion sites. There is a methionine present in exon 2 of the allele with a 47 bp deletion, however, it has been deleted in all other mutated alleles and the reduction in protein is consistent between both knockout lines. The next methionine present is in exon 6 of the gene (Figure 3.4d). This would lead to a reduction in protein size by roughly 30 kDa to 220 kDa, which matches the slight reduction seen in the size of CACNA1C protein on the Western blot. This is the most likely explanation for the residual protein expression seen in the knockout lines (Figure 3.3b). As both lines contain out-of-frame deletions in exon 2 and showed a similar reduction in expression of CACNA1C the data obtained from each line was pooled for analysis in future chapters.

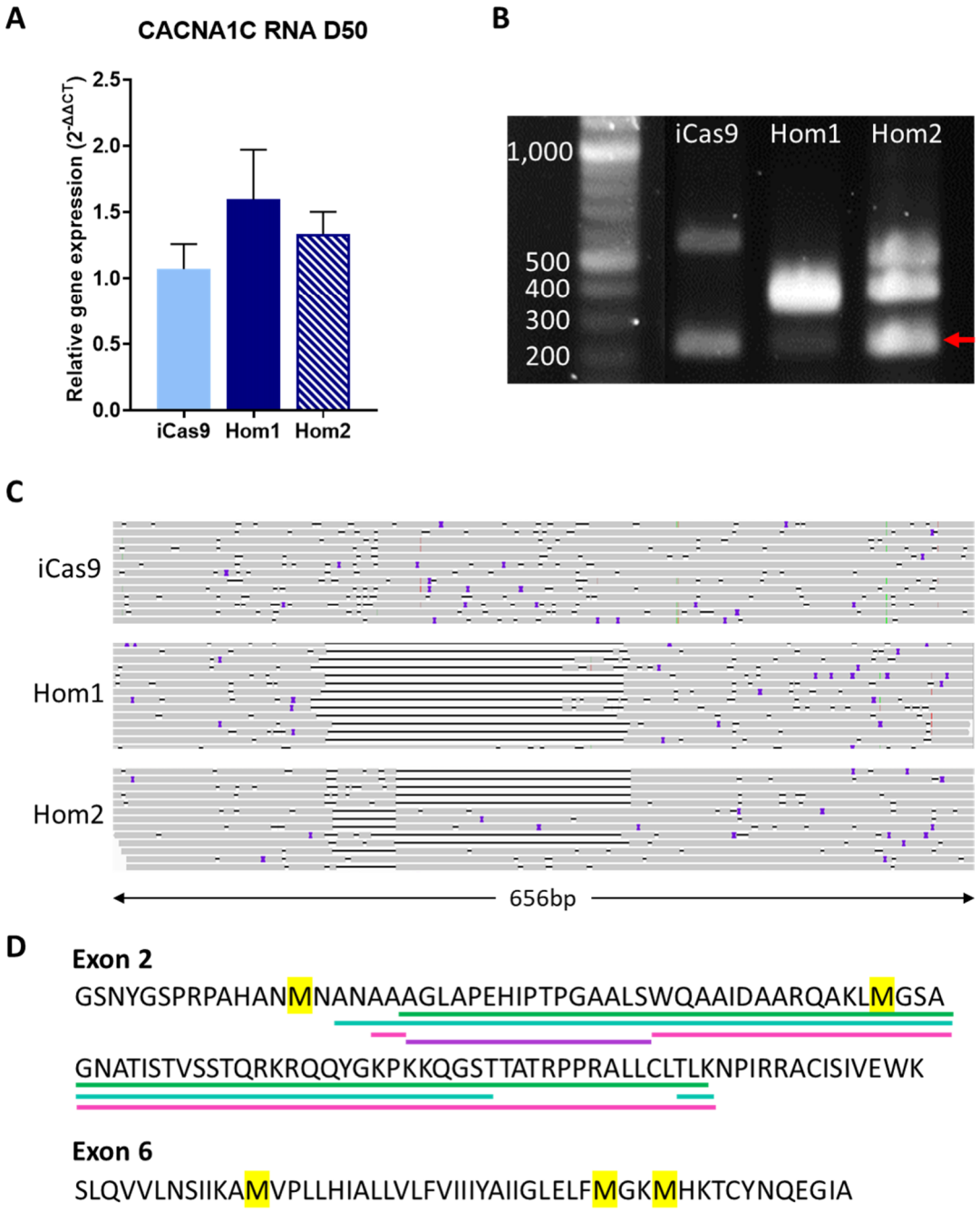

Figure 3.4 CACNA1C transcripts in knockout lines. (A) RNA expression of CACNA1C in Day 50 neurons relative to GAPDH and the iCas9 control line. Graph represents summary data from 6 samples across two differentiations (B) PCR amplification of exon 1 to 4 of CACNA1C RNA at Day 50. Arrow highlights additional band present around 200bp (C) Sequencing reads spanning exon 1 to 4 of CACNA1C day 50 RNA, black bars denote deletions. (D) Amino acid sequence of exon 2 and 6 of CACNA1C, methionine is highlighted in yellow. The position of each deletion is denoted by the coloured lines.

3.2.4 Characterisation of Atypical Timothy Syndrome line

iPSCs were derived from peripheral blood cells of an Atypical Timothy Syndrome patient carrying a novel point mutation in CACNA1C. The lines were generated by Olena Petter. Cells were genotyped to confirm no CNVs had been introduced to the line following reprogramming. They were genotyped using an Illumina Global Screening Array v3.0 and data analysed using PennCNV. No CNVs were present in the line. The point mutation (A1521P) occurs in exon 38 of CACNA1C at the end of the sixth transmembrane segment of domain IV (Figure 3.5a). Predicted pathogenicity of the mutation was performed using two sites. PolyPhen-2 predicted the mutation to be probably damaging with a score of 1.0 out of 1.0 (Adzhubei et al. 2010). Provean predicted the mutation to be deleterious with a median score of -4.807, scores equal to -2.5 or below are considered deleterious (Choi et al. 2012). The results from these sites indicates that there is a very high probability that the mutation will affect the function of Cav1.2.

Based on studies of other Timothy Syndrome mutations it is likely that this mutation will have a gain of function effect on Cav1.2 (Splawski et al. 2004; Splawski et al. 2005; Boczek et al. 2015; Wemhöner et al. 2015; Landstrom et al. 2016; Ozawa et al. 2018). To see if the point mutation also affects expression of CACNA1C samples from day 50 neurons were analysed using Western blot (Figure 3.5b). We did not have access to a familial control; therefore, the IBJ4 iPSC line was used as a control against the ATS line for all experiments. There was no significant difference in CACNA1C protein expression between the control and ATS line determined by t test ($p=0.7425$). This suggests that any differences found in the ATS line in future experiments are due to altered function of Cav1.2 and not altered expression.

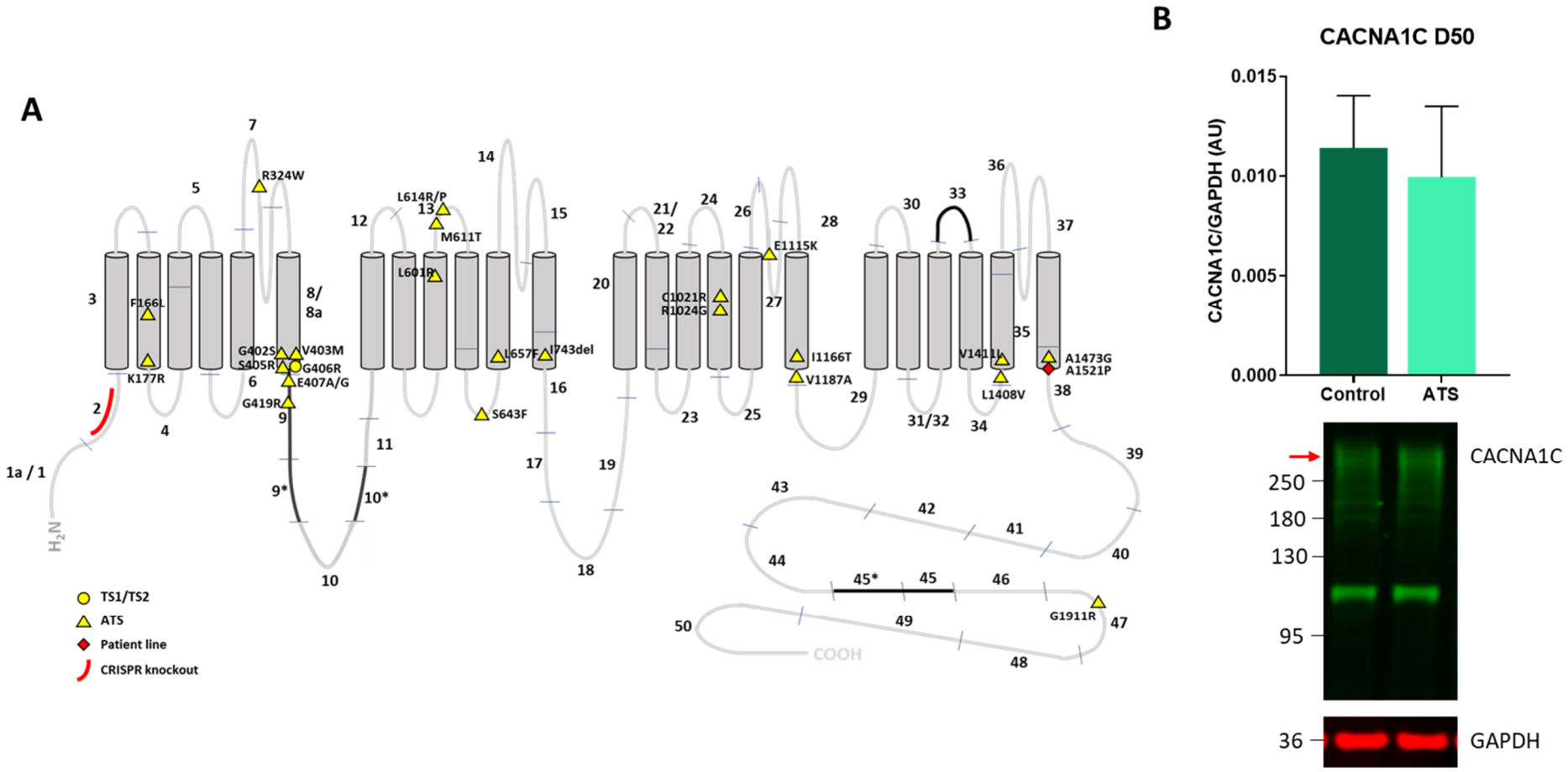

Figure 3.5 ATS line mutation and expression. (A) Schematic of CACNA1C structure indicating the position of published Timothy Syndrome mutations (yellow symbols) and the position of the mutation in the ATS patient line used in this thesis (red symbol). The red line indicates the position of the deletions in the knockout lines. (B) Expression of CACNA1C in Day 50 neurons in the IBJ4 control and ATS lines. CACNA1C expression was normalised to GAPDH. Figure B shows summary data from 6 samples across two differentiations for each line.

3.3 Discussion

This chapter describes the derivation of human iPSC lines that can be used to study the role of CACNA1C in neuronal development and increased risk of psychiatric disease. Lines modelling loss of CACNA1C were generated using an inducible-Cas9 (iCas9) iPSC line and guides targeting the first constitutive exon of CACNA1C (González et al. 2014). The iCas9 system was used as once expression is induced the only step required is the transfection of gRNAs. Other methods require cloning to produce plasmids or viral vectors allowing co-expression of Cas9 and gRNAs or co-transfection of the Cas9 protein with the guide (Kabadi et al. 2014; Zuris et al. 2015). The efficacy of guides is highly variable and multiple guides are usually tried in order to generate knockouts (Hiranniramol et al. 2020). This would mean generating multiple plasmids with different guides if using co-expression plasmids. However, with the iCas9 platform multiple gRNAs can be purchased for use immediately. Initially, each guide was used alone for CRISPR-Cas9 targeting. However, none of the guides used produced any clones containing an indel. Therefore, all 3 guides were transfected at once with the expectation that this would increase the chance of a mutation as if 2 or more guides cut the DNA strand it would lead to a large deletion between the cut sites, which is harder to repair than a single cut. Use of 3 guides led to the generation of 2 clones containing homozygous deletions in CACNA1C. No heterozygous deletions were found, which may be due to the enhanced efficiency of generating indels with multiple guides.

Using multiple guides enhanced the efficiency of gene editing, however this also leads to a higher risk of off-target mutations. Therefore, the knockout lines were screened for possible off-targets using targeted amplicon sequencing. Targeted amplicon sequencing is very sensitive and has a detection limit of 0.01% for off-targets (Hendel et al. 2015). It uses algorithms to generate potential off-target sites for guides based on mismatches in the genome and gRNA sequences (Concordet and Haeussler 2018). Some algorithms have also incorporated DNA structure, such as bulges in the DNA or RNA into predicting off-targets (Bae et al. 2014). This list of potential off-target sites can then be screened by PCR and sequencing. These lists

are ranked by size of the mismatches and bulges and mostly limited to 4bp mismatches. Off-targets could occur with higher mismatches or bulges and would be missed when screening sites, however the risk of these off-targets is very low (Hsu et al. 2013). Unbiased approaches such as GUIDE-Seq, which integrates double stranded oligodeoxynucleotides into double-strand breaks, have been generated to reduce the risk of missing these rare off-targets. However, this approach is less sensitive than amplicon sequencing (0.1% vs 0.01% detection limit) (Tsai et al. 2015). It is useful when using heterogenous cells for experiments, but subcloned cells containing the on-target mutation are very unlikely to contain these rare unpredicted off-target events, particularly as they seem to be rare in human pluripotent stem cells specifically (Smith et al. 2014; Veres et al. 2014). Therefore, targeted amplicon sequencing was used alone to determine if off-targets were present in the two knockout lines. As no off-target mutations were found at the screened sites we can be confident that it is unlikely there any off-target mutations in the lines. The use of two different lines also provides further confidence that if the same results are seen in both lines it is due to loss of CACNA1C and not an unknown off-target effect.

To validate loss of CACNA1C protein in the homozygous lines a time-course investigating CACNA1C expression across neuronal differentiation first had to be carried out. It has been previously shown that functional VGCCs are not expressed in human ESCs, although one study has shown that CACNA1C RNA and protein is expressed in human ESC lines, the channels are not functional (Malmersjö et al. 2010; Forostyak et al. 2016; Huang et al. 2017). Due to the evidence that no functional channels are expressed and the lack of sensitivity of the Cav1.2 antibody used it was not expected that it would be clearly detected in our iPSC samples therefore a time-course starting from day 10 of the differentiation, once neuroepithelial cells had been generated, was carried out. The time-course showed an increase in expression of CACNA1C over time. This time-dependent increase has also been shown in RNA-seq data looking at CACNA1C expression over cortical differentiation of human ESCs (van de Leemput et al. 2014). There was no visible protein expression of CACNA1C at day 10 and very little at day 30 of the differentiation once immature neurons have been generated. This suggests a lack of expression of CACNA1C in neural progenitor

cells (NPCs). However, it has previously been shown that human ESC-derived NPCs express functional LTCCs; Forostyak *et al.* (2016) showed protein expression of Cav1.2 specifically in ESC-derived NPCs. These channels are also important in the generation of neurons from NPCs as blockade of LTCCs during differentiation of rodent NPCs leads to a reduction in the number of neurons (D'Ascenzo et al. 2006; Lepski et al. 2013). CACNA1C is a larger protein (250kDa) and as mentioned previously antibodies available for it are not very sensitive, making it difficult to detect on a Western blot. It is therefore possible that CACNA1C is expressed in NPCs and immature neurons but was not at levels high enough to be detected on the Western blot.

The two homozygous lines were tested for loss of CACNA1C protein in day 50 neurons. The deletions on each allele in both lines cause a 2bp frameshift that leads to the generation of a stop codon at the start of exon 3. As both exon 2 and 3 are constitutive exons it was expected that this would lead to a complete loss of protein. However, both lines only showed around a 75% reduction in CACNA1C protein. qRT-PCR showed that RNA expression of CACNA1C was not reduced, implying a lack of nonsense-mediated decay. The two possibilities that could explain residual protein expression are exon-skipping and translation re-initiation (Smits et al. 2019). Exon 2 is constitutive and the exon-exon boundary between exons 2 and 3 encode a shared amino acid. Therefore, if exon-skipping was to occur both exons would be skipped, which would cause loss of the first transmembrane domain in the protein and disrupt the protein function. Sequencing of the transcripts suggested that this had not happened. This left translation re-initiation as a possible explanation. Based on the transcript sequence and slight reduction in protein size on the western blot we predict that translation re-initiation occurs at the methionine in exon 6 of CACNA1C in the knockout lines. This would generate a truncated protein missing the N-terminus and first 4 transmembrane domains. Loss of the transmembrane domains will disrupt the ability of Cav1.2 to form functional channels. In addition, the N-terminus and intracellular loops in this part of the channel are required for trafficking of the channel to the plasma membrane via interaction with the β subunit and CaMKII (Antzelevitch et al. 2007; Fang and Colecraft 2011; Simms et al. 2015). This

means any protein that is produced in the knockout lines is likely to remain in the cytoplasm and will not form functional calcium channels.

The ATS line contains a point mutation in exon 38 of CACNA1C (A1521P). Western blot showed that the mutation does not affect expression of the protein, but prediction sites suggested the mutation is highly damaging so is therefore likely to affect function of the channel. The best way to determine the effect of the mutation on Cav1.2 function would be to perform patch clamp experiments, however due to time constraints this was not carried out. Instead, we can use information from the effect of other CACNA1C mutations to predict the effect of the A1521P mutation on channel function. Typical TS mutations (G402S and G406R) lead to impaired voltage dependent inactivation (VDI) of the channel, this has a gain-of-function effect on Cav1.2 due to prolonged opening of the channel (Splawski et al. 2005; Walsh et al. 2018). Mutations in exon 14 (S643F) and exon 28 (I1166T) also cause impaired VDI, but they also alter Cav1.2 channel current and activation (Boczek et al. 2015; Wemhöner et al. 2015; Ozawa et al. 2018). The only ATS mutations that have been studied that does not cause a gain of function effect are E115K in exon 27, which causes a loss of ion selectivity of the channel allowing inward potassium and sodium currents but reduced inward calcium current and L1408V in exon 35 which causes a reduction in current density (Ye et al. 2019; Rodan et al. 2021). The E115K mutation occurs on one of the re-entrant loops of the channel, which is important for cation selectivity and the L1408V mutation occurs on an intracellular loop (Figure 3.5a). As the mutation in the ATS iPSC line occurs at the end of a transmembrane domain it is likely to have a similar gain-of-function effect on the channel as the mutations in exon 8 and exon 28.

In addition to TS-causing mutations in CACNA1C there are also mutations that cause LQT syndrome only. The effect of these mutations on channel function may provide further insight into the effect of the mutation in our patient line. In particular there is a mutation in CACNA1C two amino acids downstream of the mutation in our patient line that causes LQT syndrome (Wemhöner et al. 2015). This mutation is at amino acid 1523 when aligned to the same CACNA1C transcript as our patient

mutation but is referred to as I1475M in the publication as it is aligned to a different transcript (Bateman et al. 2015). The mutation had no effect on current amplitude but showed a gain of function shift in voltage-dependent activation and impaired VDI leading to an overall gain of function effect on Cav1.2. When combining the information of the effect of this mutation and the TS mutations we can predict that the A1521P mutation is likely to have a gain of function effect on Cav1.2 function via impaired VDI and possibly a leftward shift in voltage dependent activation.

3.3.1 Conclusion

This chapter describes the generation of CACNA1C homozygous knockout iPSC lines. Although the lines show residual protein expression further analysis of RNA transcripts suggest that the protein produced will not be functional. Therefore, the lines will be used to model full functional knockout of CACNA1C in iPSC derived neurons. In addition, the ATS patient line was characterised and showed no changes to CACNA1C expression, however *in silico* analysis predicted that the mutation is highly damaging, and we predict it will have a gain of function effect on Cav1.2. Both the knockout and ATS lines will be used to elucidate the role of CACNA1C in neuronal development and network activity.

4 Phenotypic analysis of CACNA1C knockout and atypical Timothy Syndrome iPSC lines during cortical differentiation

4.1 Introduction

Calcium signalling plays an important role in neurodevelopment, including dendritic growth, neuronal migration, and neuron specification (Rosenberg and Spitzer 2011; Mire et al. 2012; Kanamori et al. 2013; Vitali et al. 2018). Spontaneous calcium waves increase during corticogenesis and have been linked to the generation of different neuronal subtypes (Weissman et al. 2004). TS models suggest that Cav1.2 specifically plays a role in the types of neurons that are generated during neurodevelopment. TS has been linked to the generation of cortical layer neurons, with a decrease in the number of cells expressing lower layer markers but an increase in upper layer markers in iPSC-derived neurons generated from TS1 patients (Paşca et al. 2011). Both iPSC-derived neurons and mouse models of TS have shown that layer V neurons specifically have decreased expression of SATB2, which is necessary for the specification of callosal projection neurons. However, they also show an increase in CTIP2 expression, which is necessary for subcerebral projection neurons. The opposite effect is found following loss of one copy of CACNA1C in mice along with a reduction of TBR1, a marker of layer VI cortico-thalamic projection neurons (Panagiotakos et al. 2019). Research in iPSC-derived neurons has also shown that TS patient lines have increased expression of GAD67, TH and CALY, enzymes required to produce the neurotransmitters GABA, noradrenaline and dopamine (Paşca et al. 2011). In addition to neurotransmitter production, TS1 mutations have been shown to impair the migration of both excitatory and inhibitory neurons and cause increased dendritic retraction (Krey et al. 2013; Birey et al. 2017; Kamijo et al. 2018).

LTCCs generally have also been shown to be involved in the overall generation of neurons from NPCs. In culture, when rodent NPCs are differentiated in the presence of nifedipine they produce less neurons, and these neurons are more poorly differentiated with fewer synapses. However, the opposite occurs in the presence of

LTCC activator Bay K 8644, more neurons are produced and they are more electrophysiologically mature (D'Ascenzo et al. 2006; Lepski et al. 2013). Cav1.2 has also been shown to play a role in the generation of neurons in the adult brain. Conditional and heterozygous knockout models of Cav1.2 in rodents has been shown to reduce the number of new neurons produced in the hippocampus during adult neurogenesis (Lee et al. 2016; Temme et al. 2016; Völkening et al. 2017; Moon et al. 2018). This suggests a role for Cav1.2 specifically in neuron generation.

Cav1.2 channels are likely to affect neurodevelopment via activation of various downstream signalling pathways. One pathway that has been implicated in the differentiation of NPCs into neurons via LTCCs is CREB. During differentiation of cultured rodent NPCs into neurons, phosphorylation of CREB is increased. Phosphorylation of CREB allows it to bind to cAMP response elements (CRE) which leads to increased expression of a range of neuronal genes (Herold et al. 2011). However when the LTCC blocker nifedipine is added to the cultures this increase in CREB is blocked, in addition to reducing differentiation and synapse formation (Lepski et al. 2013). LTCCs can activate CREB via two pathways, CaMKII or ERK1/2 signalling. Two different rodent models have shown that loss of CACNA1C leads to decreased phosphorylation of ERK1/2 and CREB (Moosmang et al. 2005; Tigaret et al. 2021). Conversely activation of CREB, CaMKII and ERK1/2 have all been shown to be increased in TS1 models (Li et al. 2016; Servili et al. 2020). In addition to this genes linked to CREB signalling, such as EGRI, FOS, FOSB, GAD1 and TH are also upregulated in TS1 patient iPSC-derived neurons (Paşca et al. 2011).

4.1.1 Chapter Aims

CACNA1C knockout iPSCs and ATS patient iPSCs were differentiated into excitatory cortical neurons. This chapter will investigate changes to the expression of developmental and neuronal markers across the neuronal differentiation protocol. This chapter will also investigate changes to the activation of downstream molecules ERK1/2 and CREB, as this may play a role in neuron generation.

4.2 Results

4.2.1 Phenotypic analysis of NPC markers

The results from Chapter 3 and other studies show that the expression of CACNA1C follows a time-dependent increase across the course of a neuronal differentiation. It is not functionally expressed in iPSCs and is present at low levels in NPCs (Forostyak et al. 2016). Therefore, it is unlikely to have any effect on the generation of NPCs. To confirm that this was the case RNA samples were taken at day 10 and 20 of the differentiation. Neural induction with LDN and SB leads to the generation of neuroepithelial cells by day 10. Over the next 10 days neural rosettes form (Figure 4.1a) and by day 20 the cells start to generate neurons (Figure 4.1b).

Expression of Nestin, Pax6 and FoxG1 were measured in all lines as these are markers of NPCs. Nestin is an intermediate filament protein that is used as a general neural stem cell marker (Lendahl et al. 1990). Pax6 and FoxG1 are both transcription factors and are markers for neuroepithelial cells and telencephalic-specific forebrain neural stem cells, respectively (Callaerts et al. 1997; Chambers et al. 2009; Manuel et al. 2011). The telencephalon forms part of the forebrain, particularly the cerebral cortex. The were no significant changes to the expression of these genes at day 10 and 20 of the differentiation in CACNA1C knockout lines when compared to the iCas9 control line (Figure 4.1c-e). The ATS line showed no significant differences in Nestin and Pax6 expression but did show a significant increase in expression of FoxG1 at day 20 (3.115±1.638 vs 11.217±2.230 fold change relative to day 10 control) (Figure 4.1f-h). Table 4.1 presents a summary of the statistics for the gene expression data.

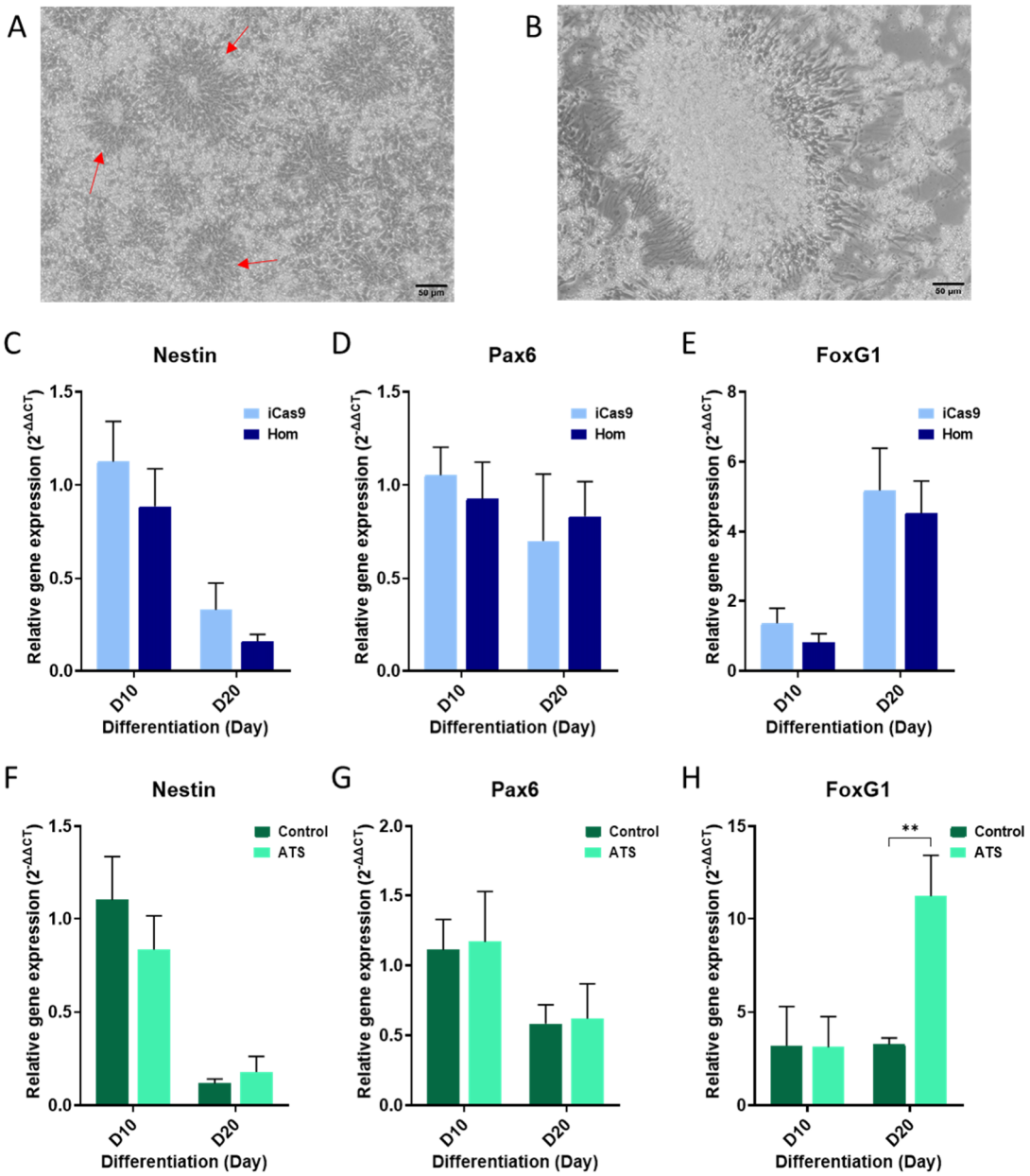

*Figure 4.1 Gene expression of NPC markers during the first 20 days of neuronal differentiation. (A) Image of neural rosettes at Day 11, ATS line (B) Image of cells at Day 21 once NPCs have started to generate neurons, ATS line. (C-E) RNA expression of Nestin, Pax6 and FoxG1 in iCas9 and Hom lines at day 10 and 20. (F-H) RNA expression of Nestin, Pax6 and FoxG1 in control and ATS lines. All genes were normalised to GAPDH and show expression level relative to the relevant control line at day 10. Plots represent summary data from 6 samples across two differentiations except the Hom line which represents data from two differentiations each of both Hom1 and Hom2 lines (12 samples total) (** p<0.01).*

Groups	Gene	Main Effect	2 Way ANOVA	Sidak's multiple comparisons
iCas9 Hom	Nestin	Time	F (1, 32) = 19.61, **P=0.0001**	No post-hoc comparisons
		Genotype	F (1, 32) = 1.407, P=0.2443	
	Pax6	Time	F (1, 32) = 0.9044, P=0.3487	No post-hoc comparisons
		Genotype	F (1, 32) = 0.0002, P=0.9901	
	FoxG1	Time	F (1, 32) = 21.59, **P<0.0001**	No post-hoc comparisons
		Genotype	F (1, 32) = 0.5466. P=0.4651	
Control ATS	Nestin	Time	F (1, 20) = 27.81, **P<0.0001**	No post-hoc comparisons
		Genotype	F (1, 20) = 0.4418, P=0.5138	
	Pax6	Time	F (1, 20) = 4.522, **P=0.0461**	No post-hoc comparisons
		Genotype	F (1, 20) = 0.03419, P=0.8552	
	FoxG1	Time	F (1, 20) = 5.481, **P=0.0297**	
		Genotype	F (1, 20) = 5.079, **P=0.0356**	D10 P=0.9993
				D20 **P =0.0085**

Table 4.1 Summary of statistics for gene expression of Nestin, Pax6 and FoxG1. Data was analysed using Two-way ANOVA followed by Sidak's multiple comparison test.

4.2.2 Impact of CACNA1C on the generation of neurons

Previous research has shown that blockade of LTCCs impairs the differentiation of rodent NPCs into neurons (D'Ascenzo et al. 2006; Lepski et al. 2013). To investigate if CACNA1C has a specific role in the generation of neurons in human cells the levels of neuronal markers MAP2 and β-III-tubulin were analysed. A larger number of immature neurons are produced by day 30 of the differentiation protocol and mature over time until the final timepoint at day 50. Therefore, the levels of Map2 and β-III-tubulin were analysed over this window. CACNA1C knockout lines showed a significant decrease in Map2 expression compared to iCas9 following two-way ANOVA (Figure 4.2a). However, post-hoc analysis did not show a significant difference at any specific time point (Day 30 1.742±0.769 vs 1.748±0.328, Day 40 3.103±0.769 vs 1.736±0.332, Day 50 3.119±0.169 vs 2.157±0.276). As both Map2 and β-III-tubulin are neuronal markers it was expected for them both to show decreased expression in the Hom line. The data at day 40 (3.127±1.151 vs 1.401±0.435) and day 50 (3.862±0.588 vs 2.112±0.342) suggest a trend towards a decrease in β-III-tubulin expression, however due to the high variability of the data, particularly at day 30 (2.109±1.288 vs 4.995±1.523), there was no significant difference in β-III-tubulin expression between iCas9 and Hom lines (Figure 4.2b). As the knockout lines showed

a decrease in MAP2 levels, it was expected that the ATS line may show the opposite trend, however the ATS line showed no significant changes to Map2 expression (Figure 4.2c). The ATS line also showed no changes to β-III-tubulin expression across the differentiation from day 30-50 (Figure 4.2d). Table 4.2 presents a summary of the statistics for this data.

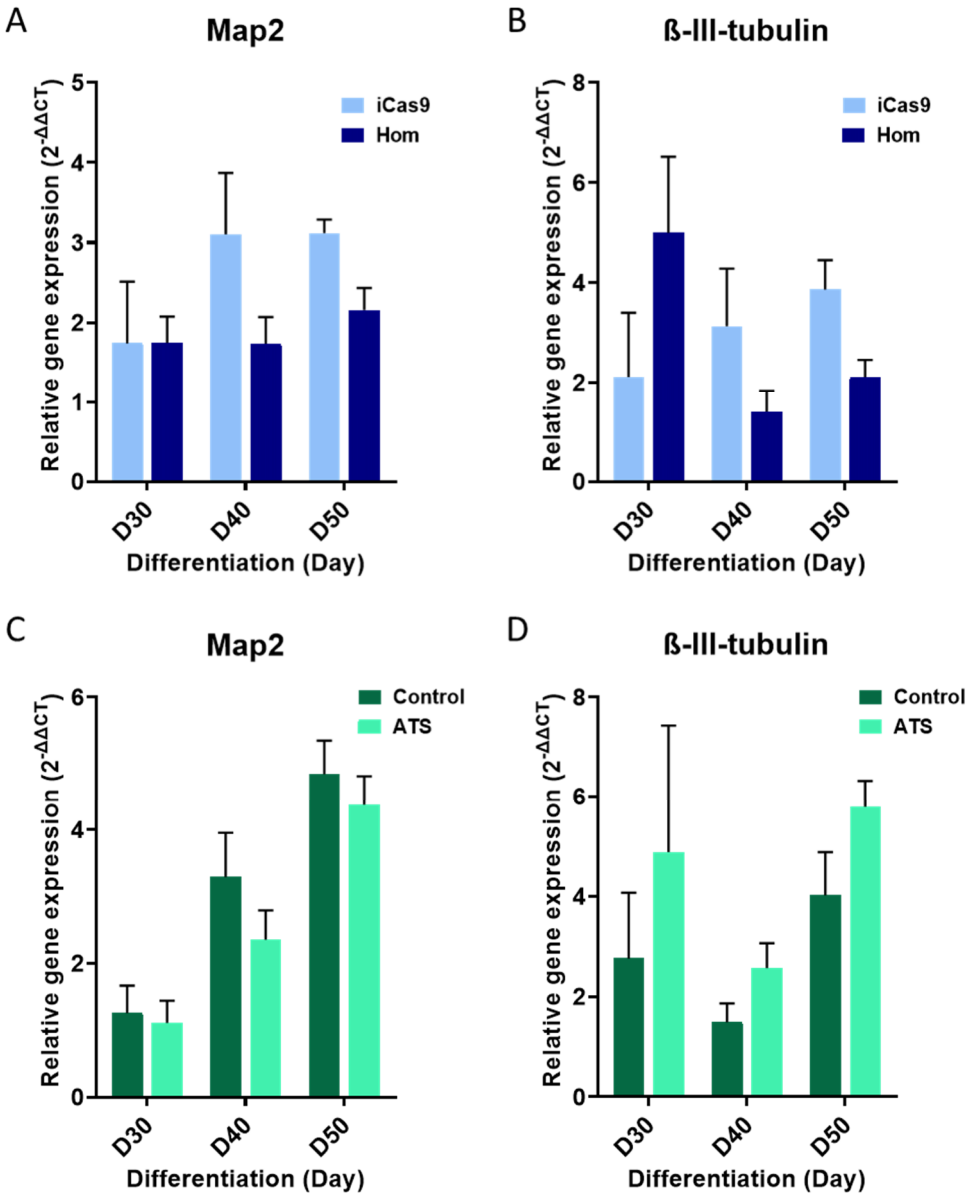

Figure 4.2 Relative gene expression of Map2 and ß-III-tubulin from day 30 to 50 of neuronal differentiation. (A-B) Expression of neuronal markers Map2 and ß-III-tubulin in iCas9 and Hom lines. (C-D) Expression of Map2 and ß-III-tubulin in IBJ4 and ATS lines. All genes were normalised to GAPDH and show expression level relative to the relevant control line at day 30. Plots represent summary data from 6 samples across two differentiations, except the Hom line which represents data from two differentiations each of both Hom1 and Hom2 lines (12 samples total).

Groups	Gene	Main Effect	2 Way ANOVA	Sidak's multiple comparisons
iCas9 Hom	Map2	Time	F (2, 48) = 2.214, P=0.1204	
		Genotype	F (1, 48) = 4.592, **P=0.0372**	D30 P>0.999
				D40 P=0.0983
				D50 P=0.3433
	β-III-tubulin	Time	F (2, 48) = 0.7167, P=0.4935	No post-hoc comparisons
		Genotype	F (1, 48) = 0.04980, P=0.8244	
Control ATS	Map2	Time	F (2, 30) = 26.01, **P<0.0001**	No post-hoc comparisons
		Genotype	F (1, 30) = 1.790, P=0.1910	
	β-III-tubulin	Time	F (2, 30) = 2.632, P=0.0885	No post-hoc comparisons
		Genotype	F (1, 30) = 2.564, P=0.1198	

Table 4.2 Summary of statistics for gene expression of Map2 and β-III-tubulin. Data was analysed using Two-way ANOVA followed by Sidak's multiple comparison test.

To determine whether the decrease in MAP2 RNA expression in the CACNA1C knockout lines also occurred at the protein level lines were fixed and stained for MAP2 at day 50 of the differentiation (Figure 4.3a). Knockout lines showed a significant decrease in MAP2 expression relative to DAPI as determined by T-test (1.403±0.082 vs 0.7604±0.0640, t(16)=5.954, p<0.0001) (Figure 4.3b). In addition, groups of cells that appeared to have a similar morphology to neuronal rosettes were counted; these were identified by radial arrangement of cells, however due to a lack of staining for markers cannot be conclusively identified as rosettes. Homozygous lines showed a significant increase in the number of these rosette-like structures as determined by T-test (0.1713±0.0243 vs 0.4355±0.01917, t(16)=8.210, p<0.0001). This increase in rosette-like structures suggests a greater proportion of NPCs are still present in the culture and thus may explain the decrease in expression of MAP2 seen at both the RNA and protein level. The ATS line was also stained to analyse MAP2 expression and rosette-like strucutre numbers. There was no difference in MAP2 expression as determined by Welch's T-test (1.033±0.166 vs 1.148±0.054, t(6.023)=0.6554, p=0.5364), consistent with the findings at RNA level, suggesting no differences in the number of neurons between control and ATS. However, there was a decrease in the number of rosette-like structures in the ATS line determined by T-test (0.2868±0.0407 vs 0.1559±0.0304, t(10)=2.575, p=0.0277).

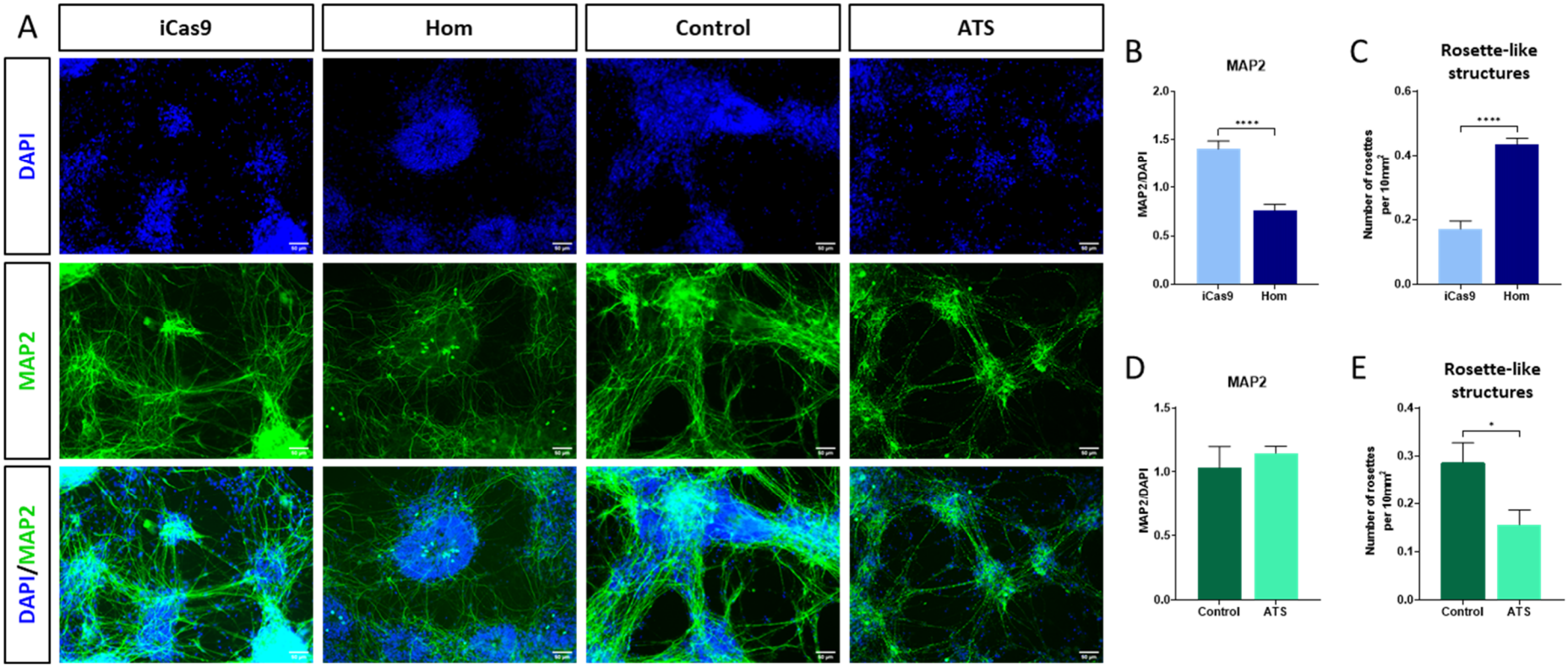

Figure 4.3 Immunostaining of MAP2 (green) and DAPI (blue) at day 50 in iCas9, Hom, control and ATS neurons. (A) Example images of staining (B, D) Quantification of MAP2 positive neurons relative to DAPI, measured by area of positive cells. (C, E) Number of rosettes present relative to the area of DAPI positive cells. Plots represent summary data from 6 samples across one differentiation, except the Hom line which represents data from one differentiation each of both Hom1 and Hom2 lines (12 samples total).

4.2.3 Analysis of neuronal subtypes

The neuronal differentiation protocol produces mostly cortical glutamatergic neurons. However, a small percentage of the neurons produced are GABAergic (Plumbly et al. 2019). The presence of GABAergic neurons is important for the generation of synchronised neuronal activity, which will be discussed in Chapter 5, and imbalances in excitatory and inhibitory signalling has been consistently implicated in psychiatric disorders, particularly ASD (Fatemi et al. 2002; Yip et al. 2009; Mariani et al. 2015; Marchetto et al. 2017). To investigate if CACNA1C alters this balance the expression of glutamatergic markers (vGlut1 and vGlut2) and GABAergic markers (GAD65, GAD67, VGAT and LHX6) was tested in day 50 neurons (Figure 4.4). Knockout of CACNA1C had no significant effect on the expression of glutamatergic markers. However, it led to a significant decrease in GAD65 expression ($t(16)=7.124$, $p=0.000002$, adjusted $p=0.00001$). Expression of the other GABAergic markers (GAD67, VGAT and LHX6) was also lower in knockout lines compared to control but this was not statistically significant (Table 4.4). The ATS line also had no effect on the expression of glutamatergic markers. However, it did have the opposite effect of the Hom lines, showing a significant increase in GAD65 expression, ($t(10)=3.172$, $p=0.0099$, adjusted $p=0.0392$). There were no significant differences in the other GABAergic markers that were analysed, as in the knockout line.

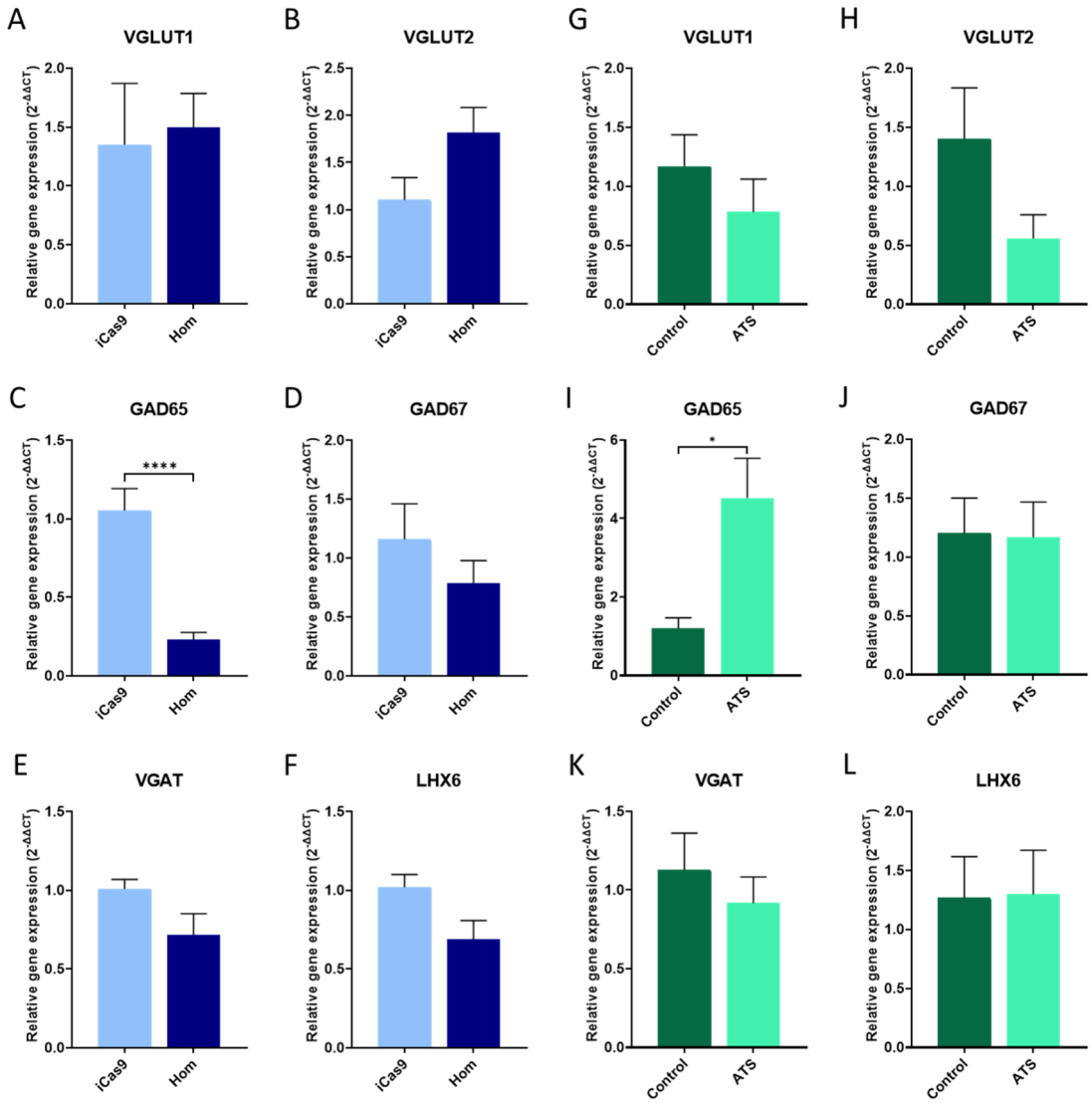

*Figure 4.4 Relative gene expression of Glutamatergic and GABAergic markers at Day 50 of neuronal differentiation. (A-F) Expression of glutamatergic markers (VGLUT1 and VGLUT2) and GABAergic markers (GAD65, GAD67, VGAT and LHX6) in iCas9 and Hom lines. (G-L) Expression of glutamatergic markers (VGLUT1 and VGLUT2) and GABAergic markers (GAD65, GAD67, VGAT and LHX6) in Control and ATS lines. All genes were normalised to GAPDH and show expression level relative to the relevant control line. Plots represent summary data from 6 samples across two differentiations except the Hom line which represents data from two differentiations each of both Hom1 and Hom2 lines (12 samples total) (**** p<0.0001).*

Gene	iCas9 vs Hom			Control vs ATS		
	Fold Change (mean±SEM)	**P value**	**Adjusted P value**	**Fold Change (mean±SEM)**	**P value**	**Adjusted P value**
VGLUT1	2.21±0.76	0.7897	0.7897	0.78±0.28	0.3383	0.3383
VGLUT2	1.81±0.27	0.1097	0.2074	0.55±0.20	0.1060	0.2008
GAD65	0.23±0.05	**0.000002**	**0.00001**	4.56±1.01	**0.0099**	**0.0392**
GAD67	0.78±0.19	0.2938	0.2938	1.17±0.30	0.9338	0.9956
VGAT	0.71±0.13	0.1582	0.2913	0.92±0.17	0.4791	0.8586
LHX6	0.69±0.12	0.0834	0.2299	1.29±0.37	0.9546	0.9956

Table 4.3 Summary of statistics for gene expression analysis of glutamatergic and GABAergic markers at day 50. Data was analysed using unpaired t-test, Holm-Sidak correction for multiple comparisons was used to generate adjusted P values

To identify if the changes to the enzymes responsible for GABA production also occurred at protein level neurons were stained at day 50 for both GAD65 and GAD67 (Figure 4.5a). If the amount of both GAD65- and GAD67-positive staining was altered this would suggest an overall change in the number of GABAergic neurons as opposed to a change in the amount of GAD65 expressed in each neuron. The knockout lines showed a significant decrease in both GAD65 (0.0907±0.0026 vs 0.0489±0.0108, $t(7)=2.620$, $p=0.0344$) and GAD67 (0.2283±0.0021 vs 0.1021±0.0298, $t(5.051)=4.22$, $p=0.0081$) expression compared to the iCas9 line (Figure 4.5b-c). The ATS line showed the opposite effect with an increase in both GAD65 (0.0294±0.0060 vs 0.0911±0.0127, $t(4)=4.396$, $p=0.0117$) and GAD67 (0.0345±0.0024 vs 0.05673±0.0053, $t(4)=3.795$, $p=0.0192$) expression (Figure 4.5d-e).

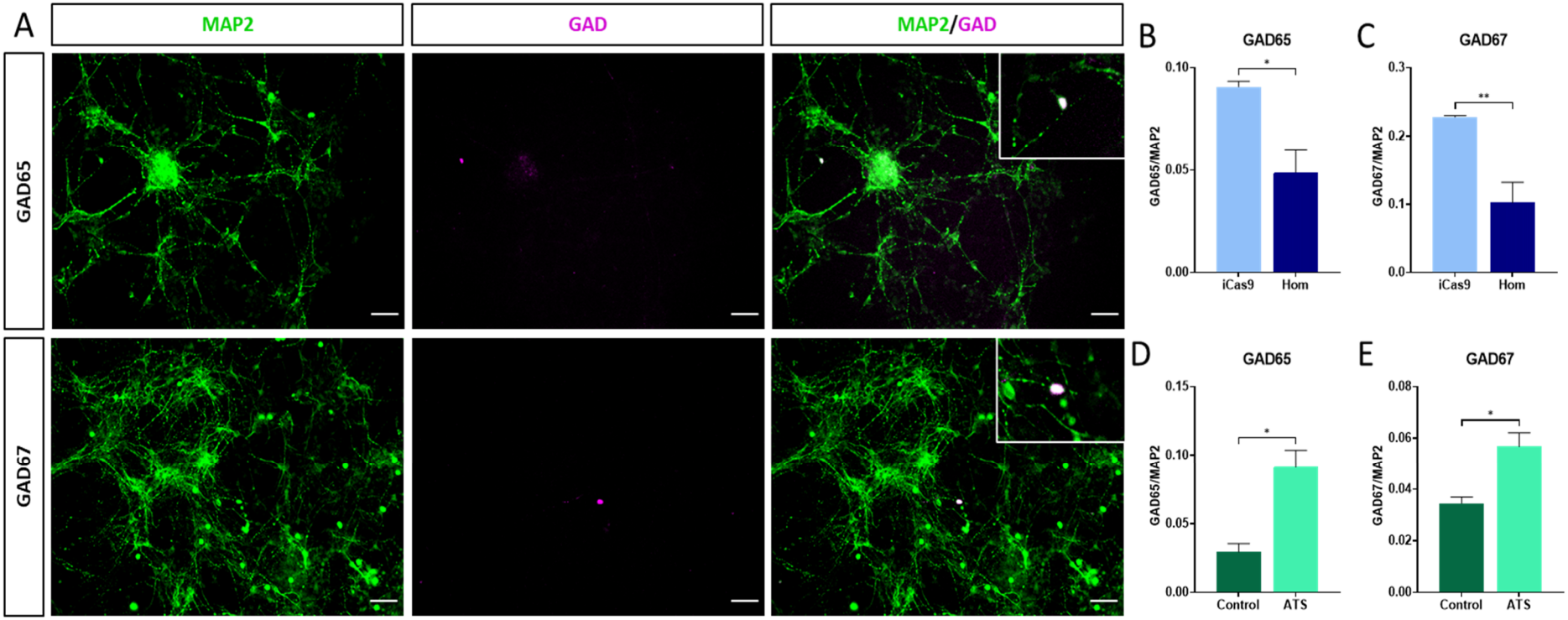

Figure 4.5 GAD65 and GAD67 immunostaining in day 50 neurons (A) Example of immunostaining of MAP2 (green) and GAD65 or GAD67 (pink). All images are of ATS line. (B, D) Quantification of GAD65 expression relative to MAP2, measured by area of positive cells. (C, E) Quantification of GAD67 expression relative to MAP2I, measured by area of positive cells. Plots represent summary data from 3 samples across one differentiation, except the Hom line which represents data from one differentiation each of both Hom1 and Hom2 lines (6 samples total).

The cortical neurons produced by this differentiation protocol have a mostly lower layer identity, with low expression of upper layer markers, due to the sequential generation of cortical layers from lower to upper layers (Shi et al. 2012). The expression of cortical layer markers has been shown to be altered in iPSC-derived neurons from patients with TS and the opposite effect occurs in a heterozygous CACNA1C model (Paşca et al. 2011; Panagiotakos et al. 2019). Therefore, the expression of cortical layer markers TBR1, CUX1, CTIP2 and SATB2 were tested in the ATS and homozygous lines (Figure 4.6). TBR1 is expressed in deep layer VI neurons and also in layer I Cajal-Retzius cells, whereas SATB2 and CUX1 are expressed in upper layer projection neurons (layers II-III) (Hevner et al. 2001; Britanova et al. 2008; Franco et al. 2012; Mukhtar and Taylor 2018) (Figure 4.6i). CTIP2 is expressed in subcerebral projection neurons in layer V. SATB2 is also present in a small number of neurons in layers IV and V as a marker of corticothalamic projection neurons and CTIP2 can also be expressed in a small amount of upper layer neurons (Chen et al. 2005; Alcamo et al. 2008) (Britanova et al. 2008). None of the layer markers were significantly different in both the homozygous and ATS lines. However, the knockout and ATS lines appeared to have opposite effects on TBR1 expression with the knockout showing a trend towards an increase in TBR1 gene expression and the ATS line a decrease compared to controls. Table 4.4 presents a summary of the statistics for this data.

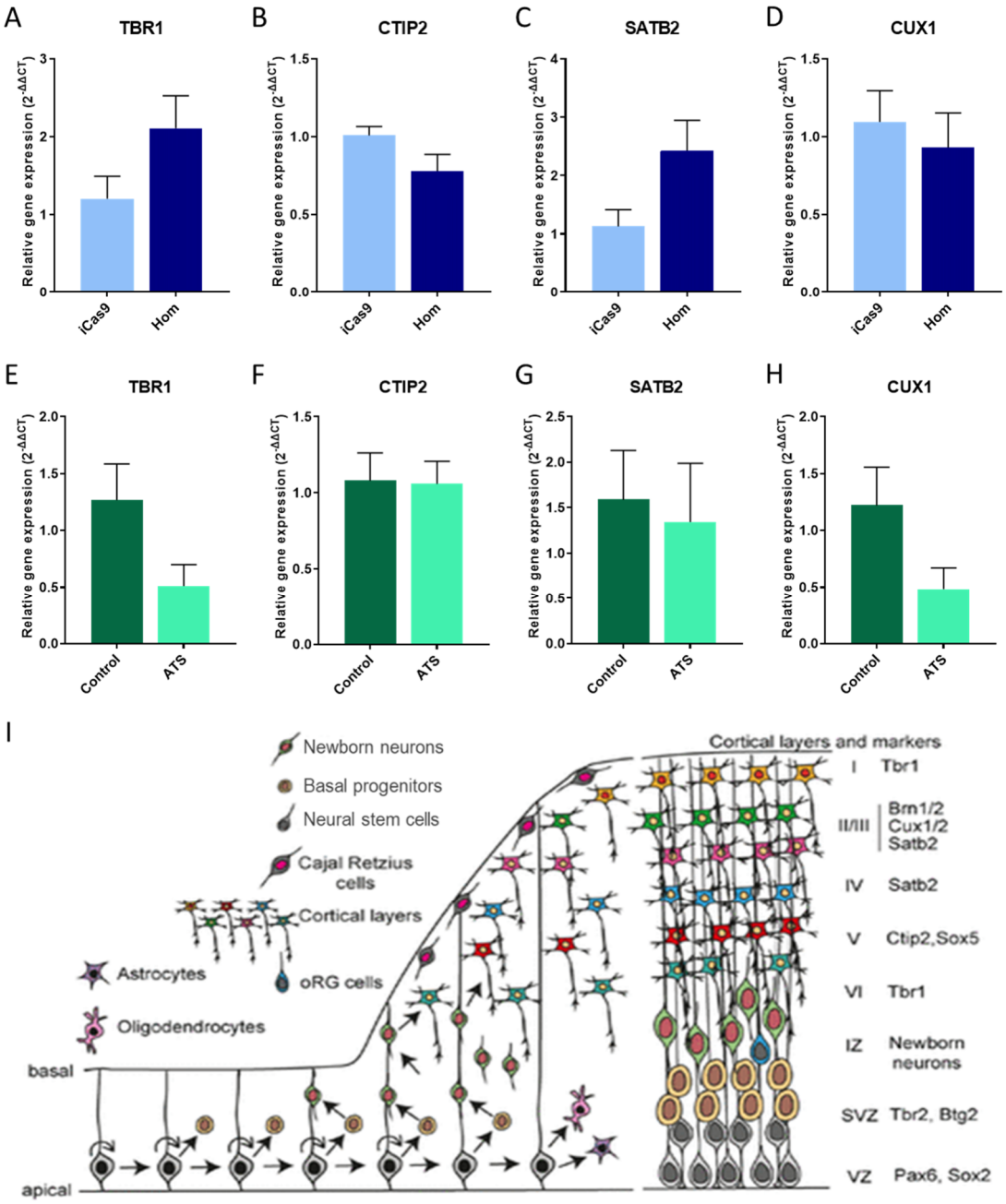

Figure 4.6 Relative gene expression of cortical layer markers at day 50 of neuronal differentiation. (A-D) Expression of TBR1, CTIP2, SATB2 and CUX1 in Hom lines relative to iCas9. (E-H) Expression of TBR1, CTIP2, SATB2 and CUX1 in ATS line relative to control. All genes were normalised to GAPDH. Plots represent summary data from 6 samples across two differentiations except the Hom line which represents data from two differentiations each of both Hom1 and Hom2 lines (12 samples total). (I) Diagram of cortical development. Formation of different cortical layers; neurons are generated sequentially from deep to upper layers and specified by different transcription factors as shown in the diagram. IZ = intermediate zone, SVZ = subventricular zone, VZ = ventricular zone. (Figure from Mukhtar & Taylor, 2018).

Gene	iCas9 vs Hom			Control vs ATS		
	Fold Change (mean±SEM)	P value	Adjusted P value	Fold Change (mean±SEM)	P value	Adjusted P value
TBR1	2.11±0.42	0.1719	0.4216	0.51±0.19	0.0679	0.2451
CTIP2	0.78±0.11	0.1668	0.4216	1.05±0.15	0.9249	0.9500
SATB2	2.43±0.52	0.1099	0.3723	1.34±0.65	0.7765	0.9500
CUX1	0.93±0.22	0.6406	0.6406	0.48±0.19	0.0838	0.2451

Table 4.4 Summary of statistics for gene expression analysis of cortical layer markers at day 50. Data was analysed using unpaired t-test, Holm-Sidak correction for multiple comparisons was used to generate adjusted P values.

4.2.4 Analysis of downstream ERK1/2 and CREB signalling

It has previously been shown that blockade of L-type calcium channels leads to a reduction in the generation of neurons via CREB signalling (D'Ascenzo et al. 2006; Lepski et al. 2013). As CACNA1C homozygous lines showed a reduction in MAP2 expression it was hypothesised that this may be due to a reduction in CREB signalling. Cav1.2 channels can activate CREB-dependent gene expression via two main pathways; activation of CaM kinases and the Ras-ERK pathway (Wu et al. 2001). We investigated whether knockout of CACNA1C reduced CREB phosphorylation via the Ras-ERK pathway during multiple timepoints of the differentiation. Day 20 was chosen as this is the timepoint when the culture is mostly NPCs but are starting to generate neurons and day 30 as there is mostly immature neurons by this timepoint. There was a significant reduction in ERK1/2 and CREB signalling at both these timepoints in the Hom lines (Figure 4.7a-b, d-e). ERK1/2 and CREB phosphorylation was also checked once mature neurons had been generated at day 50 of the differentiation. Loss of CACNA1C led to a reduction in ERK1/2 phosphorylation (Figure 4.7c). There was no difference in phosphorylation of CREB at day 50 in the Hom line when measured relative to total CREB (Figure 4.7f). However, there was a reduction in total CREB expression relative to GAPDH, which means there was an overall reduction in CREB phosphorylation in the homozygous lines (Figure 4.7g).

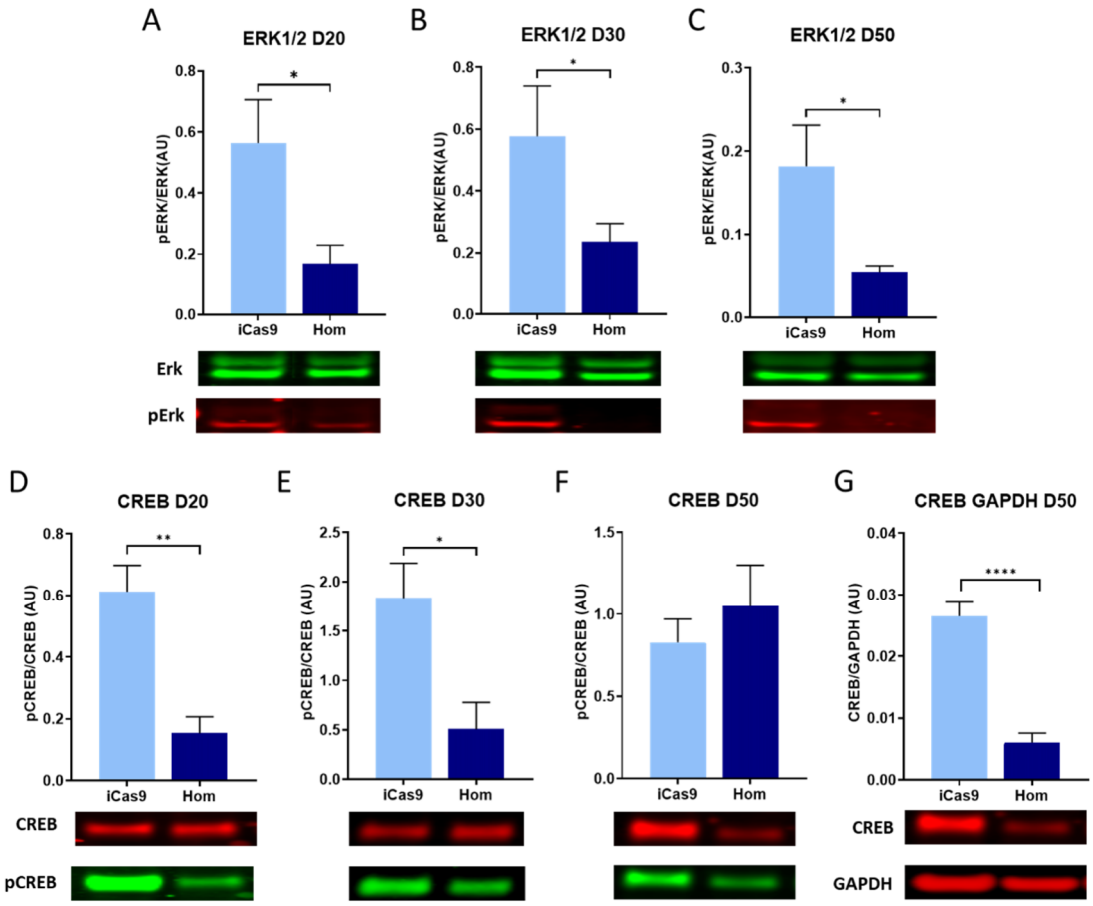

Figure 4.7 Phosphorylation of ERK1/2 and CREB in iCas9 and CACNA1C Hom lines. (A-C) Phosphorylation of ERK1/2 at day 20, 30 and 50 of neuronal differentiation. ERK1/2 phosphorylation is measured as pERK divided by total ERK expression. (D-F) Phosphorylation of CREB at day 20, 30 and 50 of neuronal differentiation. CREB phosphorylation is measured as pCREB divided by total CREB expression. (G) Total CREB expression at day 50, measured by CREB divided by GAPDH expression. Plots represent summary data from 6 samples across two differentiations of the iCas9 line. The Hom data represents 6 samples from 2 differentiations of the Hom2 line and 3-6 samples from 1-2 differentiations of the Hom1 line.

	Time-point	Protein expression (mean ± SEM)		P value	Adjusted P value
		iCas9	Hom		
pERK/ ERK	Day 20	0.5633 ± 0.1425	0.1678 ± 0.0613	**0.0128**	**0.0128**
	Day 30	0.5766 ± 0.1631	0.2352 ± 0.0592	**0.0402**	**0.0402**
	Day 50	0.1818 ± 0.0494	0.0548 ± 0.0075	**0.0036**	**0.0073**
pCREB/ CREB	Day 20	0.6119 ± 0.0856	0.1533 ± 0.0530	**0.0003**	**0.0006**
	Day 30	1.834 ± 0.3550	0.5049 ± 0.2710	**0.0099**	**0.0196**
	Day 50	0.8271 ± 0.1434	1.049 ± 0.2496	0.544	0.544
CREB/ GAPDH	Day 50	0.0265 ± 0.0022	0.0061 ± 0.0015	**0.000001**	**0.000003**

Table 4.5 Summary of statistics for western blot analysis of iCas9 and Hom lines. Data was analysed using unpaired t-test, Holm-Sidak correction for multiple comparisons was used to generate adjusted P values.

ERK1/2 and CREB phosphorylation was also measured in the ATS line in comparison to control (Figure 4.8). It was expected that the ATS line would show the opposite result to the homozygous lines. However, there was no significant difference in ERK1/2 and CREB phosphorylation at any time point between the control and ATS lines. Although there were no significant changes, the ATS line showed a consistent trend towards increased phosphorylation of both ERK1/2 and CREB at day 20 and 30 of the differentiation, the opposite effect that the CACNA1C Homozygous lines have on Erk1/2 and CREB phosphorylation. This is particularly apparent for ERK1/2 phosphorylation at Day 20 ($p=0.0536$), the time point when neurons are starting to be generated from NPCs and CREB signalling is particularly important. There was no difference in Erk1/2 or CREB phosphorylation at day 50 of the differentiation once mature neurons have been generated. Table 4.5 and Table 4.6 present a summary of the statistics for the Western blot data for the Hom and ATS lines, respectively.

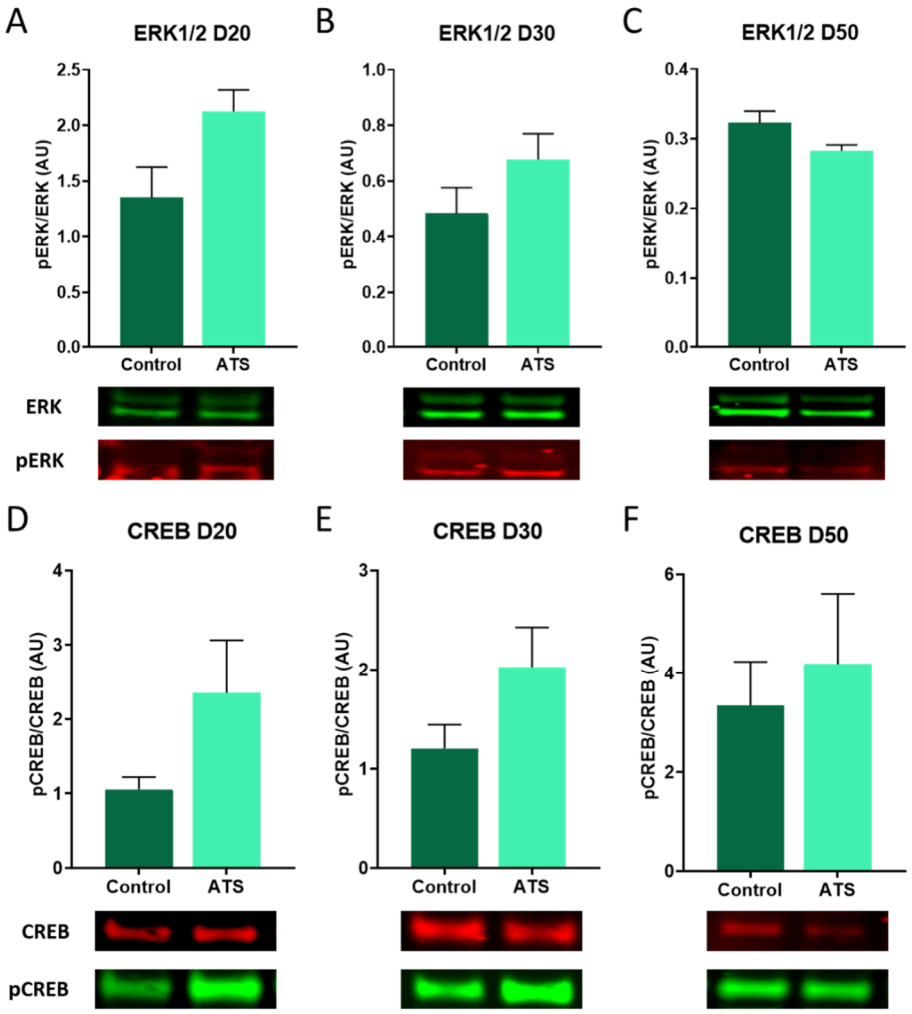

Figure 4.8 Phosphorylation of ERK1/2 and CREB in Control and ATS lines. (A-C) Phosphorylation of ERK1/2 at day 20, 30 and 50 of neuronal differentiation. ERK1/2 phosphorylation is measured as pERK divided by total ERK expression. (D-F) Phosphorylation of CREB at day 20, 30 and 50 of neuronal differentiation. CREB phosphorylation is measured as pCREB divided by total CREB expression. Plots represent summary data from 6 samples across two differentiations for each line.

	Time-point	Protein expression (mean ± SEM)		P value	Adjusted P value
		Control	ATS		
pERK/ERK	Day 20	1.351 ± 0.2738	2.126 ± 0.1931	0.0536	0.1044
	Day 30	0.4837 ± 0.0923	0.6773 ± 0.2260	0.1688	0.1704
	Day 50	0.3226 ± 0.0171	0.2827 ± 0.0084	0.0633	0.1225
pCREB/ CREB	Day 20	1.057 ± 0.1648	2.351 ± 0.7134	0.1074	0.1074
	Day 30	1.204 ± 0.2397	2.027 ± 0.4005	0.1082	0.1704
	Day 50	3.348 ± 0.8843	4.189 ± 1.416	0.6253	0.6252

Table 4.6 Summary of statistics for western blot analysis of Control and ATS lines. Data was analysed using unpaired t-test, Holm-Sidak correction for multiple comparisons was used to generate adjusted P values.

4.3 Discussion

This chapter describes the effect CACNA1C on the generation of cortical neurons focusing on expression of neuronal markers and related downstream signalling. Loss of CACNA1C had no effect on the expression of NPC markers (Pax6, Nestin, FoxG1) during the first 20 days of neuronal differentiation. However, the ATS line showed an increase in the telencephalic neural stem cell marker FoxG1 at day 20. FoxG1 is a transcriptional repressor fundamental for brain development and is widely expressed in the forebrain during development and in mature neurons (Xuan et al. 1995; Martynoga et al. 2005; Tian et al. 2012). Point mutations, deletions, and duplications of FoxG1 can all lead to FoxG1 syndrome, a severe neurodevelopmental disorder with symptoms that include ASD, seizures, mental retardation, and facial dysmorphia (Brunetti-Pierri et al. 2010; Mencarelli et al. 2010; Pontrelli et al. 2014). Many of these symptoms overlap with those seen in Timothy Syndrome, highlighting a potential for overlap in disease mechanisms. FoxG1 plays a role in regulating neural stem cell proliferation and supressing premature neuronal differentiation (Martynoga et al. 2005; Manuel et al. 2011). It is also involved in dorsoventral patterning in the telencephalon, including the generation of different cortical layers; FoxG1 represses the layer VI marker TBR1 and is important for the generation of upper-layer neurons (Siegenthaler et al. 2008; Toma et al. 2014; Cargnin et al. 2018).

In addition to this FoxG1 plays a role in regulating the excitatory/inhibitory balance in cortical neurons. FoxG1 is expressed in both dorsal and ventral telencephalic progenitors. But is expressed at higher levels in ventral progenitors, which produce inhibitory GABAergic neurons (Danesin and Houart 2012). Both increases and decreases in FoxG1 expression have been associated with an increased production of GABAergic neurons. Patient iPSC-derived neurons containing point mutations and deletions in FoxG1 showed increased expression of inhibitory markers, including GAD1, NKX2.1 and GluD1 (Patriarchi et al. 2016). However, organoids generated from patients with ASD showed increased expression of FoxG1 and GABAergic markers. RNA interference targeting FoxG1 restored expression of these GABAergic markers to normal levels (Mariani et al. 2015). The increase in FoxG1 at day 20 in the ATS line,

therefore, may lead to an increase in ventral telencephalic progenitors and thus lead to the increase in expression of GAD enzymes seen in the ATS line at Day 50.

Based on previous studies implicating LTCCs in neuronal differentiation we expected to see a decrease in the expression of neuronal markers in the CACNA1C knockout lines (D'Ascenzo et al. 2006; Lepski et al. 2013). There was a significant decrease in MAP2 expression across the differentiation from day 30 to day 50, although this was not significant at any specific time point it was most clear at day 40 and 50. β-III-tubulin also showed a trend towards decreased expression at day 40 and 50 although this was not significant. To confirm that loss of CACNA1C impaired neuronal differentiation, neurons were also stained at day 50 of the differentiation. Knockout lines showed a decrease in MAP2 expression relative to DAPI, indicating lower numbers of neurons. As the cells were too dense to count individually the area of DAPI was measured. This means we cannot conclusively say there are less MAP2-positive neurons as this measure can be influenced by neuron size and morphology. Staining with a nuclear, neuronal marker such as NeuN would have been a better alternative for counting the number of neurons in the culture. However, the knockout lines also showed a higher number of neuronal rosette-like structures in the culture. Suggesting a higher proportion of NPCs are still present and thus less mature neurons. These results suggest that loss of CACNA1C specifically leads to a deficit in differentiation of neurons from NPCs.

The ATS line showed no alteration in the expression of neuronal markers at RNA level or when stained for MAP2. This suggests that the gain-of-function mutation does not lead to an increase in neuron production. However, the ATS line did show a decrease in the number of rosette-like structures present in the culture. The structures were counted based on morphology not a protein stain, therefore rosette-like structures with larger lumens are more easily identifiable and those with small lumens in high density areas are more likely to have been missed. A stain such as N-cadherin to clearly mark neuronal rosettes would be required to conclusively say that there are alterations to the number of neuronal rosettes in knockout and patient lines. As there were no changes to MAP2 expression it is possible that the ATS line produced smaller

or less circular rosettes that are harder to identify, leading to a reduction in the number of rosette-like structures counted. Studies investigating rosette formation in other neurodevelopmental disorders have also shown deficits in rosette structure. Formation of rosettes from ASD patient-derived iPSC have been shown to be impaired, rosette diameter was smaller and had a less organised structure, although more rosettes were present in the cultures (Adhya et al. 2021). iPSCs-derived rosettes from patients carrying the 15q11.2 CNV deletion, which is associated with schizophrenia and ASD, also displayed disruption of the rosette structure (Yoon et al. 2014). Neuronal rosettes in 2D culture mimics neural tube formation during *in vivo* development. Changes to neural rosette formation may impact the generation of different cortical layer neurons, which has previously been shown to be altered in Timothy Syndrome (Paşca et al. 2011; Panagiotakos et al. 2019).

It has been shown that calcium signalling plays a role in the formation of neuronal rosettes. Blockade of intracellular calcium stores leads to a loss of rosette formation, but acute blockade of LTCCs had no impact on rosette formation (Hříbková et al. 2018). This suggests acute changes to calcium influx via Cav1.2 would not impact rosette structure. However, long term changes which alter downstream signalling pathways due to either loss of the channel or a gain-of-function mutation may have an impact on rosette formation, structure, or maintenance. Rho/ROCK signalling has been shown to be important in rosette formation and structure. Inhibition of Rho/ROCK activity increases the number of neuronal rosettes but reduces rosette organisation and lumen size, whereas activation of Rho/ROCK signalling impairs rosette initiation (Townshend et al. 2020). This signalling pathway has previously been shown to be altered in classical TS neurons. TS Cav1.2 channels showed deficits in binding with Gem leading to increased dendritic retraction; Gem is a small GTP-binding protein that inhibits Rho/ROCK signalling. Decreased recruitment of Gem by TS-Cav1.2 channels leads to increased activation of Rho and dendritic retraction (Krey et al. 2013). It is possible that Rho/ROCK signalling is also increased in the ATS line, leading to a reduction in rosette formation. Future experiments staining cells for N-cadherin, a protein that marks the centre of neural rosettes at multiple timepoints

across differentiation, would help to determine the effect of Cav1.2 on rosette structure (Elkabetz et al. 2008).

The ATS line and knockout lines showed opposing changes in expression of GAD65 and GAD67, the enzymes responsible for GABA production. At the RNA level the ATS line showed an increase in GAD65 expression and the knockout lines a decrease in GAD65. GAD65 is responsible for production of GABA at synapses specifically, compared to GAD67 which synthesises GABA for activity unrelated to neurotransmission, such as synaptogenesis (Soghomonian and Martin 1998). This suggests a reduction in synaptic GABA transmission, which is likely to lead to changes in neuronal activity. Although GAD67 expression showed no difference at the RNA level it was altered at the protein level. Knockout lines showed a reduction in both GAD65 and GAD67 staining relative to MAP2 expression and the ATS line showed increased expression of GAD65 and GAD67. This suggests Cav1.2 is important for the regulation of GABA production both at the synapse and in the cytoplasm. However, due to the high density of neurons that were stained, the number of GABAergic neurons could not be counted, therefore we cannot confirm if Cav1.2 alters the number of GABAergic neurons or the amount of GAD expression within individual neurons.

Several other studies have also shown that Cav1.2 impacts GABAergic signalling. A TS2-neo mouse model has shown an increase in VGAT-positive synaptic density in layer 4 of the barrel somatosensory cortex, although puncta were smaller in size. They also showed increased migration of inhibitory neurons into the neocortex (Horigane et al. 2020). Human organoid models from TS patients have also shown changes to the migration of inhibitory interneurons, however they showed a deficit in migration. TS interneurons showed an increase in the number of saltations but a decrease in the distance of these saltations which led to an overall decrease in migration distance. The neurons also showed upregulation of GABA receptor subunits, GABRA4, GABRG1 and GABRG2, following RNA-seq analysis (Birey et al. 2017; Birey et al. 2021). iPSC-derived neurons from TS patients have also been shown to have increased GAD67 expression compared to control neurons following

depolarisation with KCl (Paşca et al. 2011). In comparison blockade of LTCCs has shown to decrease surface expression of GABA-A receptors, decrease the number of Parvalbumin (PV) neurons and decrease GAD65, GAD67 and VGAT protein expression (Jiang and Swann 2005; Saliba et al. 2009; Saliba et al. 2012; Cohen et al. 2016; Horn and Nicoll 2018). Additionally a heterozygous CACNA1C knockout rat model showed a decrease in the number of GAD67+ and PV+ neurons in the dentate gyrus of the hippocampus (Moon 2018). These studies all show that Cav1.2 plays an important role in the production of GABAergic neurons and GABAergic signalling.

In addition to impacting the production of GABAergic neurons, Cav1.2 has also been shown to be implicated in the specification of different cortical layer neurons (Paşca et al. 2011; Panagiotakos et al. 2019). Analysis of the CACNA1C homozygous and ATS lines at day 50 of the neuronal differentiation did not show any significant changes in the expression of cortical layer markers TBR1, CUX1, CTIP2 and SATB2. Even though it was not significant, the homozygous lines showed slightly increased SATB2 and decreased CTIP2 expression which supports changes shown in a heterozygous Cav1.2 knockout mouse model. In this study, CTIP2 and SATB2 cells were quantified at embryonic day 16.5 once layer V of the cortex has been mostly formed. They found that loss of one copy of Cav1.2 led to a reduction in CTIP2+ cells and an increase in SATB2+ cells in the cortical plate. The changes to CTIP2 and SATB2 expression occur in the opposite direction in classical TS compared to the heterozygous model (Panagiotakos et al. 2019). As the ATS line is predicted to have a similar gain-of-function mutation to classical TS we predicted it would also show decreased SATB2 and increased CTIP2 expression. However, there was no change in RNA expression of either gene. This highlights that different TS mutations can have different phenotypes and that is important not to generalise findings from classical TS iPSCs to patients with ATS mutations. However, the changes found by Panagiotakos and colleagues are also specific to layer V neurons and the protocol used to generate iPSC-derived neurons produces both upper- and lower-layer neurons. CTIP2 and SATB2 expression is not restricted to layer V and Cav1.2 may have less of an effect on expression of these genes in other layers. In support of this, Pasca and colleagues found that changes to SATB2 and CTIP2 expression only occurred in lower layer

neurons but there was no difference in upper layers (Paşca et al. 2011). This may explain why the changes to CTIP2 and SATB2 expression in the homozygous lines was not large enough to be significant and no changes were seen in the ATS line.

The number of TBR1+ cells was also shown to be reduced in the Cav1.2 heterozygous mouse model (Panagiotakos et al. 2019). TBR1 neurons form layer VI of the cortex and thus are generated early in cortex development (Hevner et al. 2001). We did not find any significant changes in TBR1 expression, but the knockout line did show a trend toward an increase in TBR1, with the ATS lines showing a non-significant decrease in expression. As these changes occur in opposing directions it is likely that Cav1.2 does have an impact on TBR1 expression. However, these finding are in the opposite direction to that found by Panagiotakos and colleagues. This is possibly due to the different models and time-points that were used. They used a mouse model and looked early in development when only the deep layer V neurons have been generated. It is hard to compare iPSC-derived neurons to a developmental stage but both lower and upper layers have been generated in this model suggesting it is equivalent to later cortical development. Although TBR1 is mainly expressed in early born deep layer neurons it is also expressed at low levels in upper layer neurons (Srinivasan et al. 2012). Therefore, as with SATB2 and CTIP2, Cav1.2 may have different effects on TBR1 expression depending on whether it is expressed in upper- or lower-layer neurons.

Another possibility is that Cav1.2 may change the timing of the specification of different cortical layer neurons. In the developing cortex, cortical neurons are formed in an inside-out pattern with lower layer neurons being generated before upper layers (Mukhtar and Taylor 2018). Cortical iPSC-derived neurons generated using the dual-SMAD protocol also show this sequential formation of layers (Shi et al. 2012). Panagiotakos and colleagues showed changes in CTIP2 and SATB2 expression specifically during the formation of cortical layer V neurons (Panagiotakos et al. 2019). Therefore, it is possible that by only looking at Day 50 of the neuronal differentiation we may have missed changes in the timing of the expression of different cortical layer markers. Staining in addition to qRT-PCR analysis would also

allow us to conclusively say whether there are changes to the numbers of different cortical layer neurons.

The changes to neuronal differentiation in the knockout and ATS lines are likely to occur due to changes in activity-dependent gene expression via Cav1.2. The channel is coupled to gene expression via activation of the CREB pathway. CREB can be activated by Cav1.2 via the CaMKII or ERK1/2 signalling; we investigated activation of Erk1/2 and CREB signalling in the knockout and ATS lines. The homozygous knockout lines showed a significant decrease in ERK1/2 and CREB signalling at multiple timepoints across the neuronal differentiation. This confirms findings in rodent models that show loss of Cav1.2 leads to a reduction in basal CREB phosphorylation via the ERK1/2 pathway. Moosmang and colleagues showed that basal levels of pCREB were reduced in hippocampus and neocortex specific Cav1.2 knockout mice. They also showed that induction of LTP and the corresponding increases in pERK1/2 and pCREB levels was impaired in knockout mice (Moosmang et al. 2005). Decreased basal pERK1/2 and pCREB has also been shown to occur in the dorsal hippocampus of heterozygous Cav1.2 rats. These rats showed synaptic plasticity and behavioural deficits, but activation of the ERK1/2 pathway via a TrkB receptor activator rescued these deficits as well as pERK1/2 and pCREB levels (Tigaret et al. 2021).

The classical TS mutation (G406R) has been shown to increase CREB signalling. Li and colleagues used chimeric Cav1.2 channels in HEK cells to show that both calcium influx and voltage-dependent conformational change of Cav1.2 are required to increase CREB phosphorylation. They fused Cav1.2 to a P2X2 channel, which is ATP-gated and Ca^{2+} permeable. This meant Ca^{2+} influx could be stimulated independent of the channel opening. Cd^{2+} was used to block Ca^{2+} influx through the Cav1.2 channel, while still allowing the conformational change to occur following depolarisation. They then showed that the increase in pCREB occurred via CaMKII signalling and blockade of CaMKII via pharmacology or shRNA blocked the increase in pCREB following depolarisation, whereas blockade of ERK1/2 signalling had no effect. Next, they used the chimeric Cav1.2-P2X2 channels to investigate the effect of TS mutations. They showed that the G406R mutation caused higher increases in

CaMKII puncta and nuclear pCREB following depolarisation compared to control. However, the G402S mutation, which appears to have a more cardiac-specific phenotype, was not significantly different from the control (Li et al. 2016; Bauer et al. 2021). This suggests that the G406R but not the G402S mutation alters voltage-dependent conformational changes to Cav1.2 which leads to increased CREB signalling, contributing to the neurodevelopmental phenotype seen in TS1. Servili and colleagues also showed that the G406R but not the G402S mutation alters CREB phosphorylation. They showed that basal pCREB levels were elevated in HEK cells transfected with the Cav1.2-G406R channel compared to control or G402S channels. However, in contradiction to the other study, they showed that this could be reversed by inhibition of mitogen-activated protein kinase kinase (MEK) or ERK1/2 (Servili et al. 2020). Both studies showed that the G406R mutation alters the voltage-dependent conformational change to Cav1.2 to increase CREB phosphorylation. Servili suggested that the increased basal CREB levels for G406R were due to a negative shift in voltage dependent activation, thus increasing the channel open probability and spontaneous channel activity at basal conditions. In contrast the G402S channel causes a positive shift in voltage dependent activation so spontaneous channel opening is less likely to occur (Servili et al. 2020).

The ATS line did not show any significant changes to ERK1/2 or CREB phosphorylation. However, there was a trend towards an increase in pERK1/2 and pCREB at day 20 and 30 of the neuronal differentiation. At these timepoints many neurons are being generated from NPCs. It has previously been shown that CREB phosphorylation via LTCC activity is important for this process (Lepski et al. 2013). Whereas at day 50, the culture is comprised of mainly mature neurons so there is less CREB signalling at basal conditions. There were no changes to ERK1/2 or CREB phosphorylation at this timepoint in the ATS line. It is possible that there is not enough activation of Cav1.2 in mature neurons to see the effect of the mutation and the cells require a depolarising stimulus to see changes to CREB signalling. Servili and Li both used HEK cells to investigate Cav1.2-CREB signalling. These cells do not contain any endogenous VGCCs so the effects of Cav1.2 would be much clearer than in iPSC-derived neurons that express other channels and receptors that can also

induce CREB signalling. Indeed, Pasca and colleagues found that genes downstream of CREB where enriched in TS neurons compared to control only following depolarisation (Paşca et al. 2011). Both the knockout and ATS lines showed changes in pERK1/2 matching the changes to pCREB, this suggests that increased ERK1/2 signalling is responsible for the increases in pCREB. Based on previous studies investigating LTCC downstream signalling it is possible that CaMKII signalling is also altered and plays a role in the activation of CREB signalling. This would need to be investigated and pharmacology could be used to help determine the contribution of ERK1/2 and CaMKII signalling pathways to CREB phosphorylation and downstream gene expression in the different cell lines.

The CACNA1C homozygous lines showed a reduction in MAP2 expression and had a higher number of neuronal rosettes at day 50 of neuronal differentiation compared to control. CREB signalling is responsible for controlling the expression of a large number of genes. It is upregulated during neuronal differentiation in NPCs and young neurons. Studies have shown that upregulation of CREB, via LTCCs, is required for the production of neurons from NPCs (D'Ascenzo et al. 2006; Lepski et al. 2013). Therefore, the reduction in differentiation of neurons in the knockout lines is highly likely to be due to the reduction in CREB phosphorylation. The ATS line did not show increased MAP2 expression, as would be expected from increased Cav1.2 activity. However, the ATS line only showed increased ERK1/2 and CREB phosphorylation at day 20 and day 30 of the differentiation and the changes were not significant. Therefore, the increase in pCREB may not have had enough of an effect to significantly increase gene expression and induce higher rates of neuronal differentiation.

Other downstream genes of CREB include GAD65 and GAD67, which showed reduced expression in the knockout lines and increased expression in the ATS line. In Parvalbumin interneurons, increased CREB phosphorylation has been shown to increase both GAD67 and Parvalbumin expression. The increases in CREB phosphorylation and associated downstream gene expression could be blocked by nimodipine, showing activation of LTCCs are required for this signalling pathway

(Cohen et al. 2016). Alteration to GAD65 levels via CREB has been shown to occur in cortical interneurons via BDNF. BDNF binds to and activates TrkB receptors which leads to CREB phosphorylation via Ras-ERK1/2 signalling. pCREB then binds to the GAD65 promoter region to induce GAD65 transcription (Sánchez-Huertas and Rico 2011). BDNF transcription is also dependent on CREB signalling, therefore increased activation of Cav1.2 in the ATS line may lead to increased GAD65 expression either directly via increased pCREB or via subsequent increases in BDNF transcription (Figure 4.9) (Dolmetsch et al. 2001).

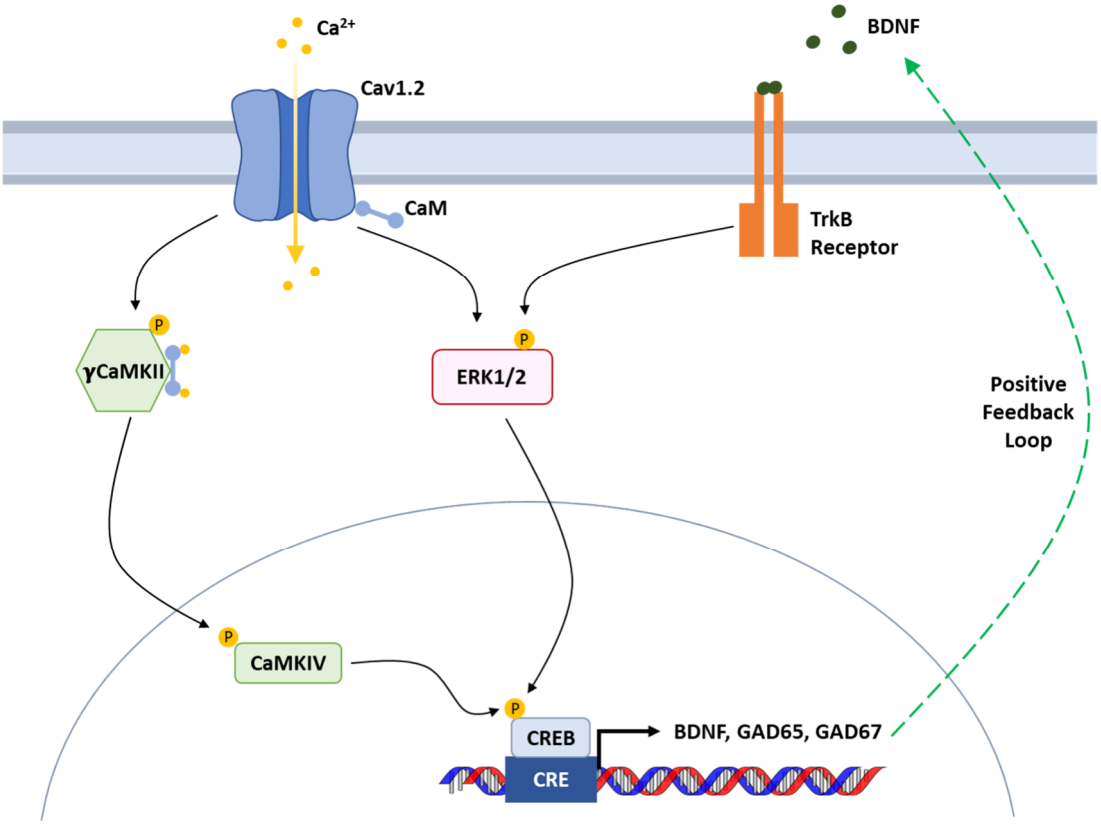

Figure 4.9 Proposed pathway of GAD65 and GAD67 transcription. Opening of Cav1.2 channels leads to phosphorylation of CREB via either CaMKII or ERK1/2 signalling. Phosphorylated CREB binds to CRE promoter sites in the genome and can induce transcription of genes including BDNF, GAD65 and GAD67. Increased expression of BDNF leads increased activation of TrkB receptors. These receptors increase CREB phosphorylation via ERK1/2 signalling, leading to a positive feedback loop of increased CREB-dependent gene expression and thus increased GAD65 and GAD67.

4.3.1 Conclusion

This chapter describes the phenotypic analysis of CACNA1C knockout and ATS lines. Loss of CACNA1C lead to an impairment in neuronal differentiation, shown by a decrease in MAP2 expression at RNA and protein level and increase in the number of neuronal rosettes. The ATS line, carrying a predicted gain-of-function mutation, had no effect on the expression of neuronal markers MAP2 or β-III-tubulin, however it did show an increase in FoxG1 expression at day 20. This change in FoxG1 may be a potential mechanism for changes in neuronal subtype seen in the ATS line. Loss of CACNA1C led to decreased expression of GAD65 and GAD67, enzymes responsible for the production of GABA, whereas the ATS line showed an increase in GAD65 and GAD67 expression. This suggests that Cav1.2 plays an important role in controlling the strength of synaptic GABAergic transmission. Although no significant changes were found, the results from this chapter also support previous studies showing that Cav1.2 plays a role in the generation of different cortical layers. Cav1.2 is responsible for coupling electrical activity to gene transcription. The opposing changes to ERK1/2 and CREB phosphorylation seen in the knockout and ATS lines are a likely mechanism for the changes that occur to MAP2 and GAD expression. Overall, these findings show that Cav1.2 plays an important role in cortical development and the generation of different neuron subtypes, which may contribute towards the pathology of neurodevelopmental and psychiatric disorders.

5 The effect of loss of CACNA1C and an ATS point mutation on neuronal network activity

5.1 Introduction

The formation of functional neuronal networks is a key aspect of brain development and synchronised activity has been observed *in vivo*, in *ex vivo* brain slices and in cultured neurons, suggesting it is an important intrinsic property of neurons (Ikegaya et al. 2004; Chiappalone et al. 2005; MacLean et al. 2005; Fujisawa et al. 2008; Pastalkova et al. 2008). Neuronal networks and associated cognitive behaviours have been shown to be disrupted in neuropsychiatric disorders, including schizophrenia and ASD (Lynall et al. 2010; Keown et al. 2013; Hahamy et al. 2015; Krajcovic et al. 2019; Yan et al. 2020; Bochet et al. 2021). There have currently been no studies investigating neuronal network activity in TS. However, as ASD and seizures are common symptoms of TS, it is highly likely that neuronal network activity is also disrupted in this disorder. Additionally, LTCCs have been shown to play an important role in neuronal activity; including regulation of synaptic plasticity, neuronal oscillations, epileptiform activity and shaping the firing of individual neurons, so changes to Cav1.2 expression or function are likely to impact network activity.

Cav1.2 is required for the induction of LTP, and thus regulates synaptic plasticity and the connectivity between neurons. Rodent models have shown that deletion of Cav1.2 causes a reduction in LTP in the amygdala and hippocampus, which is also associated with behavioural deficits including spatial memory, fear memory acquisition and contextual fear conditioning (Moosmang et al. 2005; Langwieser et al. 2010; Tigaret et al. 2021). On a single neuronal level Cav1.2 is important in shaping action potentials. Prolonged opening of Cav1.2 channels in TS neurons leads to prolonged depolarisation and wider action potentials (Paşca et al. 2011). In addition to this, Cav1.2 associates with calcium and voltage activated potassium (BK_{Ca}) channels to play a role in the afterhyperpolarisation (AHP) phase of action potentials, specifically slow AHPs which occur after bursts of action potentials (Shah and Haylett

2000; Berkefeld et al. 2006; Lima and Marrion 2007; Berkefeld and Fakler 2008). As Cav1.2 is involved in the refractory period following burst firing, this provides a potential mechanism of how it may influence synchronised network activity. Pharmacological studies have shown that oscillatory activity in rodents is dependent on LTCCs. Synchronised calcium transients in cultured hippocampal and cortical neurons are reduced by application of LTCC antagonists (Przewlocki et al. 1999; Jun He et al. 2005). *Ex vivo* hippocampal slice recordings have shown that LTCC activation is required for theta frequency slow spiking oscillations (Hansen et al. 2014). Finally, in iPSC-derived neurons blockade of LTCCs alters the pattern of synchronised burst activity by reducing the interval between bursts (Plumbly et al. 2019).

In addition to the role of Cav1.2 directly on neuronal activity, the homozygous and ATS neurons showed changes to the expression of GAD65, which is responsible for the production of synaptic GABA. Changes in GABAergic signalling may also contribute towards alterations in network activity; it is well documented that GABAergic interneurons are important for synchronised neuronal activity (Cobb et al. 1995; Sanchez-Vives and McCormick 2000; Blatow et al. 2003; Mann and Paulsen 2007; Gonzalez-Burgos and Lewis 2008). Cultured mouse cortical neurons and human iPSC-derived neurons have shown that blockade of GABA-A receptors causes increased firing frequency and reduced interval between synchronised bursts (Odawara et al. 2014; Lu et al. 2015; Odawara et al. 2016). The proportion of GABAergic to glutamatergic neurons has also been shown to influence the pattern of synchronised bursts (Chen and Dzakpasu 2010; Iida et al. 2018). Additionally the formation of synchronised activity in iPSC neurons is associated with the switch of GABA from depolarising to hyperpolarising, further highlighting the importance of GABAergic signalling in the development of co-ordinated networks (Mäkinen et al. 2018).

5.1.1 Chapter Aims

This chapter will investigate the role of CACNA1C on neuronal network activity. Neuronal activity of homozygous and ATS neurons will be recorded using multi-

electrode arrays and analysed to identify changes to basal excitability and synchronised network behaviour. Following this, pharmacological interventions will be tested to attempt to rescue the phenotypes seen. Pharmacology will target LTCCs, GABAergic signalling and ERK1/2-CREB signalling based on the changes seen to Homozygous and ATS neurons in the previous chapter.

5.2 Results

5.2.1 Overview of MEA experiment design

MEA experiments can provide a large amount of data, however a few considerations are required when designing the experiments. MEA recordings allow analysis of two main components of neuronal activity. First the general excitability of cultures, measured by spike detection. The second component is the analysis of network activity, which is carried out using array wide spike detection rates (ASDR), a measure which has been used by a number of previous studies for analysis of synchronised activity in MEA cultures (Sun et al. 2010; Mok et al. 2012; Lu et al. 2015; Plumbly et al. 2019).

Three main measures using spike detection are used to measure the general excitability of the cultures (Figure 5.1a). Average spikes per electrode is the medium number of spikes that occurs in each electrode across the 10-minute recording. The median is used instead of the mean as it controls for electrodes that are much more or less active than others and provides a more representative view of overall activity. The second measure is average spike rate, calculated by the number of spikes divided by the length of the recoding for each electrode. The median spike rate was then calculated using the values from each electrode. The third measure is the total number of bursts. A burst is classified as 3 spikes occurring within a 300 ms period and the total number of these bursts occurring across the recording was classified as the total bursts.

Network characteristics of the cultures is measured by generating the ASDR for each electrode. The ASDR is calculated by splitting the electrode data into 200 ms bins and counting the number of spikes in each bin. The ASDR plots in this chapter show the total number of spikes occurring in each 200ms bin in all electrodes across the length of the recording (Figure 5.1b). These plots show clear bursts of synchronised activity across the recordings and are used to analyse the network activity. The synchronised burst interval is the primary measure of synchronised network activity in the cultures

and has been shown to be influenced by both GABAergic signalling and LTCCs (Plumbly et al. 2019). Synchronised bursts are defined by bursts containing at least 40% of the number of spikes as the max ASDR and the mean interval between these synchronised bursts is used to determine the synchronised burst interval. Max ASDR describes the maximum number of spikes in a 200 ms bin and is also a useful measure of synchronicity as the more synchronised the culture is the higher the number of spikes occurring at once.

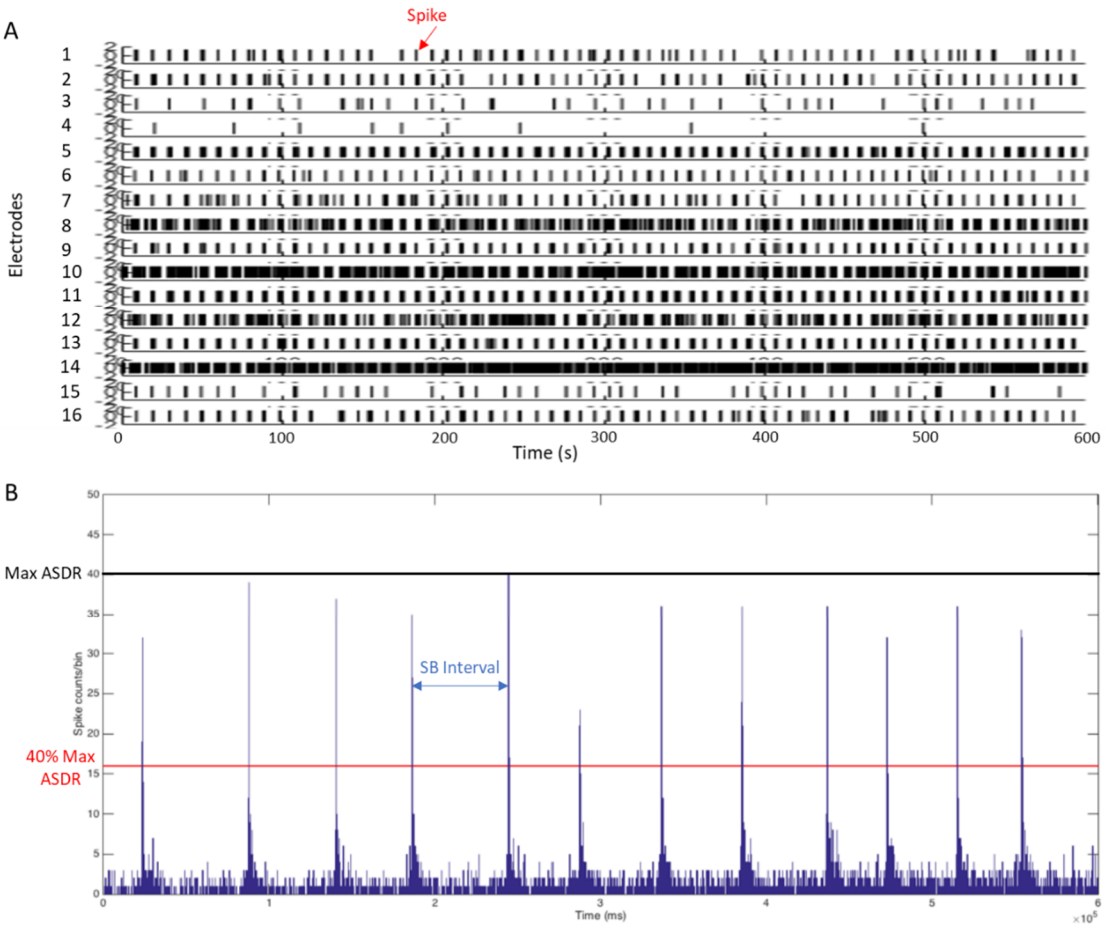

Figure 5.1 Raster and ASDR plots showing MEA analysis measures. (A) Raster plot, each row shows the activity of a different electrode in the well across the recording. The vertical black lines denote a spike occurring. The number of spikes occurring for each electrode are used to calculate general excitability of the cultures. (B) ASDR plot; Y-axis shows number of spikes per 200ms bin, X-axis shows time. Network activity is described by two measures; the max ASDR, calculated by the maximum number of spikes occurring in a 200ms bin. Synchronised burst interval is calculated by measuring the time between synchronised bursts. To be classified as a synchronised burst there must be at least 40% of the number of spikes of the max ASDR in the 200ms bin (peaks above the red line).

When plating neurons onto MEA plates it is particularly important to ensure even plating of an equal amount of cells so as not to affect the general excitability statistics. If the number of neurons plated in the cultures varies it will affect the number of spikes per electrode and spike rate. Additionally, it is important that there is even coverage of the neurons across the electrodes so as not to impact these measures. The cultures are checked under the microscope prior to recording and any wells with less than 80% coverage of electrodes are not used for analysis. To record synchronised activity in neuronal cultures any NPCs present in the culture must be removed, otherwise the formation of new neurons disrupts the formation of synchronised bursts, so cultures are treated with DAPT. Additionally, neurons are cultured using astrocyte-conditioned media to improve maturation of the neurons. However, if the astrocytes used to condition the media become stressed, this will adversely affect the neuronal activity. Therefore, neuronal activity is regularly checked as is the condition of the astrocytes using a microscope.

5.2.2 Formation of synchronised network activity in CACNA1C knockout line

Differentiated neurons from control and CACNA1C Hom lines were plated onto MEAs to identify basal excitability and network characteristics. For this experiment the IBJ4 cell line was used as a control and only the CACNA1C Hom2 line was used due to technical issues meaning no iCas9 or Hom1 neurons were available for the experiment. The iCas9 line is derived from the IBJ4 line so they should show equivalent network properties. Following plating on MEAs, neurons were treated with DAPT to remove NPCs from the culture and allow synchronised network activity to form over the next 50 days. The lines were recorded 60 days post-plating (60DPP) and analysed to identify if any differences occurred between the control and Hom neurons (Figure 5.2).

Basal activity of the cultures was measured by average number of spikes per electrode, average spike rate and total number of bursts (Figure 5.2c-e). The knockout lines showed a trend towards an increase in all these basal excitability measures as measured by Welch's T-test (Spikes/Electrode $t(2.443)=5.032$,

p=0.0581; Spike Rate t(2.343)=5.030, p=0.0658, Total bursts t(2.053)=5.111 p=0.0941). However, none of these changes were significantly different, this is likely due to the variation in the Hom neurons, with half of the wells showing increased basal excitability, but half showing excitability measures similar to control.

Network characteristics of the cultures was measured by average synchronised burst (SB) interval and maximum array-wide spike detection rate (max ASDR) (Figure 5.2f-g). The Hom line showed a significant decrease in SB interval compared to control as determined by unpaired T-test (t(2.423)=11, p=0.0338), which matches previous findings showing blockade of LTCCs reduces the SB interval of iPSC-derived neurons (Plumbly et al. 2019). There was no significant difference in the max ASDR between control and Hom lines as determined by Welch's T-test (t(2.034)=5.072, p=0.0969). This measure also showed the same pattern as the basal excitability characteristics with half of the wells showing an increased max ASDR and half were similar to control. These results suggest that loss of CACNA1C leads to a specific effect on the pattern of network activity by altering the interval between synchronised bursts.

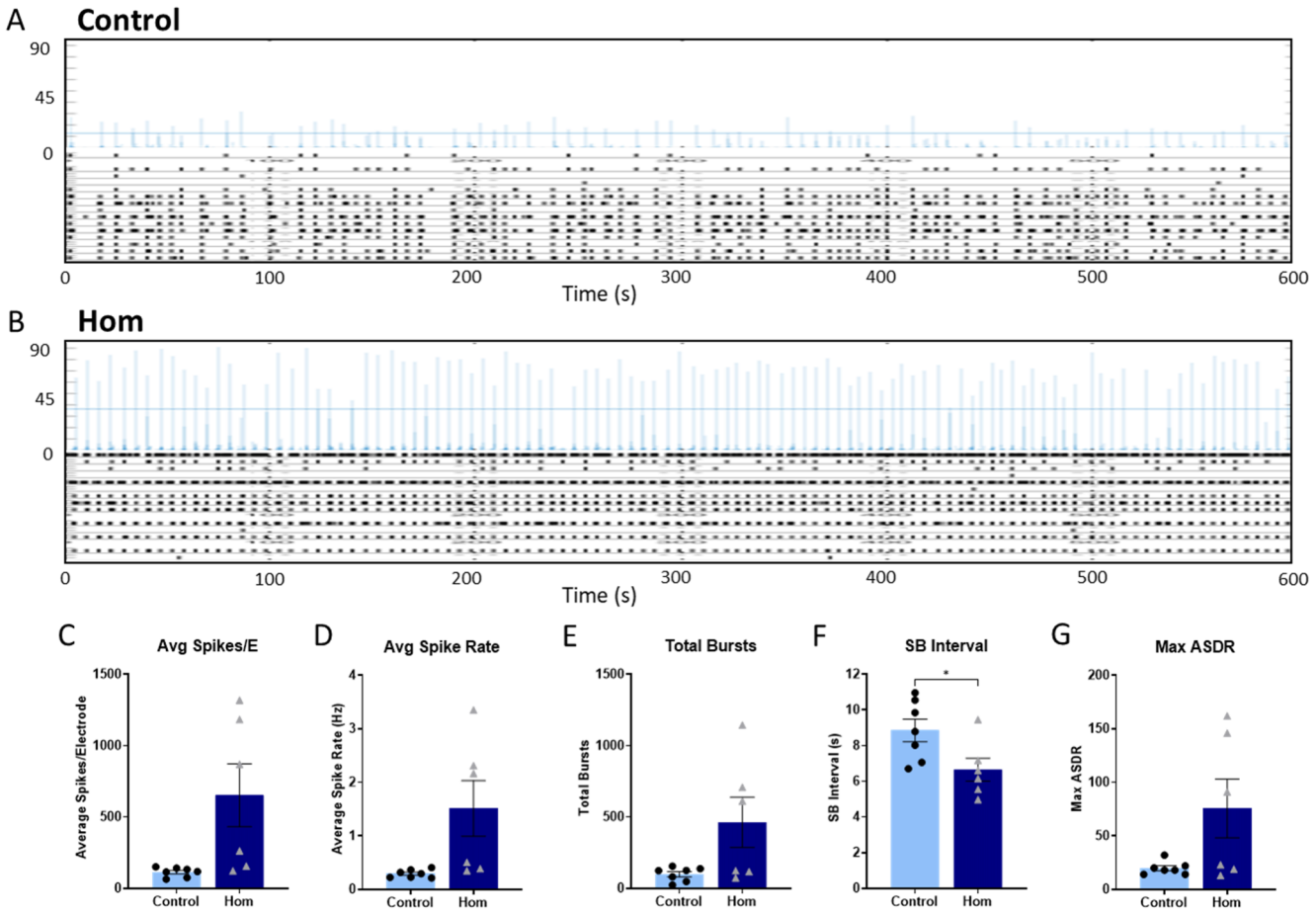

*Figure 5.2 Neuronal network activity of Control and Hom neurons on MEAs 60 days after plating. (A-B) Representative ASDR (top) and raster(bottom) plots showing spontaneous activity from a well of Control and Hom neurons. Basal excitability measured by (C) average spikes per electrode, (D) average spike rate and (E) total number of bursts. Synchronicity measured by (F) average synchronised burst (SB) interval and (G) maximum array-wide spike detection rate (ASDR). The plots represent data from one differentiation with 7 wells of control neurons and 6 wells of ATS neurons. (*p<0.05)*

5.2.3 *Effect of GABA-A receptor activation on network activity in CACNA1C knockout line*

As discussed in the previous results chapter, knockout of CACNA1C leads to decreased expression of GAD enzymes suggesting a decrease in synaptic GABA signalling. Therefore, the GABA-A receptor positive allosteric modulator diazepam was applied to the cultures to see if augmenting GABA signalling would rescue the SB interval deficit seen in the Hom line. Figure 5.8 Figure 5.3 shows raster plots of the response to 50nM diazepam for one well of the Control and Hom lines. Figure 5.4 shows summary data of the excitability and network characteristics used to measure the activity of the cultures. The statistics for this data is summarised in Table 5.3. Diazepam had no effect on the average spikes per electrode (Control, 199.92±71.15 vs 163.08±61.51; Hom, 1167.33±580.10 vs 1280.00±725.78), the average spike rate (Control, 0.57±0.16 Hz vs 0.36±0.12 Hz; Hom, 2.61±0.86 Hz vs 3.03±1.32 Hz) or total bursts (Control, 177.67±84.38 vs 96±49.24; Hom, 649.33±224.68 vs 654.00±224.91)(Figure 5.4a-c).

Diazepam did affect the SB interval, but only in the Control line and had no effect on the Hom SB interval length. The Control line showed a significant increase in the average interval between synchronised bursts (8.01±0.54 s vs 12.37±1.32 s). There was no difference in SB interval length in the Hom line following diazepam incubation (4.97±0.62 s vs 5.12±0.63 s). At baseline there was a significant difference in the SB interval between the Control and Hom line, as previously shown at 60DPP, which remained following diazepam application as only the Control line showed an increase in MAP interval (Figure 5.4d). Diazepam had no effect on max ASDR (Control, 24.00±7.08 vs 18.83±6.11; Hom 79.50±27.14 vs 91.17±34.14). These results suggest that increased GABAergic signalling via diazepam affects the pattern of synchronised bursts. However, loss of CACNA1C leads to a loss of sensitivity to the drug, likely due to a reduction in GABA production via GAD65 and GAD67.

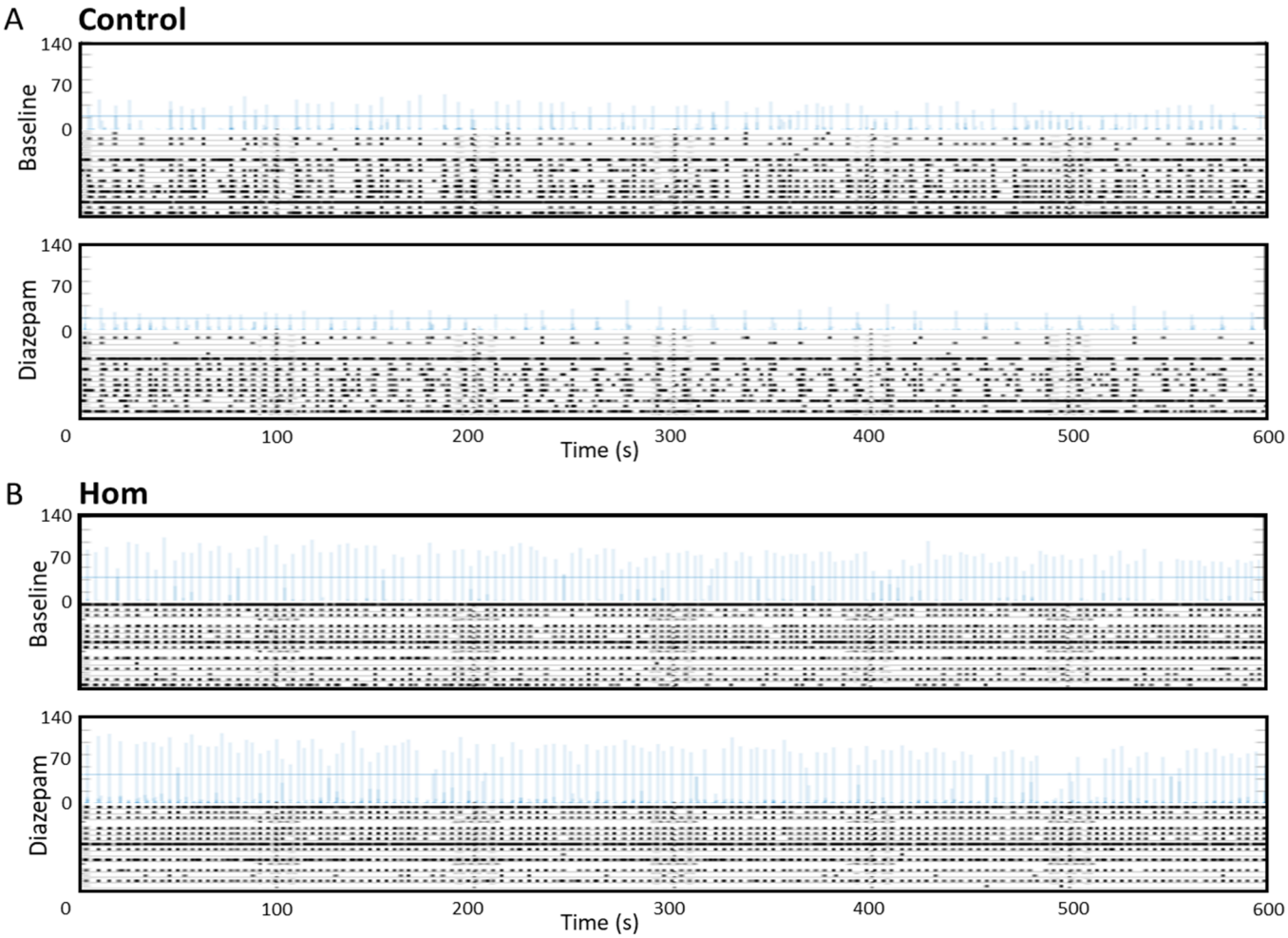

Figure 5.3 Effect of GABA-A receptor activation on neuronal network activity of Control and Hom iPSC-derived neurons. (A and B) Representative ASDR and raster plots showing spontaneous activity from a well of Control and Hom neurons before and after application of 50nM diazepam.

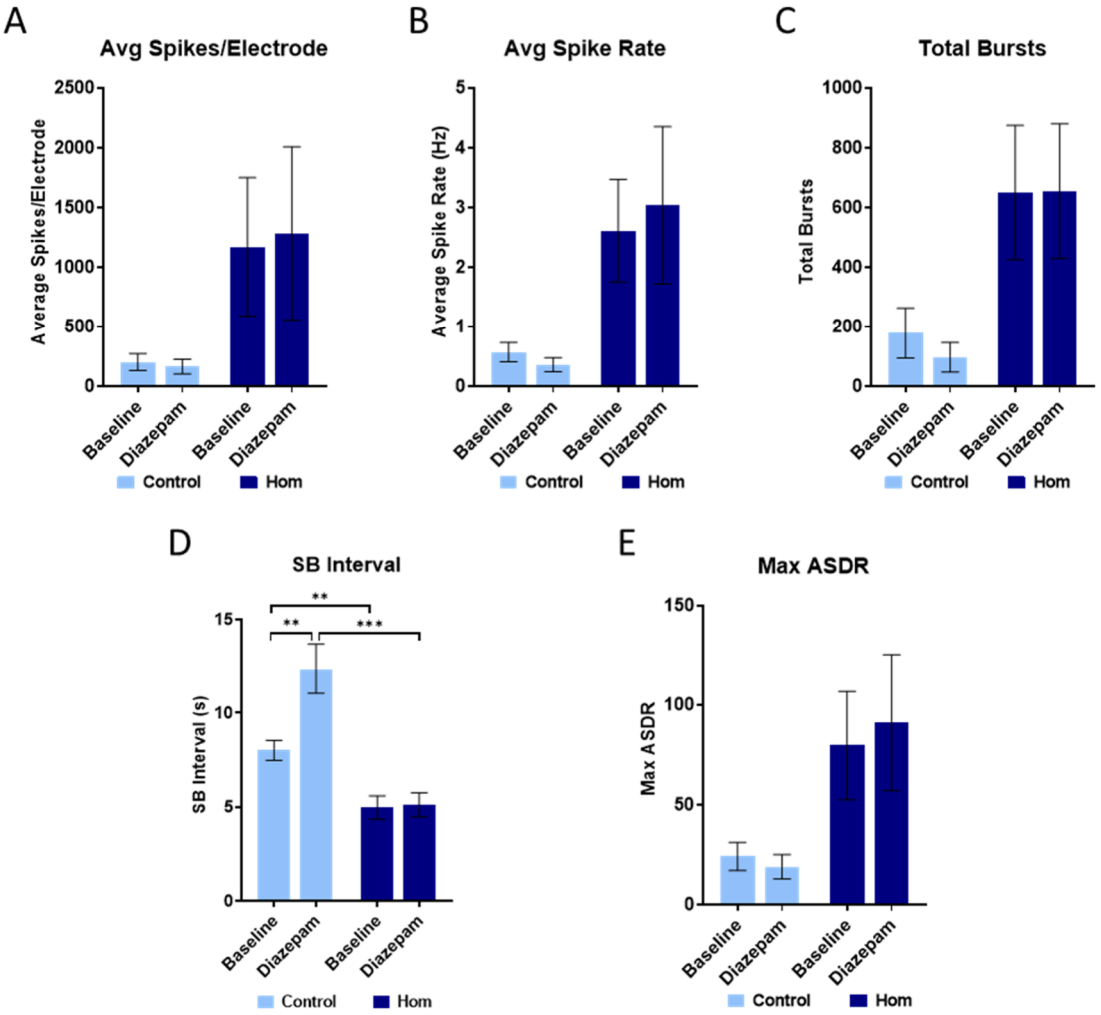

*Figure 5.4 Neuronal excitability and network characteristics following application of 50nM diazepam in control and Hom iPSC-derived neurons. Basal excitability measured by (A) average spikes per electrode, (B) average spike rate and (C) total number of bursts. Synchronicity measured by (D) average synchronised burst (SB) interval and (E) maximum array-wide spike detection rate (ASDR). The plots represent data from one differentiation with 6 wells of control neurons and 6 wells of Hom neurons. (*p<0.05, **p<0.01, ***p<0.001)*

Diazepam	Main Effect	2 Way ANOVA	Holm-Sidak's multiple comparisons
Average Spikes / Electrode	Interaction	F (1, 10) = 0.8076, P=0.3900	No post-hoc comparisons
	Treatment	F (1, 10) = 0.2078, P=0.6582	
	Genotype	F (1, 10) = 2.531, P=0.1427	
Average Spike Rate	Interaction	F (1, 10) = 1.117, P=0.3154	No post-hoc comparisons
	Treatment	F (1, 10) = 0.1308, P=0.7251	
	Genotype	F (1, 10) = 4.770, P=0.0539	
Total Bursts	Interaction	F (1, 10) = 2.823, P=0.1238	No post-hoc comparisons
	Treatment	F (1, 10) = 2.246, P=0.1649	
	Genotype	F (1, 10) = 4.850, P=0.0522	
SB Interval	**Interaction**	**F (1, 10) = 11.33, P=0.0072**	
	Treatment	**F (1, 10) = 12.91, P=0.0049**	**Control, Baseline vs Diazepam P=0.0018**
			Hom, Baseline vs Diazepam P=0.8757
	Genotype	**F (1, 10) = 25.98, P=0.0005**	**Baseline, Control vs Hom P=0.0374**
			Diazepam, Control vs Hom P=0.0004
Max ASDR	Interaction	F (1, 10) = 4.229, P=0.0668	No post-hoc comparisons
	Treatment	F (1, 10) = 0.6305, P=0.4456	
	Genotype	F (1, 10) = 4.176, P=0.0682	

Table 5.1 Summary of statisitcs for effect of diazepam on excitability and network characteristics in Control and Hom neurons. Data was analysed by repeated measures Two-way ANOVA followed by Holm-Sidak multiple comparison test.

5.2.4 Formation of synchronised network activity in ATS line

Differentiated neurons from control and ATS lines were plated onto MEAs to identify basal excitability and network characteristics. As with the previous MEA experiments, neurons were treated with DAPT to remove NPCs from the culture and allow synchronised network activity to form over the next 50 days. The lines were recorded 50 days post-plating (50DPP) and analysed to identify if any differences occurred between the control and ATS neurons (Figure 5.5). The control and ATS lines did not show any differences in overall activity as measured by average spikes per electrode (t(0.5996)=7, p=0.5677) and average spike rate (t(0.0982)=7, p=0.9245), determined by unpaired T-test (Figure 5.5c-d). However, the ATS line showed a significant

decrease in the total number of bursts as determined by Welch's T-test ($t(3.449)=4.577$, $p=0.0210$) (Figure 5.5e). This decrease in the number of bursts can be explained by the changes to the network characteristics of the culture. The ATS line showed a significant increase in the SB interval compared to control as determined by Mann Whitney test ($U=0$, $p=0.0159$) (Figure 5.5f). As shown by the ASDR plot and Figure 5.5g, the SB interval is much more variable in the ATS line, showing groups of bursts followed by variable larger intervals. The ATS line also displayed a significant increase in the max ASDR as determined by unpaired T-test ($t(2.519)=7$, $p=0.0399$) (Figure 5.5h). This shows that the ATS line is more highly synchronised than the control line, however the bursts occur less often and the pattern of the synchronised burst behaviour is less regular compared to the control line.

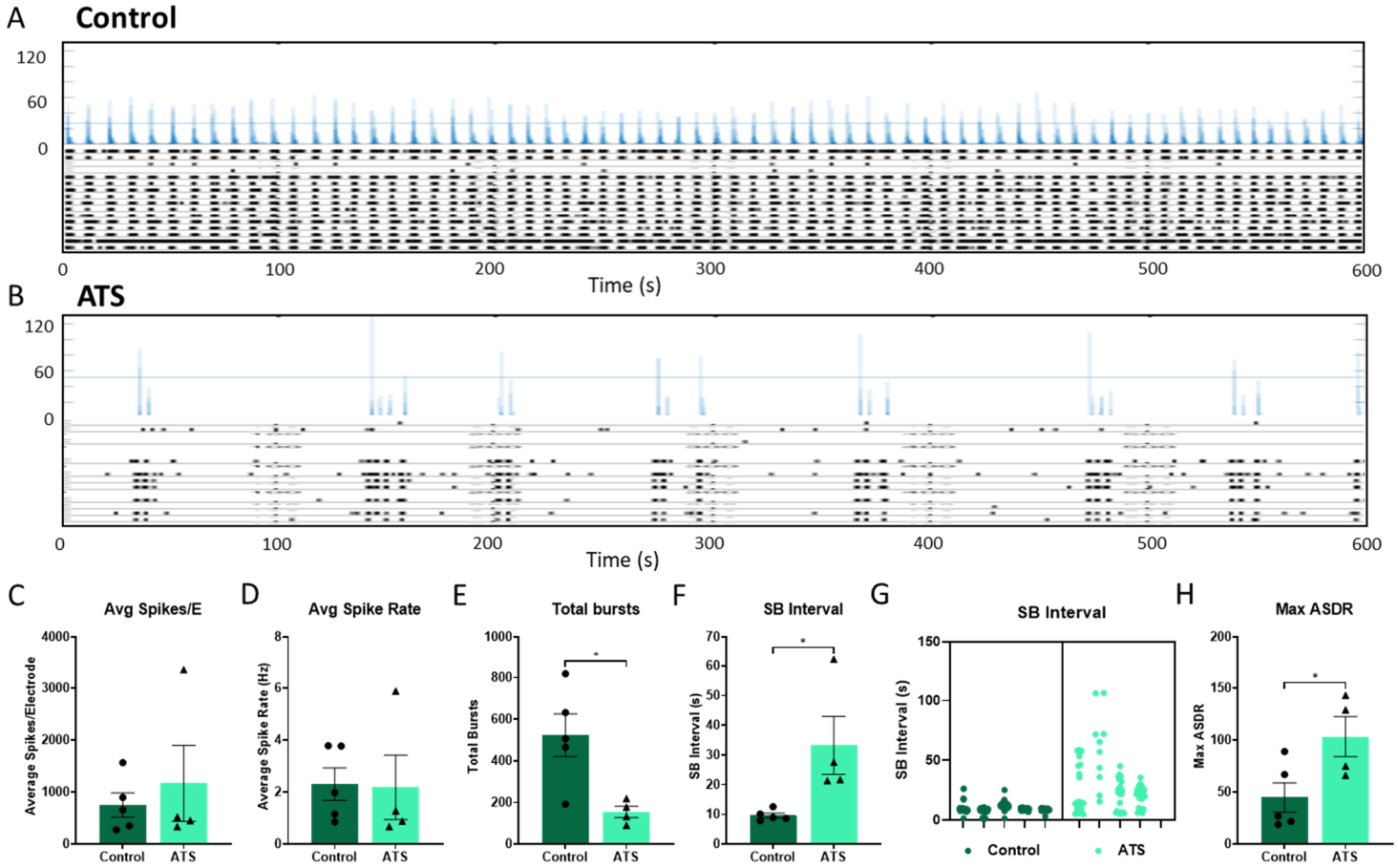

*Figure 5.5 Neuronal network activity of Control and ATS neurons on MEAs 50 days after plating. (A-B) Representative ASDR (top) and raster(bottom) plots showing spontaneous activity from a well of Control and ATS neurons. Basal excitability measured by (C) average spikes per electrode, (D) average spike rate and (E) total number of bursts. Synchronicity measured by (F) average synchronised burst (SB) interval, (G) plots showing all SB interval lengths for each well over the 10-minute recording and (H) maximum array-wide spike detection rate (ASDR). The plots represent data from one differentiation with 5 wells of control neurons and 4 wells of ATS neurons. (*p<0.05)*

5.2.5 Effect of LTCC antagonism on network activity in ATS line

TS is caused by a gain of function mutation in Cav1.2 so we tested the effect of blockade of LTCCs on neuronal network activity using diltiazem to see if this would rescue the activity in the ATS line compared to control. Figure 5.6 shows ASDR and raster plots of the response to 5µM diltiazem for one well of the Control and ATS lines and an example electrode recording from each well. Figure 5.7 shows summary data of the excitability and network characteristics used to measure the activity of the cultures. The statistics for this data is summarised in Table 5.2. Diltiazem had no effect on general excitability of the cultures, as measured by average spikes per electrode (Control, 990±237.54 vs 1172.5±377.8; ATS, 518.4±115.4 vs 620.4±57.3), average spike rate (Control, 2.19±0.57 Hz vs 2.26±0.67 Hz; ATS, 1.40±0.53 Hz vs 2.18±0.97 Hz) and total bursts (Control, 557.8±119.3 vs 502.8±138.4; ATS, 139.8±33.3 vs 236.8±42.9) (Figure 5.7a-c). However, it did have a significant effect on the synchronicity of the cultures. The ATS line showed a clear response to diltiazem, with a significant reduction in the average interval between synchronised bursts (33.77±8.60 s vs 13.90±0.84 s) and a more regular interval between each burst (Figure 5.7d-e). At baseline there was a significant difference in the SB interval between the Control and ATS line, as also shown at 50DPP. However, following application of diltiazem this difference was lost due to the reduction in SB interval in the ATS line. The control line also showed a slight reduction in the SB interval (9.66±0.82 s vs 6.83±1.23 s), although this was not significant. Diltiazem did not affect the max ASDR of the cultures, and the genotype effect previously shown in 50DPP recordings was present both at baseline (Control, 33.20±10.70; ATS, 93.50±21.55) and following diltiazem (Control, 22.80±5.83; ATS, 77.75±10.32) application (Figure 5.7f). These results suggest that diltiazem can rescue the pattern of synchronised bursting activity, but the cultures still show increased synchronicity as shown by higher max ASDR and lower total number of bursts compared to the control.

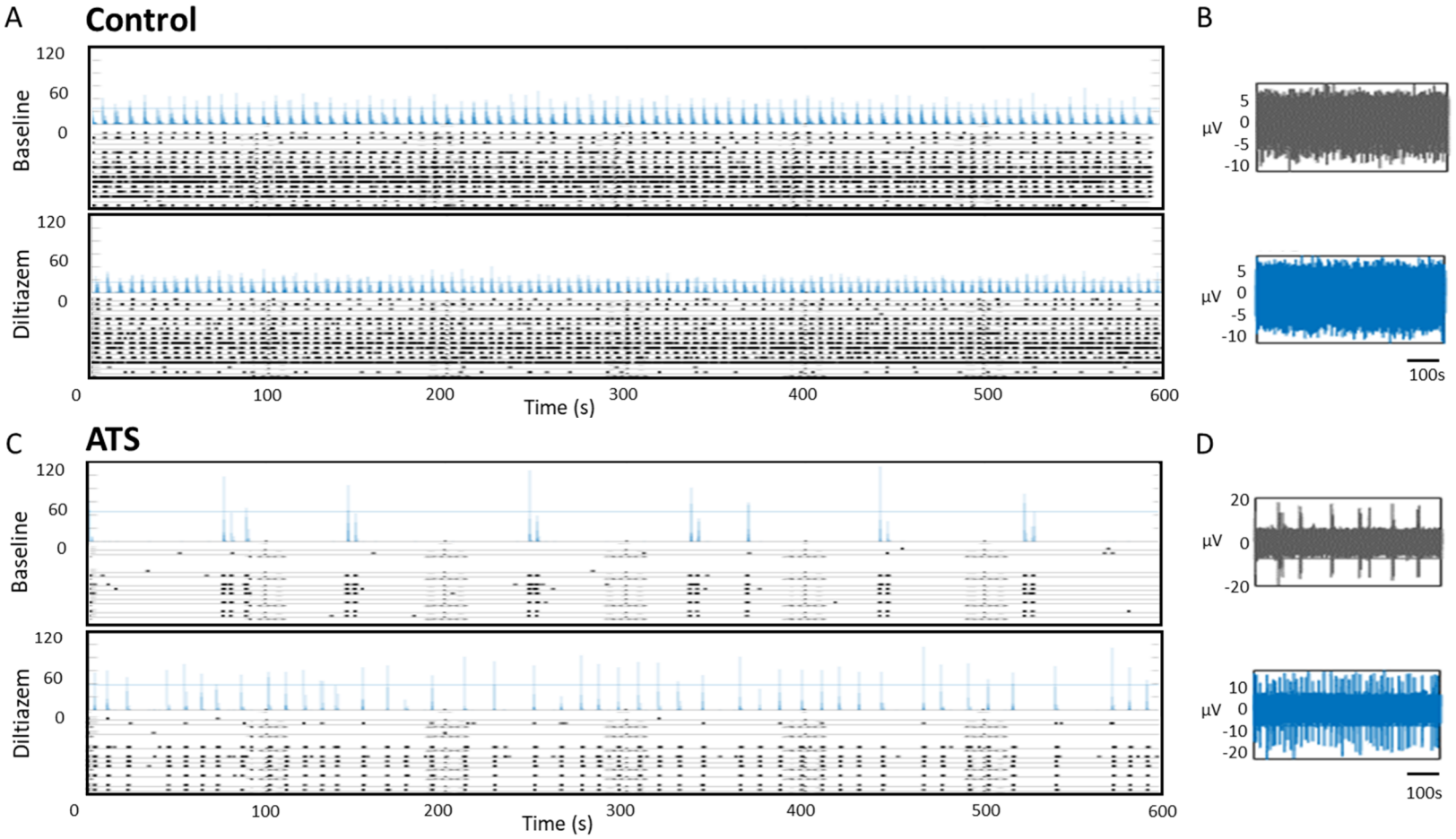

Figure 5.6 Effect of blockade of LTCCs on neuronal network activity of Control and ATS iPSC-derived neurons. (A and C) Representative raster and ASDR plots showing spontaneous activity of Control and ATS neurons before and after application of 5µM diltiazem. (B and D) Representative voltage traces from one electrode of the Control and ATS neuron cultures before and after application of diltiazem. The voltages traces are from the same well as the raster and ASDR plots.

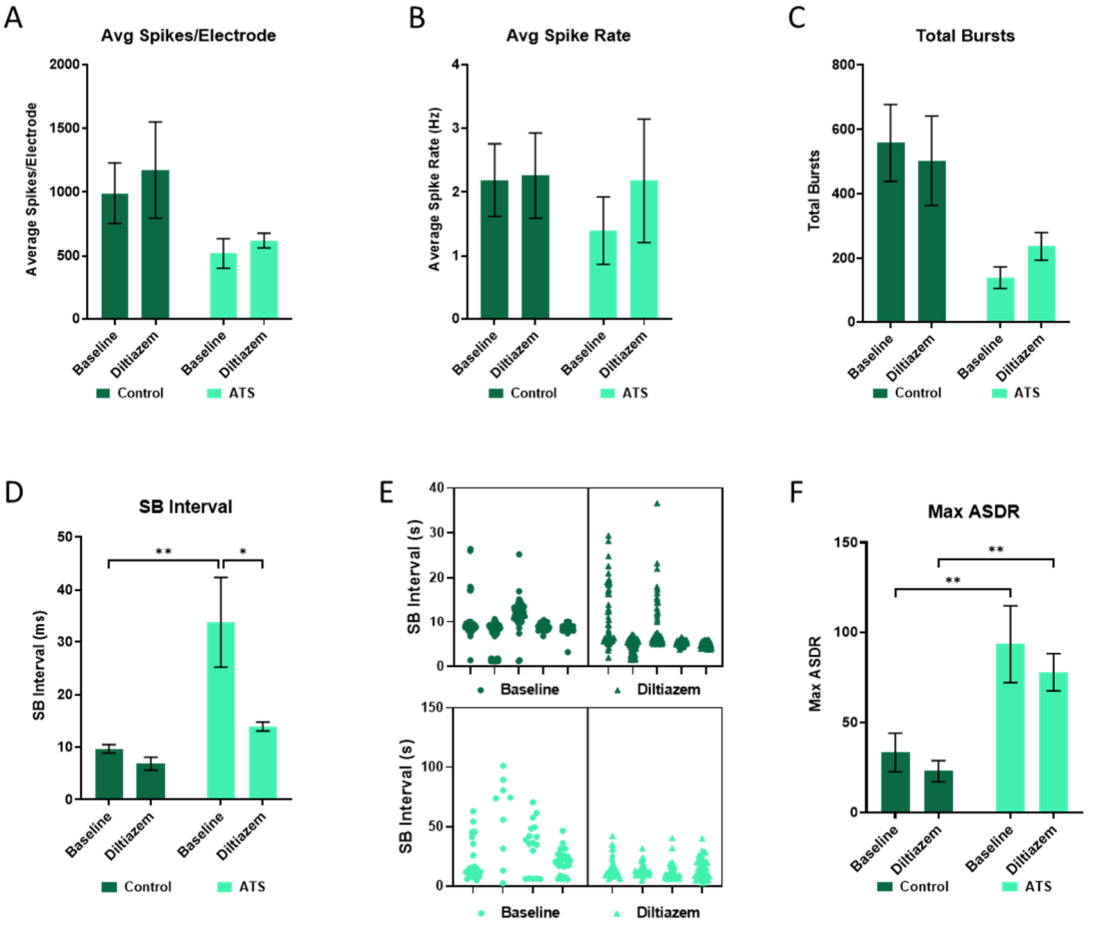

*Figure 5.7 Neuronal excitability and network characteristics following application of 5µM diltiazem in control and ATS iPSC-derived neurons. (A-C) Basal excitability measured by average spikes per electrode, average spike rate and total number of bursts. (D) Average synchronised burst (SB) interval in each condition. (E) Plots showing all SB interval lengths for each well over the 10-minute recording. (F) Maximum array-wide spike detection rate (ASDR) in each condition. The plots represent data from one differentiation with 5 wells of control neurons and 4 wells of ATS neurons. (*p<0.05, **p<0.01)*

Diltiazem	Main Effect	2 Way ANOVA	Holm-Sidak multiple comparisons
Average Spikes / Electrode	Interaction	F (1, 7) = 0.1323, P=0.7268	No post-hoc comparisons
	Treatment	F (1, 7) = 1.652, P=0.2395	
	Genotype	F (1, 7) = 2.144, P=0.1865	
Average Spike Rate	Interaction	F (1, 7) = 2.064, P=0.1940	No post-hoc comparisons
	Treatment	F (1, 7) = 2.977, P=0.1281	
	Genotype	F (1, 7) = 0.2119, P=0.6593	
Total Bursts	Interaction	F (1, 7) = 3.508, P=0.1032	No post-hoc comparisons
	Treatment	F (1, 7) = 0.2679, P=0.6207	
	Genotype	F (1, 7) = 5.585, P=0.0501	
SB Interval	**Interaction**	F (1, 7) = 4.513, P=0.0712	
	Treatment	**F (1, 7) = 8.004, P=0.0254**	Ctrl, Baseline vs Diltiazem P=0.6135
			ATS, Baseline vs Diltiazem P=0.0376
	Genotype	**F (1, 7) = 17.20, P=0.0043**	**Baseline, Ctrl vs ATS P=0.0024**
			Diltiazem, Ctrl vs ATS P=0.3904
Max ASDR	Interaction	F (1, 7) = 0.1904, P=0.6757	
	Treatment	F (1, 7) = 4.550, P=0.0704	
	Genotype	**F (1, 7) = 11.94, P=0.0106**	**Baseline, Ctrl vs ATS P=0.0087**
			Diltiazem, Ctrl vs ATS P=0.0087

Table 5.2 Summary of statisitcs for effect of diltiazem on excitability and network characteristics in Control and ATS neurons. Data was analysed by repeated measures Two-way ANOVA followed by Holm-Sidak multiple comparison test.

5.2.6 Effect of GABA-A receptor antagonism on network activity in ATS line

As discussed in the previous results chapter, the ATS line showed increased expression of GAD enzymes, particularly GAD65, suggesting an increase in synaptic GABA signalling. Therefore, the GABA-A receptor antagonist bicuculline was applied to the cultures to see if reducing GABA signalling would rescue the ATS network activity phenotype. Figure 5.8 shows raster plots of the response to 10µM bicuculline for one well of the Control and ATS lines and an example electrode recording from each well. Figure 5.9 shows summary data of the excitability and network characteristics used to measure the activity of the cultures. The statistics for this data is summarised in Table 5.3. Like diltiazem, bicuculline had no effect on the average

spikes per electrode (Control, 726.60±206.60 vs 989.50±274.98; ATS, 770.375±579.20 vs 1225.50±780.25) or the average spike rate (Control, 2.13±0.64 Hz vs 3.50±1.41 Hz; ATS, 2.23±1.77 Hz vs 3.93±2.40 Hz) (Figure 5.9a-b). However, it did have a significant effect on total bursts following repeated measures 2-way ANOVA ($F(1, 7) = 8.817$, $P = 0.0208$) (Figure 5.9c). Both lines showed an increase in the total number of bursts following bicuculline (Control, 553.40±125.93 vs 682.80±144.47; ATS, 277.00±121.65 vs 525.25±182.13); but this was not significant in either line following post-hoc tests.

Like diltiazem, bicuculline had a significant effect on the pattern of synchronised bursting in the ATS line. The ATS line showed a significant reduction in the average interval between synchronised bursts (27.73±8.48 s vs 9.56±2.47 s) and a more regular interval between each burst, although some larger intervals remained (Figure 5.9d-e). At baseline there was a significant difference in the SB interval between the Control and ATS line, as previously shown. However, following application of bicuculline this difference was lost, due to the reduction in SB interval in the ATS line. As with diltiazem, the control line also showed a slight reduction in the SB interval (8.24±1.24 s vs 5.50±0.58 s), although this was not significant. Bicuculline had no significant effect on max ADR (Control, 36.00±6.63 vs 58.80±13.11; ATS 138.50±75.23 vs 97.25±39.62). These results suggest that application of bicuculline has a similar effect to diltiazem, with rescue of the pattern of synchronised bursts, as shown by a reduction in the SB interval.

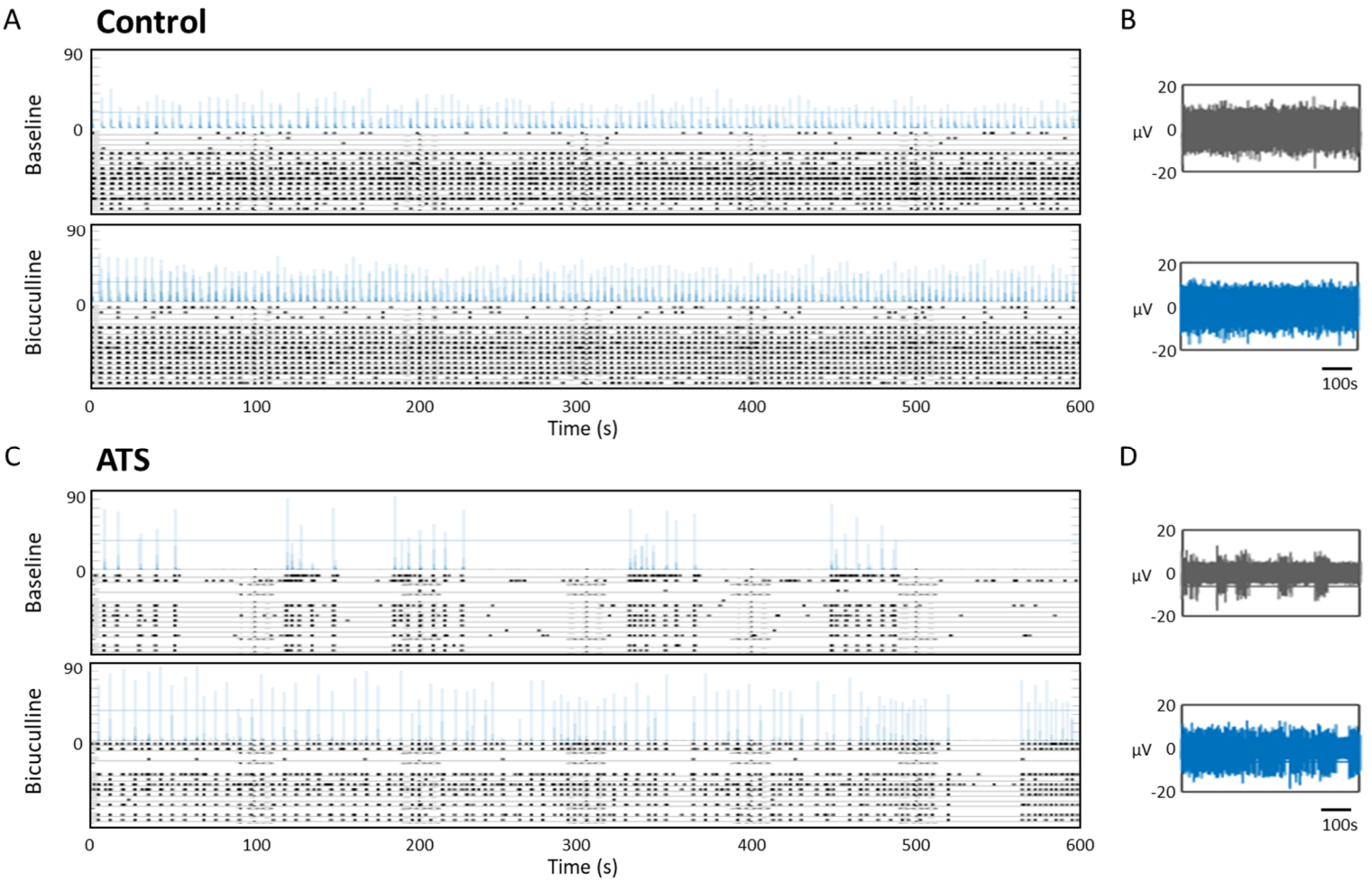

Figure 5.8 Effect of blockade of GABA-A receptors on neuronal network activity of Control and ATS iPSC-derived neurons. (A and C) Representative raster and ASDR plots showing spontaneous activity of Control and ATS neurons before and after application of 10µM bicuculline. (B and D) Representative voltage traces from one electrode of the Control and ATS neuron cultures before and after application of bicuculline. The voltages traces are from the same well as the raster and ASDR plots.

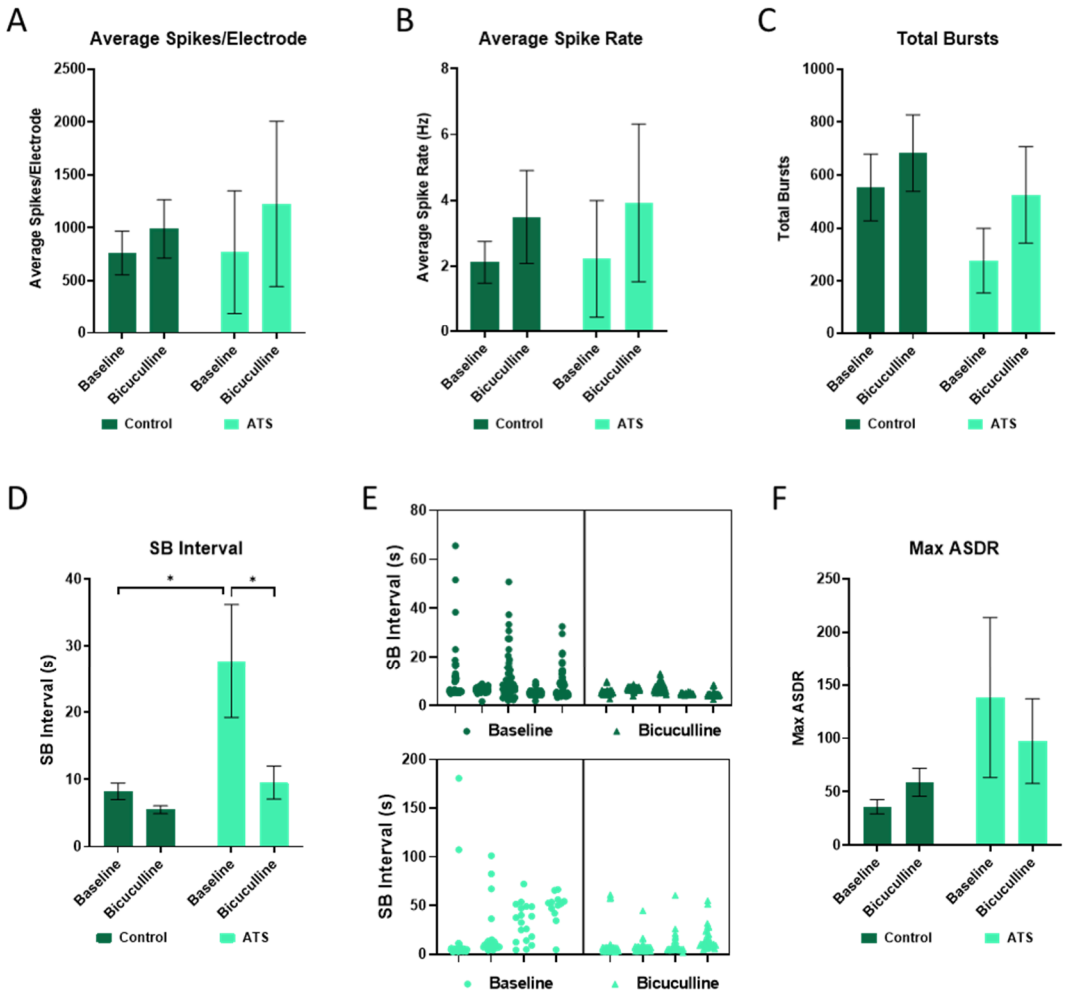

Figure 5.9 Neuronal excitability and network characteristics following application of 10µM bicuculline in control and ATS iPSC-derived neurons. (A-C) Basal excitability measured by average spikes per electrode, average spike rate and total number of bursts. (D) Average synchronised burst (SB) interval in each condition. (E) Plots showing all SB interval lengths for each well over the 10-minute recording. (F) Maximum array-wide spike detection rate (ASDR) in each condition. The plots represent data from one differentiation with 5 wells of control neurons and 4 wells of ATS neurons. ($p \leq 0.05$)*

Bicuculline	Main Effect	2 Way ANOVA	Holm-Sidak multiple comparisons
Average Spikes / Electrode	Interaction	F (1, 7) = 0.3751, P=0.5596	No post-hoc comparisons
	Treatment	F (1, 7) = 3.349, P=0.1099	
	Genotype	F (1, 7) = 0.03663, P=0.8536	
Average Spike Rate	Interaction	F (1, 7) = 0.03449, P=0.8579	No post-hoc comparisons
	Treatment	F (1, 7) = 3.032, P=0.1252	
	Genotype	F (1, 7) = 0.01708, P=0.8997	
Total Bursts	Interaction	F (1, 7) = 0.8732, P=0.3812	
	Treatment	**F (1, 7) = 8.817, P=0.0208**	Control, Baseline vs Bicuculline P=0.1708
			ATS, Baseline vs Bicuculline P=0.0678
	Genotype	F (1, 7) = 1.237, P=0.3029	
SB Interval	**Interaction**	**F (1, 7) = 6.766, P=0.0354**	
	Treatment	**F (1, 7) = 12.43, P=0.0097**	Control, Baseline vs Bicuculline P=0.7301
			ATS, Baseline vs Bicuculline P=0.0143
	Genotype	**F (1, 7) = 6.167, P=0.0420**	**Baseline, Control vs ATS P=0.0143**
			Bicuculline, Control vs ATS P=0.7301
Max ASDR	Interaction	F (1, 7) = 3.368, P=0.1091	No post-hoc comparisons
	Treatment	F (1, 7) = 0.2795, P=0.6134	
	Genotype	F (1, 7) = 1.894, P=0.2112	

Table 5.3 Summary of statisitcs for effect of bicuculline on excitability and network characteristics in Control and ATS neurons. Data was analysed by repeated measures Two-way ANOVA followed by Holm-Sidak multiple comparison test.

5.2.7 Effect of MEK inhibitor on network activity in ATS line

Although the ATS line showed no significant changes to ERK1/2 and CREB signalling, it was significantly reduced in the CACNA1C homozygous lines and other studies have shown CREB signalling is upregulated in classical TS (Paşca et al. 2011; Li et al. 2016; Servili et al. 2020). This suggests that Cav1.2 plays an important role in regulating CREB-dependent gene expression. In addition, activation of this pathway via a TrkB agonist has been shown to rescue behavioural deficits and long-term potentiation in a heterozygous CACNA1C rat model (Tigaret et al. 2021). Therefore, we investigated whether targeting ERK1/2 signalling via the MEK inhibitor selumitinib would alter

neuronal network activity in both the control and ATS lines. Selumitinib was used at 1µM based on a previous cell study showing this dose maximally inhibits phosphorylation of ERK1/2 (Alquezar et al. 2015). The cultures were recorded 1 hour and 21 hours after application of selumitinib as it targets gene expression pathways so may take longer to affect neuronal activity, compared to targeting ion channels or receptors. Figure 5.10 shows raster plots of the response to selumitinib for one well of the Control and ATS lines and an example electrode recording from each well. Figure 5.11 shows summary data of the excitability and network characteristics used to measure the activity of the cultures. The statistics for this data is summarised in Table 5.4.

Selumitinib had no effect on average spikes per electrode (Control, 1286.20±217.28 vs 1107.60±161.36 vs 1248.68±252.68; ATS, 820.87±240.19 vs 956.75±143.04 vs 737.25±277.30) (Figure 5.11a). There was also no effect on the average spike rate (Control, 3.12±0.68 Hz vs 2.84±0.72 Hz vs 3.58±0.848 Hz; ATS, 2.37±1.09 Hz vs 2.63±1.13 Hz vs 2.20±1.16 Hz), although repeated measures 2-way ANOVA showed a significant interaction effect between treatment and genotype ($F(2, 14) = 14.10$, $P=0.0004$). Post-hoc tests did not find any significant effects between control and ATS or following drug treatment in either line. Selumitinib also had no effect on total bursts, with the only significant effect being between Control and ATS at each time-point (Baseline, 722.20±87.69 vs 224.50±49.98; 1 h, 704.80±106.125 vs 259.75±46.89; 21 h, 695.20±84.08 vs 188.75±51.99). This suggest that Selumitinib has no effect on the general excitability of the cultures. Selumitinib also had no effect on the SB interval in both control (12.63±3.26 s vs 14.80±6.98 s vs 13.57±2.85 s) and TS (25.99±1.31 s vs 18.76±0.70 s vs 29.90±2.971) cultures. However, it did have a significant effect on max ASDR ($F(2, 14) = 30.02$, $P<0.0001$). There were no significant differences in max ASDR following 1 hour incubation in the control (48.80±10.61 vs 41.8±10.523) and ATS (166.25±26.088 vs 173.50±24.62) lines. However, after 21 hours both lines showed a significant increase in max ASDR (Control, 48.80±10.61 vs 71.60±7.64; ATS, 166.25±26.088 vs 199.00±28.393), suggesting an increase in synchronicity of the cultures.

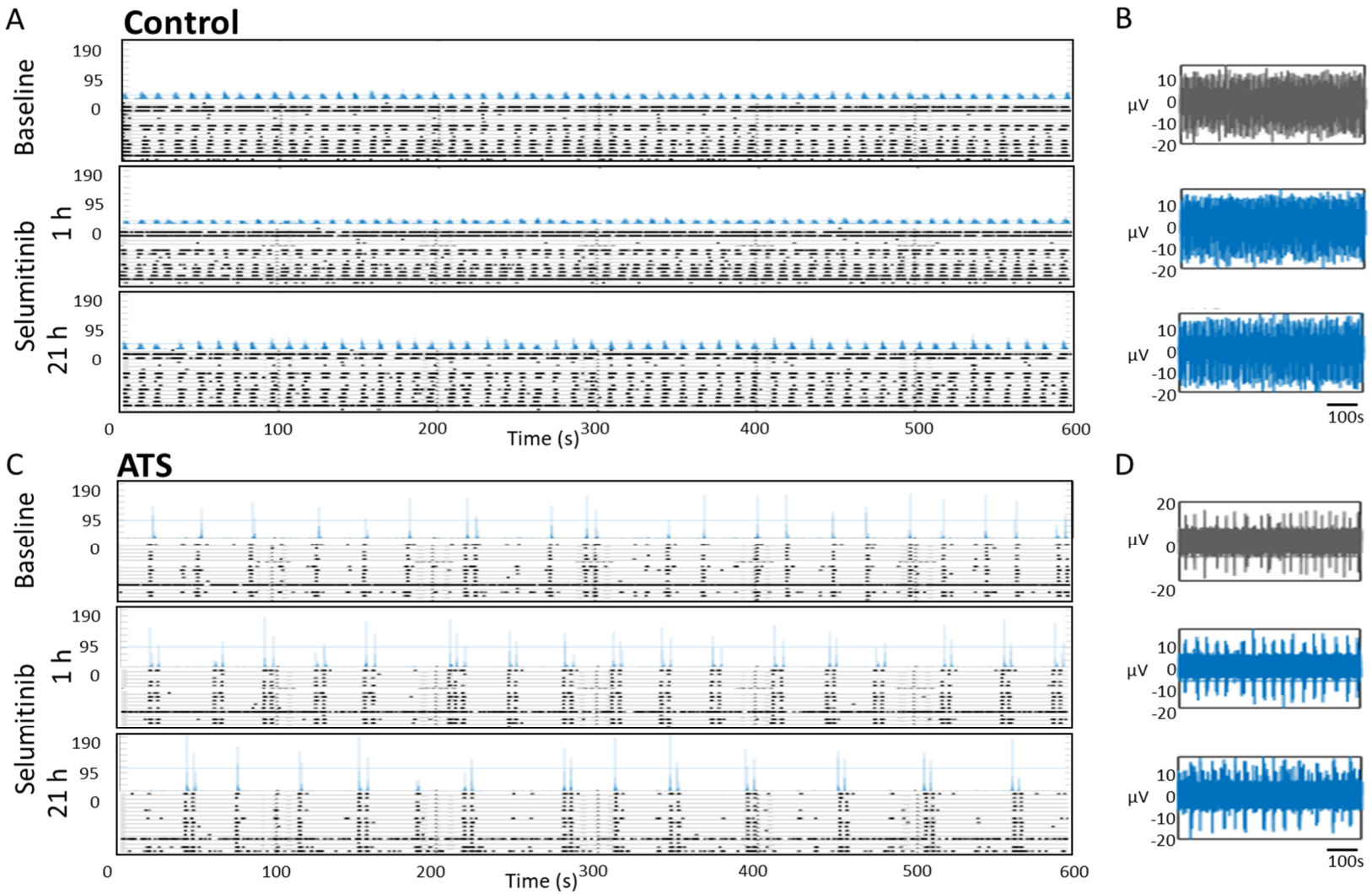

Figure 5.10 Effect of blockade of MEK signalling on neuronal network activity of Control and ATS iPSC-derived neurons. (A and C) Representative raster and ASDR plots showing spontaneous activity of Control and ATS neurons before and after application of 1μM selumitinib at 1 hour and 21 hours post-application. (B and D) Representative voltage traces from one electrode of the Control and ATS neuron cultures before and after (1 hour and 21 hours) application of selumitinib. The voltages traces are from the same well as the raster and ASDR plots.

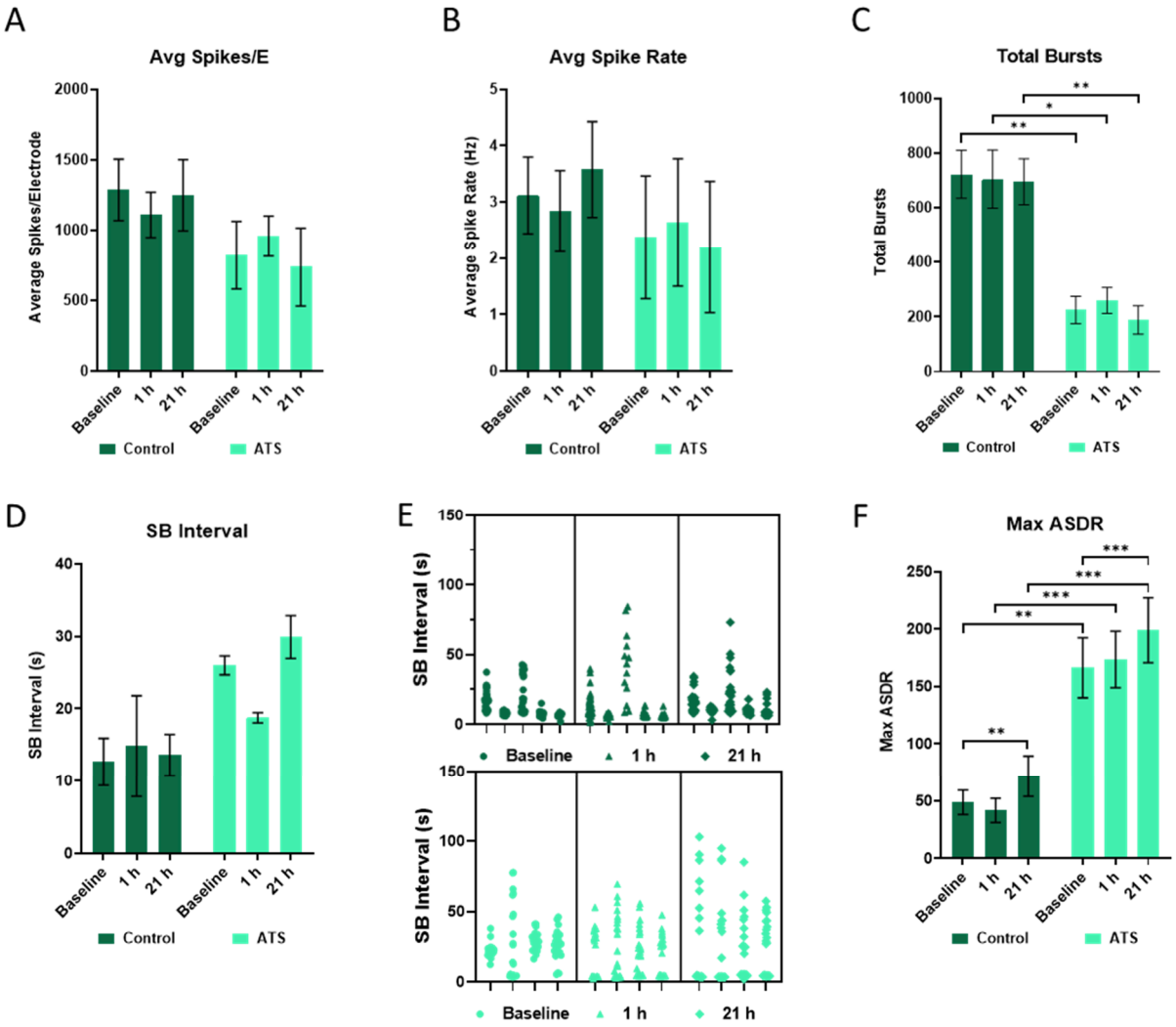

*Figure 5.11 Neuronal excitability and network characteristics 1 hour and 21 hours after application of 1μM selumitinib in control and ATS iPSC-derived neurons. (A-C) Basal excitability measured by average spikes per electrode, average spike rate and total number of bursts. (D) Average synchronised burst (SB) interval in each condition. (E) Plots showing all SB interval lengths for each well over the 10-minute recording. (F) Maximum array-wide spike detection rate (ASDR) in each condition. The plots represent data from one differentiation with 5 wells of control neurons and 4 wells of ATS neurons. (*p≤0.05, **p≤0.01, ***p≤0.001)*

Selumitinib	Main Effect	2 Way ANOVA	Holm-Sidak multiple comparisons
Average Spikes / Electrode	Interaction	F (2, 14) = 1.707, P=0.2171	No post-hoc comparisons
	Treatment	F (1.760, 12.32) = 0.1680, P=0.8213	
	Genotype	F (1, 7) = 1.690, P=0.2348	
Average Spike Rate	**Interaction**	**F (2, 14) = 14.10, P=0.0004**	Control, Baseline vs 1h P=0.1674
			Control, Baseline vs 21h P=0.0683
	Treatment	F (1.943, 13.60) = 1.218	ATS, Baseline vs 1h P=0.1632
			ATS, Baseline vs 21h P=0.2445
	Genotype	F (1, 7) = 0.3541	Baseline, Control vs ATS P=0.5864
			1 h, Control vs ATS P=0.8846
			21 h, Control vs ATS P=0.3775
Total Bursts	Interaction	F (2, 14) = 0.7901, P=0.4730	
	Treatment	F (1.566, 10.96) = 1.284, P=0.3053	
	Genotype	**F (1, 7) = 19.25, P=0.0032**	**Baseline, Control vs ATS P=0.0073**
			1 h, Control vs ATS P=0.0308
			21 h, Control vs ATS P=0.0054
SB Interval	Interaction	F (2, 14) = 3.545, P=0.0568	No post-hoc comparisons
	Treatment	F (1.682, 11.78) = 2.087, P=0.1709	
	Genotype	F (1, 7) = 5.254, P=0.0556	
Max ASDR	Interaction	F (2, 14) = 1.566, P=0.2433	
	Treatment	**F (2, 14) = 30.02, P<0.0001**	Control, Baseline vs 1h P=0.3984
			Control, Baseline vs 21h P=0.003
			ATS, Baseline vs 1h P=0.3984
			ATS, Baseline vs 21h P=0.0007
	Genotype	**F (1, 7) = 21.16, P=0.0025**	**Baseline, Control vs ATS P=0.0016**
			1 h, Control vs ATS P=0.0007
			21 h, Control vs ATS P=0.0010

Table 5.4 Summary of statisitcs for effect of selumitnib after 1 hour and 21 hours on excitability and network characteristics in Control and ATS neurons. Data was analysed by repeated measures Two-way ANOVA followed by Holm-Sidak multiple comparison test.

5.3 Discussion

This chapter describes the role of CACNA1C on neuronal network activity. Results from both the homozygous knockout and ATS line show that CACNA1C has a clear impact on synchronised neuronal network activity, but no effect on basal excitability. The Hom line showed a reduction in the synchronised burst interval; this effect has also been shown to occur following acute application of LTCC blockers (Plumbly et al. 2019). Both diltiazem and nimodipine led to a reduction in the synchronised burst interval, but blockade of T-type or P/Q type VGCCs had no effect on the synchronicity of iPSC-derived neurons, showing LTCCs specifically are important in controlling the pattern of synchronised bursts. The results from the Hom line show that loss of Cav1.2 alone is enough to alter the synchronised burst interval, though this does not mean that Cav1.3 does not also contribute towards synchronised network activity. Interestingly, chronic loss of CACNA1C throughout the neuronal differentiation had the same effect on network activity as acute blockade of LTCCs. This suggests that the changes in network activity in the Hom line are not due to changes occurring during neuronal development, but instead are due to the role of Cav1.2 in mature neurons and thus is likely to be rescuable by restoring Cav1.2 function. The LTCC activator Bay K8644 had been planned to be tested to see if increased activation of Cav1.3 would rescue the SB interval, however due to technical issues and time constraints this could not be completed. However, it would be a valuable future experiment to identify if both Cav1.2 and Cav1.3 play the same role in network activity. It would also be interesting to see the effect of Bay K 8644 on control neurons and if it produces a similar phenotype to the ATS line.

The ATS line had the opposite effect on network activity to the Hom line, but also showed additional changes. Although the synchronised burst interval was increased in the ATS line, the interval was also more varied with groups of synchronised bursts occurring followed by longer periods of inactivity. The max ASDR was increased, and total number of bursts decreased, suggesting an increased synchronicity between neurons in the ATS cultures. Calcium signalling has been shown to be important for the maturation of neurons. In these experiments, astrocyte-conditioned media is

used to increase maturation of the neurons. However, Rushton and colleagues showed that astrocyte-conditioned media (ACM) could be replaced by media with a high calcium concentration, GABA or Bay K 8644 to produce fully functional neurons. They showed that Bay K 8644 hyperpolarised neurons to enhance excitability and increase spontaneous activity (Rushton et al. 2013). The ATS line did not show any changes to basal excitability compared to control, however this is likely to be due to the use of ACM to enhance the excitability of both control and ATS neurons. As the ATS line contains a predicted gain-of-function mutation in CACNA1C we tested diltiazem to see if it would rescue the network phenotype. Application of diltiazem caused a reduction in the SB interval in the control line, although it was not significant, matching previous studies showing this effect (Plumbly et al. 2019). It had a much larger effect on the ATS line, with a significant reduction in synchronised length and increased regularity of the bursts. There was no effect on the max ASDR or total bursts, indicating that blockade of LTCCs rescues only the pattern of bursting behaviour and not the increase in synchronicity.

Previous studies have shown that GABA signalling is important in the regulation of neuronal network activity and the Homozygous and ATS lines showed opposing changes to expression of GAD enzymes (Odawara et al. 2014; Lu et al. 2015; Odawara et al. 2016). Therefore, we targeted GABA signalling in both lines to try to rescue the changes to network activity. The Hom line shows a reduction in GAD enzyme expression so diazepam was used to augment GABA signalling. Whereas the ATS line shows increased GAD expression so bicuculline was used on this line. In the control line, diazepam caused a significant increase in the SB interval without altering basal excitability or any other measures of network activity. Bicuculline had the opposite effect causing a decrease in SB interval, although this was not significant, with no effect on spike number or rate. Other studies have also shown that GABA-A receptor activation is important for controlling the pattern of network activity. Activation of GABA-A receptors with either agonists or PAMs causes an increased interval between synchronised bursts (Bader et al. 2017). Antagonism of GABA-A receptors has the opposite effect, bicuculline and other antagonists decrease the SB interval in cultured neurons (Lu et al. 2015; Odawara et al. 2016; Plumbly et al. 2019). However, all these

studies except one also showed that modulation of GABA-A receptor activation also alters basal excitability measures such as the spike rate. The concentrations of bicuculline and diazepam used are comparative between studies, so this does not explain the different results. The other study that did not show changes to basal excitability was also carried out in cortical iPSC neurons, generated using a similar protocol (Plumbly et al. 2019). Therefore, it is possible that the opposing results are due to differences in the proportion of GABAergic neurons present in the culture. The other experiments were carried out using primary rodent neurons. In the rodent brain and thus primary cultures, GABAergic neurons make up roughly 20% of cortical neurons (Sahara et al. 2012; Bader et al. 2017). However, the iPSC-derived neurons in this experiment are mostly glutamatergic neurons with a small proportion (less than 5%) of GABAergic neurons (Plumbly et al. 2019). This suggests that when there is a low proportion of GABAergic neurons, GABA-A receptor pharmacology does not modulate basal excitability of neurons. However, it is still able to affect the network activity, suggesting that the co-ordinated activity of neuronal networks is much more sensitive and dependent on GABAergic signalling than basal excitability characteristics.

In contrast to the control neurons the Hom line showed no response to diazepam treatment. This could be for several reasons. First, diazepam acts as a positive allosteric modulator, so is still reliant on the release of GABA to activate GABA-A receptors. As GAD65 and GAD67 expression is significantly reduced in the Hom line there may not be enough GABA being released for Diazepam to have a meaningful effect. The second reason could be that the expression of GABA-A receptors is also reduced in the Hom line as studies have shown that modulation of LTCC activity alters the expression of GABA-A receptor subunits at the synapse. Chronic blockade (24 hours) of LTCCs with nifedipine leads to a reduction in the number of GABA-A receptors at synaptic sites via increased proteasomal degradation and decreased membrane insertion (Saliba et al. 2009). Whereas acute activation (5-10 minutes) of LTCCs with Bay K 8644 leads to an increase in surface expression of GABA-A receptors via CamKII-dependent phosphorylation of the GABA-A receptor β3 subunit (Saliba et

al. 2012). Therefore, chronic loss of Cav1.2 may lead to a reduction in GABA-A receptor expression leading to a loss of sensitivity to diazepam treatment.

Antagonism of GABA-A receptors in the ATS line with bicuculline rescued the SB interval. This was not surprising as bicuculline has previously been shown to reduce the synchronised burst interval and GABA signalling is increased in the ATS line (Lu et al. 2015; Odawara et al. 2016; Plumbly et al. 2019). Perhaps more interesting is the fact that acute blockade of LTCCs and GABA-A receptors has the same effect on network activity. Cav1.2 has been shown to be expressed on the soma and dendrites of both glutamatergic and GABAergic neurons, so changes to neuronal activity via Cav1.2 could occur via glutamatergic or GABAergic neurons (Obermair et al. 2004). In glutamatergic neurons, Cav1.2 may alter bursting activity by modulating the post burst-AHP phase. Cav1.2 associates with BK channels to induce this refractory period of hyperpolarisation. Therefore, loss or blockade of Cav1.2 may lead to reduced activation of BK channels and a shorter AHP period. However, as LTCC blockade has the same effect as GABA-A antagonism and GABAergic signalling has been shown to be important for the generation and pattern of network burst activity, it is likely that Cav1.2 influences this pathway. Neuronal activity is highly regulated, and studies have shown that chronic alterations in neuronal activity can lead to homeostatic synaptic scaling of GABAergic synaptic strength (Kilman et al. 2002; Hartman et al. 2006; Swanwick et al. 2006). It is likely that this occurs via LTCCs and their role in coupling neuronal activity to gene expression. It has also been shown that blockade of LTCCs with nifedipine for 24 hours leads to a reduction in GABA-A receptor expression (Saliba et al. 2009). However, activation of LTCCs has been shown to increase membrane expression of GABA-A receptors within 5-10 minutes of drug application (Saliba et al. 2012). Therefore, it is likely that acute application of a LTCC blocker could cause a reduction in GABA-A receptor expression after 10 minutes. This reduction in expression would have a similar effect to the application of bicuculline, in that the number of activated GABA-A receptors would be reduced and thus the SB interval increased. These findings suggest that Cav1.2 is an important modulator of GABAergic signalling and that both acute blockade and chronic loss of Cav1.2 leads to synaptic scaling that reduces the effect of GABA on neuronal cultures.

Blockade of ERK1/2 signalling had no effect on the burst pattern of either the control or ATS neurons. The only effect it had was to increase the max ASDR after 21 hours, suggesting an increase in synchronisation of the neurons. Although ERK1/2 signalling was not increased in the ATS neurons, it was decreased in the knockout lines. Additionally, a TrkB agonist, which increases ERK1/2 and CREB phosphorylation has been shown to restore deficits in synaptic plasticity in heterozygous mouse (Tigaret et al. 2021). Therefore, we had hypothesised that targeting ERK1/2 signalling would also alter the SB interval of neuronal networks. While inhibition of ERK1/2 did not alter the burst pattern of control and ATS lines it is possible that activation of ERK1/2 via the TrkB agonist may have had an effect in the knockout line. We had planned to test this but due to technical issues and time constraints the experiment was not carried out. The lack of response to selumitinib in the neuronal cultures however does suggest that Cav1.2 is not modulating neuronal activity via ERK1/2-dependent changes in gene expression. Cav1.2 activates multiple signalling pathways, and it is possible that a different pathway is involved in modulating network activity. This would also fit with the hypothesis that Cav1.2 may modulate GABA-A receptor expression as studies have shown that CaMKII phosphorylates GABA-A receptors in neuronal cells. This leads to alterations in the subunit composition of the receptors and increased GABA currents (Houston and Smart 2006). Saliba and colleagues also showed that LTCC activation specifically leads to increased CaMKII phosphorylation of the β subunit of GABA-A receptors and thus insertion of the receptors onto the membrane (Saliba et al. 2012).

As ATS is a developmental disorder with symptoms including ASD and intellectual disability it is interesting to see how these findings compare to other neurodevelopmental disorders. Studies looking at non-syndromic ASD have shown alterations in the neuronal activity of ASD neurons. One study showed that ASD neurons had reduced frequency and half-width of spontaneous excitatory post-synaptic potentials (sEPSCs) associated with a decrease in synaptic markers (Liu et al. 2017). Marchetto and colleagues looked specifically at neurons derived from ASD patients with macrocephaly. They showed that ASD neurons showed a decrease in

the number of synchronised bursts and a decrease in the ASDR, suggesting a reduction in synchronicity of the cultures. However, they found no change in sEPSPs in ASD neurons (Marchetto et al. 2017). Another study also showed a reduction in connectivity but no change to the basal firing rate of neurons; ASD neurons showed a reduction in the number of bursting electrodes and dynamic complexity of the cultures (Amatya et al. 2019). There are also a few studies looking at the effect of neurodevelopmental disorders caused by genetic mutations on neuronal network activity. Patients-derived neurons containing mutations in TSC2, which causes a rare multisystem disorder with severe neurodevelopmental effects including ASD, have been shown to have increased neuronal excitability but decreased synchronicity. TSC2 neurons displayed a higher firing rate but decreased number of synchronised bursts with a larger interval between these bursts. The neurons showed an increase in the number of spikes occurring outside of bursts and less connectivity between electrodes (Alsaqati et al. 2020). Neurons derived from patients with 1q21.1 deletions, a copy number variant associated with schizophrenia, autism and epilepsy, also showed an increased spike rate and increase in the duration of synchronised bursts (Chapman et al. 2021). The results between these studies are variable, although they suggest a general phenotype of hyperexcitability coupled with reduced synchronicity for neurodevelopmental disorders. The ATS line did not show any changes in basal excitability but there were clear alterations in the network activity of cultures, with changes to the frequency of synchronised bursts appearing to be a common phenotype between disorders.

5.3.1 Conclusion

This chapter describes the analysis of neuronal activity and network properties in the CACNA1C knockout and ATS lines. CACNA1C does not impact basal neuronal activity but has a clear impact on network activity behaviour. Loss of CACNA1C leads to specific reduction in the interval between synchronised bursts, similar to that seen following acute blockade of LTCCs. The ATS line showed an increased interval between synchronised bursts, which was also more variable compared to control. The bursting pattern of the ATS line could be rescued by either blockade of LTCCs or

GABA-A receptors; suggesting that Cav1.2 and GABA-A receptors may have a common mechanism for controlling network activity. However, diazepam was unable to rescue the reduced SB interval in the knockout line, likely due to reduced GABAergic signalling leading to loss of sensitivity to the drug. Blockade of ERK1/2 signalling had no effect on the bursting pattern of either control or ATS neurons, suggesting that activation of this pathway is not required for Cav1.2 to alter network activity. Overall, these findings highlight that Cav1.2 is an important modulator of network activity in neurons and it likely that it does this by altering the strength of GABAergic signalling.

6 General Discussion

6.1 Summary of findings

6.1.1 Chapter 3: Generation and validation of CACNA1C mutant iPSC lines and an Atypical Timothy Syndrome patient iPSC line

The key aims of this project were to identify the role of CACNA1C in neuronal differentiation and neuronal network activity. To do this we used two different cell lines: a line carrying a point mutation in CACNA1C from a patient with ATS, and a CACNA1C knockout line. This chapter described the generation and validation of these lines.

Key Findings:

- Two CACNA1C knockout lines were generated using an inducible CRISPR-Cas9 iPSC line
- Homozygous deletions in exon 2 led to a 75% reduction of Cav1.2 protein. The remaining protein is likely to be present due to translation re-initiation in exon 6 and therefore is unlikely to be functional.
- The ATS line contains a novel point mutation (A1521P) in exon 38 of CACNA1C that is predicted to have a gain of function effect and be highly damaging.
- The point mutation has no effect on levels of expression of Cav1.2 protein in neurons.

6.1.2 Chapter 4: Phenotypic analysis of CACNA1C knockout and atypical Timothy Syndrome iPSC lines during cortical differentiation

Previous studies have shown that LTCCs play an important role in neuronal differentiation via CREB signalling. This chapter described the specific effect of alterations to Cav1.2 expression/function on neuronal differentiation and associated downstream signalling pathways.

Key Findings:

- The ATS line showed an increase in RNA expression of the transcription factor FoxG1 in NPCs (day 20).
- Loss of CACNA1C leads to a reduction in the expression of the neuronal marker MAP2 at RNA and protein level. There was a corresponding increase in the number of rosettes present in cultures, which suggests a deficit in differentiation of NPCs to neurons.
- The ATS line showed no changes to MAP2 expression but did show a reduction in the number of rosettes. This highlights a clear role for Cav1.2 in either rosette formation or maintenance.
- The knockout and ATS lines showed opposing effects on protein expression of GAD65 and GAD67. Loss of CACNA1C led to a reduction, whereas the ATS line showed an increase.
- There were no significant changes to RNA expression of glutamatergic markers or cortical layer markers.
- Loss of Cav1.2 led to a clear reduction in pERK1/2 and pCREB across multiple time-points of neuronal differentiation. pERK1/2 was reduced at Day 20 (NPCs), 30 (immature neurons) and 50 (mature neurons). pCREB was also decreased at day 20 and 30, however at day 50 there was also a reduction in total CREB expression.
- The ATS line showed no significant changes to pERK1/2 and pCREB expression. However, there was a trend towards an increase in phosphorylation of both proteins at day 20 and day 30 of neuronal differentiation.

6.1.3 Chapter 5: The effect of loss of CACNA1C and an ATS point mutation on neuronal network activity

Neuronal network function has commonly shown to be disrupted in neuropsychiatric disorders. This chapter described how Cav1.2 impacts neuronal network activity using the CACNA1C knockout line and ATS line.

Key Findings:

- Loss of CACNA1C had no significant effect on basal excitability of neurons but led to a reduction in the interval between synchronised bursts.
- Activation of GABA-A receptors with diazepam leads to an increase in the synchronised burst (SB) interval of control neurons. However, it had no effect on knockout neurons, suggesting a loss of sensitivity to diazepam.
- Basal excitability of the ATS line was no different to control line, but network activity was significantly altered. The SB interval was larger but also more variable in the ATS line. There was also a reduction in the total bursts and an increase in max ASDR which suggests an increased synchronisation, with more neurons firing at the same time.
- Blockade of LTCCs with diltiazem led to a reduction in the SB interval in both the control and ATS neurons. In the control line, this caused a reduction in SB interval like that seen in the CACNA1C knockout line. In the ATS line it led to a rescue of network activity, with more regular bursting.
- Blockade of GABA-A receptors with bicuculline also led to a reduction in the SB interval in both the control and ATS neurons. Bicuculline had a very similar effect to diltiazem in both lines.
- Blockade of MEK signalling with selumitinib had little effect on neuronal activity in the control and ATS lines. After 21 hours of treatment, both the control and ATS lines showed a significant increase in the Max ASDR. There was no effect on basal excitability or the SB interval. Blockade of MEK was unable to rescue the alterations in network activity in the ATS line.

6.2 Context and points of discussion

6.2.1 Neuronal development

Loss of Cav1.2 led to a reduction in the expression of the neuronal marker MAP2 and a corresponding increase in the number of rosettes still present at day 50 of the neuronal differentiation. These findings suggest that Cav1.2 is important for the

differentiation of NPCs into neurons. Interestingly the ATS line showed no change to MAP2 expression, however there was a decrease in the number of rosettes in the culture. As discussed in Chapter 4, LTCCs have been shown to be required for the differentiation of NPCs into neurons in rodent cultures and loss of Cav1.2 specifically is associated with a reduction in adult hippocampal neurogenesis (D'Ascenzo et al. 2006; Lepski et al. 2013). Alterations during neurodevelopment is thought to be a key contributor towards the development of both schizophrenia and ASD (Sacco et al. 2018). Indeed alterations to neurogenesis in animal models leads to behavioural alterations associated with schizophrenia (Iwata et al. 2008; Maekawa et al. 2009). Schizophrenia iPSC-derived NPCs have been shown to have an altered proliferation rate and also alterations in the WNT signalling cascade, an important pathway for neuronal patterning, proliferation and migration (Brennand et al. 2011; Topol et al. 2015; Murai et al. 2016). Another study found deficits in the generation of dentate granule neurons from schizophrenia iPSCs. NPCs had reduced levels of NEUROD1, PROX1 and TBR1 (Yu et al. 2014). Interestingly blockade of LTCCs has been shown to reduce NEUROD1 expression and block excitation-induced neurogenesis (Deisseroth et al. 2004). Additionally the number of TBR1-positive cells has been shown to be reduced during early cortical development in a Cav1.2 heterozygous mouse model (Panagiotakos et al. 2019).

In ASD, many of the associated risk genes are involved in neurodevelopment (Chow et al. 2012; Casanova and Casanova 2014). Post-mortem studies have also shown structural changes that could be linked to abnormal neurogenesis, such as reduced cell density in the septal subventricular zone, subtle difference in hippocampal size, and increased amygdala volume in children but not adolescents with ASD (Schumann et al. 2004; Nicolson et al. 2006; Kotagiri et al. 2014). iPSC studies have shown that ASD patients with macrocephaly have an impaired ability to form neural rosettes and altered cell proliferation leading to delayed production of neurons (Marchetto et al. 2017; Adhya et al. 2021). This was associated with changes to GAD67 and TBR1 expression, which are also altered by changes to Cav1.2 expression/function (Paşca et al. 2011; Moon 2018; Panagiotakos et al. 2019). RNA-seq studies have also shown dysregulation of the differentiation pathway in ASD iPSC-derived neurons,

supporting findings from post-mortem studies (DeRosa et al. 2018). CNVs associated with both schizophrenia and ASD have also shown altered proliferation of neuronal progenitors. A 16p11.2 deletion mouse model, which harbours the gene that encodes ERK1, showed an increase in ERK signalling, which was thought to drive the increase in cyclinD1 expression and premature cell-cycle exit of radial glia and intermediate progenitors leading to altered expression of different cortical layers (Pucilowska et al. 2015). This is supported by the finding that deletion of MAPK1 and MAPK2 promotes cell-cycle elongation and premature progenitor pool depletion (Pucilowska et al. 2012). ERK1/2 and CREB signalling was altered in the CACNA1C knockout and ATS lines during differentiation and is likely to be responsible for changes to downstream gene expression that alter neuronal differentiation (D'Ascenzo et al. 2006; Lepski et al. 2013). Changes to NPC function and neuronal differentiation could contribute to a wide variety of changes seen in neuropsychiatric disorders, including the abundance of different neuron types, abnormal neuronal migration and organisation, and altered neuron morphology or structure (Wegiel et al. 2010; Bakhshi and Chance 2015; Muraki and Tanigaki 2015; Gilbert and Man 2017; Pan et al. 2019). These changes are likely to lead to changes in neuronal connectivity and activity, which are seen in schizophrenia and ASD (Lynall et al. 2010; Keown et al. 2013; Hahamy et al. 2015; Krajcovic et al. 2019).

6.2.2 GABAergic signalling

The knockout and ATS lines showed opposite phenotypes in terms of the expression of GAD65 and GAD67, enzymes required to produce GABA. Their response to pharmacology targeting GABA-A receptors when recording neuronal network activity further suggests that GABAergic signalling is influenced by Cav1.2. Changes to GABAergic neurons has consistently been shown to occur in psychiatric disorders. Post-mortem studies have shown decreases in expression of GAD67 in the prefrontal cortex along with decreases in expression of parvalbumin and GABA receptors occurs in schizophrenia (Akbarian et al. 1995; Volk et al. 2000; Ishikawa et al. 2005; Thompson et al. 2009; de Jonge et al. 2017). In-situ hybridisation studies suggest that these decreases in GAD67 are due to a decrease in GAD67 expression per neuron,

not a decrease in the number of GABAergic neurons. Specifically, dysfunction of parvalbumin interneurons have been implicated in schizophrenia (Lewis et al.; Lodge et al. 2009). The expression of parvalbumin interneurons was not investigated in these experiments as parvalbumin interneurons are hard to generate from iPSCs and the protocol used in these experiments generates mostly excitatory neurons, so there would have been negligible expression of parvalbumin (Keefe and Li 2020). However, it has been shown that the number of parvalbumin interneurons is decreased in a heterozygous CACNA1C rat model, suggesting that Cav1.2 may directly impact this subpopulation of GABAergic neurons (Moon 2018).

Studies investigating BPD generally show an increase in GABA-related genes. BPD patient-derived iPSC neurons have shown increased GAD67 and NKX2.1 RNA expression, a transcription factor required for generation of ventral GABAergic neurons (Chen et al. 2014; Kim et al. 2015). RNA sequencing experiments have also shown that GABA receptor pathways are enriched in neural stem cells from BPD patient-derived iPSCs. These studies suggest increases in GABAergic signalling are associated with BPD and decreases are more associated with schizophrenia. For ASD, both increased and decreased GABA signalling has been shown to occur. Post-mortem studies have shown increased GAD65 and GAD67 expression in the brains of ASD patients (Fatemi et al. 2002; Yip et al. 2009). However iPSC studies have shown both increases and decreases in the number of GABAergic neurons and the expression of GABA receptors (Mariani et al. 2015; Liu et al. 2017; Marchetto et al. 2017; Adhya et al. 2021). A recent paper describing 25 individuals with novel mutations in CACNA1C suggests that both gain and loss of function of CACNA1C may lead to ASD symptoms, supporting the idea that perturbations to GABA signalling in either direction can lead to the development of this disorder (Rodan et al. 2021).

It is likely that the alterations to GABAergic signalling are responsible for the changes to neuronal network activity in the knockout and ATS lines. The knockout line showed a reduction in the SB interval compared to control. This was the same effect as acute blockade of either LTCCs or GABA-A receptors. Additionally, it has previously been shown that application of diltiazem to a culture already treated with bicuculline has

no additional effect on the SB interval (Plumbly 2017). These findings suggests that there may be common mechanism leading to the reduction in SB interval. Blocking GABA-A receptors will directly impact the activation of neurons to alter network activity. However, Cav1.2 opens in response to neuron depolarisation and is important for coupling neuronal activity to gene expression. As the strength of GABAergic signalling is dynamic and dependent on neuronal activity, this provides a potential mechanism for Cav1.2 to alter synaptic GABA signalling and thus network activity (Kilman et al. 2002; Hartman et al. 2006; Swanwick et al. 2006). We have shown that loss of Cav1.2 leads to a reduction in GAD65 and GAD67 expression, and studies suggest that GAD65 and GAD67 transcription is dependent on CREB signalling which is also reduced in the knockout lines (Sánchez-Huertas and Rico 2011; Cohen et al. 2016). A reduction in the production of GABA will reduce the activation of GABA-A receptors at the synapses and thus alter network activity. However, this is unlikely to be the only way that Cav1.2 alters GABAergic signalling. There is evidence that LTCCs and Cav1.2 specifically also alter the expression of GABA-A receptors. TS neurons have been shown to have increased expression of GABA-A receptor subunits (GABRA4, GABRG1 and GABRG2) (Birey et al. 2017; Birey et al. 2021). Interestingly, GABRA4 has also been associated with ASD (Ma et al. 2005). Acute activation of LTCCs also leads to increased surface expression of GABA-A receptors, whereas blockade of LTCCs leads to a reduction (Saliba et al. 2009; Saliba et al. 2012). This suggests that both acute and chronic reduction of Cav1.2 leads to a reduction of GABA-A receptors and therefore alters the bursting activity of neurons.

6.3 Study Limitations

6.3.1 Residual Cav1.2 protein expression

The CACNA1C knockout lines contained out-of-frame mutations on each allele that should have led to complete loss of Cav1.2. However, western blot analysis showed that there was still roughly 25% protein expression of Cav1.2 in both these lines. Analysis of the RNA transcripts suggests that there is no residual wild-type RNA being produced and it is most likely that translation re-initiation is occurring to produce a

slightly truncated protein. It is possible that the remaining protein expression may have a dominant-negative effect, this would not be an issue as the lines are meant to model complete loss of Cav1.2 function. However, we cannot be sure that the residual protein does not still have any functional effects and that the lines are representative of a complete loss of Cav1.2. Residual protein expression is a common issue when generating knockout lines and, in the future, it may be useful to target multiple regions of the gene to ensure complete knockout of the target protein.

6.3.2 Unknown effect of ATS mutation on Cav1.2 function

Based on the effect of other nearby mutations in CACNA1C we predicted that the ATS mutation (A1521P) would have a gain-of-function effect on Cav1.2. The results from the ATS line tend to mirror the effects of the knockout line, suggesting that this is the case. However, the effect of point mutations in CACNA1C are variable and we do not know the specific effect of the mutation on Cav1.2 channel function. Determining this would be helpful for comparing the phenotypes seen in the ATS line to other TS mutations.

6.3.3 Variability in differentiation of iPSCs

A common issue in iPSC experiments is that different lines can display a large amount of variability in differentiation potential and genetic stability. One of the main sources of variability is the genetic background of different lines which can lead to phenotypic variation (Kilpinen et al. 2017). The CACNA1C knockout lines were derived from the iCas9 line, which was used as a control for these experiments so there was no difference in genetic background between these lines. The IBJ4 line, which was used as a control line for the ATS experiments also has the same genetic background as the iCas9 and knockout lines. However, the ATS line was derived from a patient and thus has a different genetic background which is likely to introduce variation and may affect the results. As the ATS line generally mirrored the effects of the knockout line we can be confident that the phenotypes we see are real. However, correcting the CACNA1C point mutation in the ATS line to make a control line with

the same genetic background would provide a better control line to reduce background variability.

Although the genetic background is the main source of variability in iPSC experiments, additional variation also occurs in routine cell culture. Sources of variation include passage number, culture medium, growth rate and cell culture technique (Volpato and Webber 2020). In the experiments in this thesis, we ensured lines had similar passage numbers and that they were as low as possible for neuronal differentiations as it is has been shown that cells accumulate mutations over extended culturing (Yoshihara et al. 2017). Although differentiations are carried out following standardised protocols, they are long and complex, and slight changes can introduce variability (Volpato et al. 2018). Control and knockout or patient lines were differentiated at the same time to ensure there was no difference in the differentiation procedure, however variation may be introduced between different differentiations. Due to this variability, it is important to repeat experiments over multiple differentiations to show phenotypes are reproducible. The majority of experiments in chapter 4 were carried out across multiple differentiations, however the immunofluorescence experiments and the MEA experiments in chapter 5 only contain data from one differentiation. Ideally, all experiments would have been carried out over multiple differentiations.

6.3.4 Variability in MEA recordings

Neuronal activity can be highly variable between cultures of the same line. This is particularly highlighted by the results of the homozygous line which showed a bimodal distribution for all the measures except synchronised burst interval. This distribution is surprising considering neurons plated into different MEA wells came from neurons from the same differentiation. Additionally, the same control line was used for the homozygous and ATS experiments, but they also showed large differences in the basal activity and network activity measures, with only the synchronised burst interval appearing to be consistent. The knockout and ATS MEA experiments were carried out at different times and as previously stated iPSCs can

show high variability between independent differentiations. Another aspect that may contribute to the variability is the use of astrocyte-conditioned media. It is important for enhancing maturation of neurons and has been shown to increase spontaneous activity of neurons (Rushton et al. 2013). As the knockout and ATS MEA experiments were carried out at different times the batch of astrocyte-conditioned media used was not the same, thus introducing more variability into the composition of the media which may affect spontaneous neuronal activity. These issues with variability could be overcome by increasing the number of wells for each group and repeating the experiment across more differentiations to increase the power of the experiments.

6.4 Future Directions

6.4.1 Comparison of different TS mutations

Timothy syndrome was originally classified by a specific mutation in CACNA1C (G406R) (Splawski et al. 2004; Splawski et al. 2005). However, the number of different mutations in CACNA1C that cause this multi-system disorder has rapidly expanded in recent years (Rodan et al. 2021). Timothy Syndrome patients have widely varying phenotypes and the mutations have been shown to have varying effects on Cav1.2 function (Splawski et al. 2005; Ozawa et al. 2018; Ye et al. 2019; Bisabu et al. 2020; Rodan et al. 2021). This thesis focused on the effect of a novel mutation (A1521P) in CACNA1C. Patch clamp experiments need to be carried out to identify the effect of this mutation on channel function in comparison to other TS mutations. However, the mutation had a clear effect on neuronal network activity that could be rescued by LTCC or GABA-A receptor blockade. Before this, studies have only investigated classical TS mutations (G406R) in neurons, and none have investigated its effect on neuronal network activity. We cannot generalise the findings from one TS mutation to other mutations; therefore, identifying the effect of different TS mutations on Cav1.2 channel function and comparing this to their effect on neuronal network activity will help to identify if a general gain-of-function effect leads to the same

phenotype. This system can also be used to see if the same pharmacological interventions can rescue the phenotypes shown in different patient-derived neurons.

6.4.2 GABAergic signalling

This thesis has shown that Cav1.2 has a clear impact on GABAergic signalling. There is evidence to suggest that Cav1.2 may affect both the production of GABAergic neurons and the strength of GABAergic signalling at the synapse. We have hypothesised that the expression of GABA-A receptors is altered in the knockout and Timothy Syndrome lines and that this is responsible for the changes to neuronal network activity. Therefore, it is important to investigate the expression of different GABA-A receptor subunits to support this hypothesis. The protocol used in this thesis generates mostly excitatory cortical neurons with a small proportion of GABAergic neurons. However, GABAergic neurons account for roughly 20% of neurons in the cortex, so this system is not representative of normal GABAergic signalling strength (Sahara et al. 2012; Bader et al. 2017). To further elucidate the effects of Cav1.2, iPSCs can be differentiated separately into glutamatergic and GABAergic neurons. Generation of GABAergic neurons can be independently analysed, and the amount of glutamatergic and GABAergic neurons that are mixed together can then be controlled to see if this alters the effect of Cav1.2 on neuronal network activity. In addition, different combinations of control glutamatergic, control GABAergic, TS/knockout glutamatergic and TS/knockout GABAergic neurons can be tested to identify the contribution of glutamatergic and GABAergic neurons to phenotypes including network activity and synapse composition.

6.4.3 Neuronal rosette formation and maintenance

CACNA1C knockout cultures showed an increase in the number of rosettes present in the culture, whereas the ATS line showed a reduction in the number of rosettes. This was measured at day 50, once cultures are mostly mature neurons, so suggests there may be changes to the maintenance of NPCs. But additional experiments investigating rosette formation and maintenance would help determine which

aspect is altered. The rosettes were identified based on morphology and not a protein stain. Cells can be stained for markers such as N-cadherin, which marks the apical side of a rosette allowing the number of rosettes to be more accurately counted. This would also provide information as to whether the structure of the rosette is altered, as studies have shown that Rho signalling, which is downstream of Cav1.2, impacts rosette organisation and lumen size (Krey et al. 2013; Townshend et al. 2020). Cultures can be stained at multiple time points throughout the differentiation to help determine whether formation or maintenance of rosettes is altered.

6.5 Conclusions

The work in this project demonstrates that Cav1.2 has an important impact on neuronal differentiation. Loss of Cav1.2 leads to deficits in neuronal production and a reduction in the expression of enzymes GAD65 and GAD67. Whereas a gain of function mutation in Cav1.2 leads to an increase in expression of GAD enzymes. These changes are likely to occur via altered activation of downstream signalling pathways; ERK1/2 and CREB. Changes to Cav1.2 expression/function also led to alterations in neuronal network activity, specifically altering the interval between synchronised bursts. Pharmacological targeting of either LTCCs or GABA-A receptors can rescue the changes seen in the ATS line. However, the knockout line showed a loss of sensitivity to GABA-A receptor activation. These results suggest that changes to GABAergic signalling are responsible for the changes to neuronal network activity seen in the CACNA1C knockout and ATS patient lines.

References

Abudayyeh, O.O. et al. 2017. RNA targeting with CRISPR–Cas13. *Nature* 550(7675), pp. 280–284.

Adhya, D. et al. 2021. Atypical Neurogenesis in Induced Pluripotent Stem Cells From Autistic Individuals. *Biological Psychiatry* 89(5), pp. 486–496.

Adzhubei, I.A. et al. 2010. A method and server for predicting damaging missense mutations. *Nature Methods* 7(4), pp. 248–249.

Aicardi, G. and Schwartzkroin, P.A. 1990. Suppression of epileptiform burst discharges in CA3 neurons of rat hippocampal slices by the organic calcium channel blocker, verapamil. *Experimental Brain Research* 81(2), pp. 288–296.

Akbarian, S., Kim, J.J., Potkin, S.G., Hagman, J.O., Tafazzoli, A., Bunney, W.E. and Jones, E.G. 1995. Gene Expression for Glutamic Acid Decarboxylase is Reduced without Loss of Neurons in Prefrontal Cortex of Schizophrenics. *Archives of General Psychiatry* 52(4), pp. 258–266.

Alcamo, E.A., Chirivella, L., Dautzenberg, M., Dobreva, G., Fariñas, I., Grosschedl, R. and McConnell, S.K. 2008. Satb2 Regulates Callosal Projection Neuron Identity in the Developing Cerebral Cortex. *Neuron* 57(3), pp. 364–377.

Aldred, S., Moore, K.M., Fitzgerald, M. and Waring, R.H. 2003. Plasma amino acid levels in children with autism and their families. *Journal of Autism and Developmental Disorders* 33(1), pp. 93–97.

Allen, G. and Courchesne, E. 2003. Differential effects of developmental cerebellar abnormality on cognitive and motor functions in the cerebellum: An fMRI study of autism. *American Journal of Psychiatry* 160(2), pp. 262–273.

Allen, G., Müller, R.A. and Courchesne, E. 2004. Cerebellar function in autism: Functional magnetic resonance image activation during a simple motor task. *Biological Psychiatry* 56(4), pp. 269–278.

Alquezar, C., Esteras, N., Encarnación, A. de la, Moreno, F., de Munain, A.L. and Martín-Requero, A. 2015. Increasing progranulin levels and blockade of the ERK1/2 pathway: Upstream and downstream strategies for the treatment of progranulin deficient frontotemporal dementia. *European Neuropsychopharmacology* 25(3), pp. 386–403.

Alsaqati, M., Heine, V.M. and Harwood, A.J. 2020. Pharmacological intervention to restore connectivity deficits of neuronal networks derived from ASD patient iPSC with a TSC2 mutation. *Molecular Autism* 11(1), pp. 1–13.

Altier, C. et al. 2011. The Cavβ subunit prevents RFP2-mediated ubiquitination and proteasomal degradation of L-type channels. In: *Nature Neuroscience*. Nature Publishing Group, pp. 173–182.

Amare, A.T. et al. 2019. Bivariate genome-wide association analyses of the broad depression phenotype combined with major depressive disorder, bipolar disorder or schizophrenia reveal eight novel genetic loci for depression. *Molecular Psychiatry* , pp. 1–10.

Amatya, D.N. et al. 2019. Dynamical Electrical Complexity Is Reduced during Neuronal Differentiation in Autism Spectrum Disorder. *Stem Cell Reports* 13(3), pp. 474–484.

Andrade, A., Brennecke, A., Mallat, S., Brown, J., Gomez-Rivadeneira, J., Czepiel, N. and Londrigan, L.

2019. Genetic Associations between Voltage-Gated Calcium Channels and Psychiatric Disorders. *International Journal of Molecular Sciences* 20(14), p. 3537.

Antzelevitch, C. et al. 2007. Loss-of-Function Mutations in the Cardiac Calcium Channel Underlie a New Clinical Entity Characterized by ST-Segment Elevation, Short QT Intervals, and Sudden Cardiac Death. *Circulation* 115(4), pp. 442–449.

Arber, C. et al. 2015. Activin a directs striatal projection neuron differentiation of human pluripotent stem cells. *Development (Cambridge)* 142(7), pp. 1375–1386.

B, T., P, B., F, H., M, R. and F, R. 2016. Heritability of autism spectrum disorders: a meta-analysis of twin studies. *Journal of child psychology and psychiatry, and allied disciplines* 57(5), pp. 585–595.

Bader, B.M., Steder, A., Klein, A.B., Frølund, B., Schroeder, O.H.U. and Jensen, A.A. 2017. Functional characterization of GABAA receptor-mediated modulation of cortical neuron network activity in microelectrode array recordings. *PLOS ONE* 12(10), p. e0186147.

Bading, H., Ginty, D.D. and Greenberg, M.E. 1993. Regulation of gene expression in hippocampal neurons by distinct calcium signaling pathways. *Science* 260(5105), pp. 181–186.

Bae, S., Park, J. and Kim, J.-S. 2014. Cas-OFFinder: a fast and versatile algorithm that searches for potential off-target sites of Cas9 RNA-guided endonucleases. *Bioinformatics* 30(10), pp. 1473–1475.

Baio, J. et al. 2018. Prevalence of autism spectrum disorder among children aged 8 Years - Autism and developmental disabilities monitoring network, 11 Sites, United States, 2014. *MMWR Surveillance Summaries* 67(6)

Bakhshi, K. and Chance, S.A. 2015. The neuropathology of schizophrenia: A selective review of past studies and emerging themes in brain structure and cytoarchitecture. *Neuroscience* 303, pp. 82–102.

Bardy, C. et al. 2015. Neuronal medium that supports basic synaptic functions and activity of human neurons in vitro. *Proceedings of the National Academy of Sciences of the United States of America* 112(20), pp. E2725–E2734.

Barrangou, R. et al. 2007. CRISPR Provides Acquired Resistance Against Viruses in Prokaryotes. *Science* 315(5819), pp. 1709–1712.

Bartels, P., Yu, D., Huang, H., Hu, Z., Herzig, S. and Soong, T.W. 2018. Alternative Splicing at N Terminus and Domain I Modulates CaV1.2 Inactivation and Surface Expression. *Biophysical Journal* 114(9), pp. 2095–2106.

Bateman, A. et al. 2015. UniProt: A hub for protein information. *Nucleic Acids Research* 43(D1), pp. D204–D212.

Bauer, E.P., Schafe, G.E. and LeDoux, J.E. 2002. NMDA Receptors and L-Type Voltage-Gated Calcium Channels Contribute to Long-Term Potentiation and Different Components of Fear Memory Formation in the Lateral Amygdala. *Journal of Neuroscience* 22(12), pp. 5239–5249.

Bauer, R., Timothy, K.W. and Golden, A. 2021. Update on the Molecular Genetics of Timothy Syndrome. *Frontiers in Pediatrics* 9, p. 668546.

Baurand, A. et al. 2017. Incomplete Timothy syndrome secondary to a mosaic mutation of the CACNA1C gene diagnosed using next-generation sequencing. *American Journal of Medical Genetics,*

Part A 173(2), pp. 531–536.

Bean, B.P. 2007. The action potential in mammalian central neurons. *Nature Reviews Neuroscience 2007 8:6* 8(6), pp. 451–465.

Beasley, C.L. and Reynolds, G.P. 1997. Parvalbumin-immunoreactive neurons are reduced in the prefrontal cortex of schizophrenics. *Schizophrenia Research* 24(3), pp. 349–355.

Berkefeld, H. et al. 2006. BKCa-Cav channel complexes mediate rapid and localized Ca 2+-activated K+ signaling. *Science* 314(5799)

Berkefeld, H. and Fakler, B. 2008. Repolarizing responses of BKCa-cav complexes are distinctly shaped by their cav subunits. *Journal of Neuroscience* 28(33), pp. 8238–8245.

Di Biase, V., Obermair, G.J., Szabo, Z., Altier, C., Sanguesa, J., Bourinet, E. and Flucher, B.E. 2008. Stable membrane expression of postsynaptic CaV1.2 calcium channel clusters is independent of interactions with AKAP79/150 and PDZ proteins. *Journal of Neuroscience* 28(51), pp. 13845–13855.

Bigos, K.L. et al. 2010. Genetic Variation in CACNA1C Affects Brain Circuitries Related to Mental Illness. *Archives of General Psychiatry* 67(9), pp. 939–945.

Bingmann, D. and Speckmann, E.J. 1989. Specific suppression of pentylenetetrazol-induced epileptiform discharges in CA3 neurons (hippocampal slice, guinea pig) by the organic calcium antagonists flunarizine and verapamil. *Experimental Brain Research* 74(2), pp. 239–248.

Birey, F. et al. 2017. Assembly of functionally integrated human forebrain spheroids. *Nature* 545(7652), pp. 54–59.

Birey, F. et al. 2021. Dissecting the molecular basis of human interneuron migration in forebrain assembloids from Timothy syndrome. *bioRxiv* , p. 2021.06.14.448277.

Bisabu, K.K. et al. 2020. Novel Gain-of-Function Variant in CACNA1C Associated With Timothy Syndrome, Multiple Accessory Pathways, and Noncompaction Cardiomyopathy. *Circulation: Genomic and Precision Medicine* 13, pp. 707–709.

Blatow, M. et al. 2003. A Novel Network of Multipolar Bursting Interneurons Generates Theta Frequency Oscillations in Neocortex. *Neuron* 38(5), pp. 805–817.

Bochet, A. et al. 2021. Early alterations of large-scale brain networks temporal dynamics in young children with autism. *Communications Biology 2021 4:1* 4(1), pp. 1–10.

Boczek, N.J. et al. 2013. Exome Sequencing and Systems Biology Converge to Identify Novel Mutations in the L-Type Calcium Channel, *CACNA1C* , Linked to Autosomal Dominant Long QT Syndrome. *Circulation: Cardiovascular Genetics* 6(3), pp. 279–289.

Boczek, N.J. et al. 2015. Novel Timothy syndrome mutation leading to increase in CACNA1C window current. *Heart Rhythm* 12(1), pp. 211–219.

Boissart, C. et al. 2013. Differentiation from human pluripotent stem cells of cortical neurons of the superficial layers amenable to psychiatric disease modeling and high-throughput drug screening. *Translational Psychiatry* 3(8), pp. e294–e294.

Bray, N.J. and Hill, M.J. 2016. Translating Genetic Risk Loci into Molecular Risk Mechanisms for Schizophrenia. *Schizophrenia Bulletin*

Breitenkamp, A.F.S., Matthes, J., Nass, R.D., Sinzig, J., Lehmkuhl, G., Nürnberg, P. and Herzig, S. 2014. Rare Mutations of CACNB2 Found in Autism Spectrum Disease-Affected Families Alter Calcium Channel Function. Zwick, M. E. ed. *PLoS ONE* 9(4), p. e95579.

Brennand, K. et al. 2015. Phenotypic differences in hiPSC NPCs derived from patients with schizophrenia. *Molecular Psychiatry* 20(3), pp. 361–368.

Brennand, K.J. et al. 2011. Modelling schizophrenia using human induced pluripotent stem cells. *Nature* 473(7346), pp. 221–225.

Britanova, O. et al. 2008. Satb2 Is a Postmitotic Determinant for Upper-Layer Neuron Specification in the Neocortex. *Neuron* 57(3), pp. 378–392.

Brunetti-Pierri, N. et al. 2010. Duplications of FOXG1 in 14q12 are associated with developmental epilepsy, mental retardation, and severe speech impairment. *European Journal of Human Genetics 2011 19:1* 19(1), pp. 102–107.

Bukalo, O., Campanac, E., Hoffman, D.A. and Fields, R.D. 2013. Synaptic plasticity by antidromic firing during hippocampal network oscillations. *Proceedings of the National Academy of Sciences of the United States of America* 110(13), pp. 5175–5180.

Burashnikov, E. et al. 2010. Mutations in the cardiac L-type calcium channel associated with inherited J-wave syndromes and sudden cardiac death. *Heart Rhythm* 7(12), pp. 1872–1882.

Callaerts, P., Halder, G. and Gehring, W.J. 1997. Pax-6 in development and evolution. *Annual Review of Neuroscience* 20, pp. 483–532.

Cardno, A.G. and Gottesman, I.I. 2000. Twin Studies of Schizophrenia: From Bow-and-Arrow Concordances to Star Wars Mx and Functional Genomics. *J. Med. Genet. (Semin. Med. Genet.)* 97, pp. 12–17.

Cargnin, F., Kwon, J.-S., Katzman, S., Chen, B., Lee, J.W. and Lee, S.-K. 2018. FOXG1 Orchestrates Neocortical Organization and Cortico-Cortical Connections. *Neuron* 100(5), pp. 1083-1096.e5.

Casanova, E.L. and Casanova, M.F. 2014. Genetics studies indicate that neural induction and early neuronal maturation are disturbed in autism. *Frontiers in Cellular Neuroscience* 0, p. 397.

Catterall, W.A. 2010. Ion channel voltage sensors: Structure, function, and pathophysiology. *Neuron* 67(6), pp. 915–928.

Catterall, W.A., Perez-Reyes, E., Snutch, T.P. and Striessnig, J. 2005. International Union of Pharmacology. XLVIII. Nomenclature and structure-function relationships of voltage-gated calcium channels. *Pharmacological Reviews* 57(4), pp. 411–425.

Chambers, S.M., Fasano, C.A., Papapetrou, E.P., Tomishima, M., Sadelain, M. and Studer, L. 2009. Highly efficient neural conversion of human ES and iPS cells by dual inhibition of SMAD signaling. *Nature Biotechnology* 27(3), pp. 275–280.

Chapman, G. et al. 2021. Using induced pluripotent stem cells to investigate human neuronal phenotypes in 1q21.1 deletion and duplication syndrome. *Molecular Psychiatry 2021* , pp. 1–12.

Charlson, F., Ommeren, M. van, Flaxman, A., Cornett, J., Whiteford, H. and Saxena, S. 2019. New WHO prevalence estimates of mental disorders in conflict settings: a systematic review and meta-analysis.

The Lancet 394(10194), pp. 240–248.

Charney, A.W. et al. 2017. Evidence for genetic heterogeneity between clinical subtypes of bipolar disorder. *Translational Psychiatry* 7(1), pp. e993–e993.

Chen, B., Schaevitz, L.R. and McConnell, S.K. 2005. Fezl regulates the differentiation and axon targeting of layer 5 subcortical projection neurons in cerebral cortex. *Proceedings of the National Academy of Sciences of the United States of America* 102(47), pp. 17184–17189.

Chen, B., Wang, S.S., Hattox, A.M., Rayburn, H., Nelson, S.B. and McConnell, S.K. 2008. The Fezf2-Ctip2 genetic pathway regulates the fate choice of subcortical projection neurons in the developing cerebral cortex. *Proceedings of the National Academy of Sciences of the United States of America* 105(32), pp. 11382–11387.

Chen, H.M., DeLong, C.J., Bame, M., Rajapakse, I., Herron, T.J., McInnis, M.G. and O'Shea, K.S. 2014. Transcripts involved in calcium signaling and telencephalic neuronal fate are altered in induced pluripotent stem cells from bipolar disorder patients. *Translational Psychiatry* 4(3), pp. e375–e375.

Chen, R.S., Deng, T.C., Garcia, T., Sellers, Z.M. and Best, P.M. 2007. Calcium channel γ subunits: A functionally diverse protein family. *Cell Biochemistry and Biophysics* 47(2), pp. 178–186.

Chen, X. and Dzakpasu, R. 2010. Observed network dynamics from altering the balance between excitatory and inhibitory neurons in cultured networks. *Physical Review E* 82(3), p. 031907.

Chiappalone, M., Novellino, A., Vajda, I., Vato, A., Martinoia, S. and van Pelt, J. 2005. Burst detection algorithms for the analysis of spatio-temporal patterns in cortical networks of neurons. *Neurocomputing* 65–66(SPEC. ISS.), pp. 653–662.

Cho, S.W., Kim, S., Kim, Y., Kweon, J., Kim, H.S., Bae, S. and Kim, J.S. 2014. Analysis of off-target effects of CRISPR/Cas-derived RNA-guided endonucleases and nickases. *Genome Research* 24(1), pp. 132–141.

Choi, Y., Sims, G.E., Murphy, S., Miller, J.R. and Chan, A.P. 2012. Predicting the Functional Effect of Amino Acid Substitutions and Indels. de Brevern, A. G. ed. *PLoS ONE* 7(10), p. e46688.

Chow, M.L. et al. 2012. Age-Dependent Brain Gene Expression and Copy Number Anomalies in Autism Suggest Distinct Pathological Processes at Young Versus Mature Ages. *PLOS Genetics* 8(3), p. e1002592.

Clark, M. et al. 2018. Long-read sequencing reveals the splicing profile of the calcium channel gene CACNA1C in human brain. *bioRxiv* , p. 260562.

Clark, M.B. et al. 2020. Long-read sequencing reveals the complex splicing profile of the psychiatric risk gene CACNA1C in human brain. *Molecular Psychiatry* 25(1), pp. 37–47.

Clark, N.C. et al. 2003. Neurological phenotype and synaptic function in mice lacking the Ca V1.3 α subunit of neuronal L-type voltage-dependent Ca 2+ channels. *Neuroscience* 120(2), pp. 435–442.

Cobb, S.R., Buhl, E.H., Halasy, K., Paulsen, O. and Somogyi, P. 1995. Synchronization of neuronal activity in hippocampus by individual GABAergic interneurons. *Nature 1995 378:6552* 378(6552), pp. 75–78.

Cohen, S.M. et al. 2018. Calmodulin shuttling mediates cytonuclear signaling to trigger experience-

dependent transcription and memory. *Nature Communications* 9(1), pp. 1–12.

Cohen, S.M., Ma, H., Kuchibhotla, K.V., Watson, B.O., Buzsáki, G., Froemke, R.C. and Tsien, R.W. 2016. Excitation-Transcription Coupling in Parvalbumin-Positive Interneurons Employs a Novel CaM Kinase-Dependent Pathway Distinct from Excitatory Neurons. *Neuron* 90(2), pp. 292–307.

Colson, C., Mittre, H., Busson, A., Leenhardt, A., Denjoy, I., Fressard, V. and Troadec, Y. 2019. Unusual clinical description of adult with Timothy syndrome, carrier of a new heterozygote mutation of CACNA1C. *European Journal of Medical Genetics* 62(7), p. 103648.

Colvert, E. et al. 2015. Heritability of Autism Spectrum Disorder in a UK Population-Based Twin Sample. *JAMA Psychiatry* 72(5), pp. 415–423.

Concordet, J.P. and Haeussler, M. 2018. CRISPOR: Intuitive guide selection for CRISPR/Cas9 genome editing experiments and screens. *Nucleic Acids Research* 46(W1), pp. W242–W245.

Le Couteur, A.L., Gottesman, I., Bolton, P., Simonoff, E., Yuzda, E., Rutter, M. and Bailey, A. 1995. Autism as a strongly genetic disorder evidence from a british twin Study. *Psychological Medicine* 25(1), pp. 63–77.

Cox, D.B.T., Gootenberg, J.S., Abudayyeh, O.O., Franklin, B., Kellner, M.J., Joung, J. and Zhang, F. 2017. RNA editing with CRISPR-Cas13. *Science (New York, N.Y.)* 358(6366), pp. 1019–1027.

Coyle, J.T. 2012. NMDA Receptor and Schizophrenia: A Brief History. *Schizophrenia Bulletin* 38(5), pp. 920–926.

D'Ascenzo, M., Piacentini, R., Casalbore, P., Budoni, M., Pallini, R., Azzena, G.B. and Grassi, C. 2006. Role of L-type Ca^{2+} channels in neural stem/progenitor cell differentiation. *European Journal of Neuroscience* 23(4), pp. 935–944.

Danesin, C. and Houart, C. 2012. A Fox stops the Wnt: implications for forebrain development and diseases. *Current Opinion in Genetics & Development* 22(4), pp. 323–330.

Dao, D.T. et al. 2010. Mood Disorder Susceptibility Gene CACNA1C Modifies Mood-Related Behaviors in Mice and Interacts with Sex to Influence Behavior in Mice and Diagnosis in Humans. *Biological Psychiatry* 68(9), pp. 801–810.

Deisseroth, K., Heist, E.K. and Tsien, R.W. 1998. Translocation of calmodulin to the nucleus supports CREB phosphorylation in hippocampal neurons. *Nature* 392(6672), pp. 198–202.

Deisseroth, K., Singla, S., Toda, H., Monje, M., Palmer, T.D. and Malenka, R.C. 2004. Excitation-neurogenesis coupling in adult neural stem/progenitor cells. *Neuron* 42(4), pp. 535–552.

Demyttenaere, K. et al. 2004. Prevalence, Severity, and Unmet Need for Treatment of Mental Disorders in the World Health Organization World Mental Health Surveys. *JAMA* 291(21), p. 2581.

DeRosa, B.A. et al. 2018. Convergent Pathways in Idiopathic Autism Revealed by Time Course Transcriptomic Analysis of Patient-Derived Neurons. *Scientific Reports 2018 8:1* 8(1), pp. 1–15.

Dolmetsch, R. and Geschwind, D.H. 2011. The human brain in a dish: The promise of iPSC-derived neurons. *Cell* 145(6), pp. 831–834.

Dolmetsch, R.E., Pajvani, U., Fife, K., Spotts, J.M. and Greenberg, M.E. 2001. Signaling to the nucleus by an L-type calcium channel-calmodulin complex through the MAP kinase pathway. *Science (New*

York, N.Y.) 294(5541), pp. 333–9.

Dragunow, M. 2008. The adult human brain in preclinical drug development. *Nature Reviews Drug Discovery* 7(8), pp. 659–666.

Dufendach, K.A. et al. 2018. Clinical Outcomes and Modes of Death in Timothy Syndrome: A Multicenter International Study of a Rare Disorder. *JACC: Clinical Electrophysiology* 4(4), pp. 459–466.

Dufendach, K.A., Giudicessi, J.R., Boczek, N.J. and Ackerman, M.J. 2013. Maternal mosaicism confounds the neonatal diagnosis of type 1 timothy syndrome. *Pediatrics* 131(6), p. e1991.

Eckart, N., Song, Q., Yang, R., Wang, R., Zhu, H., McCallion, A.S. and Avramopoulos, D. 2016. Functional Characterization of Schizophrenia-Associated Variation in CACNA1C. Potash, J. B. ed. *PLOS ONE* 11(6), p. e0157086.

Edvardsen, J., Torgersen, S., Røysamb, E., Lygren, S., Skre, I., Onstad, S. and Øien, P.A. 2008. Heritability of bipolar spectrum disorders. Unity or heterogeneity? *Journal of Affective Disorders* 106(3), pp. 229–240.

Edwards, S.L., Beesley, J., French, J.D. and Dunning, M. 2013. Beyond GWASs: Illuminating the dark road from association to function. *American Journal of Human Genetics* 93(5), pp. 779–797.

Elkabetz, Y., Panagiotakos, G., Shamy, G. Al, Socci, N.D., Tabar, V. and Studer, L. 2008. Human ES cell-derived neural rosettes reveal a functionally distinct early neural stem cell stage. *Genes & Development* 22(2), pp. 152–165.

Empson, R.M. and Jefferys, J.G.R. 2001. Ca2+ entry through L-type Ca2+ channels helps terminate epileptiform activity by activation of a Ca2+ dependent afterhyperpolarization in hippocampal CA3. *Neuroscience* 102(2), pp. 297–306.

Fakhoury, M. 2015. Autistic spectrum disorders: A review of clinical features, theories and diagnosis. *International Journal of Developmental Neuroscience* 43, pp. 70–77.

Fang, K. and Colecraft, H.M. 2011. Mechanism of auxiliary β-subunit-mediated membrane targeting of L-type (CaV1.2) channels. *Journal of Physiology* 589(18), pp. 4437–4455.

Fatemi, S.H., Halt, A.R., Stary, J.M., Kanodia, R., Schulz, S.C. and Realmuto, G.R. 2002. Glutamic acid decarboxylase 65 and 67 kDa proteins are reduced in autistic parietal and cerebellar cortices. *Biological psychiatry* 52(8), pp. 805–10.

Ferreira, M.A.R. et al. 2008. Collaborative genome-wide association analysis supports a role for ANK3 and CACNA1C in bipolar disorder. *Nature Genetics* 40(9), pp. 1056–1058.

Folstein, S.E. and Rosen-Sheidley, B. 2001. Genetics of autism: Complex aetiology for a heterogeneous disorder. *Nature Reviews Genetics* 2(12), pp. 943–955.

Forostyak, O., Forostyak, S., Kortus, S., Sykova, E., Verkhratsky, A. and Dayanithi, G. 2016. Physiology of Ca2+ signalling in stem cells of different origins and differentiation stages. *Cell Calcium* 59(2–3), pp. 57–66.

Franco, S.J., Gil-Sanz, C., Martinez-Garay, I., Espinosa, A., Harkins-Perry, S.R., Ramos, C. and Müller, U. 2012. Fate-Restricted Neural Progenitors in the Mammalian Cerebral Cortex. *Science* 337(6095), pp. 746–749.

Freir, D.B. and Herron, C.E. 2003. Inhibition of L-type voltage dependent calcium channels causes impairment of long-term potentiation in the hippocampal CA1 region in vivo. *Brain Research* 967(1–2), pp. 27–36.

Fu, Y., Foden, J.A., Khayter, C., Maeder, M.L., Reyon, D., Joung, J.K. and Sander, J.D. 2013. High-frequency off-target mutagenesis induced by CRISPR-Cas nucleases in human cells. *Nature Biotechnology* 31(9), pp. 822–826.

Fujisawa, S., Amarasingham, A., Harrison, M.T. and Buzsáki, G. 2008. Behavior-dependent short-term assembly dynamics in the medial prefrontal cortex. *Nature Neuroscience* 11(7), pp. 823–833.

Fukuyama, M. et al. 2014. Long QT syndrome type 8: novel CACNA1C mutations causing QT prolongation and variant phenotypes. *EP Europace* 16(12), pp. 1828–1837.

Gabdoulline, R. et al. 2015. Differences in the early development of human and mouse embryonic stem cells. *PLoS ONE* 10(10)

Gardner, R.J.M. et al. 2019. Penetrance and expressivity of the R858H *CACNA1C* variant in a five-generation pedigree segregating an arrhythmogenic channelopathy. *Molecular Genetics & Genomic Medicine* 7(1), p. e00476.

Gaugler, T. et al. 2014. Most genetic risk for autism resides with common variation. *Nature Genetics* 46(8), pp. 881–885.

Gejman, P. V, Sanders, A.R. and Duan, J. 2010. The role of genetics in the etiology of schizophrenia. *The Psychiatric clinics of North America* 33(1), pp. 35–66.

Gershon, E.S. et al. 2014. A rare mutation of CACNA1C in a patient with bipolar disorder and decreased gene expression associated with a bipolar-associated common SNP of CACNA1C in brain. *Molecular Psychiatry* 19(8), pp. 890–894.

Ghanizadeh, A., Sahraeizadeh, A. and Berk, M. 2014. A head-to-head comparison of aripiprazole and risperidone for safety and treating autistic disorders, a randomized double blind clinical trial. *Child Psychiatry and Human Development* 45(2), pp. 185–192.

Gilbert, J. and Man, H.-Y. 2017. Fundamental Elements in Autism: From Neurogenesis and Neurite Growth to Synaptic Plasticity. *Frontiers in Cellular Neuroscience* 0, p. 359.

Gilbert, L.A. et al. 2014. Genome-Scale CRISPR-Mediated Control of Gene Repression and Activation. *Cell* 159(3), pp. 647–661.

Gillis, J. et al. 2012. Long QT, syndactyly, joint contractures, stroke and novel CACNA1C mutation: Expanding the spectrum of Timothy syndrome. *American Journal of Medical Genetics Part A* 158A(1), pp. 182–187.

Girirajan, S. et al. 2012. Phenotypic Heterogeneity of Genomic Disorders and Rare Copy-Number Variants. *New England Journal of Medicine* 367(14), pp. 1321–1331.

Gogtay, N., Vyas, N.S., Testa, R., Wood, S.J. and Pantelis, C. 2011. Age of onset of schizophrenia: Perspectives from structural neuroimaging studies. *Schizophrenia Bulletin* 37(3), pp. 504–513.

Gomez-Ospina, N. et al. 2013. A Promoter in the Coding Region of the Calcium Channel Gene CACNA1C Generates the Transcription Factor CCAT. Muotri, A. R. ed. *PLoS ONE* 8(4), p. e60526.

Gomez-Ospina, N., Tsuruta, F., Barreto-Chang, O., Hu, L. and Dolmetsch, R. 2006. The C Terminus of the L-Type Voltage-Gated Calcium Channel CaV1.2 Encodes a Transcription Factor. *Cell* 127(3), pp. 591–606.

Gonzalez-Burgos, G. and Lewis, D.A. 2008. GABA Neurons and the Mechanisms of Network Oscillations: Implications for Understanding Cortical Dysfunction in Schizophrenia. *Schizophrenia Bulletin* 34(5), pp. 944–961.

González, F., Zhu, Z., Shi, Z.-D., Lelli, K., Verma, N., Li, Q. V and Huangfu, D. 2014. An iCRISPR platform for rapid, multiplexable, and inducible genome editing in human pluripotent stem cells. *Cell stem cell* 15(2), pp. 215–226.

Gore, A. et al. 2011. Somatic coding mutations in human induced pluripotent stem cells. *Nature* 471(7336), pp. 63–67.

Graef, I.A., Mermelstein, P.G., Stankunas, K., Hellson, J.R., Delsseroth, K., Tsien, R.W. and Crabtree, G.R. 1999. L-type calcium channels and GSK-3 regulate the activity of NF-ATc4 in hippocampal neurons. *Nature* 401(6754), pp. 703–708.

Green, E.K. et al. 2010. The bipolar disorder risk allele at CACNA1C also confers risk of recurrent major depression and of schizophrenia. *Molecular Psychiatry* 15(10), pp. 1016–1022.

Green, E.K. et al. 2013. Replication of bipolar disorder susceptibility alleles and identification of two novel genome-wide significant associations in a new bipolar disorder case-control sample. *Molecular Psychiatry* 18(12), pp. 1302–1307.

Grove, J. et al. 2019. Identification of common genetic risk variants for autism spectrum disorder. *Nature Genetics* 51(3), pp. 431–444.

Grzadzinski, R., Huerta, M. and Lord, C. 2013. DSM-5 and autism spectrum disorders (ASDs): An opportunity for identifying ASD subtypes. *Molecular Autism* 4(1), p. 12.

Guan, F. et al. 2014. MIR137 gene and target gene CACNA1C of miR-137 contribute to schizophrenia susceptibility in Han Chinese. *Schizophrenia Research* 152(1), pp. 97–104.

Gunhanlar, N. et al. 2017. A simplified protocol for differentiation of electrophysiologically mature neuronal networks from human induced pluripotent stem cells. *Molecular Psychiatry* 23(5), pp. 1336–1344.

Gupta, R.M. and Musunuru, K. 2014. Expanding the genetic editing tool kit: ZFNs, TALENs, and CRISPR-Cas9. *The Journal of clinical investigation* 124(10), pp. 4154–61.

Haeussler, M. et al. 2016. Evaluation of off-target and on-target scoring algorithms and integration into the guide RNA selection tool CRISPOR. *Genome Biology* 17(1), p. 148.

Hagberg, B. 1995. Rett syndrome: clinical peculiarities and biological mysteries. *Acta Pædiatrica* 84(9), pp. 971–976.

Hahamy, A., Behrmann, M. and Malach, R. 2015. The idiosyncratic brain: distortion of spontaneous connectivity patterns in autism spectrum disorder. *Nature Neuroscience 2015 18:2* 18(2), pp. 302–309.

Hallmayer, J. et al. 2011. Genetic heritability and shared environmental factors among twin pairs with

autism. *Archives of General Psychiatry* 68(11), pp. 1095–1102.

Hama, H., Hara, C., Yamaguchi, K. and Miyawaki, A. 2004. PKC Signaling Mediates Global Enhancement of Excitatory Synaptogenesis in Neurons Triggered by Local Contact with Astrocytes. *Neuron* 41(3), pp. 405–415.

Hamshere, M.L. et al. 2013. Genome-wide significant associations in schizophrenia to ITIH3/4, CACNA1C and SDCCAG8, and extensive replication of associations reported by the Schizophrenia PGC. *Molecular Psychiatry* 18(6), pp. 708–712.

Hansen, A.K., Nedergaard, S. and Andreasen, M. 2014. Intrinsic Ca $^{2+}$ -dependent theta oscillations in apical dendrites of hippocampal CA1 pyramidal cells in vitro. *Journal of Neurophysiology* 112(3), pp. 631–643.

Hartman, K.N., Pal, S.K., Burrone, J. and Murthy, V.N. 2006. Activity-dependent regulation of inhibitory synaptic transmission in hippocampal neurons. *Nature Neuroscience 2006 9:5* 9(5), pp. 642–649.

Hashimoto, M. and Takemoto, T. 2015. Electroporation enables the efficient mRNA delivery into the mouse zygotes and facilitates CRISPR/Cas9-based genome editing. *Scientific Reports* 5(1), pp. 1–8.

Hazlett, H.C. et al. 2005. Magnetic resonance imaging and head circumference study of brain size in autism: Birth through age 2 years. *Archives of General Psychiatry* 62(12), pp. 1366–1376.

He, K. et al. 2014. CACNA1C, schizophrenia and major depressive disorder in the Han Chinese population. *British Journal of Psychiatry* 204(1), pp. 36–39.

Hendel, A., Fine, E.J., Bao, G. and Porteus, M.H. 2015. Quantifying on- and off-target genome editing. *Trends in Biotechnology* 33(2), pp. 132–140.

Hennessey, J.A. et al. 2014. A CACNA1C Variant Associated with Reduced Voltage-Dependent Inactivation, Increased CaV1.2 Channel Window Current, and Arrhythmogenesis. *PLOS ONE* 9(9), p. e106982.

Herbert, M.R. et al. 2004. Localization of White Matter Volume Increase in Autism and Developmental Language Disorder. *Annals of Neurology* 55(4), pp. 530–540.

Herold, S., Jagasia, R., Merz, K., Wassmer, K. and Lie, D.C. 2011. CREB signalling regulates early survival, neuronal gene expression and morphological development in adult subventricular zone neurogenesis. *Molecular and Cellular Neuroscience* 46(1), pp. 79–88.

Hevner, R.F. et al. 2001. Tbr1 Regulates Differentiation of the Preplate and Layer 6. *Neuron* 29(2), pp. 353–366.

Hilker, R. et al. 2018. Heritability of Schizophrenia and Schizophrenia Spectrum Based on the Nationwide Danish Twin Register. *Biological Psychiatry* 83(6), pp. 492–498.

Hiranniramol, K., Chen, Y., Liu, W. and Wang, X. 2020. Generalizable sgRNA design for improved CRISPR/Cas9 editing efficiency. Luigi Martelli, P. ed. *Bioinformatics* 36(9), pp. 2684–2689.

de Hoog, C.L., Fan, W.-T., Goldstein, M.D., Moran, M.F. and Koch, C.A. 2000. Calmodulin-Independent Coordination of Ras and Extracellular Signal-Regulated Kinase Activation by Ras-GRF2. *Molecular and Cellular Biology* 20(8), pp. 2727–2733.

Hoppa, M.B., Lana, B., Margas, W., Dolphin, A.C. and Ryan, T.A. 2012. α2δ expression sets presynaptic

calcium channel abundance and release probability. *Nature* 486(7401), pp. 122–125.

Horigane, S. ichiro et al. 2020. A mouse model of Timothy syndrome exhibits altered social competitive dominance and inhibitory neuron development. *FEBS Open Bio* 10(8), pp. 1436–1446.

Horn, M.E. and Nicoll, R.A. 2018. Somatostatin and parvalbumin inhibitory synapses onto hippocampal pyramidal neurons are regulated by distinct mechanisms. *Proceedings of the National Academy of Sciences* 115(3), pp. 589–594.

Houston, C.M. and Smart, T.G. 2006. CaMK-II modulation of GABAA receptors expressed in HEK293, NG108-15 and rat cerebellar granule neurons. *European Journal of Neuroscience* 24(9), pp. 2504–2514.

Hříbková, H., Grabiec, M., Klemová, D., Slaninová, I. and Sun, Y.-M. 2018. Calcium signaling mediates five types of cell morphological changes to form neural rosettes. *Journal of Cell Science* 131(3)

Hsu, P.D. et al. 2013. DNA targeting specificity of RNA-guided Cas9 nucleases. *Nature Biotechnology* 31(9), pp. 827–832.

Hu, B.Y., Weick, J.P., Yu, J., Ma, L.X., Zhang, X.Q., Thomson, J.A. and Zhang, S.C. 2010. Neural differentiation of human induced pluripotent stem cells follows developmental principles but with variable potency. *Proceedings of the National Academy of Sciences of the United States of America* 107(9), pp. 4335–4340.

Huang, J.J. et al. 2017. Functional expression of the Ca2+ signaling machinery in human embryonic stem cells. *Acta Pharmacologica Sinica* 38(12), pp. 1663–1672.

Iida, S., Shimba, K., Sakai, K., Kotani, K. and Jimbo, Y. 2018. Synchronous firing patterns of induced pluripotent stem cell-derived cortical neurons depend on the network structure consisting of excitatory and inhibitory neurons. *Biochemical and Biophysical Research Communications* 501(1), pp. 152–157.

Ikeda, M. et al. 2018. Genome-Wide Association Study Detected Novel Susceptibility Genes for Schizophrenia and Shared Trans-Populations/Diseases Genetic Effect. *Schizophrenia Bulletin* 45(4), pp. 824–834.

Ikegaya, Y., Aaron, G., Cossart, R., Aronov, D., Lampl, I., Ferster, D. and Yuste, R. 2004. Synfire Chains and Cortical Songs: Temporal Modules of Cortical Activity. *Science* 304(5670), pp. 559–564.

Ishikawa, M., Mizukami, K., Iwakiri, M. and Asada, T. 2005. Immunohistochemical and immunoblot analysis of γ-aminobutyric acid B receptor in the prefrontal cortex of subjects with schizophrenia and bipolar disorder. *Neuroscience Letters* 383(3), pp. 272–277.

Iwamoto, K., Bundo, M. and Kato, T. 2005. Altered expression of mitochondria-related genes in postmortem brains of patients with bipolar disorder or schizophrenia, as revealed by large-scale DNA microarray analysis. *Human molecular genetics* 14(2), pp. 241–53.

Iwata, Y. et al. 2008. Irradiation in Adulthood as a New Model of Schizophrenia. *PLOS ONE* 3(5), p. e2283.

Jašović-Gašić, M., Vuković, O., Pantović, M., Cvetić, T. and Marić-Bojović, N. 2012. ANTIPSYCHOTICS - HISTORY OF DEVELOPMENT AND FIELD OF INDICATION, NEW WINE -OLD GLASSESS. *Psychiatria*

Danubina 24, pp. 342–344.

Jiang, M. and Swann, J.W.W. 2005. A role for L-type calcium channels in the maturation of parvalbumin-containing hippocampal interneurons. *Neuroscience* 135(3), pp. 839–850.

Jiang, Y.H. et al. 2013. Detection of clinically relevant genetic variants in autism spectrum disorder by whole-genome sequencing. *American Journal of Human Genetics* 93(2), pp. 249–263.

Johansson, V., Kuja-Halkola, R., Cannon, T.D., Hultman, C.M. and Hedman, A.M. 2019. A population-based heritability estimate of bipolar disorder – In a Swedish twin sample. *Psychiatry Research* 278, pp. 180–187.

Johny, M. Ben, Yang, P.S., Bazzazi, H. and Yue, D.T. 2013. Dynamic switching of calmodulin interactions underlies Ca2+ regulation of CaV1.3 channels. *Nature Communications* 4(1), pp. 1–13.

de Jonge, J.C., Vinkers, C.H., Hulshoff Pol, H.E. and Marsman, A. 2017. GABAergic mechanisms in schizophrenia: Linking postmortem and In vivo studies. *Frontiers in Psychiatry* 8(AUG), p. 118.

Jun He, J., Wei Zhou, W., Shaoqun Zeng, S. and Qingming Luo, Q. 2005. L-type calcium channels mediate synchronized spontaneous Ca^{2+}spikes in cultured cortical networks. In: *2005 IEEE Engineering in Medicine and Biology 27th Annual Conference*., pp. 1783–1785.

Just, M.A., Cherkassky, V.L., Keller, T.A., Kana, R.K. and Minshew, N.J. 2007. Functional and anatomical cortical underconnectivity in autism: evidence from an FMRI study of an executive function task and corpus callosum morphometry. *Cerebral cortex (New York, N.Y. : 1991)* 17(4), pp. 951–61.

Kabadi, A., Ousterout, D., Hilton, I. and Gersbach, C. 2014. Multiplex CRISPR/Cas9-based genome engineering from a single lentiviral vector. *Nucleic Acids Res* 42(19), p. e147.

Kamijo, S. et al. 2018. A Critical Neurodevelopmental Role for L-Type Voltage-Gated Calcium Channels in Neurite Extension and Radial Migration. *The Journal of neuroscience : the official journal of the Society for Neuroscience* 38(24), pp. 5551–5566.

Kanamori, T., Kanai, M.I., Dairyo, Y., Yasunaga, K., Morikawa, R.K. and Emoto, K. 2013. Compartmentalized Calcium Transients Trigger Dendrite Pruning in Drosophila Sensory Neurons. *Science* 340(6139), pp. 1475–1478.

Kaplanis, J. et al. 2020. Evidence for 28 genetic disorders discovered by combining healthcare and research data. *Nature 2020 586:7831* 586(7831), pp. 757–762.

Kathuria, A., Lopez-Lengowski, K., Vater, M., McPhie, D., Cohen, B.M. and Karmacharya, R. 2020. Transcriptome analysis and functional characterization of cerebral organoids in bipolar disorder. *Genome medicine* 12(1), p. 34.

Kato, T. 2008. Role of mitochondrial DNA in calcium signaling abnormality in bipolar disorder. *Cell Calcium* 44(1), pp. 92–102.

Kato, T. 2019. Current understanding of bipolar disorder: Toward integration of biological basis and treatment strategies. *Psychiatry and Clinical Neurosciences* 73(9), pp. 526–540.

Keefe, F. and Li, M. 2020. Pluripotent stem cell derived inhibitory interneurons - Principles and applications in health and disease. *Neural Regeneration Research* 15(2), pp. 251–252.

Keown, C.L., Shih, P., Nair, A., Peterson, N., Mulvey, M.E. and Müller, R.A. 2013. Local Functional

Overconnectivity in Posterior Brain Regions Is Associated with Symptom Severity in Autism Spectrum Disorders. *Cell Reports* 5(3), pp. 567–572.

Kilman, V., Rossum, M.C.W. van and Turrigiano, G.G. 2002. Activity Deprivation Reduces Miniature IPSC Amplitude by Decreasing the Number of Postsynaptic GABAA Receptors Clustered at Neocortical Synapses. *Journal of Neuroscience* 22(4), pp. 1328–1337.

Kilpinen, H. et al. 2017. Common genetic variation drives molecular heterogeneity in human iPSCs. *Nature 2017 546:7658* 546(7658), pp. 370–375.

Kim, K. et al. 2011. Donor cell type can influence the epigenome and differentiation potential of human induced pluripotent stem cells. *Nature Biotechnology* 29(12), pp. 1117–1119.

Kim, K.H. et al. 2015. Transcriptomic Analysis of Induced Pluripotent Stem Cells Derived from Patients with Bipolar Disorder from an Old Order Amish Pedigree. *PLOS ONE* 10(11), p. e0142693.

Kipanyula, M.J., Kimaro, W.H. and Etet, P.F.S. 2016. The Emerging Roles of the Calcineurin-Nuclear Factor of Activated T-Lymphocytes Pathway in Nervous System Functions and Diseases. *Journal of Aging Research* 2016

Klei, L. et al. 2012. Common genetic variants, acting additively, are a major source of risk for autism. *Molecular Autism* 3(1), p. 9.

Kmet, M., Guo, C., Edmondson, C. and Chen, B. 2013. Directed Differentiation of Human Embryonic Stem Cells into Corticofugal Neurons Uncovers Heterogeneous Fezf2-Expressing Subpopulations. *PLoS ONE* 8(6)

Konermann, S., Lotfy, P., Brideau, N.J., Oki, J., Shokhirev, M.N. and Hsu, P.D. 2018. Transcriptome Engineering with RNA-Targeting Type VI-D CRISPR Effectors. *Cell* 173(3), pp. 665-676.e14.

Konradi, C., Eaton, M., MacDonald, M.L., Walsh, J., Benes, F.M. and Heckers, S. 2004. Molecular Evidence for Mitochondrial Dysfunction in Bipolar Disorder. *Archives of General Psychiatry* 61(3), pp. 300–308.

Kosaki, R., Ono, H., Terashima, H. and Kosaki, K. 2018. Timothy syndrome-like condition with syndactyly but without prolongation of the QT interval. *American Journal of Medical Genetics Part A* 176(7), pp. 1657–1661.

Koschak, A., Reimer, D., Huber, I., Grabner, M., Glossmann, H., Engel, J. and Striessnig, J. 2001. α1D (Cav1.3) Subunits Can Form L-type Ca2+ Channels Activating at Negative Voltages. *Journal of Biological Chemistry* 276(25), pp. 22100–22106.

Kotagiri, P., Chance, S.A., Szele, F.G. and Esiri, M.M. 2014. Subventricular zone cytoarchitecture changes in Autism. *Developmental Neurobiology* 74(1), pp. 25–41.

Krajcovic, B., Fajnerova, I., Horacek, J., Kelemen, E., Kubik, S., Svoboda, J. and Stuchlik, A. 2019. Neural and neuronal discoordination in schizophrenia: From ensembles through networks to symptoms. *Acta Physiologica* 226(4), p. e13282.

Krey, J.F., Paşca, S.P., Shcheglovitov, A., Yazawa, M., Schwemberger, R., Rasmusson, R. and Dolmetsch, R.E. 2013. Timothy syndrome is associated with activity-dependent dendritic retraction in rodent and human neurons. *Nature Neuroscience* 16(2), pp. 201–209.

Krystal, J.H. et al. 1994. Subanesthetic Effects of the Noncompetitive NMDA Antagonist, Ketamine, in Humans: Psychotomimetic, Perceptual, Cognitive, and Neuroendocrine Responses. *Archives of General Psychiatry* 51(3), pp. 199–214.

Kujawa, M.J. and Nemeroff, C.B. 2006. The biology of bipolar disorder. In: *Bipolar Disorders*. Kluwer Academic Publishers, pp. 281–314.

Kwon, J. et al. 2012. Neuronal Differentiation of a Human Induced Pluripotent Stem Cell Line (FS-1) Derived from Newborn Foreskin Fibroblasts. *International Journal of Stem Cells* 5(2), pp. 140–145.

Kwon, Y.-W. et al. 2014. Comparative Study of Efficacy of Dopaminergic Neuron Differentiation between Embryonic Stem Cell and Protein-Based Induced Pluripotent Stem Cell. Johnson, R. ed. *PLoS ONE* 9(1), p. e85736.

Lally, J., Gaughran, F., Timms, P. and Curran, S.R. 2016. Treatment-resistant schizophrenia: Current insights on the pharmacogenomics of antipsychotics. *Pharmacogenomics and Personalized Medicine* 9, pp. 117–129.

Lancaster, B., Hu, H., Ramakers, G.M.J. and Storm, J.F. 2001. Interaction between synaptic excitation and slow afterhyperpolarization current in rat hippocampal pyramidal cells. *The Journal of Physiology* 536(3), pp. 809–823.

Landstrom, A.P. et al. 2016. Novel long QT syndrome-associated missense mutation, L762F, in CACNA1C-encoded L-type calcium channel imparts a slower inactivation tau and increased sustained and window current. *International Journal of Cardiology* 220, pp. 290–298.

Langwieser, N., Christel, C.J., Kleppisch, T., Hofmann, F., Wotjak, C.T. and Moosmang, S. 2010. Homeostatic switch in Hebbian plasticity and fear learning after sustained loss of Cav1.2 calcium channels. *Journal of Neuroscience* 30(25), pp. 8367–8375.

Lee, A.S. et al. 2016. The Neuropsychiatric Disease-Associated Gene cacna1c Mediates Survival of Young Hippocampal Neurons,,. *eNeuro*

van de Leemput, J. et al. 2014. CORTECON: a temporal transcriptome analysis of in vitro human cerebral cortex development from human embryonic stem cells. *Neuron* 83(1), pp. 51–68.

Lendahl, U., Zimmerman, L.B. and McKay, R.D.G. 1990. CNS stem cells express a new class of intermediate filament protein. *Cell* 60(4), pp. 585–595.

Lepski, G., Jannes, C.E., Nikkhah, G., Bischofberger, J. and Cherubini, E. 2013. cAMP promotes the differentiation of neural progenitor cells in vitro via modulation of voltage-gated calcium channels.

Lewis, D.A., Curley, A.A., Glausier, J.R. and Volk, D.W. Cortical parvalbumin interneurons and cognitive dysfunction in schizophrenia. *Trends in Neurosciences* 35(1), pp. 57–67.

Li, B., Tadross, M.R. and Tsien, R.W. 2016. Sequential ionic and conformational signaling by calcium channels drives neuronal gene expression. *Science* 351(6275), pp. 863–867.

Li, H., Pink, M.D., Murphy, J.G., Stein, A., Dell'Acqua, M.L. and Hogan, P.G. 2012. Balanced interactions of calcineurin with AKAP79 regulate Ca 2+-calcineurin-NFAT signaling. *Nature Structural and Molecular Biology* 19(3), pp. 337–345.

Li, J. et al. 2015. Schizophrenia Related Variants in CACNA1C also Confer Risk of Autism. Zheng, D. ed.

PLOS ONE 10(7), p. e0133247.

Li, Z. et al. 2017. Genome-wide association analysis identifies 30 new susceptibility loci for schizophrenia. *Nature Genetics* 49(11), pp. 1576–1583.

Lima, P.A. and Marrion, N. V. 2007. Mechanisms underlying activation of the slow AHP in rat hippocampal neurons. *Brain Research* 1150(1), pp. 74–82.

Liu, X. et al. 2017. Idiopathic Autism: Cellular and Molecular Phenotypes in Pluripotent Stem Cell-Derived Neurons. *Molecular Neurobiology* 54(6), pp. 4507–4523.

Liu, Y. et al. 2011. Meta-analysis of genome-wide association data of bipolar disorder and major depressive disorder. *Molecular Psychiatry* 16(1), pp. 2–4.

Liu, Y., Liu, H., Sauvey, C., Yao, L., Zarnowska, E.D. and Zhang, S.C. 2013. Directed differentiation of forebrain GABA interneurons from human pluripotent stem cells. *Nature Protocols* 8(9), pp. 1670–1679.

Livak, K.J. and Schmittgen, T.D. 2001. Analysis of Relative Gene Expression Data Using Real-Time Quantitative PCR and the 2−ΔΔCT Method. *Methods* 25(4), pp. 402–408.

Livide, G. et al. 2015. GluD1 is a common altered player in neuronal differentiation from both MECP2-mutated and CDKL5-mutated iPS cells. *European Journal of Human Genetics* 23(2), pp. 195–201.

Lodge, D.J., Behrens, M.M. and Grace, A.A. 2009. A Loss of Parvalbumin-Containing Interneurons Is Associated with Diminished Oscillatory Activity in an Animal Model of Schizophrenia. *Journal of Neuroscience* 29(8), pp. 2344–2354.

Lu, A.T.-H., Dai, X., Martinez-Agosto, J.A. and Cantor, R.M. 2012. Support for calcium channel gene defects in autism spectrum disorders. *Molecular Autism 2012 3:1* 3(1), pp. 1–9.

Lu, C., Chen, Q., Zhou, T., Bozic, D., Fu, Z., Pan, J.Q. and Feng, G. 2015. Micro-electrode array recordings reveal reductions in both excitation and inhibition in cultured cortical neuron networks lacking Shank3. *Molecular Psychiatry 2016 21:2* 21(2), pp. 159–168.

Lu, J. et al. 2016. Generation of serotonin neurons from human pluripotent stem cells. *Nature Biotechnology* 34(1), pp. 89–94.

Lynall, M.-E., Bassett, D.S., Kerwin, R., McKenna, P.J., Kitzbichler, M., Muller, U. and Bullmore, E. 2010. Functional Connectivity and Brain Networks in Schizophrenia. *Journal of Neuroscience* 30(28), pp. 9477–9487.

Ma, D.Q. et al. 2005. Identification of Significant Association and Gene-Gene Interaction of GABA Receptor Subunit Genes in Autism. *The American Journal of Human Genetics* 77(3), pp. 377–388.

Ma, H. et al. 2014. γcaMKII shuttles Ca2+/CaM to the nucleus to trigger CREB phosphorylation and gene expression. *Cell* 159(2), pp. 281–294.

MacLean, J.N., Watson, B.O., Aaron, G.B. and Yuste, R. 2005. Internal Dynamics Determine the Cortical Response to Thalamic Stimulation. *Neuron* 48(5), pp. 811–823.

Madison, J.M. et al. 2015. Characterization of bipolar disorder patient-specific induced pluripotent stem cells from a family reveals neurodevelopmental and mRNA expression abnormalities. *Molecular Psychiatry* 20(6), pp. 703–717.

Maekawa, M. et al. 2009. Arachidonic Acid Drives Postnatal Neurogenesis and Elicits a Beneficial Effect on Prepulse Inhibition, a Biological Trait of Psychiatric Illnesses. *PLOS ONE* 4(4), p. e5085.

Mäkinen, M.E.-L., Ylä-Outinen, L. and Narkilahti, S. 2018. GABA and Gap Junctions in the Development of Synchronized Activity in Human Pluripotent Stem Cell-Derived Neural Networks. *Frontiers in Cellular Neuroscience* 0, p. 56.

Malhi, G.S. and Outhred, T. 2016. Therapeutic Mechanisms of Lithium in Bipolar Disorder: Recent Advances and Current Understanding. *CNS Drugs* 30(10), pp. 931–949.

Malmersjö, S., Liste, I., Dyachok, O., Tengholm, A., Arenas, E. and Uhlén, P. 2010. Ca2+ and cAMP signaling in human embryonic stem cell-derived dopamine neurons. *Stem Cells and Development* 19(9), pp. 1355–1364.

Mandegar, M.A. et al. 2016. CRISPR Interference Efficiently Induces Specific and Reversible Gene Silencing in Human iPSCs. *Cell Stem Cell* 18(4), pp. 541–553.

Mann, E.O. and Paulsen, O. 2007. Role of GABAergic inhibition in hippocampal network oscillations. *Trends in Neurosciences* 30(7), pp. 343–349.

Manuel, M.N., Martynoga, B., Molinek, M.D., Quinn, J.C., Kroemmer, C., Mason, J.O. and Price, D.J. 2011. The transcription factor Foxg1 regulates telencephalic progenitor proliferation cell autonomously, in part by controlling Pax6 expression levels. *Neural Development* 6(1), p. 9.

Marchetto, M.C. et al. 2017. Altered proliferation and networks in neural cells derived from idiopathic autistic individuals. *Molecular Psychiatry* 22(6), pp. 820–835.

Marchetto, M.C.N. et al. 2010. A model for neural development and treatment of rett syndrome using human induced pluripotent stem cells. *Cell* 143(4), pp. 527–539.

Mariani, J. et al. 2015. FOXG1-Dependent Dysregulation of GABA/Glutamate Neuron Differentiation in Autism Spectrum Disorders. *Cell* 162(2), pp. 375–390.

Maroof, A.M. et al. 2013. Directed differentiation and functional maturation of cortical interneurons from human embryonic stem cells. *Cell Stem Cell* 12(5), pp. 559–572.

Martynoga, B., Morrison, H., Price, D.J. and Mason, J.O. 2005. Foxg1 is required for specification of ventral telencephalon and region-specific regulation of dorsal telencephalic precursor proliferation and apoptosis. *Developmental Biology* 283(1), pp. 113–127.

Mazurek, M.O., Handen, B.L., Wodka, E.L., Nowinski, L., Butter, E. and Engelhardt, C.R. 2014. Age at First Autism Spectrum Disorder Diagnosis. *Journal of Developmental & Behavioral Pediatrics* 35(9), pp. 561–569.

McCracken, J.T. et al. 2002. Risperidone in Children with Autism and Serious Behavioral Problems. *New England Journal of Medicine* 347(5), pp. 314–321.

McDougle, C.J. et al. 2005. Risperidone for the core symptom domains of autism: Results from the study by the Autism Network of the Research Units on Pediatric Psychopharmacology. *American Journal of Psychiatry* 162(6), pp. 1142–1148.

McNeill, R. V., Ziegler, G.C., Radtke, F., Nieberler, M., Lesch, K.P. and Kittel-Schneider, S. 2020. Mental health dished up—the use of iPSC models in neuropsychiatric research. *Journal of Neural Transmission*

127(11), pp. 1547–1568.

McRory, J.E. et al. 2004. The CACNA1F Gene Encodes an L-Type Calcium Channel with Unique Biophysical Properties and Tissue Distribution. *Journal of Neuroscience* 24(7), pp. 1707–1718.

Mencarelli, M.A. et al. 2010. Novel FOXG1 mutations associated with the congenital variant of Rett syndrome. *Journal of Medical Genetics* 47(1), pp. 49–53.

Merikangas, K.R., Akiskal, H.S., Angst, J., Greenberg, P.E., Hirschfeld, R.M.A., Petukhova, M. and Kessler, R.C. 2007. Lifetime and 12-month prevalence of bipolar spectrum disorder in the national comorbidity survey replication. *Archives of General Psychiatry* 64(5), pp. 543–552.

Mertens, J. et al. 2015. Differential responses to lithium in hyperexcitable neurons from patients with bipolar disorder. *Nature* 527(7576), pp. 95–99.

Mire, E. et al. 2012. Spontaneous activity regulates Robo1 transcription to mediate a switch in thalamocortical axon growth. *Nature Neuroscience* 15(8), pp. 1134–1143.

Miyamoto, S., Miyake, N., Jarskog, L.F., Fleischhacker, W.W. and Lieberman, J.A. 2012. Pharmacological treatment of schizophrenia: A critical review of the pharmacology and clinical effects of current and future therapeutic agents. *Molecular Psychiatry* 17(12), pp. 1206–1227.

Mok, S.Y., Nadasdy, Z., Lim, Y.M. and Goh, S.Y. 2012. Ultra-slow oscillations in cortical networks in vitro. *Neuroscience* 206, pp. 17–24.

Molnár, Z. and Clowry, G. 2012. Cerebral cortical development in rodents and primates. In: *Progress in Brain Research*. Elsevier B.V., pp. 45–70.

Moon, A.L. 2018. *The impact of genetic variation in CACNA1C and prepubertal stress on hippocampal function*. Cardiff University.

Moon, A.L., Haan, N., Wilkinson, L.S., Thomas, K.L. and Hall, J. 2018. CACNA1C: Association With Psychiatric Disorders, Behavior, and Neurogenesis. *Schizophrenia Bulletin* 44(5), pp. 958–965.

Moosmang, S. et al. 2005. Role of hippocampal Cav1.2 Ca2+ channels in NMDA receptor-independent synaptic plasticity and spatial memory. *Journal of Neuroscience* 25(43), pp. 9883–9892.

Morgan, S.L. and Teyler, T.J. 1999. VDCCs and NMDARs Underlie Two Forms of LTP in CA1 Hippocampus In Vivo. *Journal of Neurophysiology* 82(2), pp. 736–740.

Mukhtar, T. and Taylor, V. 2018. Untangling Cortical Complexity During Development. *Journal of Experimental Neuroscience* 12, p. 117906951875933.

Murai, K. et al. 2016. The TLX-miR-219 cascade regulates neural stem cell proliferation in neurodevelopment and schizophrenia iPSC model. *Nature Communications 2016 7:1* 7(1), pp. 1–15.

Muraki, K. and Tanigaki, K. 2015. Neuronal migration abnormalities and its possible implications for schizophrenia. *Frontiers in Neuroscience* 0(FEB), p. 74.

Muratore, C.R., Srikanth, P., Callahan, D.G. and Young-Pearse, T.L. 2014. Comparison and Optimization of hiPSC Forebrain Cortical Differentiation Protocols. Dottori, M. ed. *PLoS ONE* 9(8), p. e105807.

Murphy, T.H., Worley, P.F. and Baraban, J.M. 1991. L-type voltage-sensitive calcium channels mediate synaptic activation of immediate early genes. *Neuron* 7(4), pp. 625–635.

Ngui, E.M., Khasakhala, L., Ndetei, D. and Roberts, L.W. 2010. Mental disorders, health inequalities

and ethics: A global perspective. *International Review of Psychiatry* 22(3), pp. 235–244.

Nicolson, R. et al. 2006. Detection and mapping of hippocampal abnormalities in autism. *Psychiatry Research: Neuroimaging* 148(1), pp. 11–21.

Nugud, A.A. et al. 2021. Case Report: Expanding the Phenotypic Spectrum of Timothy Syndrome Type 1: A Sporadic Case With a de novo CACNA1C Pathogenic Variant and Segmental Ileal Dilatation. *Frontiers in Pediatrics* 0, p. 372.

Nyegaard, M. et al. 2010. CACNA1C (rs1006737) is associated with schizophrenia. *Molecular Psychiatry* 15(2), pp. 119–121.

O'dushlaine, C. et al. 2015. Psychiatric genome-wide association study analyses implicate neuronal, immune and histone pathways. *Nature Neuroscience 2015 18:2* 18(2), pp. 199–209.

Obermair, G.J., Szabo, Z., Bourinet, E. and Flucher, B.E. 2004. Differential targeting of the L-type Ca2+ channel alpha1C (CaV1.2) to synaptic and extrasynaptic compartments in hippocampal neurons. *European Journal of Neuroscience* 19(8), pp. 2109–2122.

Odawara, A., Katoh, H., Matsuda, N. and Suzuki, I. 2016. Physiological maturation and drug responses of human induced pluripotent stem cell-derived cortical neuronal networks in long-term culture. *Scientific Reports 2016 6:1* 6(1), pp. 1–14.

Odawara, A., Saitoh, Y., Alhebshi, A.H., Gotoh, M. and Suzuki, I. 2014. Long-term electrophysiological activity and pharmacological response of a human induced pluripotent stem cell-derived neuron and astrocyte co-culture. *Biochemical and Biophysical Research Communications* 443(4), pp. 1176–1181.

Oliveria, S.F., Dell'Acqua, M.L. and Sather, W.A. 2007. AKAP79/150 Anchoring of Calcineurin Controls Neuronal L-Type Ca2+ Channel Activity and Nuclear Signaling. *Neuron* 55(2), pp. 261–275.

Opatowsky, Y., Chen, C.C., Campbell, K.P. and Hirsch, J.A. 2004. Structural analysis of the voltage-dependent calcium channel β subunit functional core and its complex with the α1 interaction domain. *Neuron* 42(3), pp. 387–399.

Owen, M.J., Sawa, A. and Mortensen, P.B. 2016. Schizophrenia. *The Lancet* 388(10039), pp. 86–97.

Ozawa, J., Ohno, S., Saito, H., Saitoh, A., Matsuura, H. and Horie, M. 2018. A novel CACNA1C mutation identified in a patient with Timothy syndrome without syndactyly exerts both marked loss- and gain-of-function effects. *HeartRhythm Case Reports* 4(7), pp. 273–277.

Ozonoff, S. et al. 2011. Recurrence risk for autism spectrum disorders: A baby siblings research consortium study. *Pediatrics* 128(3)

P, M., F, R., M, A., P, S., R, K. and A, C. 2003. The heritability of bipolar affective disorder and the genetic relationship to unipolar depression. *Archives of general psychiatry* 60(5), pp. 497–502.

Pan, Y.-H., Wu, N. and Yuan, X.-B. 2019. Toward a Better Understanding of Neuronal Migration Deficits in Autism Spectrum Disorders. *Frontiers in Cell and Developmental Biology* 7(SEP)

Panagiotakos, G. et al. 2019. Aberrant calcium channel splicing drives defects in cortical differentiation in timothy syndrome. *eLife* 8

Pardiñas, A.F. et al. 2018. Common schizophrenia alleles are enriched in mutation-intolerant genes and in regions under strong background selection. *Nature Genetics* 50(3), pp. 381–389.

Paşca, S.P. et al. 2011. Using iPSC-derived neurons to uncover cellular phenotypes associated with Timothy syndrome. *Nature Medicine* 17(12), pp. 1657–1662.

Pastalkova, E., Itskov, V., Amarasingham, A. and Buzsáki, G. 2008. Internally generated cell assembly sequences in the rat hippocampus. *Science* 321(5894), pp. 1322–1327.

Patriarchi, T. et al. 2016. Imbalance of excitatory/inhibitory synaptic protein expression in iPSC-derived neurons from FOXG1 patients and in foxg1 mice. *European Journal of Human Genetics* 24(6), pp. 871–880.

Pattanayak, V., Lin, S., Guilinger, J.P., Ma, E., Doudna, J.A. and Liu, D.R. 2013. High-throughput profiling of off-target DNA cleavage reveals RNA-programmed Cas9 nuclease specificity. *Nature Biotechnology* 31(9), pp. 839–843.

Paulus, F.M. et al. 2014. Association of rs1006737 in *CACNA1C* with alterations in prefrontal activation and fronto-hippocampal connectivity. *Human Brain Mapping* 35(4), pp. 1190–1200.

Periyasamy, S. et al. 2019. Association of Schizophrenia Risk with Disordered Niacin Metabolism in an Indian Genome-wide Association Study. *JAMA Psychiatry* 76(10), pp. 1026–1034.

Peterson, B.Z., Lee, J.S., Mulle, J.G., Wang, V., De Leon, M. and Yue, D.T. 2000. Critical determinants of Ca2+-dependent inactivation within an EF-hand motif of L-type Ca2+ channels. *Biophysical Journal* 78(4), pp. 1906–1920.

Pfrieger, F.W. and Barres, B.A. 1997. Synaptic efficacy enhanced by glial cells in vitro. *Science* 277(5332), pp. 1684–1687.

Pinggera, A. et al. 2015. CACNA1D de novo mutations in autism spectrum disorders activate cav1.3 l-type calcium channels. *Biological Psychiatry* 77(9), pp. 816–822.

Plumbly, W. 2017. *The creation of a platform for investigating the network function of human pluripotent stem cell derived neurons in development and disease*. Cardiff University.

Plumbly, W., Brandon, N., Deeb, T.Z., Hall, J. and Harwood, A.J. 2019. L-type voltage-gated calcium channel regulation of in vitro human cortical neuronal networks. *Scientific Reports* 9(1), pp. 1–12.

Po', C. et al. 2019. Photosensitive epilepsy and long QT: expanding Timothy syndrome phenotype. *Clinical Neurophysiology* 130(11), pp. 2134–2136.

Pontrelli, G. et al. 2014. Epilepsy in Patients With Duplications of Chromosome 14 Harboring FOXG1. *Pediatric Neurology* 50(5), pp. 530–535.

Prabhakar, D. and Balon, R. 2010. Late-onset bipolar disorder: A case for careful appraisal. *Psychiatry* 7(1), pp. 34–37.

Przewlocki, R., Parsons, K.L., Sweeney, D.D., Trotter, C., Netzeband, J.G., Siggins, G.R. and Gruol, D.L. 1999. Opioid enhancement of calcium oscillations and burst events involving NMDA receptors and L-type calcium channels in cultured hippocampal neurons. *Journal of Neuroscience* 19(22), pp. 9705–9715.

Pucilowska, J., Puzerey, P.A., Karlo, J.C., Galán, R.F. and Landreth, G.E. 2012. Disrupted ERK Signaling during Cortical Development Leads to Abnormal Progenitor Proliferation, Neuronal and Network Excitability and Behavior, Modeling Human Neuro-Cardio-Facial-Cutaneous and Related Syndromes.

Journal of Neuroscience 32(25), pp. 8663–8677.

Pucilowska, J., Vithayathil, J., Tavares, E.J., Kelly, C., Karlo, J.C. and Landreth, G.E. 2015. The 16p11.2 Deletion Mouse Model of Autism Exhibits Altered Cortical Progenitor Proliferation and Brain Cytoarchitecture Linked to the ERK MAPK Pathway. *Journal of Neuroscience* 35(7), pp. 3190–3200.

Purcell, S.M. et al. 2014. A polygenic burden of rare disruptive mutations in schizophrenia. *Nature* 506(7487), pp. 185–190.

Raffaelli, G., Saviane, C., Mohajerani, M.H., Pedarzani, P. and Cherubini, E. 2004. BK potassium channels control transmitter release at CA3-CA3 synapses in the rat hippocampus. *The Journal of Physiology* 557(1), pp. 147–157.

Ramaswami, G. and Geschwind, D.H. 2018. Genetics of autism spectrum disorder. In: *Handbook of Clinical Neurology*. Elsevier B.V., pp. 321–329.

Ran, F.A., Hsu, P.D., Wright, J., Agarwala, V., Scott, D.A. and Zhang, F. 2013. Genome engineering using the CRISPR-Cas9 system. *Nature Protocols* 8(11), pp. 2281–2308.

Randall, A. and Tsien, R.W. 1995. Pharmacological dissection of multiple types of Ca2+ channel currents in rat cerebellar granule neurons. *Journal of Neuroscience* 15(4), pp. 2995–3012.

Ripke, S. et al. 2013. Genome-wide association analysis identifies 13 new risk loci for schizophrenia. *Nature Genetics* 45(10), pp. 1150–1159.

Ripke, S. et al. 2014. Biological insights from 108 schizophrenia-associated genetic loci. *Nature* 511(7510), pp. 421–427.

Robicsek, O. et al. 2013. Abnormal neuronal differentiation and mitochondrial dysfunction in hair follicle-derived induced pluripotent stem cells of schizophrenia patients. *Molecular Psychiatry* 18(10), pp. 1067–1076.

Rodan, L.H. et al. 2021. Phenotypic expansion of CACNA1C-associated disorders to include isolated neurological manifestations. *Genetics in Medicine 2021* , pp. 1–11.

Roost, M.S. et al. 2017. DNA methylation and transcriptional trajectories during human development and reprogramming of isogenic pluripotent stem cells. *Nature Communications 2017 8:1* 8(1), pp. 1–11.

Rosenberg, S.S. and Spitzer, N.C. 2011. Calcium Signaling in Neuronal Development. *Cold Spring Harbor Perspectives in Biology* 3(10), p. a004259.

Roussos, P. et al. 2014. A Role for Noncoding Variation in Schizophrenia. *Cell Reports* 9(4), pp. 1417–1429.

De Rubeis, S. et al. 2014. Synaptic, transcriptional and chromatin genes disrupted in autism. *Nature* 515(7526), pp. 209–215.

Ruderfer, D.M. et al. 2014. Polygenic dissection of diagnosis and clinical dimensions of bipolar disorder and schizophrenia. *Molecular Psychiatry* 19(9), pp. 1017–1024.

Rund, B.R. 2018. The research evidence for schizophrenia as a neurodevelopmental disorder. *Scandinavian Journal of Psychology* 59(1), pp. 49–58.

Rushton, D.J., Mattis, V.B., Svendsen, C.N., Allen, N.D. and Kemp, P.J. 2013. Stimulation of GABA-

induced Ca2+ influx enhances maturation of human induced pluripotent stem cell-derived neurons. *PLoS ONE* 8(11)

Sacco, R., Cacci, E. and Novarino, G. 2018. Neural stem cells in neuropsychiatric disorders. *Current Opinion in Neurobiology* 48, pp. 131–138.

Sah, P. and Bekkers, J.M. 1996. Apical dendritic location of slow afterhyperpolarization current in hippocampal pyramidal neurons: Implications for the integration of long-term potentiation. *Journal of Neuroscience* 16(15), pp. 4537–4542.

Sahara, S., Yanagawa, Y., O'Leary, D.D.M. and Stevens, C.F. 2012. The Fraction of Cortical GABAergic Neurons Is Constant from Near the Start of Cortical Neurogenesis to Adulthood. *Journal of Neuroscience* 32(14), pp. 4755–4761.

Saliba, R.S., Gu, Z., Yan, Z. and Moss, S.J. 2009. Blocking L-type voltage-gated Ca2+ channels with dihydropyridines reduces γ-aminobutyric acid type A receptor expression and synaptic inhibition. *Journal of Biological Chemistry* 284(47), pp. 32544–32550.

Saliba, R.S., Kretschmannova, K. and Moss, S.J. 2012. Activity-dependent phosphorylation of GABAA receptors regulates receptor insertion and tonic current. *EMBO Journal* 31(13), pp. 2937–2951.

Sánchez-Huertas, C. and Rico, B. 2011. CREB-Dependent Regulation of GAD65 Transcription by BDNF/TrkB in Cortical Interneurons. *Cerebral Cortex* 21(4), pp. 777–788.

Sanchez-Vives, M. V. and McCormick, D.A. 2000. Cellular and network mechanisms of rhythmic recurrent activity in neocortex. *Nature Neuroscience 2000 3:10* 3(10), pp. 1027–1034.

Sanjana, N.E., Shalem, O. and Zhang, F. 2014. Improved vectors and genome-wide libraries for CRISPR screening. *Nature Methods* 11(8), pp. 783–784.

Schroder, E., Byse, M. and Satin, J. 2009. L-Type Calcium Channel C Terminus Autoregulates Transcription. *Circulation Research* 104(12), pp. 1373–1381.

Schumann, C.M. et al. 2004. The Amygdala Is Enlarged in Children But Not Adolescents with Autism; the Hippocampus Is Enlarged at All Ages. *Journal of Neuroscience* 24(28), pp. 6392–6401.

Servili, E., Trus, M. and Atlas, D. 2019. Ion occupancy of the channel pore is critical for triggering excitation-transcription (ET) coupling. *Cell Calcium* 84, p. 102102.

Servili, E., Trus, M., Sajman, J., Sherman, E. and Atlas, D. 2020. Elevated basal transcription can underlie timothy channel association with autism related disorders. *Progress in Neurobiology* 191, p. 101820.

Shah, M. and Haylett, D.G. 2000. Ca $^{2+}$ Channels Involved in the Generation of the Slow Afterhyperpolarization in Cultured Rat Hippocampal Pyramidal Neurons. *Journal of Neurophysiology* 83(5), pp. 2554–2561.

Shi, Y., Kirwan, P. and Livesey, F.J. 2012. Directed differentiation of human pluripotent stem cells to cerebral cortex neurons and neural networks. *Nature Protocols* 7(10), pp. 1836–1846.

Shimmura, C. et al. 2011. Alteration of plasma glutamate and glutamine levels in children with high-functioning autism. *PLoS ONE* 6(10)

Siegenthaler, J.A., Tremper-Wells, B.A. and Miller, M.W. 2008. Foxg1 Haploinsufficiency Reduces the

Population of Cortical Intermediate Progenitor Cells: Effect of Increased p21 Expression. *Cerebral Cortex* 18(8), pp. 1865–1875.

Simms, B.A., Souza, I.A., Rehak, R. and Zamponi, G.W. 2015. The Cav1.2 N terminus contains a CaM kinase site that modulates channel trafficking and function. *Pflugers Archiv European Journal of Physiology* 467(4), pp. 677–686.

Simms, B.A. and Zamponi, G.W. 2014. Neuronal Voltage-Gated Calcium Channels: Structure, Function, and Dysfunction. *Neuron* 82(1), pp. 24–45.

Sinnegger-Brauns, M.J. et al. 2009. Expression and 1,4-dihydropyridine-binding properties of brain L-type calcium channel isoforms. *Molecular Pharmacology* 75(2), pp. 407–414.

Sklar, P. et al. 2008. Whole-genome association study of bipolar disorder. *Molecular Psychiatry* 13(6), pp. 558–569.

Sklar, P. et al. 2011. Large-scale genome-wide association analysis of bipolar disorder identifies a new susceptibility locus near ODZ4. *Nature Genetics* 43(10), pp. 977–985.

Smith, C. et al. 2014. Whole-genome sequencing analysis reveals high specificity of CRISPR/Cas9 and TALEN-based genome editing in human iPSCs. *Cell Stem Cell* 15(1), pp. 12–13.

Smits, A.H. et al. 2019. Biological plasticity rescues target activity in CRISPR knock outs. *Nature Methods* 16(11), pp. 1087–1093.

Smoller, J.W. et al. 2013. Identification of risk loci with shared effects on five major psychiatric disorders: A genome-wide analysis. *The Lancet* 381(9875), pp. 1371–1379.

Soghomonian, J.J. and Martin, D.L. 1998. Two isoforms of glutamate decarboxylase: why? *Trends in Pharmacological Sciences* 19(12), pp. 500–505.

Song, J., Bergen, S.E., Kuja-Halkola, R., Larsson, H., Landén, M. and Lichtenstein, P. 2015. Bipolar disorder and its relation to major psychiatric disorders: a family-based study in the Swedish population. *Bipolar Disorders* 17(2), pp. 184–193.

Splawski, I. et al. 2004. CaV1.2 Calcium Channel Dysfunction Causes a Multisystem Disorder Including Arrhythmia and Autism. *Cell* 119(1), pp. 19–31.

Splawski, I. et al. 2005. Severe arrhythmia disorder caused by cardiac L-type calcium channel mutations. *Proceedings of the National Academy of Sciences* 102(23), pp. 8089–8096.

Srinivasan, K. et al. 2012. A network of genetic repression and derepression specifies projection fates in the developing neocortex. *Proceedings of the National Academy of Sciences* 109(47), pp. 19071–19078.

Stahl, E.A. et al. 2019. Genome-wide association study identifies 30 loci associated with bipolar disorder. *Nature Genetics* 51(5), pp. 793–803.

Stanika, R.I., Villanueva, I., Kazanina, G., Brian Andrews, S. and Pivovarova, N.B. 2012. Comparative impact of voltage-gated calcium channels and NMDA receptors on mitochondria-mediated neuronal injury. *Journal of Neuroscience* 32(19), pp. 6642–6650.

Starnawska, A. et al. 2016. CACNA1C hypermethylation is associated with bipolar disorder. *Translational Psychiatry* 6(6), p. e831.

Stotz, S.C., Jarvis, S.E. and Zamponi, G.W. 2004. Functional roles of cytoplasmic loops and pore lining transmembrane helices in the voltage-dependent inactivation of HVA calcium channels. *Journal of Physiology* 554(2), pp. 263–273.

Straub, H., Köhling, R., Frieler, A., Grigat, M. and Speckmann, E.J. 1999. Contribution of L-type calcium channels to epileptiform activity in hippocampal and neocortical slices of guinea-pigs. *Neuroscience* 95(1), pp. 63–72.

Suhara, T., Nakayama, K., Inoue, O., Fukuda, H., Shimizu, M., Mori, A. and Tateno, Y. 1992. D1 dopamine receptor binding in mood disorders measured by positron emission tomography. *Psychopharmacology* 106(1), pp. 14–8.

Sullivan, P.F., Kendler, K.S. and Neale, M.C. 2003. Schizophrenia as a Complex Trait: Evidence From a Meta-analysis of Twin Studies. *Archives of General Psychiatry* 60(12), pp. 1187–1192.

Sun, J.J., Kilb, W. and Luhmann, H.J. 2010. Self-organization of repetitive spike patterns in developing neuronal networks in vitro. *European Journal of Neuroscience* 32(8), pp. 1289–1299.

Sun, X., Wang, J.F., Tseng, M. and Young, L.T. 2006. Downregulation in components of the mitochondrial electron transport chain in the postmortem frontal cortex of subjects with bipolar disorder. *Journal of Psychiatry and Neuroscience* 31(3), pp. 189–196.

Swanwick, C.C., Murthy, N.R. and Kapur, J. 2006. Activity-dependent scaling of GABAergic synapse strength is regulated by brain-derived neurotrophic factor. *Molecular and Cellular Neuroscience* 31(3), pp. 481–492.

Sweatt, J.D. 2010. Long-Term Potentiation—A Candidate Cellular Mechanism for Information Storage in the Central Nervous System. In: *Mechanisms of Memory*. Elsevier, pp. 150–189.

Szegedi, A. and Egan, M. 2012. CHAPTER 2. The Pathophysiology of Schizophrenia., pp. 13–34.

Takahashi, K., Tanabe, K., Ohnuki, M., Narita, M., Ichisaka, T., Tomoda, K. and Yamanaka, S. 2007. Induction of Pluripotent Stem Cells from Adult Human Fibroblasts by Defined Factors. *Cell* 131(5), pp. 861–872.

Takahashi, S., Glatt, S.J., Uchiyama, M., Faraone, S. V. and Tsuang, M.T. 2015. Meta-analysis of data from the Psychiatric Genomics Consortium and additional samples supports association of CACNA1C with risk for schizophrenia. *Schizophrenia Research* 168(1–2), pp. 429–433.

Tanabe, T. et al. 1988. Primary structure of the receptor for calcium channel blockers from skeletal muscle. *Nature* 328(6128), pp. 313–318.

Tang, X., Zhou, L., Wagner, A.M., Marchetto, M.C.N., Muotri, A.R., Gage, F.H. and Chen, G. 2013. Astroglial cells regulate the developmental timeline of human neurons differentiated from induced pluripotent stem cells. *Stem Cell Research* 11(2), pp. 743–757.

Tang, Z.Z., Liang, M.C., Lu, S., Yu, D., Yu, C.Y., Yue, D.T. and Soong, T.W. 2004. Transcript scanning reveals novel and extensive splice variations in human l-type voltage-gated calcium channel, Cav1.2 alpha1 subunit. *The Journal of biological chemistry* 279(43), pp. 44335–43.

Teh, D.B.L., Ishizuka, T. and Yawo, H. 2014. Regulation of later neurogenic stages of adult-derived neural stem/progenitor cells by L-type Ca^{2+} channels. *Development, Growth & Differentiation* 56(8),

pp. 583–594.

Telezhkin, V. et al. 2016. Forced cell cycle exit and modulation of GABA $_A$, CREB, and GSK3β signaling promote functional maturation of induced pluripotent stem cell-derived neurons. *American Journal of Physiology-Cell Physiology* 310(7), pp. C520–C541.

Temme, S.J., Bell, R.Z., Fisher, G.L. and Murphy, G.G. 2016. Deletion of the mouse homolog of CACNA1C disrupts discrete forms of hippocampal-dependent memory and neurogenesis within the dentate gyrus. *eNeuro* 3(6)

Thompson, M., Weickert, C.S., Wyatt, E. and Webster, M.J. 2009. Decreased glutamic acid decarboxylase67 mRNA expression in multiple brain areas of patients with schizophrenia and mood disorders. *Journal of Psychiatric Research* 43(11), pp. 970–977.

Thompson, M.A., Ginty, D.D., Bonni, A. and Greenberg, M.E. 1995. L-type voltage-sensitive Ca2+ channel activation regulates c-fos transcription at multiple levels. *Journal of Biological Chemistry* 270(9), pp. 4224–4235.

Tian, C. et al. 2012. Foxg1 Has an Essential Role in Postnatal Development of the Dentate Gyrus. *Journal of Neuroscience* 32(9), pp. 2931–2949.

Tian, Y. et al. 2014. Alteration in basal and depolarization induced transcriptional network in iPSC derived neurons from Timothy syndrome. *Genome Medicine* 6(10), p. 75.

Tigaret, C.M. et al. 2021. Neurotrophin receptor activation rescues cognitive and synaptic abnormalities caused by hemizygosity of the psychiatric risk gene Cacna1c. *Molecular Psychiatry 2021* , pp. 1–13.

Tokumitsu, H. and Soderling, T.R. 1996. Requirements for calcium and calmodulin in the calmodulin kinase activation cascade. *Journal of Biological Chemistry* 271(10), pp. 5617–5622.

Toma, K., Kumamoto, T. and Hanashima, C. 2014. The Timing of Upper-Layer Neurogenesis Is Conferred by Sequential Derepression and Negative Feedback from Deep-Layer Neurons. *Journal of Neuroscience* 34(39), pp. 13259–13276.

Topol, A., Zhu, S., Tran, N., Simone, A., Fang, G. and Brennand, K.J. 2015. Altered WNT Signaling in Human Induced Pluripotent Stem Cell Neural Progenitor Cells Derived from Four Schizophrenia Patients. *Biological Psychiatry* 78(6), pp. e29–e34.

Townshend, R.F. et al. 2020. Effect of Cell Spreading on Rosette Formation by Human Pluripotent Stem Cell-Derived Neural Progenitor Cells. *Frontiers in Cell and Developmental Biology* 0, p. 1072.

Tsai, S.Q. et al. 2015. GUIDE-seq enables genome-wide profiling of off-target cleavage by CRISPR-Cas nucleases. *Nature Biotechnology* 33(2), pp. 187–198.

Tully, I.J. 2020. *Exploring the link between CHD2 mutations and double strand break repair in developing neurons*. Cardiff University.

Ullian, E.M., Christopherson, K.S. and Barres, B.A. 2004. Role for glia in synaptogenesis. *GLIA* 47(3), pp. 209–216.

Veltman, M.W.M., Craig, E.E. and Bolton, P.F. 2005. Autism spectrum disorders in Prader-Willi and Angelman syndromes: A systematic review. *Psychiatric Genetics* 15(4), pp. 243–254.

Veres, A. et al. 2014. Low incidence of Off-target mutations in individual CRISPR-Cas9 and TALEN targeted human stem cell clones detected by whole-genome sequencing. *Cell Stem Cell* 15(1), pp. 27–30.

Vigo, D., Thornicroft, G. and Atun, R. 2016. Estimating the true global burden of mental illness. *The Lancet Psychiatry* 3(2), pp. 171–178.

Vitali, I. et al. 2018. Progenitor Hyperpolarization Regulates the Sequential Generation of Neuronal Subtypes in the Developing Neocortex. *Cell* 174(5), pp. 1264-1276.e15.

Volk, D.W., Austin, M.C., Pierri, J.N., Sampson, A.R. and Lewis, D.A. 2000. Decreased Glutamic Acid Decarboxylase67 Messenger RNA Expression in a Subset of Prefrontal Cortical γ-Aminobutyric Acid Neurons in Subjects With Schizophrenia. *Archives of General Psychiatry* 57(3), pp. 237–245.

Völkening, B., Schönig, K., Kronenberg, G., Bartsch, D. and Weber, T. 2017. Deletion of psychiatric risk gene *Cacna1c* impairs hippocampal neurogenesis in cell-autonomous fashion. *Glia* 65(5), pp. 817–827.

Volpato, V. et al. 2018. Reproducibility of Molecular Phenotypes after Long-Term Differentiation to Human iPSC-Derived Neurons: A Multi-Site Omics Study. *Stem Cell Reports* 11(4), pp. 897–911.

Volpato, V. and Webber, C. 2020. Addressing variability in iPSC-derived models of human disease: guidelines to promote reproducibility. *Disease Models & Mechanisms* 13(1)

Wadel, K., Neher, E. and Sakaba, T. 2007. The Coupling between Synaptic Vesicles and Ca2+ Channels Determines Fast Neurotransmitter Release. *Neuron* 53(4), pp. 563–575.

Walsh, M.A. et al. 2018. A multicentre study of patients with Timothy syndrome. *EP Europace* 20(2), pp. 377–385.

Wang, L. et al. 2015. Differentiation of hypothalamic-like neurons from human pluripotent stem cells. *Journal of Clinical Investigation* 125(2), pp. 796–808.

Wegiel, J. et al. 2010. The neuropathology of autism: defects of neurogenesis and neuronal migration, and dysplastic changes. *Acta Neuropathologica 2010 119:6* 119(6), pp. 755–770.

Weinberger, D.R. 1987. Implications of Normal Brain Development for the Pathogenesis of Schizophrenia. *Archives of General Psychiatry* 44(7), pp. 660–669.

Weisskopf, M.G., Bauer, E.P. and LeDoux, J.E. 1999. L-type voltage-gated calcium channels mediate NMDA-independent associative long-term potentiation at thalamic input synapses to the amygdala. *Journal of Neuroscience* 19(23), pp. 10512–10519.

Weissman, T.A., Riquelme, P.A., Ivic, L., Flint, A.C. and Kriegstein, A.R. 2004. Calcium waves propagate through radial glial cells and modulate proliferation in the developing neocortex. *Neuron* 43(5), pp. 647–661.

Wemhöner, K. et al. 2015. Gain-of-function mutations in the calcium channel CACNA1C (Cav1.2) cause non-syndromic long-QT but not Timothy syndrome. *Journal of Molecular and Cellular Cardiology* 80, pp. 186–195.

Williams, S. and Boksa, P. 2010. Gamma oscillations and schizophrenia. *Journal of psychiatry & neuroscience : JPN* 35(2), pp. 75–7.

Wong, L.C., Wu, Y.T., Hsu, C.J., Weng, W.C., Tsai, W.C. and Lee, W.T. 2019. Cognition and evolution of

movement disorders of FOXG1-related syndrome. *Frontiers in Neurology* 10(MAY)

Wu, G.Y., Deisseroth, K. and Tsien, R.W. 2001. Activity-dependent CREB phosphorylation: Convergence of a fast, sensitive calmodulin kinase pathway and a slow, less sensitive mitogen-activated protein kinase pathway. *Proceedings of the National Academy of Sciences of the United States of America* 98(5), pp. 2808–2813.

Xiao, X., Chang, H. and Li, M. 2017. Molecular mechanisms underlying noncoding risk variations in psychiatric genetic studies. *Molecular Psychiatry* 22(4), pp. 497–511.

Xie, S. et al. 2020. The Familial Risk of Autism Spectrum Disorder with and without Intellectual Disability. *Autism Research* 13(12), pp. 2242–2250.

Xu, W. and Lipscombe, D. 2001. Neuronal Cav1.3α1 L-type channels activate at relatively hyperpolarized membrane potentials and are incompletely inhibited by dihydropyridines. *Journal of Neuroscience* 21(16), pp. 5944–5951.

Xuan, S., Baptista, C.A., Balas, G., Tao, W., Soares, V.C. and Lai, E. 1995. Winged helix transcription factor BF-1 is essential for the development of the cerebral hemispheres. *Neuron* 14(6), pp. 1141–1152.

Yan, W., Zhang, R., Zhou, M., Lu, S., Li, W., Xie, S. and Zhang, N. 2020. Relationships between abnormal neural activities and cognitive impairments in patients with drug-naive first-episode schizophrenia. *BMC Psychiatry 2020 20:1* 20(1), pp. 1–9.

Yang, J., Elllnor, P.T., Sather, W.A., Zhang, J.F. and Tsien, R.W. 1993. Molecular determinants of Ca2+ selectivity and ion permeation in L-type Ca2+ channels. *Nature* 366(6451), pp. 158–161.

Yatham, L.N. et al. 2010. Brain serotonin-2 receptors in acute mania. *British Journal of Psychiatry* 196(1), pp. 47–51.

Ye, D., Tester, D.J., Zhou, W., Papagiannis, J. and Ackerman, M.J. 2019. A pore-localizing CACNA1C-E1115K missense mutation, identified in a patient with idiopathic QT prolongation, bradycardia, and autism spectrum disorder, converts the L-type calcium channel into a hybrid nonselective monovalent cation channel. *Heart Rhythm* 16(2), pp. 270–278.

Yip, J., Soghomonian, J.J. and Blatt, G.J. 2009. Decreased GAD65 mRNA levels in select subpopulations of neurons in the cerebellar dentate nuclei in autism: An in situ hybridization study. *Autism Research* 2(1), pp. 50–59.

Yoo, H. 2015. Genetics of Autism Spectrum Disorder: Current Status and Possible Clinical Applications. *Experimental Neurobiology* 24(4), pp. 257–72.

Yoon, K.J. et al. 2014. Modeling a Genetic Risk for Schizophrenia in iPSCs and Mice Reveals Neural Stem Cell Deficits Associated with Adherens Junctions and Polarity. *Cell Stem Cell* 15(1), pp. 79–91.

Yoshihara, M., Hayashizaki, Y. and Murakawa, Y. 2017. Genomic Instability of iPSCs: Challenges Towards Their Clinical Applications. *Stem Cell Reviews and Reports* 13(1), pp. 7–16.

Yoshimizu, T. et al. 2015. Functional implications of a psychiatric risk variant within CACNA1C in induced human neurons. *Molecular Psychiatry*

Yu, D.X. et al. 2014. Modeling hippocampal neurogenesis using human pluripotent stem cells. *Stem*

Cell Reports 2(3), pp. 295–310.

Yu, H.M., Wen, J., Wang, R., Shen, W.H., Duan, S. and Yang, H.T. 2008. Critical role of type 2 ryanodine receptor in mediating activity-dependent neurogenesis from embryonic stem cells. *Cell Calcium* 43(5), pp. 417–431.

Yu, J. et al. 2007. Induced pluripotent stem cell lines derived from human somatic cells. *Science* 318(5858), pp. 1917–1920.

Zheng, F. et al. 2014. Further evidence for genetic association of CACNA1C and schizophrenia: New risk loci in a Han Chinese population and a meta-analysis. *Schizophrenia Research* 152(1), pp. 105–110.

Zuris, J.A. et al. 2015. Cationic lipid-mediated delivery of proteins enables efficient protein-based genome editing in vitro and in vivo. *Nature Biotechnology* 33(1), pp. 73–80.